

**Attachment 5**

**2CAN030706**

**Holtec Licensing Report for ANO Unit 2 Partial Rerack  
(Non-Proprietary)**



Holtec Center, 555 Lincoln Drive West, Marlton, NJ 08053

Telephone (856) 797-0900  
Fax (856) 797-0909

***LICENSING REPORT FOR ANO UNIT 2  
PARTIAL RERACK***

FOR

***ENTERGY***

**Holtec Report No: HI-2063601**

**Holtec Project No: 1572**

**Report Class : SAFETY RELATED**

# HOLTEC INTERNATIONAL

DOCUMENT NUMBER: HI-2063601

PROJECT NUMBER: 1572

DOCUMENT ISSUANCE AND REVISION STATUS										
DOCUMENT NAME: LICENSING REPORT FOR ANO UNIT 2 PARTIAL RERACK					DOCUMENT CATEGORY: <input type="checkbox"/> GENERIC <input checked="" type="checkbox"/> PROJECT SPECIFIC					
No.	Document Portion††	REVISION No. <u>0</u>			REVISION No. _____			REVISION No. _____		
		Author's Initials	Date Approved	VIR #	Author's Initials	Date Approved	VIR #	Author's Initials	Date Approved	VIR #
1.	Chapter 1	ER	3/20/2007	859498						
2.	Chapter 2	ER	3/20/2007	557031						
3.	Chapter 3	ER	3/20/2007	286352						
4.	Chapter 4	KC	3/27/2007	674418						
5.	Chapter 5	DMM	3/20/2007	628952						
6.	Chapter 6	ER	3/20/2007	710764						
7.										
8.										
9.										
11.										
12.										

†† Chapter, section or appendix number. \* Including Appendix A.

# HOLTEC INTERNATIONAL

DOCUMENT NUMBER: HI-2063601

PROJECT NUMBER: 1572

## DOCUMENT CATEGORIZATION

In accordance with the Holtec Quality Assurance Manual and associated Holtec Quality Procedures (HQPs), this document is categorized as a:

- Calculation Package<sup>3</sup> (Per HQP 3.2)       Technical Report (Per HQP 3.2)(Such as a Licensing Report)
- Design Criterion Document (Per HQP 3.4)       Design Specification (Per HQP 3.4)
- Other (Specify):

## DOCUMENT FORMATTING

The formatting of the contents of this document is in accordance with the instructions of HQP 3.2 or 3.4 except as noted below:

## DECLARATION OF PROPRIETARY STATUS

- Nonproprietary       Holtec Proprietary       Privileged Intellectual Property (PIP)

Documents labeled Privileged Intellectual Property contain extremely valuable intellectual/commercial property of Holtec International. They cannot be released to external organizations or entities without explicit approval of a company corporate officer. The recipient of Holtec's proprietary or Top Secret document bears full and undivided responsibility to safeguard it against loss or duplication.

### Notes:

1. This document has been subjected to review, verification and approval process set forth in the Holtec Quality Assurance Procedures Manual. Password controlled signatures of Holtec personnel who participated in the preparation, review, and QA validation of this document are saved in the N-drive of the company's network. The Validation Identifier Record (VIR) number is a random number that is generated by the computer after the specific revision of this document has undergone the required review and approval process, and the appropriate Holtec personnel have recorded their password-controlled electronic concurrence to the document.
2. A revision to this document will be ordered by the Project Manager and carried out if any of its contents is materially affected during evolution of this project. The determination as to the need for revision will be made by the Project Manager with input from others, as deemed necessary by him.
3. Revisions to this document may be made by adding supplements to the document and replacing the "Table of Contents", this page and the "Revision Log".

## Table of Contents

Chapter 1: Overview of the Project.....	1-1
1.1 Introduction.....	1-1
1.2 The Imperative for Reracking.....	1-1
1.3 Report Contents Summary.....	1-1
1.4 References.....	1-3
Chapter 2: Principal Design Criteria and Applicable Codes.....	2-1
2.1 Principal Design Criteria.....	2-1
2.2 Reference Codes and Standards.....	2-1
Chapter 3: Mechanical Design and Materials Considerations.....	3-1
3.1 Mechanical Design Considerations.....	3-1
3.1.1 Overview of Rack’s Mechanical Design.....	3-1
3.1.2 Mechanical Design Objectives.....	3-1
3.1.3 Design Characteristics of Rack Modules.....	3-2
3.2 Material Considerations.....	3-6
3.2.1 Structural Materials.....	3-6
3.2.2 Neutron Absorber Material.....	3-7
3.2.3 Characteristics of Metamic™.....	3-8
3.3 References.....	3-10
Chapter 4: Criticality Safety Analysis.....	4-1
4.1 Introduction and Summary.....	4-1
4.2 Methodology.....	4-3
4.3 Acceptance Criteria.....	4-5
4.4 Assumptions.....	4-6
4.5 Input Data.....	4-6
4.5.1 Fuel Assembly Specification.....	4-6
4.5.2 Core Operating Parameters.....	4-7
4.5.3 Axial Burnup Distribution.....	4-7
4.5.4 Burnable Absorbers.....	4-7
4.5.5 ANO Unit 2 Storage Rack Specification.....	4-7
4.5.5.1 Region 1 Style Storage Racks.....	4-7
4.5.5.2 Region 2 Style Storage Racks.....	4-8
4.5.5.3 Gaps Between Adjacent Racks.....	4-9
4.5.6 New Fuel Vault and Fuel Handling Equipment.....	4-9
4.6 Computer Codes.....	4-9
4.7 Analysis.....	4-10
4.7.1 Region 1.....	4-10
4.7.1.1 Identification of Reference Fuel Assembly.....	4-11
4.7.1.2 Eccentric Fuel Assembly Positioning.....	4-11
4.7.1.3 Uncertainties Due to Manufacturing Tolerances.....	4-11
4.7.1.4 Temperature and Water Density Effects.....	4-12
4.7.1.5 Calculation of Maximum $k_{eff}$ .....	4-13
4.7.1.6 Soluble Boron Concentration for Maximum $k_{eff}$ of 0.95.....	4-13
4.7.1.7 Abnormal and Accident Conditions.....	4-13
4.7.1.7.1 Abnormal Temperature.....	4-14
4.7.1.7.2 Dropped Assembly - Horizontal.....	4-14
4.7.1.7.3 Dropped Assembly – Vertical Into Fuel Storage Cell.....	4-14

4.7.1.7.4	Dropped Assembly – Vertical Onto Rack Wall .....	4-15
4.7.1.7.5	Abnormal Location of a Fuel Assembly .....	4-15
4.7.1.7.5.1	Misloaded Fresh Fuel Assembly.....	4-15
4.7.1.7.5.2	Mislocated Fresh Fuel Assembly.....	4-15
4.7.2	Region 2.....	4-16
4.7.2.1	Identification of Reference Fuel Assembly.....	4-16
4.7.2.2	Core Moderator Temperature Effect for Depletion Calculations.....	4-16
4.7.2.3	Reactivity Effect of Burnable Absorbers During Depletion .....	4-17
4.7.2.4	Reactivity Effect of Axial Burnup Distribution.....	4-17
4.7.2.5	Isotopic Compositions .....	4-18
4.7.2.6	Uncertainty in Depletion Calculations.....	4-18
4.7.2.7	Eccentric Fuel Assembly Positioning.....	4-19
4.7.2.8	Uncertainties Due to Manufacturing Tolerances .....	4-19
4.7.2.9	Temperature and Water Density Effects.....	4-21
4.7.2.10	Determination of Burnup Versus Enrichment Values for the Central Region.....	4-21
4.7.2.11	Determination of Burnup Versus Enrichment Values for Peripheral Cells .....	4-21
4.7.2.12	Calculation of Maximum $k_{eff}$ .....	4-22
4.7.2.13	Soluble Boron Concentration for Maximum $k_{eff}$ of 0.95 .....	4-22
4.7.2.14	Abnormal and Accident Conditions.....	4-23
4.7.2.14.1	Abnormal Temperature.....	4-23
4.7.2.14.2	Dropped Assembly - Horizontal.....	4-24
4.7.2.14.3	Dropped Assembly - Vertical .....	4-24
4.7.2.14.4	Abnormal Location of a Fuel Assembly .....	4-24
4.7.2.14.4.1	Misloaded Fresh Fuel Assembly.....	4-24
4.7.2.14.4.2	Mislocated Fresh Fuel Assembly.....	4-25
4.7.3	Interfaces Within and Between Racks .....	4-26
4.7.3.1	Normal Conditions.....	4-26
4.7.3.2	Rack Lateral Motion – Seismic Event .....	4-27
4.7.4	Boron Dilution Evaluation.....	4-27
4.7.4.1	Low Flow Rate Dilution. ....	4-28
4.7.4.2	High Flow Rate Dilution.....	4-29
4.8	New Fuel Storage Racks Criticality Analysis.....	4-31
4.9	Fuel Handling Equipment.....	4-32
4.9.1	New Fuel Elevator and Fuel Carriage.....	4-32
4.9.2	Fuel Upender.....	4-32
4.9.3	Temporary Storage Rack in the Refuel Canal.....	4-33
4.10	References.....	4-34
Appendix 4A:	Benchmark Calculations .....	4A-1
Chapter 5:	Thermal-Hydraulic Considerations .....	5-1
5.1	Introduction.....	5-1
5.2	Cooling System Description .....	5-2
5.3	Spent Fuel Pool Decay Heat Loads.....	5-3
5.4	Minimum Time-To-Boil And Maximum Boiloff Rate .....	5-5
5.5	Maximum SFP Local Water Temperature .....	5-6
5.6	Fuel Rod Cladding Temperature.....	5-8
5.7	Results.....	5-9
5.7.1	Decay Heat.....	10
5.7.2	Minimum Time-To-Boil And Maximum Boiloff Rate.....	5-10
5.7.3	Local Water and Fuel Cladding Temperatures .....	5-10

5.8	References.....	5-11
Chapter 6:	Installation.....	6-1
6.1	Introduction.....	6-1
6.2	Rack Arrangement .....	6-3
6.3	Rack Interferences .....	6-3
6.4	SFP Cooling.....	6-4
6.5	Removal of Existing Racks and Installation of New Racks .....	6-4
6.6	Safety, Health Physics, and ALARA Methods.....	6-5
6.6.1	Safety.....	6-5
6.6.2	Health Physics .....	6-5
6.6.3	ALARA.....	6-6
6.7	Radwaste Material Control .....	6-7

## List of Tables

Table 3.1.1:	Geometric and Physical Data for the New Region 1 Racks.....	3-1
Table 3.1.3:	Listing Of Holtec Projects That Utilize A Similar Rack Design .....	3-5
Table 3.3.1:	Permissible Structural Materials .....	3-7
Table 4.5.2:	Core Operating Parameter for Depletion Analyses.....	4-36
Table 4.5.3:	Axial Burnup Profile; Burnup < 25.0 GWD/MTU, All enrichments .....	4-37
Table 4.5.4:	Axial Burnup Profile; Burnup > 25.0 GWD/MTU, All enrichments .....	4-38
Table 4.5.5:	Fuel Rack Specifications – Region 1 Racks .....	4-39
Table 4.5.6:	Fuel Rack Specifications – Region 2 Racks .....	4-40
Table 4.5.7:	Identification of Possible Rack Interaction and Minimum Distances Between Racks .....	4-41
Table 4.5.8:	New Fuel Vault and Refuel Canal Rack Dimensions .....	4-42
Table 4.7.1:	Summary of the Criticality Safety Analyses for Region 1 without Soluble Boron .....	4-43
Table 4.7.2:	Summary of the Criticality Safety Analyses for Region 1 with Soluble Boron .....	4-44
Table 4.7.2:	Summary of the Criticality Safety Analyses for Region 1 with Soluble Boron .....	4-44
Table 4.7.3:	Summary of the Criticality Safety Analyses for a Uniform Loading of Spent Fuel in Region 2 without Soluble Boron at 0 Years Cooling Time .....	4-45
Table 4.7.4:	Summary of the Criticality Safety Analyses for a Uniform Loading of Spent Fuel in Region 2 with Soluble Boron at 0 Years Cooling Time .....	4-46
Table 4.7.5:	Summary of the Criticality Safety Analyses for Region 2 without Soluble Boron for a 2x2 Checkerboard of Fresh Fuel and Empty Cells .....	4-47
Table 4.7.6:	Summary of the Criticality Safety Analyses for Low Burnup Peripheral Cells in Region 2 without Soluble Boron at 0 Years Cooling Time.....	4-48
Table 4.7.7:	Summary of the Criticality Safety Analyses for Low Burnup Peripheral Cells in Region 2 with Soluble Boron at 0 Years Cooling Time.....	4-49
Table 4.7.10:	Soluble Boron Requirements for Region 1 Accident Conditions .....	4-52
Table 4.7.11:	Soluble Boron Requirements for Region 2 Accident Conditions .....	4-53
Table 4.7.12:	Summary of Calculations for the Interfaces Between Racks and Loading Schemes... ..	4-54
Table 4.7.13:	Reactivity Effect of IFBA Rods Enrichment 4.95 wt% <sup>235</sup> U .....	4-55
Table 4.7.14:	Reactivity Effect of Fuel and Rack Tolerances for Region 1 Racks.....	4-56
Table 4.7.15:	Reactivity Effect of Temperature Variation in Region 1 Racks .....	4-57
Table 4.7.16:	Reactivity Effect of Fuel and Rack Tolerances for Region 2 Racks (0 Cooling Time).....	4-58
Table 4.7.17:	Reactivity Effect of Temperature Variation in Region 2 Racks (0 Cooling Time) .....	4-59

Table 4.8.1:	Summary of New Fuel Vault Criticality Safety Analysis.....	4-60
Table 4.9.1:	Summary of Criticality Safety Analysis for Fuel Handling Equipment .....	4-61
Table 4.9.2:	Summary of Criticality Safety Analysis for the Fuel Upender .....	4-62
Table 4.9.3:	Summary of Criticality Safety Analysis for Refuel Canal Rack.....	4-63
Table 5.3.1:	Key Input Data for Decay Heat Computations .....	5-12
Table 5.3.2:	Offload Schedule .....	5-13
Table 5.4.1:	Key Input Data for Time-To-Boil Evaluation .....	5-14
Table 5.5.1:	Key Input Data for Local Temperature Evaluation .....	5-15
Table 5.7.1:	Result of SFP Decay Heat Calculations.....	5-16
Table 5.7.2:	Results of Loss-of-Forced Cooling Evaluations .....	5-17
Table 5.7.3:	Results of Maximum Local Water and Fuel Cladding Temperature Evaluations .....	5-18

## List of Figures

FIGURE 1.2.1:	PROPOSED REGION 1 RACK MODULES (A1, A2 AND A3) LAYOUT .....	1-4
FIGURE 3.1.1:	ISOMETRIC VIEW OF A TYPICAL HOLTEC-DESIGNED REGION 1 RACK ..	3-11
FIGURE 3.1.2:	TYPICAL NEUTRON POISON ATTACHMENT .....	3-12
FIGURE 3.1.3:	TYPICAL ASSEMBLAGE OF REGION 1 CELLS .....	3-13
FIGURE 3.1.4:	TYPICAL RACK ADJUSTABLE PEDESTAL .....	3-14
FIGURE 4.5.1:	A TWO-DIMENSIONAL REPRESENTATION OF THE ACTUAL CALCULATIONAL MODEL USED FOR THE REGION 1 RACK ANALYSIS FOR UNIFORM LOADING OF SPENT FUEL. ....	4-64
FIGURE 4.5.3:	A TWO-DIMENSIONAL REPRESENTATION OF THE ACTUAL CALCULATIONAL MODEL USED FOR THE REGION 2 RACK ANALYSIS FOR CHECKERBOARD LOADING OF FRESH FUEL. ....	4-66
FIGURE 4.5.4:	A TWO-DIMENSIONAL REPRESENTATION OF THE ACTUAL CALCULATIONAL MODEL USED FOR THE REGION 2 RACK ANALYSIS FOR PERIPHERAL CELLS. ....	4-67
FIGURE 4.5.5:	A TWO-DIMENSIONAL REPRESENTATION OF THE EXISTING ANO UNIT 2 SPENT FUEL POOL LAYOUT WITH RACK REGION LAYOUT AND GAPS BETWEEN ADJACENT RACKS .....	4-68
FIGURE 4.5.6:	SKETCH OF REGION 1 RACKS, DETAILING IMPORTANT DIMENSIONS AND TOLERANCES .....	4-69
FIGURE 4.5.7:	SKETCH OF REGION 2 RACKS, DETAILING IMPORTANT DIMENSIONS AND TOLERANCES. ....	4-70
FIGURE 4.5.8:	IFBA FUEL ROD CONFIGURATION, CYCLE 18 (124 ZRB <sub>2</sub> RODS).....	4-71
FIGURE 4.5.9:	IFBA FUEL ROD CONFIGURATION, CYCLE 19 AND BEYOND (148 ZRB <sub>2</sub> RODS).....	4-72
FIGURE 4.7.1a:	FRESH FUEL CHECKERBOARD AND SPENT FUEL IN SAME REGION 2 RACK – ACCEPTABLE .....	4-73
FIGURE 4.7.1b:	FRESH FUEL CHECKERBOARD AND SPENT FUEL IN SAME REGION 2 RACK – NOT ACCEPTABLE .....	4-73
FIGURE 4.7.1c:	FRESH FUEL CHECKERBOARD AND SPENT FUEL IN SAME REGION 2 RACK – ACCEPTABLE .....	4-74

FIGURE 4.7.1d:	FRESH FUEL CHECKERBOARD AND SPENT FUEL IN SAME REGION 2 RACK – NOT ACCEPTABLE .....	4-74
FIGURE 4.7.1e:	FRESH FUEL CHECKERBOARD AND SPENT FUEL IN SAME REGION 2 RACK – NOT ACCEPTABLE .....	4-75
FIGURE 4.7.1f:	FRESH FUEL CHECKERBOARD AND SPENT FUEL IN SAME REGION 2 RACK – ACCEPTABLE .....	4-75
FIGURE 4.7.1g:	FRESH FUEL CHECKERBOARD AND SPENT FUEL IN SAME REGION 2 RACK – ACCEPTABLE .....	4-76
FIGURE 4.7.1h:	FRESH FUEL CHECKERBOARD AND SPENT FUEL IN SAME REGION 2 RACK – ACCEPTABLE .....	4-76
FIGURE 4.7.1i:	FRESH FUEL CHECKERBOARD AND SPENT FUEL IN SAME REGION 2 RACK – NOT ACCEPTABLE .....	4-77
FIGURE 4.7.2:	INTERFACE CALCULATION FOR ADJACENT REGION 2 RACKS CONTAINING FRESH FUEL CHECKERBOARDS WITH FRESH FUEL ASSEMBLIES FACING ACROSS THE GAP – NOT ACCEPTABLE .....	4-77
FIGURE 4.7.3:	INTERFACE CALCULATION FOR ADJACENT REGION 2 RACKS CONTAINING FRESH FUEL CHECKERBOARD AND UNIFORM LOADING OF SPENT FUEL - ACCEPTABLE .....	4-78
FIGURE 4.7.4:	INTERFACE CALCULATION FOR REGION 1 AND REGION 2 RACKS; FRESH FUEL CHECKERBOARD IN REGION 2 RACK –ACCEPTABLE.....	4-78
FIGURE 4.7.5:	INTERFACE CALCULATION FOR REGION 1 AND REGION 2 RACKS. UNIFORM LOADING OF SPENT FUEL IN REGION 2 RACK – ACCEPTABLE. ....	4-79
FIGURE 4.8.1:	TWO-DIMENSIONAL REPRESENTATIONS (CROSS SECTIONS) OF THE ACTUAL CALCULATIONAL MODEL USED FOR THE NEW FUEL VAULT ANALYSIS: ENTIRE VAULT (TOP) AND INDIVIDUAL ASSEMBLY (BOTTOM)	4-80
FIGURE 4.8.2:	CALCULATED $K_{EFF}$ AS A FUNCTION OF WATER DENSITY IN THE NEW FUEL VAULT.....	4-81
FIGURE 4.9.1:	TWO-DIMENSIONAL REPRESENTATION (CROSS SECTION) OF THE ACTUAL CALCULATIONAL MODEL USED FOR THE FUEL UPENDER ANALYSIS ...	4-82
FIGURE 4.9.2:	TWO-DIMENSIONAL REPRESENTATION (CROSS SECTION) OF THE ACTUAL CALCULATIONAL MODEL USED FOR THE REFUEL CANAL ANALYSIS. ...	4-83
FIGURE 5.5.1:	SCHEMATIC OF THE CFD MODEL OF THE ANO-2 SFP .....	5-19
FIGURE 5.7.1:	NORMAL OFFLOAD BOUNDING SPENT FUEL HEAT LOAD.....	5-20

FIGURE 5.7.3: CONTOURS OF STATIC TEMPERATURE IN A VERTICAL PLANE THROUGH  
THE CENTER OF THE SFP .....5-22

FIGURE 5.7.4: VELOCITY VECTOR PLOT IN A VERTICAL PLANE THROUGH THE CENTER  
OF THE SFP.....5-23

# Chapter 1: Overview of the Project

## 1.1 Introduction

Entergy is the owner and operator of Arkansas Nuclear One Unit 2 (ANO-2), a Pressurized Water Reactor (PWR) nuclear plant located approximately 70 miles northwest of Little Rock and 5 miles west of Russellville. ANO-2 features a Combustion Engineering reactor design and has a spent fuel pool located in the Auxiliary Building. The reactor has a licensed rated thermal power of 3026 MWt.

ANO-2 uses a Spent Fuel Pool (SFP) for storage of irradiated nuclear fuel in order to maintain a subcritical array, remove decay heat and provide radiation shielding. The SFP is currently licensed for a maximum of 988 fuel assemblies. The storage locations are arranged in twelve rack modules: three Region 1 racks (with poison panels for criticality control) and nine Region 2 racks (without poison panels).

## 1.2 The Imperative for Reracking

The existing Region 1 racks utilize Boraflex™ panels for neutron absorption. Due to observed degradation of the Boraflex™ panels, fuel loading restrictions have been imposed in Region 1. In order to reduce the loading restrictions, the Region 1 racks will be removed and replaced with racks containing a non-degrading neutron absorber material, Metamic™.

There are currently two Region 1 racks with a 9x9 array and one Region 1 rack with a 9x8 array, for a total of 234 Region 1 storage locations. The new racks will have the same number of fuel storage locations as the racks being replaced (i.e., there is no increase in the spent fuel storage capacity). A rack module layout showing the new Region 1 racks in the ANO-2 spent fuel pool is presented in Figure 1.2.1.

## 1.3 Report Contents Summary

This report provides the design basis, analysis methodology, and evaluation results for the proposed Region 1 storage racks at ANO-2 to support review by the U.S. Nuclear Regulatory

Commission (USNRC). The rack design and analysis methodologies employed are a direct evolution of previous license applications. This report documents the design and analyses performed for the new racks to show that they are consistent with governing requirements of the applicable codes and standards, in particular, "OT Position for Review and Acceptance of Spent Fuel Storage and Handling Applications," USNRC (1978) and 1979 Addendum thereto [1].

The new storage racks are freestanding and self-supporting. The principal construction materials for the SFP racks are SA240-304 and/or A240-304 stainless steel sheet and plate stock, and the Metamic™ neutron absorber for reactivity control. The only non-stainless material utilized in the rack is the neutron absorber material, Metamic™, whose characteristics are discussed in Chapter 3. The new racks are designed using the guidance of the OT position paper and the sections of NUREG-0800 [2] applicable to the spent fuel racks. The material procurement, analysis, fabrication, and installation of the rack modules conform to 10CFR50 Appendix B requirements.

Chapters 2 and 3 of this report provide an abstract of the design and material information on the racks, respectively. Chapter 4 provides a summary of the methods and results of the criticality evaluations performed for the spent fuel pool racks. The criticality limit is that the effective neutron multiplication factor ( $k_{\text{eff}}$ ) be less than or equal to 0.95 with the spent fuel storage racks fully loaded with fuel of the highest permissible reactivity and the pool flooded with borated water at a temperature corresponding to the highest reactivity. The maximum calculated reactivities include a margin for uncertainty in reactivity calculations, including manufacturing tolerances, and are calculated with a 95% probability at a 95% confidence level with credit for soluble boron. The criticality safety analysis sets the requirements on the neutron absorber panel length and the amount of  $B^{10}$  per unit area (i.e., loading density) for the new racks. Chapter 4 also discusses new criticality evaluations performed for the new fuel storage vault rack and fuel handling equipment. The acceptance criteria for the new fuel storage rack is  $k_{\text{eff}}$  less than or equal to 0.95 when flooded with unborated water and less than or equal to 0.98 under optimal moderation. The acceptance criteria for the fuel handling equipment is  $k_{\text{eff}}$  less than 1.0 with no credit for soluble boron and less than or equal to 0.95 with partial credit for soluble boron.

Thermal-hydraulic considerations require that, under normal conditions, the SFP bulk temperatures not exceed 120°F during a partial core offload and 150°F for a full core offload. It must further be demonstrated that, under normal conditions, localized boiling in the racks and stored fuel will not occur and that Departure from Nucleate Boiling (DNB) will not occur on fuel cladding surfaces. The thermal-hydraulic analyses carried out in support of this re-rack effort are described in Chapter 5.

Chapter 6 discusses the safety and ALARA considerations applicable to the installation of the new racks.

All computer programs utilized to perform the analyses documented in this report are benchmarked and verified. Holtec International has utilized these programs in numerous license applications over the past two decades.

The analyses presented herein demonstrate that the new racks possess sufficient margins under the guidelines mentioned in the OT Position Paper [1], namely, nuclear subcriticality, thermal-hydraulic safety, and radiological compliance.

#### **1.4 References**

- [1] USNRC, "OT Position for Review and Acceptance of Spent Fuel Storage and Handling Applications," April 14, 1978, and Addendum dated January 18, 1979.
- [2] NUREG-0800, SRP 9.1.2 and Appendix D to SRP 3.8.4, USNRC July 1981.

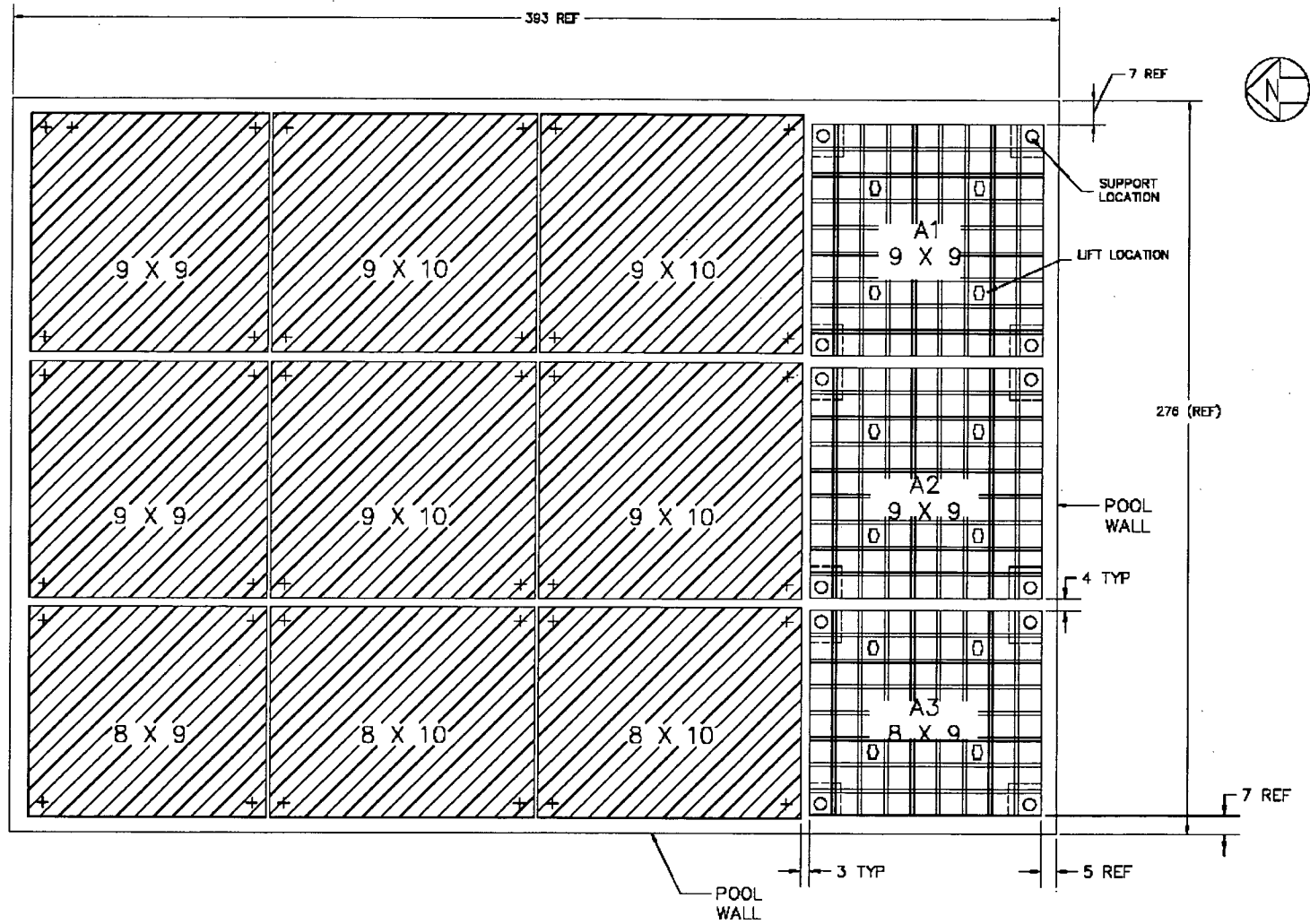


**FIGURE 1.2.1: PROPOSED REGION 1 RACK MODULES (A1, A2 AND A3) LAYOUT**

## Chapter 2: Principal Design Criteria and Applicable Codes

### 2.1 Principal Design Criteria

The key design criteria for the new Region 1 spent fuel racks are set forth in the USNRC memorandum entitled "OT Position for Review and Acceptance of Spent Fuel Storage and Handling Applications," dated 14 April 1978 as modified by amendment dated 18 January 1979. Criticality requirements are also defined in 10CFR50.68 (Criticality Accident Requirements). A brief summary of the design bases for the racks, from this OT Position Paper, is as follows:

- a. Disposition: All new rack modules are required to be freestanding.
- b. Kinematic Stability: All freestanding modules must be kinematically stable (against tipping or overturning) if a seismic event is imposed on any module.
- c. Structural Compliance: All primary stresses in the rack modules must satisfy the limits postulated in Section III Subsection NF of the ASME B&PV Code.
- d. Thermal-Hydraulic Compliance: The spatial average bulk pool temperature is required to remain below 120°F in the wake of a partial offload and below 150°F subsequent to a full core offload, with only one SFP cooling system train in operation.
- e. Criticality Compliance: The fuel storage racks must be able to store Zircaloy-4 and Optimized ZIRLO clad fuel of 5.0 weight percent (w/o) maximum enrichment while maintaining the reactivity ( $K_{eff}$ ) less than 0.95.
- f. Accident Events: In the event of postulated drop events (uncontrolled lowering of a fuel assembly, for instance), it is necessary to demonstrate that the subcritical geometry of the rack structure is not compromised.

### 2.2 Reference Codes and Standards

Inasmuch as the Region 1 spent fuel rack is a fuel storage device with the overriding mission to guarantee a sub-critical storage state for the stored spent fuel, the role of the mechanical design codes and standards is focused on ensuring the physical integrity of the rack structure during all conditions of service. For this reason, the governing NRC document (the OT Position Paper referenced in the foregoing) does not prescribe a specific code. However, Holtec International

has used ASME Section III Subsection NF as the guiding Code for stress analysis purposes, treating the rack as a linear Class 3 NF structure.

Subsection NF of the ASME Code requires the “jurisdictional boundary” of the structure to be defined. For the new Region 1 spent fuel storage racks, the jurisdictional boundary is the interface between the adjustable rack pedestals and the underlying pool structure.

The following codes, standards and practices are used as applicable for the design, construction, and assembly of the new Region 1 spent fuel storage racks. Later Code editions and addenda may be used during the design and fabrication phases provided they are reconciled with the Code of record.

a. Design Codes

- (1) American Institute of Steel Construction (AISC) Manual of Steel Construction, 7<sup>th</sup> Edition, 1970.
- (2) American Society of Mechanical Engineers (ASME), Boiler and Pressure Vessel Code, Section III, Subsection NF, 1980 Edition through Winter 1981 Addenda.
- (3) American National Standards Institute (ANSI) N210-1976, Design Objectives for Light Water Reactor Spent Fuel Storage Facilities at Nuclear Power Stations.
- (4) ANSI/ANS 8.1/N16.1-1975, Nuclear Criticality Safety in Operations with Fissionable Materials Outside Reactors.
- (5) ANSI/ANS 8.7-1974, Guide for Nuclear Criticality Safety in the Storage of Fissionable Materials.
- (6) ANSI/ANS 8.11-1975, Validation of Calculation Methods for Nuclear Criticality Safety.
- (7) ANSI/ANS-57.3-1983, Design Requirements for New Fuel Storage Facilities at Light Water Reactor Plants.
- (8) ANSI/AISC-N690-1984, Nuclear Facilities - Steel Safety Related Structure for Design, Fabrication and Erection.
- (9) ANSI/ANS 8.17-1984, Criticality Safety Criteria for the Handling, Storage and Transportation of LWR Fuel Outside Reactors.

b. Test and Inspection Codes

- (1) ASNT-TC-1A, June, 1984 American Society for Nondestructive Testing (Recommended Practice for Personnel Qualification).
- (2) ASME Section V - Nondestructive Examination, 1980 Edition through Winter 1981 Addenda.
- (3) American Society for Testing and Materials (ASTM) A262 Practices A or E, Standard Recommended Practices for Detecting Susceptibility to Intergranular Attack in Stainless Steels.

c. Material Codes

- (1) ASTM Standard - A-240.
- (2) ASME Boiler and Pressure Vessel Code, Section II - Parts A and C, 1980 Edition through Winter 1981 Addenda.
- (3) ASME Boiler and Pressure Vessel Code, Section III, Subsection NF, 1980 Edition through Winter 1981 Addenda.

d. Welding Codes

- (1) ASME Boiler and Pressure Vessel Code, Section IX - Latest Applicable Edition and Addenda.
- (2) ASME Boiler and Pressure Vessel Code, Section III, Subsection NF, 1980 Edition through Winter 1981 Addenda.
- (3) American Welding Society (AWS) Standard - D1.1, Structural Welding Code.

e. Quality Assurance, Cleanliness, Packaging, Shipping, Receiving, Storage and Handling Requirements

- (1) ANSI N45.2.2-1978, "Packaging, Shipping, Receiving, Storage and Handling of Items for Nuclear Power Plants."
- (2) ANSI N45.2.1-1980, "Cleaning of Fluid Systems and Associated Components during Construction Phase of Nuclear Power Plants."
- (3) ASME Boiler and Pressure Vessel, Section V, Nondestructive Examination, 1980 Edition through Winter 1981 Addenda, or later.

- (4) 10CFR50 Appendix B, Quality Assurance Criteria for Nuclear Power Plants and Fuel Reprocessing Plants.
- (5) ANSI - N45.2.11-1978, "Quality Assurance Requirements for the Design of Nuclear Power Plants."
- (6) ANSI 14.6-1978, "Special Lifting Devices for Shipping Containers weighing 10,000 lb. or more for Nuclear Materials."
- (7) ANSI N45.2.6-1973, "Qualifications of Inspection, Examination, and Testing Personnel for the Construction Phase of Nuclear Power Plants."
- (8) ANSI N45.2.8-1975, "Supplementary Quality Assurance Requirements for Installation, Inspection and Testing of Mechanical Equipment and Systems for the Construction Phase of Nuclear Power Plants."
- (9) ANSI N45.2.9-1979, "Requirements for Collection, Storage, and Maintenance of Quality Assurance Records for Nuclear Power Plants."
- (10) ANSI N45.2.10-1973, "Quality Assurance Terms and Definitions."
- (11) ANSI N45.2.12-1977, "Requirements for Auditing of Quality Assurance Programs for Nuclear Power Plants."
- (12) ANSI N45.2.13-1976, "Quality Assurance Requirements for Control of procurement of Items and Services for Nuclear Power Plants."
- (13) ANSI N45.2.23-1978, "Qualification of Quality Assurance Program Audit Personnel for Nuclear Power Plants."
- (14) ASME NQA-1, Quality Assurance Program Requirements for Nuclear Facility Applications, latest revision.
- (15) ASTM A380, Recommended Practice for Descaling, Cleaning and Marking Stainless Steel Parts, and Equipment.

f. Other References

- (1) Nuclear Regulatory Commission (NRC) Regulatory Guides 1.13, Rev. 2; 1.25, March 1972; 1.26, Rev. 3; 1.29, Rev. 3; 1.31, Rev. 3; 1.44; 1.60; 1.61; 1.70, Rev. 3; 1.71, Rev. 0; 1.85, latest Rev.; 1.92, Rev. 1; 1.124, Rev. 1; 3.41, Rev. 1; 8.8, Safety Guide 28; 1.38, Rev. 2.
- (2) General Design Criteria for Nuclear Power Plants, Code of Federal Regulations, Title 10, Part 50, Appendix A (GDC Nos. 1, 2, 61, 62, and 63).

- (3) NUREG-0800, Standard Review Plan, Sections 3.2.1, 3.2.2, 3.7.1, 3.7.2, 3.7.3, 3.8.4, 3.8.5, 9.1.1, 9.1.2, 9.1.3.
- (4) NUREG-0800, Branch Technical Position ASB 9-2 "Residual Decay Energy for Light Water Reactors for Long Term Cooling."
- (5) NRC Generic Letter, "Position for Review and Acceptance of Spent Fuel Storage and Handling Applications" dated April 14, 1978, and the modifications to this document of January 18, 1979.
- (6) NUREG-0612, July 1980, "Control of Heavy Loads at Nuclear Power Plants."
- (7) NRC Regulatory Issue Summary 2005-25: "Clarification of NRC Guidelines for Control of Heavy Loads' – October 31, 2005"
- (8) ANSI - N16.1-75 Nuclear Criticality Safety Operations with Fissionable Materials Outside Reactors.
- (9) ANSI - N16.9-75 Validation of Calculation Methods for Nuclear Criticality Safety.
- (10) 10CFR21 - Reporting of Defects and Non-Compliance.
- (11) NUREG-1233, Seismic Design Criteria.
- (12) 10CFR50.68 - Criticality Accident Requirements.
- (13) Dr. Lawrence Kopp, "Guidance on the Regulatory Requirements for Criticality Analysis for Fuel Storage at Light-Water Reactor Power Plants," USNRC Internal Memorandum to T. Collins, 19 August 1998.

# Chapter 3: Mechanical Design and Materials Considerations

## 3.1 Mechanical Design Considerations

### 3.1.1 Overview of Rack's Mechanical Design

The three new Region 1 rack modules are designed as cellular structures such that each fuel assembly has a square opening with a baseplate providing a support surface for the bottom nozzle of the PWR style fuel assembly.

Each rack module is a freestanding structure, made primarily from austenitic stainless steel containing honeycomb storage cells interconnected through longitudinal welds. Suitably engineered neutron absorber panels interposed between facing fuel storage assemblies provide the requisite neutron attenuation between adjacent storage cells.

A rack module layout showing the new Region 1 racks in the spent fuel pool is presented in Figure 1.2.1. Table 3.1.1 provides geometric and physical data on the new Region 1 rack modules.

<b>Table 3.1.1: Geometric and Physical Data for the New Region 1 Racks</b>									
RACK I.D.	RACK TYPE	CELL-TO-CELL PITCH		NO. OF CELLS		MODULE WIDTHS (approximate)		DRY WEIGHT (lb)	CELLS PER RACK
		N-S (in)	E-W (in)	N-S	E-W	N-S (in)	E-W (in)		
A1	Flux Trap	9.8	9.8	9	9	87.505	87.505	24,200	81
A2	Flux Trap	9.8	9.8	9	9	87.505	87.505	24,200	81
A3	Flux Trap	9.8	9.8	9	8	87.505	77.705	21,700	72

### 3.1.2 Mechanical Design Objectives

A central objective in the design of the new rack modules is to maximize structural strength while minimizing inertial mass and dynamic response. Accordingly, the rack modules have been designed to simulate a stiff linear structure that has excellent de-tuning characteristics with respect to the applicable seismic events. In addition, the rack modules are designed to meet the

functional performance objectives cited as Design Criteria presented in Chapter 2. The mechanical design attributes of the modules that enable the required performance objectives to be fulfilled are summarized below.

- i. The rack modules must be constructed in such a manner that the storage cell surfaces, which would come in contact with the fuel assembly, will be free of harmful chemicals and projections (e.g., weld splatter).
- ii. The component connection sequence and welding processes must be selected to reduce fabrication distortions.
- iii. The fabrication process should involve operational sequences that permit immediate accessibility for verification by the inspection staff.
- iv. The corners of storage cells should be connected to each other using austenitic stainless steel connector elements (Holtec refers to these elements in a flux trap rack as water gap plates) such that a honeycomb lattice construction is realized. The extent of welding is selected to detune the racks from the seismic input motion of the plant.

### **3.1.3 Design Characteristics of Rack Modules**

The Region 1 spent fuel storage racks (see isometric view in Figure 3.1.1) consist of three main subcomponents, namely:

- i. the cellular structure
- ii. the baseplate
- iii. the adjustable pedestals

The cellular structure of the fuel rack defines the storage space for the fuel. It has six principal design attributes:

- i. Each fuel assembly is confined in a square space (called a cell or box) that presents no protrusions or barriers to the insertion and withdrawal of the fuel assembly.
- ii. The height of the storage cells is set to provide full lateral support to the fuel assembly and to enable unfettered access by the fuel handling tool from the fuel handling bridge.
- iii. A neutron absorber panel (Metamic™) is attached to cell walls as required by the criticality analyses.

- iv. The neutron absorber panels are firmly held in place in all-stainless steel pockets around each cell (see Figure 3.1.2). The neutron absorber length is sized to provide complete coverage to the active fuel length.
- v. The cells are joined together using multiple connector elements (water gap plates) spaced along the rack height in the manner shown in Figure 3.1.3. Joining the cells by the connector elements results in a well-defined shear flow path, and essentially makes the box assemblage into a multi-flanged beam-type structure.
- vi. The bottom edge of the boxes that constitute the cellular region is welded to the baseplate to create an integral welded construction.

The cell-to cell connectivity in the cellular region renders it into an extremely stiff multi-flange, multi-web structure that simulates the load bearing characteristics of an elastic half space at the pedestal-to-baseplate locations.

The extensive in-body welds in the cellular region and the baseplate-to-cellular region render the fuel rack module into a stainless steel weldment that is structurally detuned from the earthquake harmonics, resulting in a sharply mitigated module response to the site's earthquake.

The baseplate is an austenitic stainless steel plate equipped with equally spaced thru-holes and a flat platform that provides the structural connection between the group of adjustable pedestals underneath it and the cellular regions above. The baseplate provides the bearing surface for the bottom fitting of the fuel assembly.

The third constituent item in the rack modules are the adjustable pedestals (refer to Figure 3.1.4) used to elevate the module baseplate above the floor of the spent fuel pool. Each rack has four adjustable pedestals attached to the bottom of the rack baseplate beneath the corner cell locations. The adjustable pedestals are used to level the racks.

The thermal-hydraulic imperatives of the fuel rack's design are satisfied by ensuring that every storage cell has a flow path to promote a gravity-driven thermosiphon cooling of the stored fuel without allowing any local hot spots on the fuel cladding that may be injurious to the long-term integrity of the fuel cladding. Analyses and results, presented in Chapter 5, confirm the efficient thermal performance of the new fuel racks.

In the event of a fuel assembly drop into a storage cell, the module baseplate provides the barrier against a direct impact on the pool liner. Thus, the racks also provide the collateral benefit of an added protection to the pool's water confinement system (the stainless steel lining of the pool cavity).

Principal design data on the new rack modules are provided in Table 3.1.2.

<b>Table 3.1.2: Module Data For SFP Racks<sup>1</sup></b>	
Storage Cell Center-to-Center Pitch	9.8 in.
Storage Cell Inner Dimension (Width)	8.58 in.
Inter-Cell Flux Trap Gap	0.76 in.
Storage Cell Length	189 in.
Neutron Absorber Material	Metamic™
Neutron Absorber Length	154 in.
Neutron Absorber Width	7.2 in.
Baseplate Thickness	0.75 in.
Baseplate Flow Hole Diameter	6 in.
Rack Pedestal Type (fixed or adjustable)	Adjustable
Rack Pedestal Height (female + male)	3-5/8 in.
Remote Lifting and Handling Provisions	Yes

In closure, the new Region 1 rack modules are the flux trap genre utilized by Holtec International in scores of wet capacity expansion projects in the U.S. and overseas (see Table 3.1.3 for a nearly complete listing). The principal causative factors relevant to rack structural failure [3.1.1] are largely eliminated, resulting in a "high margin" rack design.

<sup>1</sup> All dimensions indicate nominal values.

**TABLE 3.1.3: Listing Of Holtec Projects That Utilize A Similar Rack Design**

<b>Plant Name</b>	<b>Reactor Type</b>	<b>Utility</b>	<b>Start Date</b>	<b>Completion Date</b>
Kori 4 and Yonggwang 1	PWR	Korea Hydro and Nuclear Power	February 2005	September 2005
Shin Kori 1 & 2	PWR	Korea Hydro and Nuclear Power	December 2003	August 2008
Diablo Canyon Units 1 & 2	PWR	Pacific Gas and Electric	November 2003	March 2007
Turkey Point Units 3 & 4	PWR	Florida Power & Light	April 2003	TBD
McGuire Nuclear Station Units 3 & 4	PWR	Duke Energy Company	February 2003	June 2003
McGuire Nuclear Station Units 1 & 2	PWR	Duke Energy Company	May 2002	October 2003
Turkey Point Units 3 & 4	PWR	Florida Power & Light	May 2002	December 2004
Port St. Lucie Units 1 & 2	PWR	Florida Power & Light	October 2001	December 2004
Comanche Peak	PWR	Texas Utilities	January 2001	December 2001
V.C. Summer	PWR	South Carolina Electric & Gas Company	August 2000	March 2003
Comanche Peak	PWR	Texas Utilities	December 1999	December 2001
Byron	PWR	Commonwealth Edison Company	February 1998	ca. 2000
Braidwood	PWR	Commonwealth Edison Company	February 1998	June 2001
Yonggwang 5&6	PWR	Hanjung-KEPCO	September 1997	July 2000
Harris Station	PWR	Carolina Power & Light Company	March 1997	ca.2005
Vogtle 1	PWR	Southern Nuclear Operating company	February 1997	November 1998
Shearon Harris	PWR	Carolina Power & Light Company	October 1996	July 1997
Sizewell B	PWR	Nuclear Electric, plc	December 1995	March 1997
Angra Unit 1	PWR	FURNAS Centrais Electricas, S.A.	October 1995	October 1997
Shearon Harris	PWR	Carolina Power & Light Company	April 1995	February 1996
Kori 4 and Yonggwang 1&2	PWR	Korea Electric Power Corporation	June 1995	December 1997
Connecticut Yankee	PWR	Northeast Utilities Service Company	March 1994	September 1996
Ulchin Unit 2	PWR	Korea Electric Power Corporation	March 1995	June 1996
Ulchin Unit 1	PWR	Korea Electric Power Corporation	January 1994	August 1996

<b>TABLE 3.1.3: Listing Of Holtec Projects That Utilize A Similar Rack Design</b>				
<b>Plant Name</b>	<b>Reactor Type</b>	<b>Utility</b>	<b>Start Date</b>	<b>Completion Date</b>
Salem Nuclear Generating Station Units 1&2	PWR	Public Service Electric and Gas Company	December 1992	July 1995
Fort Calhoun Nuclear Station	PWR	Omaha Public Power District	March 1992	August 1994
Beaver Valley Unit 1	PWR	Duquesne Light Company	March 1992	July 1994
Zion Station	PWR	Commonwealth Edison Company	February 1991	October 1993
Shearon Harris Plant	PWR	Carolina Power & Light Company	July 1991	April 1992
Yonggwang Units 3&4	PWR	Korea Electric Power Corporation	March 1991	January 1992
Donald C. Cook Nuclear Plant	PWR	American Electric Power Service Corporation	April 1990	June 1993
Ulchin Unit 2	PWR	Korea Electric Power Corporation	March 1989	August 1990
Three Mile Island Unit 1	PWR	GPU Nuclear	March 1989	August 1992
Indian Point Unit 2	PWR	Consolidated Edison Company	October 1988	September 1990
Vogtle Unit 1	PWR	Georgia Power Company	August 1987	November 1988
Diablo Canyon Units 1&2	PWR	Pacific Gas and Electric Company	January 1984	July 1986

### **3.2 Material Considerations**

Safe storage of nuclear fuel in the SFP requires that the materials utilized in the rack fabrication be of proven durability and compatible with the pool water environment. This section provides a synopsis of the considerations that assure a satisfactory service life of at least 40 years for all materials used in the new fuel racks.

#### **3.2.1 Structural Materials**

Table 3.3.1 provides a listing of the structural materials that are permitted in the new spent fuel rack modules. All austenitic stainless steel materials proposed for use in the new racks have been used in numerous Light Water Reactor (LWR) pools racked by Holtec International. Many racks

have been in the pool water for decades. None has exhibited any evidence of material degradation. All materials used in the construction of the new spent fuel storage racks have been determined to be compatible with the ANO-2 spent fuel pool.

Table 3.3.1: Permissible Structural Materials	
Part	Material
Baseplate	A240-304 or SA240-304
Sheet metal stock	A240-304 or SA240-304
Pedestals	A240-304 or SA240-304 and A564-630 or SA564-630
Weld material	Type 308 or 309

### 3.2.2 Neutron Absorber Material

The Metamic™ neutron absorber material, proposed for use in the new racks, is manufactured by Metamic, LLC of Lakeland, Florida ([www.metamic.com](http://www.metamic.com)). As discussed below, Metamic™ has been subjected to rigorous tests by various organizations including Holtec International, and has been approved by the USNRC in recent dry as well as wet storage applications.

Metamic™ was developed in the mid-1990s by the Reynolds Metals Company [3.2.9] with the technical support of the Electric Power Research Institute (EPRI) for spent fuel reactivity control in dry and wet storage applications with the explicit objective to eliminate the performance frailties of aluminum cermet type of absorbers reported in the industry. Metallurgically, Metamic™ is a metal matrix composite (MMC) consisting of a matrix of aluminum reinforced with Type 1 ASTM C-750 boron carbide. Metamic™ is characterized by extremely fine aluminum (325 mesh or smaller) and boron carbide (B<sub>4</sub>C) powder. Typically, the average B<sub>4</sub>C particle size is between 10 and 40 microns. The high performance and reliability of Metamic™ derives from the fineness of the B<sub>4</sub>C particle size and uniformity of its distribution, which is solidified into a metal matrix composite structure by the powder metallurgy process. This yields excellent homogeneity and a porosity-free material.

In Metamic™'s manufacturing process, the aluminum and boron carbide powders are carefully blended without binders or other additives that could potentially adversely influence

Metamic™'s performance. The blend of powders is isostatically compacted into a green billet under high pressure and vacuum sintered to near theoretical density. The billet is extruded and subjected to multiple rolling operations to produce sheet stock of the required thickness and a tight thickness tolerance. An array of U.S. patents discloses the unique technologies that underlie the Metamic™ neutron absorber [3.2.1-3.2.4].

In recognition of the central role of the neutron absorber in maintaining the subcriticality, Holtec International utilizes appropriately rigorous technical and quality assurance criteria and acceptance protocols to ensure satisfactory neutron absorber performance over the service life of the fuel racks. Holtec International's Q.A. program ensures that Metamic™ will be manufactured under the control and surveillance of a Quality Assurance/Quality Control Program that conforms to the requirements of 10CFR50 Appendix B, "Quality Assurance Criteria for Nuclear Power Plants." Consistent with its role in reactivity control, all neutron absorbing material procured for use in the Holtec racks is categorized as Safety Related (SR). SR manufactured items, as required by Holtec's NRC-approved Quality Assurance program, must be produced to essentially preclude, to the extent possible, the potential of an error in the procurement of constituent materials and the manufacturing processes. Accordingly, material and manufacturing control processes must be established to eliminate the incidence of errors, and inspection steps are implemented to serve as an independent set of barriers to ensure that all critical characteristics defined for the material by Holtec's design team are met in the manufactured product.

### **3.2.3 Characteristics of Metamic™**

Because Metamic™ is a porosity-free material, there is no capillary path through which spent fuel pool water can penetrate Metamic™ panels and chemically react with aluminum in the interior of the material to generate hydrogen. Thus, the potential of swelling and generation of significant quantities of hydrogen is eliminated.

To determine its physical stability and performance characteristics, Metamic™ was subjected to an extensive array of tests sponsored by EPRI that evaluated the functional performance of the material at elevated temperatures (up to 900°F) and radiation levels (1E+11 rads gamma). The results of the tests documented in an EPRI report [3.2.5] indicate that Metamic™ maintains its physical and neutron absorption properties with little variation in its properties from the unirradiated state. The main conclusions provided in the above-referenced EPRI report, which endorsed Metamic™ for dry and wet storage applications on a generic basis, are summarized below:

- The metal matrix configuration produced by the powder metallurgy process with almost a complete absence of open porosity in Metamic™ ensures that its density is essentially equal to the theoretical density.
- The physical and neutronic properties of Metamic™ are essentially unaltered under exposure to elevated temperatures (750° F - 900° F).
- No detectable change in the neutron attenuation characteristics under accelerated corrosion test conditions has been observed.

Additional technical information on Metamic™ in the literature includes independent measurements of boron carbide particle distribution in Metamic™ panels, which showed extremely small particle-to-particle distance [3.2.6]. The USNRC has previously approved Metamic™ for use in both wet storage [3.2.7] and dry storage [3.2.8] applications.

Metamic™ has also been subjected to independent performance assessment tests by Holtec International in the company's Florida laboratories since 2001 [3.2.9, 10]. The three-year long experimental study simulated limiting environmental conditions in wet and dry storage. No anomalous material behavior was observed in any of the tests. These independent Holtec tests essentially confirmed earlier EPRI and other industry reports cited in the foregoing with regard to Metamic™'s suitability as a neutron absorber in fuel storage applications.

### 3.3 References

- [3.1.1] A Case for Wet Storage, by K.P. Singh, INNM Spent Fuel Management Seminar X, Washington, D.C., January 1993.
- [3.2.1] U.S. Patent # 6,332,906 entitled "Aluminum-Silicon Alloy formed by Powder", Thomas G. Haynes III and Dr. Kevin Anderson, issued December 25, 2001.
- [3.2.2] U.S. Patent # 5,965,829 entitled "Radiation Absorbing Refractory Composition and Method of Manufacture", Dr. Kevin Anderson, Thomas G. Haynes III, and Edward Oschmann, issued October 12, 1999.
- [3.2.3] U.S. Patent # 6,042,779 entitled "Extrusion Fabrication Process for Discontinuous Carbide Particulate Metal and Super Hypereutectic Al/Si Alloys", Thomas G. Haynes III and Edward Oschmann, issued March 28, 2000.
- [3.2.4] U.S. Patent Application 09/433773 entitled "High Surface Area Metal Matrix Composite Radiation Absorbing Product", Thomas G. Haynes III and Goldie Oliver, filed May 1, 2002.
- [3.2.5] "Qualification of METAMIC<sup>®</sup> for Spent Fuel Storage Application," EPRI, 1003137, Final Report, October 2001.
- [3.2.6] "METAMIC Neutron Shielding", by K. Anderson, T. Haynes, and R. Kazmier, EPRI Boraflex Conference, November 19-20 (1998).
- [3.2.7] "Safety Evaluation by the Office of Nuclear Reactor Regulation Related to Holtec International Report HI-2022871 Regarding Use of Metamic in Fuel Pool Applications," Facility Operating License Nos. DPR-51 and NPF-6, Entergy Operations, Inc., Docket No. 50-313 and 50-368, USNRC, June 2003.
- [3.2.8] USNRC Docket No. 72-1004, NRC's Safety Evaluation Report on NUHOMS 61BT (2002).
- [3.2.9] "Use of METAMIC<sup>®</sup> in Fuel Pool Applications," Holtec Information Report No. HI-2022871, Revision 1 (2002).
- [3.2.10] "Sourcebook for Metamic<sup>™</sup> Performance Assessment" by Dr. Stanley Turner, Holtec Report No. HI-2043215, Revision 2 (2006).

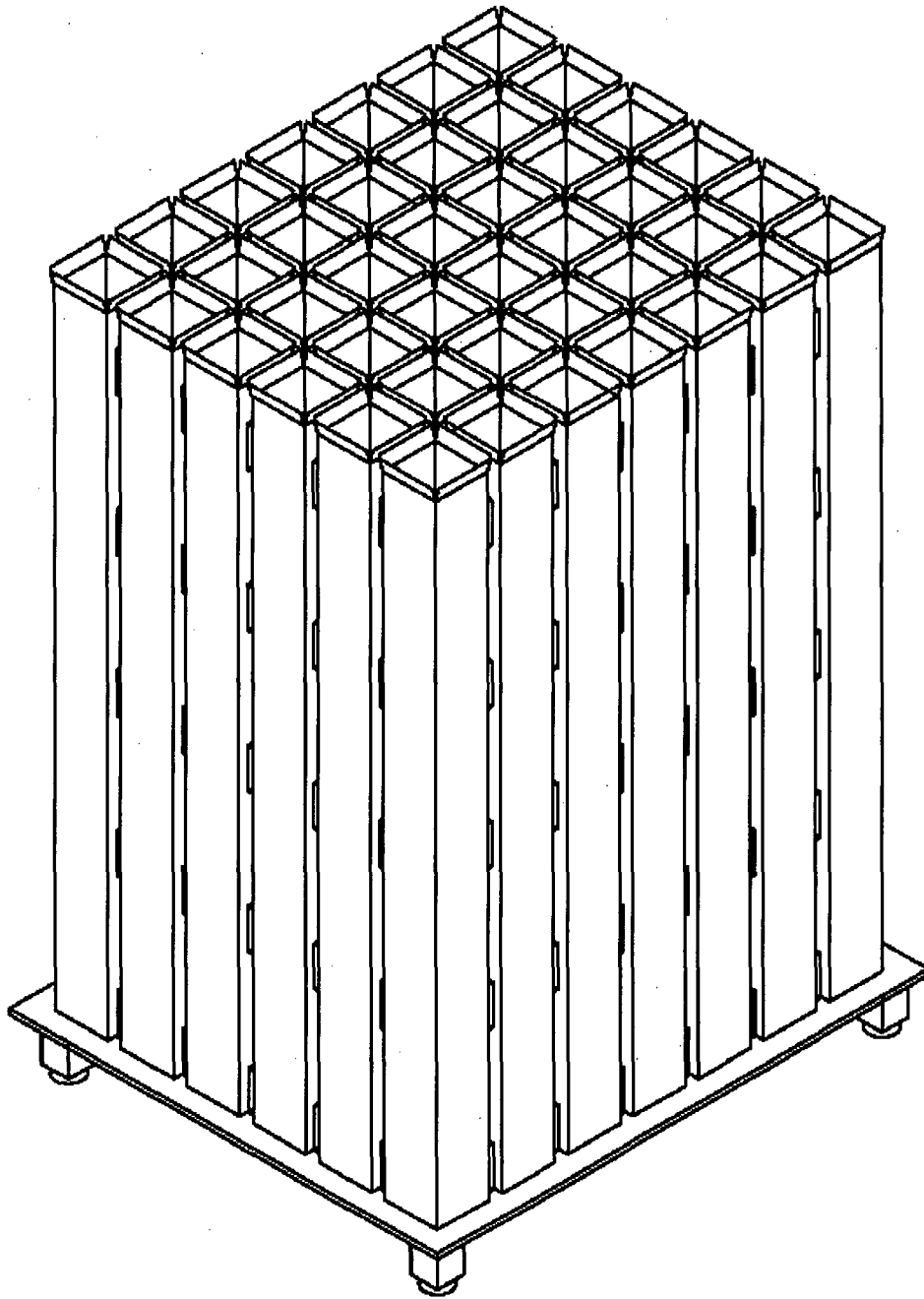


**FIGURE 3.1.1: ISOMETRIC VIEW OF A TYPICAL HOLTEC-DESIGNED REGION 1 RACK**

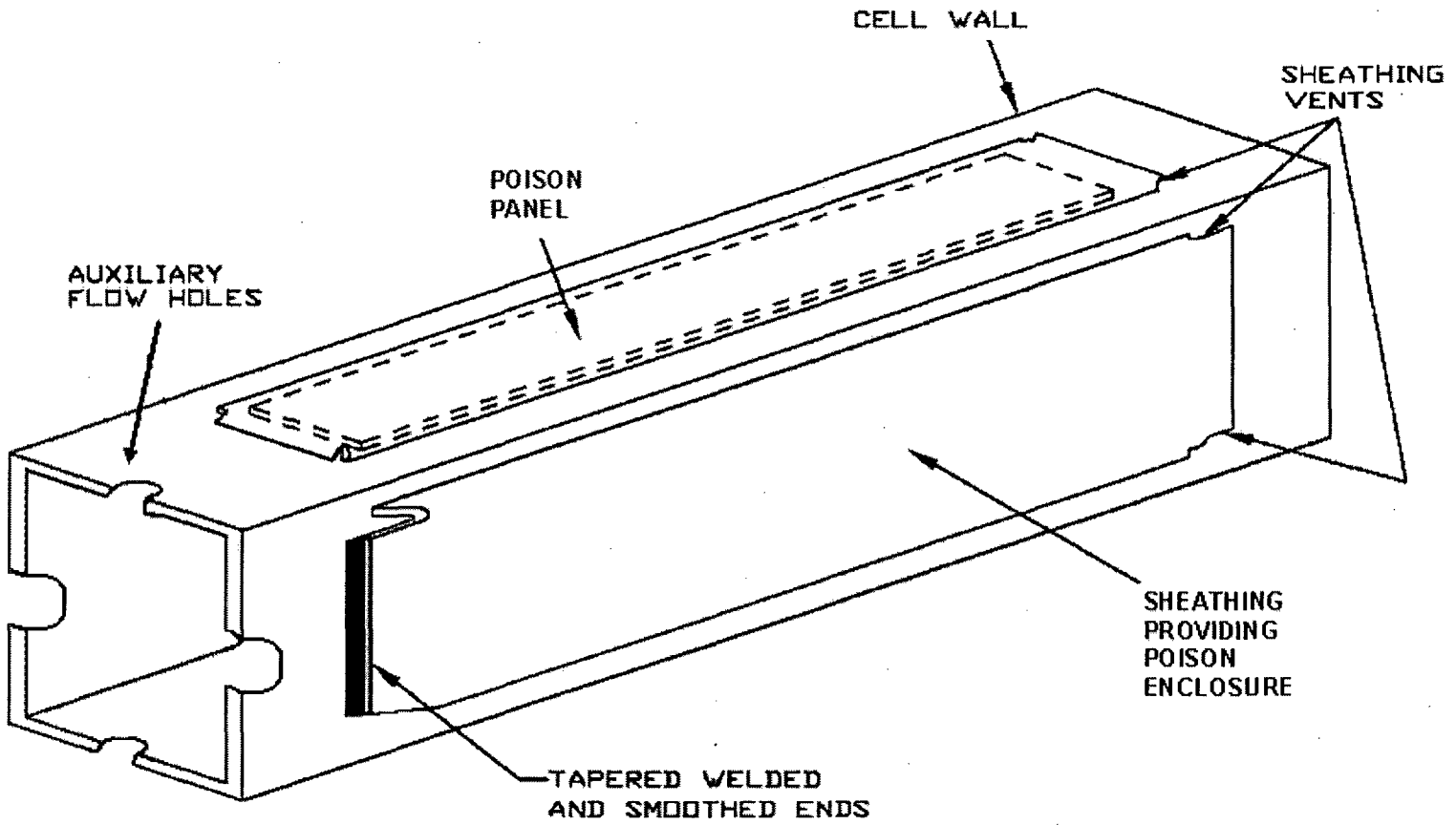


FIGURE 3.1.2: TYPICAL NEUTRON POISON ATTACHMENT

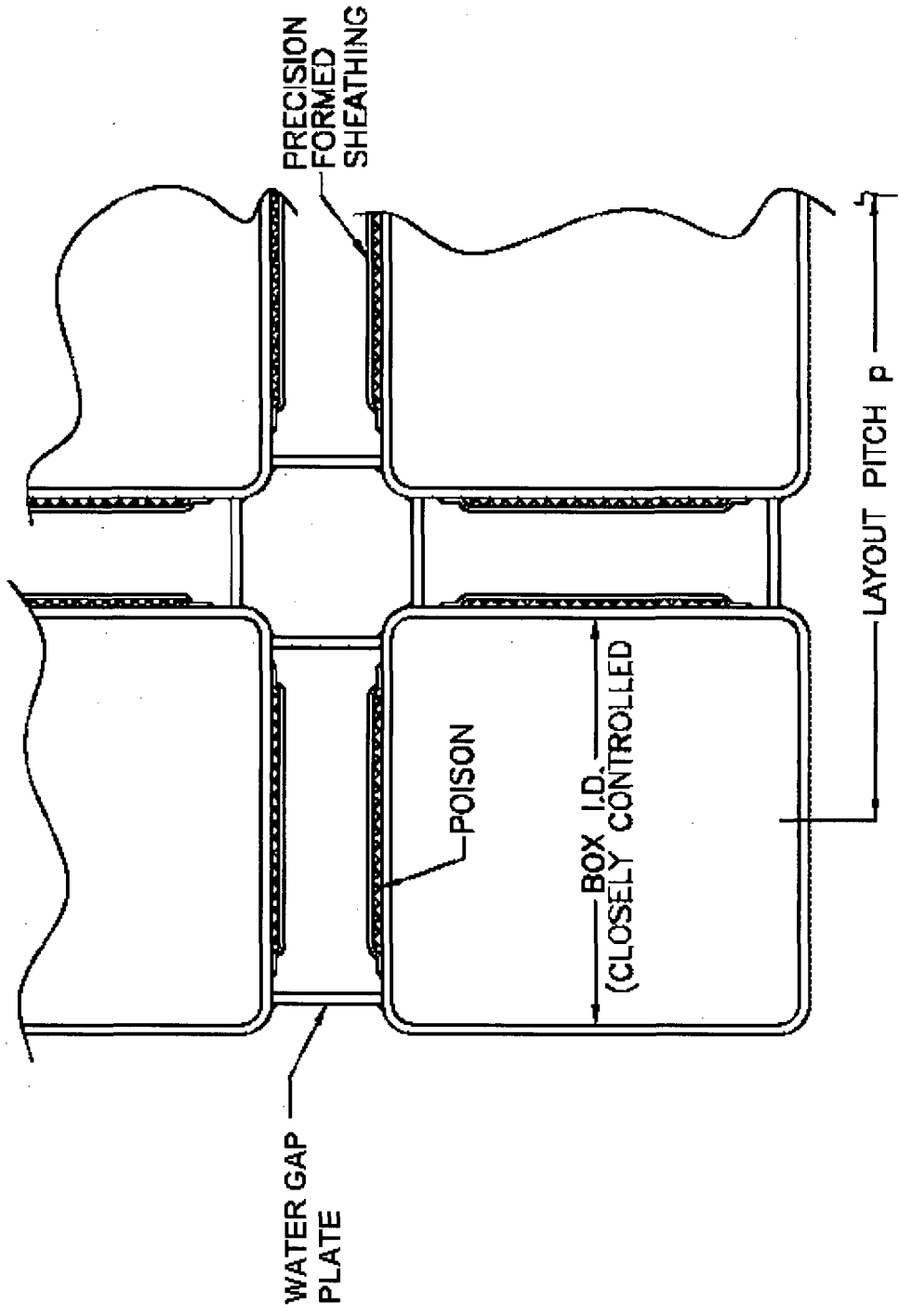
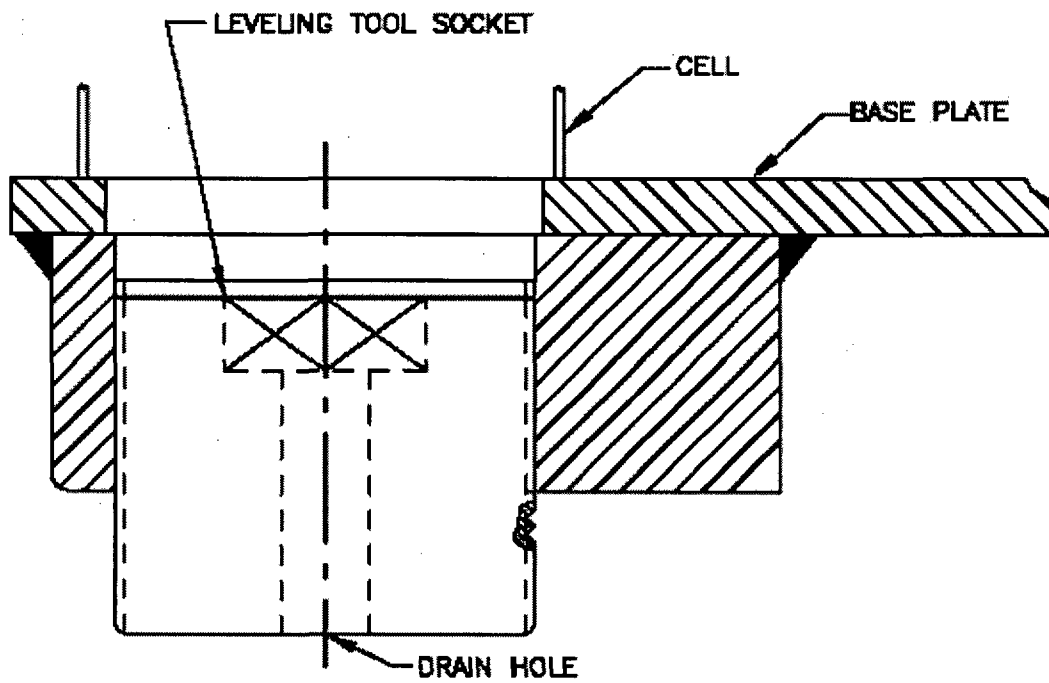
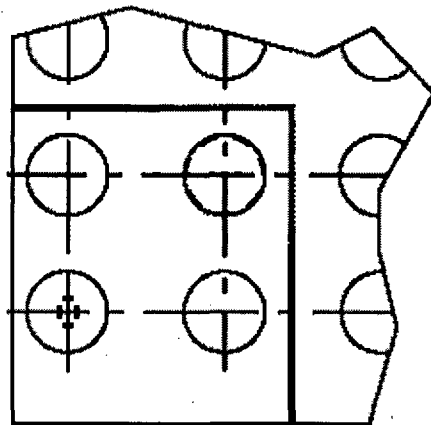


FIGURE 3.1.3: TYPICAL ASSEMBLAGE OF REGION 1 CELLS



TYPICAL ELEVATION VIEW



TYPICAL PLAN VIEWS OF RACK BASEPLATE CORNER

**FIGURE 3.1.4: TYPICAL RACK ADJUSTABLE PEDESTAL**

# Chapter 4: Criticality Safety Analysis

## 4.1 Introduction and Summary

This chapter documents the criticality safety evaluation for the storage of PWR spent nuclear fuel in Region 1 & 2 style high-density spent fuel storage racks at the ANO Unit 2 nuclear power plant operated by Entergy.

The objective of this analysis is to ensure that the effective neutron multiplication factor ( $k_{eff}$ ) is less than or equal to 0.95 with the storage racks fully loaded with fuel of the highest permissible reactivity and the pool flooded with borated water at a temperature corresponding to the highest reactivity. In addition, it is demonstrated that  $k_{eff}$  is less than 1.0 under the assumed loss of soluble boron in the pool water, i.e., assuming unborated water in the spent fuel pool. The maximum calculated reactivities include a margin for uncertainty in reactivity calculations, including manufacturing tolerances, and are calculated with a 95% probability at a 95% confidence level [4.1]. Reactivity effects of abnormal and accident conditions have also been evaluated to assure that under all credible abnormal and accident conditions, the reactivity will not exceed the regulatory limit of 0.95.

The ANO Unit 2 spent fuel pool currently contains two unique types of racks:

1. Region 1 racks: These racks were originally designed with Boraflex as the poison material in a flux-trap configuration.
2. Region 2 racks: These racks are designed to store spent fuel assemblies of a specified combination of initial enrichment and discharge burnup. These racks do not currently contain neutron absorber material.

Due to the Boraflex degradation in the Region 1 racks, future credit for Boraflex in these racks is not feasible. The proposed resolution is to replace these racks with new racks containing fixed neutron absorber. Additionally, it is proposed to re-evaluate the criticality safety of the Region 2 racks with credit for burnup and cooling time of the spent fuel.

Specifically, the following evaluations were performed for the ANO Unit 2 spent fuel pool:

- The Region 1 racks were evaluated for storage of fresh fuel assemblies with a maximum nominal initial enrichment of 4.95 wt%  $^{235}\text{U}$ . Calculation of the maximum  $k_{\text{eff}}$  is given in Table 4.7.1 with no soluble boron and Table 4.7.2 with soluble boron.
- The Region 2 racks were evaluated for storage of spent fuel assemblies with specific burnup requirements as a function of initial enrichment between 2.0 wt% and 4.95 wt%  $^{235}\text{U}$  and cooling times between 0 and 20 years. Minimum burnup values at varying enrichment and cooling time are summarized in Table 4.7.8 and the calculation of the maximum  $k_{\text{eff}}$  for 4.95 wt%  $^{235}\text{U}$  at 0 years cooling time is given in Table 4.7.3 with no soluble boron and Table 4.7.4 with soluble boron.
- The Region 2 racks were evaluated for storage of fresh fuel assemblies with a maximum nominal enrichment of 4.95 wt%  $^{235}\text{U}$  in a checkerboard configuration with empty storage cells. Calculation of the maximum  $k_{\text{eff}}$  is presented in Table 4.7.5 for the case without soluble credit.
- The Region 2 racks were evaluated for storage of lower burned assemblies on the rack periphery, facing the spent fuel pool walls. Minimum burnup versus enrichment values for the peripheral cells are summarized in Table 4.7.9 and the calculation of the maximum  $k_{\text{eff}}$  for 4.95 wt%  $^{235}\text{U}$  at 0 years cooling is given in Table 4.7.6 with no soluble boron and Table 4.7.7 with soluble boron.

Reactivity effects of abnormal and accident conditions have also been evaluated. A summary of the types of accidents analyzed and the soluble boron required to ensure that the maximum  $k_{\text{eff}}$  remains below 0.95 are shown in Table 4.7.10 and Table 4.7.11 for Region 1 and Region 2, respectively. The most limiting accident condition involves misloading a fresh fuel assembly, enriched to 4.95 wt%  $^{235}\text{U}$ , in an empty storage location of the Region 2 storage rack, when a checkerboard configuration is used. A minimum soluble boron concentration of 881 ppm must be maintained in the spent fuel pool to ensure that the maximum  $k_{\text{eff}}$  is less than 0.95 under accident conditions.

In addition to the analysis performed for each individual rack detailed above, the possibility of an increased reactivity effect due to the rack interfaces within and between the racks was analyzed. Table 4.7.12 provides a summary of the various interface calculations performed for the ANO Unit 2 spent fuel pool. Interfaces within the rack include spent and fresh fuel loading patterns within the same rack to determine acceptability. Interface calculations between racks include Region 2-Region 2 and Region 1-Region 2. The calculated reactivity from the interface

calculation is then compared to the calculated reactivity from the reference infinite array calculations. From the summary of the results in Table 4.7.12 the following conclusions may be drawn regarding the reactivity effect of the interfaces:

- In the Region 2 Racks, a fresh fuel checkerboard and uniform spent fuel loading may be placed adjacent to each other in the same rack. If both patterns are placed in a single rack, no fresh fuel assembly may be placed with more than one face adjacent to a spent fuel assembly.
- In the Region 2 racks, if adjacent racks contain a checkerboard of fresh fuel assemblies, the checkerboard must be maintained across the gap, i.e., fresh fuel assemblies may not face each other across a gap.
- In the Region 2 racks, one rack may contain a checkerboard of fresh fuel and empty storage locations and the adjacent rack may contain spent fuel with no loading restrictions.

## 4.2 Methodology

The principal method for the criticality analysis of the high-density storage racks is the three-dimensional Monte Carlo code MCNP4a [4.2]. MCNP4a is a continuous energy three-dimensional Monte Carlo code developed at the Los Alamos National Laboratory. MCNP4a was selected because it has been used previously and verified for criticality analyses and has all of the necessary features for this analysis. MCNP4a calculations used continuous energy cross-section data based on ENDF/B-V and ENDF/B-VI. Exceptions are two lumped fission products used by the CASMO-4 depletion code, that do not have corresponding cross sections in MCNP4a. For these isotopes, the CASMO-4 cross sections are used in MCNP4a. This approach has been validated in [4.3] by showing that the cross sections result in the same reactivity effect in both CASMO-4 and MCNP4a.

Benchmark calculations, presented in Appendix 4A, indicate a bias of 0.0009 with an uncertainty of  $\pm 0.0011$  for MCNP4a, evaluated with a 95% probability at the 95% confidence level [4.1]. The calculations for this analysis utilize the same computer platform and cross-section libraries used for the benchmark calculations discussed in Appendix 4A.

The convergence of a Monte Carlo criticality problem is sensitive to the following parameters: (1) number of histories per cycle, (2) the number of cycles skipped before averaging, (3) the total number of cycles and (4) the initial source distribution. The MCNP4a criticality output contains a great deal of useful information that may be used to determine the acceptability of the problem convergence. This information has been used in parametric studies to develop appropriate values for the aforementioned criticality parameters to be used in storage rack criticality calculations. Based on these studies, a minimum of 10,000 histories were simulated per cycle, a minimum of 100 cycles were skipped before averaging, a minimum of 150 cycles were accumulated, and the initial source was specified as uniform over the fueled regions (assemblies). Further, the output was reviewed to ensure that each calculation achieved acceptable convergence. These parameters represent an acceptable compromise between calculational precision and computational time.

Fuel depletion analyses during core operation were performed with CASMO-4 (using the 70-group cross-section library), a two-dimensional multigroup transport theory code based on capture probabilities [4.4-4.6]. CASMO-4 is used to determine the isotopic composition of the spent fuel. In addition, the CASMO-4 calculations are restarted in the storage rack geometry, yielding the two-dimensional infinite multiplication factor ( $k_{inf}$ ) for the storage rack to determine the reactivity effect of fuel and rack tolerances, temperature variation, depletion uncertainty, and to perform various studies. For all calculations in the spent fuel pool racks, the Xe-135 concentration in the fuel is conservatively set to zero.

The maximum  $k_{eff}$  is determined from the MCNP4a calculated  $k_{eff}$ , the calculational bias, the temperature bias, and the applicable uncertainties and tolerances (bias uncertainty, calculational uncertainty, rack tolerances, fuel tolerances, depletion uncertainty) using the following formula:

$$^2\text{Max } k_{eff} = \text{Calculated } k_{eff} + \text{biases} + [\sum_i (\text{Uncertainty}_i)^2]^{1/2}$$

---

<sup>2</sup>The maximum  $k_{eff}$  value listed in Table 4.7.1 through Table 4.7.7 may differ from the calculated value based on this formula ( $\Delta k = 0.0001$ ) due to rounding.

In the geometric models used for the calculations, each fuel rod and its cladding were described explicitly and reflecting or periodic boundary conditions were used in the radial direction which has the effect of creating an infinite radial array of storage cells.

### 4.3 Acceptance Criteria

The high-density spent fuel PWR storage racks for ANO are analyzed in accordance with the applicable codes and standards listed below. The objective of this analysis is to ensure that the effective neutron multiplication factor ( $k_{\text{eff}}$ ) is less than or equal to 0.95 with the storage racks fully loaded with fuel of the highest permissible reactivity and the pool flooded with borated water at a temperature corresponding to the highest reactivity. In addition, it is demonstrated that  $k_{\text{eff}}$  is less than 1.0 under the assumed loss of soluble boron in the pool water, i.e. assuming unborated water in the spent fuel pool. The maximum calculated reactivities include a margin for uncertainty in reactivity calculations, including manufacturing tolerances, and are calculated with a 95% probability at a 95% confidence level [4.1].

Applicable codes, standard, and regulations or pertinent sections thereof, include the following:

- *Code of Federal Regulations*, Title 10, Part 50, Appendix A, General Design Criterion 62, "Prevention of Criticality in Fuel Storage and Handling."
- USNRC Standard Review Plan, NUREG-0800, Section 9.1.2, Spent Fuel Storage, Rev. 3 - July 1981.
- USNRC letter of April 14, 1978, to all Power Reactor Licensees - OT Position for Review and Acceptance of Spent Fuel Storage and Handling Applications, including modification letter dated January 18, 1979.
- L. Kopp, "Guidance on the Regulatory Requirements for Criticality Analysis of Fuel Storage at Light-Water Reactor Power Plants," NRC Memorandum from L. Kopp to T. Collins, August 19, 1998. [4.7]
- USNRC Regulatory Guide 1.13, Spent Fuel Storage Facility Design Basis, Rev. 2 (proposed), December 1981.
- ANSI ANS-8.17-1984, Criticality Safety Criteria for the Handling, Storage and Transportation of LWR Fuel Outside Reactors.

- Code of Federal Regulation 10CFR50.68, Criticality Accident Requirements (for soluble boron)

## 4.4 Assumptions

To assure the true reactivity will always be less than the calculated reactivity, the following conservative design criteria and assumptions were employed:

- 1) Moderator is borated or unborated water at a temperature in the operating range that results in the highest reactivity, as determined by the analysis.
- 2) Neutron absorption in minor structural members is neglected, i.e., spacer grids are replaced by water.
- 3) The effective multiplication factor of an infinite radial array of fuel assemblies was used in the analyses, except for the assessment of certain abnormal/accident conditions or where neutron leakage is inherent, such as for the analysis of the peripheral rack cells.
- 4) The B<sub>4</sub>C loading in the neutron absorber panels is nominally 30.5 wt%, with an uncertainty of +0.5/-1.0 wt%.
- 5) The presence of burnable absorbers (B<sub>4</sub>C, Gadolinium, Erbium, IFBA) in fresh fuel is neglected. This is conservative as burnable absorbers would reduce the reactivity of the fresh fuel assembly. The presence of burnable absorbers in spent fuel is addressed in Section 4.7.2.3.
- 6) When multiple enrichments are used within an assembly, the average enrichment is used for all fuel pins, i.e. distributed enrichments are neglected.

## 4.5 Input Data

### 4.5.1 Fuel Assembly Specification

The spent fuel storage racks are designed to accommodate 16x16 fuel assemblies (Standard and NGF). The design specifications for these fuel assemblies, which were used for this analysis, are given in Table 4.5.1.

## **4.5.2 Core Operating Parameters**

Core operating parameters are necessary for fuel depletion calculations performed with CASMO-4. The core parameters necessary for the depletion calculations are presented in Table 4.5.2. Temperature and soluble boron values are taken as the upper bound (most conservative) of the core operating parameters of ANO Unit 2. The neutron spectrum is hardened by each of these parameters, leading to a greater production of plutonium during depletion, which results in conservative reactivity values.

## **4.5.3 Axial Burnup Distribution**

Axial burnup profiles were provided by Entergy and are documented in Table 4.5.3 and Table 4.5.4.

## **4.5.4 Burnable Absorbers**

There is the potential for burnable absorbers ( $B_4C$ , Gadolinium, Erbium, IFBA) to be located in the assembly. The design specifications for the IFBA rods are given in Table 4.5.1, Figure 4.5.8 and Figure 4.5.9.

## **4.5.5 ANO Unit 2 Storage Rack Specification**

The storage cell characteristics for the Region 1 and Region 2 storage racks which are used in the criticality evaluations are summarized in Table 4.5.5 and Table 4.5.6.

### *4.5.5.1 Region 1 Style Storage Racks*

The Region 1 storage cells are composed of stainless steel boxes separated by a gap with Metamic neutron absorber panels, (attached by stainless steel sheathing) centered on each side of the storage cell. The steel walls define the storage cells and the stainless steel sheathing supports the Metamic neutron absorber panel and defines the boundary of the flux-trap water-gap used to augment reactivity control. Stainless steel channels connect the storage cells in a rigid structure and define the flux-trap between the sheathing of the neutron absorber panels. Figure 4.5.6

provides a sketch of the Region 1 racks along with the dimensions. Additionally, the Region 1 racks contain Metamic panels and thicker sheathing on the side of the racks that face another rack and the east or west wall of the spent fuel pool, however there is no Metamic or sheathing on the side of the racks that face the south wall of the spent fuel pool.

The calculational models consist of a single storage cell with reflecting boundary conditions through the centerline of the water gap on the outer boundary of the cells, thus simulating an infinite array of Region 1 storage cells. Figure 4.5.1 shows the actual MCNP4a calculational model of the nominal Region 1 spent fuel storage cell, as drawn by the two-dimensional plotter in MCNP4a for the individual cell model.

#### *4.5.5.2 Region 2 Style Storage Racks*

The Region 2 storage cells are composed of stainless steel walls with no neutron absorber panels. The stainless steel walls are formed in such a way as to create a water gap between adjacent cells. Figure 4.5.7 provides a sketch of the Region 2 racks along with the dimensions.

The calculational models consist of either a single storage cell or a group of 49 storage cells (7x7) with reflecting boundary conditions or a group of four storage cells (2x2) with periodic boundary conditions through the centerline of the water gap on the outer boundary of the four cells, thus simulating an infinite array of Region 2 storage cells. Figure 4.5.2 and Figure 4.5.3 shows the actual MCNP4a calculational model of the nominal Region 2 spent fuel storage cell, as drawn by the two-dimensional plotter in MCNP4a for the individual cell model and the 2x2 model, respectively.

The calculational model for the peripheral cell calculations consists of a group of 49 storage cells (7x7) with the spent fuel pool wall on two sides and reflecting boundary conditions through the centerline of the water gap on the opposite two sides. Figure 4.5.4 shows a portion of the actual MCNP4a calculational model of the peripheral cells, as drawn by the two-dimensional plotter in MCNP4a.

#### 4.5.5.3 Gaps Between Adjacent Racks

In addition to the calculations for each style of rack in the ANO Unit 2 spent fuel pool, the reactivity effect of potential interaction between adjacent racks and between different loading patterns is addressed. Figure 4.5.5 shows a diagram of the existing spent fuel pool layout, including location of the different styles of racks, with respect to each other, and the distances of the gaps between adjacent Region 2 racks. The values taken from this figure are the minimum distances from the edge of the storage cell to the edge of the storage cell in the adjacent rack, denoted by a "B" for the bottom of the rack and a "T" for the top of the rack and followed by the dimension in inches. Table 4.5.7 identifies the possible rack-to-rack interactions and the minimum rack-to-rack distance. For the Region 1 to Region 2 interfaces, the distance between racks is 3 inches, however the gap was conservatively modeled as 2 inches. This is conservative as it places the racks closer to each other.

#### 4.5.6 New Fuel Vault and Fuel Handling Equipment

The storage cell characteristics for the new fuel vault and the transfer canal storage racks which are used in the criticality evaluations are summarized in Table 4.5.8.

### 4.6 Computer Codes

The following computer codes were used during this analysis.

- MCNP4a [4.2] is a three-dimensional continuous energy Monte Carlo code developed at Los Alamos National Laboratory. This code offers the capability of performing full three-dimensional calculations for the loaded storage racks. MCNP4a was run on the PCs at Holtec.
- CASMO-4, Version 2.05.14 [4.4-4.6] is a two-dimensional multigroup transport theory code developed by Studsvik of Sweden. CASMO-4 performs cell criticality calculations and burnup. CASMO-4 has the capability of analytically restarting burned fuel assemblies in the rack configuration. This code was used to determine the reactivity effects of tolerances and fuel depletion. The CASMO-4 code was run on a PC at Holtec using the N-library.

## 4.7 Analysis

This section describes the calculations that were used to determine the acceptable storage criteria for the Region 1 and Region 2 style racks. In addition, this section discusses the possible abnormal and accident conditions.

Unless otherwise stated, all calculations assumed nominal characteristics for the fuel and the fuel storage cells. The effect of the manufacturing tolerances is accounted for with a reactivity adjustment as discussed below.

As discussed in Section 4.2, MCNP4a was the primary code used in the calculations. CASMO-4 was used to determine the reactivity effect of tolerances and for depletion calculations. MCNP4a was used for reference cases and to perform calculations which are not possible with CASMO-4 (e.g. eccentric fuel positioning, axial burnup distributions, and fuel misloading).

Figures 4.5.1 through 4.5.4 are pictures of the basic calculational models used in MCNP4a. These pictures were created with the two-dimensional plotter in MCNP4a and clearly indicate the explicit modeling of fuel rods in each fuel assembly. In CASMO-4, a single cell is modeled, and since CASMO-4 is a two-dimensional code, the fuel assembly hardware above and below the active fuel length is not represented. The three-dimensional MCNP4a models assumed approximately 30 cm of water above and below the active fuel length. Additional models with more than four cells were generated with MCNP4a to investigate the effect of accident conditions. These models are discussed in the appropriate section.

### 4.7.1 Region 1

The goal of the criticality calculations for the Region 1 style racks is to qualify the racks for storage of spent fuel assemblies with design specifications as shown in Table 4.5.1 and a maximum nominal initial enrichment of 4.95 wt%  $^{235}\text{U}$ .

#### *4.7.1.1 Identification of Reference Fuel Assembly*

CASMO-4 calculations were performed to determine which of the two assembly types in Table 4.5.1 is bounding in the Region 1 racks. In the calculations, the fuel assembly is modeled in the rack configuration. For both assemblies, the presence of burnable absorbers in the fuel assembly ( $B_4C$ , Gadolinium, Erbium, IFBA) were neglected as these would reduce the reactivity of the fresh fuel assembly. The NGF assembly was determined to have the highest reactivity for fresh fuel of nominal initial enrichment of 4.95 wt%  $^{235}U$ . This assembly type is therefore used in all subsequent calculations.

#### *4.7.1.2 Eccentric Fuel Assembly Positioning*

The fuel assembly is assumed to be normally located in the center of the storage rack cell. Nevertheless, MCNP4a calculations were made with the fuel assemblies assumed to be in the corner of the storage rack cell (four-assembly cluster at closest approach). These calculations indicate that eccentric fuel positioning results in a decrease in reactivity. The highest reactivity, therefore, corresponds to the reference design with the fuel assemblies positioned in the center of the storage cells.

#### *4.7.1.3 Uncertainties Due to Manufacturing Tolerances*

In the calculation of the final  $k_{eff}$ , the effect of manufacturing tolerances on reactivity must be included. CASMO-4 was used to perform these calculations. As allowed in [4.7], the methodology employed to calculate the tolerance effects combine both the worst-case bounding value and sensitivity study approaches. The evaluations include tolerances of the rack dimensions (see Table 4.5.5) and tolerances of the fuel dimensions (see Table 4.5.1). As for the bounding assembly, calculations are performed for a nominal initial enrichment of 4.95 wt%  $^{235}U$ . The reference condition is the condition with nominal dimensions and properties. To determine the  $\Delta k$  associated with a specific manufacturing tolerance, the  $k_{inf}$  calculated for the reference condition is compared to the  $k_{inf}$  from a calculation with the tolerance included. Note that for the individual parameters associated with a tolerance, no statistical approach is utilized.

Instead, the full tolerance value is utilized to determine the maximum reactivity effect. All of the  $\Delta k$  values from the various tolerances are statistically combined (square root of the sum of the squares) to determine the final reactivity allowance for manufacturing tolerances. Only the  $\Delta k$  values in the positive direction (increasing reactivity) were used in the statistical combination. The fuel and rack tolerances included in this analysis are taken from Table 4.5.1 and Table 4.5.5 and are described below:

#### **Fuel Tolerances**

- Increased Fuel Density
- Increased Fuel Enrichment
- Fuel Rod Pitch
- Fuel Rod Cladding Outside Diameter
- Fuel Rod Cladding Inner Diameter
- Fuel Pellet Outside Diameter
- Guide Tube Outside Diameter
- Guide Tube Inside Diameter

#### **Rack Tolerances**

- Variable Cell Inner Dimension & Constant Water Gap
- Variable Water Gap & Constant Pitch
- Box Wall Thickness
- Sheathing Thickness
- Metamic Thickness
- Metamic Width
- Metamic B<sub>4</sub>C Weight Percent

Table 4.7.14 provides the reactivity effect of fuel and racks tolerances for the Region 1 racks.

#### *4.7.1.4 Temperature and Water Density Effects*

Pool water temperature effects on reactivity in the Region 1 racks have been calculated with CASMO-4 for a nominal initial enrichment of 4.95 wt% <sup>235</sup>U. The results in Table 4.7.15 show that the spent fuel pool temperature coefficient of reactivity is negative, i.e. a lower temperature results in a higher reactivity. Consequently, all CASMO-4 calculations are evaluated at 4 °C, which corresponds to the highest density of water.

In MCNP4a, the Doppler treatment and cross-sections are valid only at 300K (27 °C). Therefore, a  $\Delta k$  is determined in CASMO-4 from 27 °C to 4 °C, and is included in the final  $k_{\text{eff}}$  calculation as a bias. The temperature bias for the Region 1 racks from 27 °C (80.33 °F) to 4 °C (39.2 °F) is shown in Table 4.7.1.

#### *4.7.1.5 Calculation of Maximum $k_{\text{eff}}$*

Using the calculational model shown in Figure 4.5.1 and the reference NGF 16x16 fuel assembly, the  $k_{\text{eff}}$  in the Region 1 storage racks has been calculated with MCNP4a. The determination of the maximum  $k_{\text{eff}}$ , which is based on the formula in Section 4.2, is shown in Table 4.7.1 without soluble boron. Uncertainties associated with depletion are not applicable to the Region 1 racks. Results show that the maximum  $k_{\text{eff}}$  of the Region 1 racks is less than 1.0 at a 95% probability at a 95% confidence level with no credit for soluble boron.

#### *4.7.1.6 Soluble Boron Concentration for Maximum $k_{\text{eff}}$ of 0.95*

The calculations crediting soluble boron in the spent fuel pool to ensure that the reactivity does not exceed 0.95 are also performed. Calculations are performed at a nominal initial enrichment of 4.95 wt%  $^{235}\text{U}$  and with a soluble boron level of 400ppm and 800ppm. The minimum soluble boron requirement is determined by linear interpolation between soluble boron levels to achieve a target maximum  $k_{\text{eff}}$  of 0.9450. The maximum  $k_{\text{eff}}$ , including all applicable biases and uncertainties is below the regulatory limit of 0.95. The results for 4.95 wt% initial enrichment, including the required soluble boron are listed in Table 4.7.2.

#### *4.7.1.7 Abnormal and Accident Conditions*

The effects on reactivity of credible abnormal and accident conditions are examined in this section. This section identifies which of the credible abnormal or accident conditions will result in exceeding the limiting reactivity ( $k_{\text{eff}} \leq 0.95$ ). For those accident or abnormal conditions that result in increasing the reactivity, a minimum soluble boron concentration is determined to ensure that  $k_{\text{eff}} \leq 0.95$ . The double contingency principle of ANS-8.1/N16.1-1975 [4.8] (and the

USNRC letter of April 1978) specifies that it shall require at least two unlikely independent and concurrent events to produce a criticality accident. This principle precludes the necessity of considering the simultaneous occurrence of multiple accident conditions.

#### 4.7.1.7.1 Abnormal Temperature

All calculations for Region 1 are performed at a pool temperature of 4°C. As shown in Section 4.7.1.4 above, the temperature coefficient of reactivity is negative, therefore any increase in temperature above 4°C would cause a reduction in the reactivity. Table 4.7.15 shows the reactivity effects of increasing the temperature and including boiling in the spent fuel pool.

#### 4.7.1.7.2 Dropped Assembly - Horizontal

For the case in which a fuel assembly is assumed to be dropped on top of a rack, the fuel assembly will come to rest horizontally on top of the rack with a minimum separation distance from the active fuel region of more than 12 inches, which is sufficient to preclude neutron coupling (i.e., an effectively infinite separation). Consequently, the horizontal fuel assembly drop accident will not result in a significant increase in reactivity. Furthermore, the soluble boron in the spent fuel pool water assures that the true reactivity is always less than the limiting value for this dropped fuel accident.

#### 4.7.1.7.3 Dropped Assembly – Vertical Into Fuel Storage Cell

It is also possible to vertically drop an assembly into a location that might be occupied by another assembly or that might be empty. Such a vertical impact onto another assembly would at most cause a small compression of the stored assembly, reducing the water-to-fuel ratio and thereby reducing reactivity. A vertical drop into an empty storage cell could result in a small deformation of the baseplate. The resultant effect would be the lowering of a single assembly by the amount of the deformation. This could potentially result in the active fuel height of that assembly no longer being completely covered by the Metamic. However, the amount of

deformation for this drop would be small and restricted to a localized area of the rack around the storage cell where the drop occurs. Furthermore, the soluble boron in the spent fuel pool water assures that the true reactivity is always less than the limiting value for this dropped fuel accident.

#### 4.7.1.7.4 Dropped Assembly – Vertical Onto Rack Wall

It is possible to vertically drop an assembly onto the top of the rack such that damage to the neutron absorber may be possible. Based on a mechanical drop analysis, the maximum damage depth to the Region 1 racks is 33 inches. Credit was taken for 2000ppm soluble boron (actual pool soluble boron concentration is higher) and the top 20 inches of the metamatic material covering the active fuel length was replaced with water in all Region 1 fuel cells. The result of this postulated accident condition shows that the maximum  $k_{\text{eff}}$  is 0.8767 including bias and uncertainties.

#### 4.7.1.7.5 Abnormal Location of a Fuel Assembly

##### 4.7.1.7.5.1 Misloaded Fresh Fuel Assembly

There is no misloading accident that would result in an increase in the reactivity of the Region 1 racks because the design basis calculations are performed at a maximum nominal enrichment of 4.95 wt%  $^{235}\text{U}$ . Therefore, no calculations are performed as the design basis calculations are bounding.

##### 4.7.1.7.5.2 Mislocated Fresh Fuel Assembly

The mislocation of a fresh unburned fuel assembly could, in the absence of soluble poison, result in exceeding the regulatory limit ( $k_{\text{eff}}$  of 0.95). This could possibly occur if a fresh fuel assembly of the highest permissible enrichment (4.95 wt%) were to be accidentally mislocated outside of a storage rack adjacent to other fuel assemblies. There is no location in the pool where a fuel assembly could be located between the Region 1 racks and the spent fuel pool wall. Therefore, no calculations are necessary for the potential misloading outside the Region 1 racks.

## 4.7.2 Region 2

The goal of the criticality calculations for the PWR Region 2 style racks is to qualify the racks for storage of fuel assemblies with design specifications as shown in Table 4.5.1 and a maximum nominal initial enrichment of 4.95 wt%  $^{235}\text{U}$  that have accumulated a minimum burnup with credit for cooling times between 0 and 20 years. The purpose of the criticality calculations is to determine the initial enrichment and burnup combinations required for the storage of fuel assemblies with nominal initial enrichments up to 4.95 wt%  $^{235}\text{U}$  and for cooling times up to 20 years. Additionally, credit is taken for neutron leakage from the rack periphery, facing the spent fuel pool walls, to qualify lower burned, higher reactivity assemblies for storage in peripheral locations in the Region 2 racks. Finally, the Region 2 racks are qualified for storage of fresh fuel assemblies, in a checkerboard pattern with empty storage cells, at a maximum nominal enrichment of 4.95 wt%  $^{235}\text{U}$ .

### 4.7.2.1 Identification of Reference Fuel Assembly

CASMO-4 calculations were performed to determine which of the two assembly types in Table 4.5.1 is bounding in the Region 2 racks. In the calculations, the fuel assembly is burned in the core configuration and restarted in the rack configuration. For both assemblies, the presence of burnable absorbers in the fuel assembly ( $\text{B}_4\text{C}$ , Gadolinium, Erbium, IFBA) were neglected for determination of the reference fuel assembly. The NGF assembly was determined to have the highest reactivity for fresh fuel and low burned fuel, while the Standard assembly has the highest reactivity for high burned fuel. All subsequent calculations are performed with the NGF assembly and a bias is applied to account for the higher reactivity Standard fuel assembly, if necessary.

### 4.7.2.2 Core Moderator Temperature Effect for Depletion Calculations

For the depletion calculations, the temperature at the top of the active region is used as the moderator temperature (see Table 4.5.2). However, the reactivity in the rack is dominated by the area slightly below the top of the active region, where the moderator temperature in the core is

lower. Since the reactivity increases significantly with increasing moderator temperature, the assumption used in the depletion calculations is conservative.

#### *4.7.2.3 Reactivity Effect of Burnable Absorbers During Depletion*

The ANO Unit 2 fuel makes use of integral burnable absorbers (IBAs) such as B<sub>4</sub>C rods, Gadolinium or Erbium integrated with the fuel, or IFBA (Zirconium Diboride) coatings. Generic studies [4.10] have investigated the effect that these IBAs have on the reactivity of spent fuel assemblies. These studies have concluded that the reactivity of a spent fuel assembly with IBAs such as Gd<sub>2</sub>O<sub>3</sub>, Er<sub>2</sub>O<sub>3</sub> or B<sub>4</sub>C rods are lower than the same assembly without these IBAs. Therefore, for the purposes of the analysis presented in this report these types of IBAs are neglected. The generic studies [4.10] also found that there is a small positive reactivity effect associated with the presence of IFBA rods.

To determine the reactivity effect of the IFBA rods for the ANO Unit 2 spent fuel racks, depletion calculations were performed with CASMO-4 for the two configurations of IFBA rods shown in Figure 4.5.8 and Figure 4.5.9. These configurations correspond to a large number of IFBA rods with high <sup>10</sup>B loadings for the ZrB<sub>2</sub> coatings that are used in Cycle 18 and Cycle 19 of the ANO Unit 2 reactor, respectively. The reactivity of the fuel assembly with IFBA rods is compared to the reactivity of the fuel assembly without the IFBA rods. The maximum positive reactivity effect associated with either of the two IFBA configurations analyzed over the specified burnup range is applied as a bias to account for the presence of the IFBA rods. Table 4.7.13 presents an example of the reactivity effect due to the presence of IFBA rods for an enrichment of 4.95 wt% <sup>235</sup>U. It should be noted that this approach is extremely conservative, especially for lower enriched fuel, which would not be expected to have either the high number of IFBA rods or high <sup>10</sup>B loadings associated with the configurations analyzed.

#### *4.7.2.4 Reactivity Effect of Axial Burnup Distribution*

Initially, fuel loaded into the reactor will burn with a slightly skewed cosine power distribution. As burnup progresses, the burnup distribution will tend to flatten, becoming more highly burned

in the central regions than in the upper and lower ends. The more reactive fuel near the ends of the fuel assembly (less than average burnup) occurs in regions of lower reactivity worth due to neutron leakage. Consequently, it would be expected that over most of the burnup history, distributed burnup fuel assemblies would exhibit a slightly lower reactivity than that calculated for the average burnup. As burnup progresses, the distribution, to some extent, tends to be self-regulating as controlled by the axial power distribution, precluding the existence of large regions of significantly reduced burnup.

Generic analytic results of the axial burnup effect for assemblies without axial blankets have been provided by Turner [4.9] based upon calculated and measured axial burnup distributions. These analyses confirm the minor and generally negative reactivity effect of the axially distributed burnup compared to a flat distribution, becoming positive at burnups greater than about 30 GWD/MTU. The trends observed in [4.9] suggest the possibility of a small positive reactivity effect above 30 GWD/MTU increasing to slightly over 1%  $\Delta k$  at 40 GWD/MTU. The required burnup for the maximum enrichment is higher than 30 GWD/MTU. Therefore, a positive reactivity effect of the axially distributed burnup is possible. Calculations are performed with the axial burnup distributions from Table 4.5.3 and Table 4.5.4

#### *4.7.2.5 Isotopic Compositions*

To perform the criticality evaluation for spent fuel in MCNP4a, the isotopic composition of the fuel is calculated with the depletion code CASMO-4 and then specified as input data in the MCNP4a run. The CASMO-4 calculations to obtain the isotopic compositions for MCNP4a were performed generically, with one calculation for each enrichment, and burnups in increments of 2.5 GWD/MTU or less. The isotopic composition for any given burnup is then determined by linear interpolation.

#### *4.7.2.6 Uncertainty in Depletion Calculations*

Since critical experiment data with spent fuel is not available for determining the uncertainty in burnup-dependent reactivity calculations, an allowance for uncertainty in reactivity was assigned

based upon other considerations. Assuming the uncertainty in depletion calculations is less than 5% of the total reactivity decrement, a burnup dependent uncertainty in reactivity for burnup calculations may be assigned [4.7]. This allowance is statistically combined with the other reactivity allowances in the determination of the maximum  $k_{\text{eff}}$  for normal conditions where assembly burnup is credited. CASMO-4 was used to perform the depletion calculations.

#### *4.7.2.7 Eccentric Fuel Assembly Positioning*

The fuel assembly is assumed to be normally located in the center of the storage rack cell. In the absence of a fixed neutron absorber, the eccentric location of fuel assemblies in the storage cells may produce a positive reactivity effect. Therefore, MCNP4a calculations for a uniform loading of spent fuel assemblies and a checkerboard of fresh fuel assemblies and empty storage locations were performed with the fuel assemblies assumed to be in the corner of the storage rack cell (four-assembly cluster at closest approach). Three different enrichment and burnup combinations were analyzed for the spent fuel. These calculations indicate that eccentric fuel positioning results in an increase in reactivity.

The eccentric positioning is performed in a very conservative manner, assuming 4 assemblies in the corners of the storage cell, at closest approach to each other, and that these clusters of four assemblies are repeated throughout the rack. However, since eccentric positioning is highly unlikely to occur in this manner and recognizing that placement of fuel assemblies in the storage cells is random, the maximum reactivity effect of eccentric positioning for either spent or fresh fuel is applied as an uncertainty, and combined statistically with other uncertainties, as shown Table 4.7.3 through Table 4.7.7.

#### *4.7.2.8 Uncertainties Due to Manufacturing Tolerances*

In the calculation of the final  $k_{\text{eff}}$ , the effect of manufacturing tolerances on reactivity must be included. CASMO-4 was used to perform these calculations. As allowed in [4.7], the methodology employed to calculate the tolerance effects combine both the worst-case bounding value and sensitivity study approaches. The evaluations include tolerances of the rack

dimensions (see Table 4.5.6) and tolerances of the fuel dimensions (see Table 4.5.1). As for the bounding assembly, calculations are performed for different enrichments and burnups. The reference condition is the condition with nominal dimensions and properties. To determine the  $\Delta k$  associated with a specific manufacturing tolerance, the  $k_{inf}$  calculated for the reference condition is compared to the  $k_{inf}$  from a calculation with the tolerance included. Note that for the individual parameters associated with a tolerance, no statistical approach is utilized. Instead, the full tolerance value is utilized to determine the maximum reactivity effect. All of the  $\Delta k$  values from the various tolerances are statistically combined (square root of the sum of the squares) to determine the final reactivity allowance for manufacturing tolerances. Only the  $\Delta k$  values in the positive direction (increasing reactivity) were used in the statistical combination. The fuel and rack tolerances included in this analysis are taken from Table 4.5.1 and Table 4.5.6 and are described below:

#### **Fuel Tolerances**

- Increased Fuel Density
- Increased Fuel Enrichment
- Fuel Rod Pitch
- Fuel Rod Cladding Outside Diameter
- Fuel Rod Cladding Inner Diameter
- Fuel Pellet Outside Diameter
- Guide Tube Outside Diameter
- Guide Tube Inside Diameter

#### **Rack Tolerances**

- Variable Cell Inner Dimension & Constant Water Gap
- Variable Water Gap & Constant Pitch
- Box Wall Thickness

The reactivity effect of fuel and rack tolerances shown above were calculated for enrichments from 2.0 to 5.0 wt%  $^{235}\text{U}$  and for 0 cooling time. For longer cooling times the fuel and rack tolerances from 0 cooling time are used. Table 4.7.16 provides representative examples of the fuel and rack tolerances for the Region 2 racks.

#### 4.7.2.9 Temperature and Water Density Effects

Pool water temperature effects on reactivity in the Region 2 racks have been calculated with CASMO-4 for enrichments from 2.0 to 4.95 wt%  $^{235}\text{U}$  and cooling times from 0 to 20 years. The results in Table 4.7.17 show that the spent fuel pool temperature coefficient of reactivity is positive, i.e. a higher temperature results in a higher reactivity. Consequently, all CASMO-4 calculations are evaluated at 150 °F. Temperatures higher than 150 °F are treated as accidents and discussed in Section 4.7.2.14

In MCNP4a, the Doppler treatment and cross-sections are valid only at 300K (27 °C). Therefore, a  $\Delta k$  is determined in CASMO-4 from 27 °C (80.33 °F) to 150 °F, and is included in the final  $k_{\text{eff}}$  calculation as a bias. The temperature bias is shown in Table 4.7.3 through Table 4.7.7.

#### 4.7.2.10 Determination of Burnup Versus Enrichment Values for the Central Region

To establish a burnup versus enrichment curve (loading curve), calculations were performed at selected enrichments between 2.0 wt% and 4.95 wt%, and for burnup values slightly above and below the expected loading curve. Points on the proposed loading curve are then calculated by linear interpolation for each enrichment, based on an appropriate target value ( $\text{max } k_{\text{eff}} = 0.9950$ ) for the reactivity. Burnup at varying enrichment values and cooling times of 0, 1, 2, 3, 4, 5, 10, 15 and 20 years are presented in Table 4.7.8.

#### 4.7.2.11 Determination of Burnup Versus Enrichment Values for Peripheral Cells

To provide greater flexibility for loading spent fuel into the Region 2 racks, credit is taken for radial neutron leakage from the rack periphery. This allows fuel assemblies with lower burnups than determined in Section 4.7.2.10 to be stored on the periphery of the racks, facing the spent fuel pool walls.

To establish a burnup versus enrichment curve (loading curve) for the peripheral storage locations, calculations were performed with the center of the rack loaded with fuel at the burnup,

enrichment and cooling time combinations determined in Table 4.7.8 and the peripheral storage locations loaded with fuel at selected enrichments between 2.0 wt% and 4.95 wt%, 0 years of cooling and for burnup values slightly above and below the expected loading curve. Points on the proposed loading curve are then calculated by linear interpolation for each enrichment, based on an appropriate target value ( $\max k_{\text{eff}} = 0.9950$ ) for the reactivity. Burnup versus enrichment values for the peripheral cells are presented in Table 4.7.9.

The peripheral cells are defined as those storage cells closest to the spent fuel pool wall that have fuel assemblies located in them. Therefore, if the storage cell closest to the spent fuel pool wall is kept empty, then the second storage cell from the spent fuel pool wall may be filled with lower burnup fuel meeting the requirements of Table 4.7.9.

#### 4.7.2.12 *Calculation of Maximum $k_{\text{eff}}$*

Using the calculational model shown in Figure 4.5.2 through 4.5.4 and the reference NGF 16x16 fuel assembly, the  $k_{\text{eff}}$  in the Region 2 storage racks has been calculated with MCNP4a. A summary of the calculation of the maximum  $k_{\text{eff}}$ , which is based on the formula in Section 4.2, is shown for spent fuel of maximum nominal enrichment of 4.95 wt%  $^{235}\text{U}$  and for the fresh fuel checkerboard in Table 4.7.3 and Table 4.7.5, respectively, without soluble boron. Calculation of the maximum  $k_{\text{eff}}$  for the peripheral cell locations is presented in Table 4.7.6 without credit for soluble boron. Uncertainties associated with depletion are not applicable to the Region 2 checkerboard of fresh fuel assemblies and empty storage cells. Results show that the maximum  $k_{\text{eff}}$  of the Region 2 racks is less than 1.0 at a 95% probability and at a 95% confidence level for spent fuel and less than 0.95 at a 95% probability and at a 95% confidence level for a fresh fuel checkerboard with no credit for soluble boron.

#### 4.7.2.13 *Soluble Boron Concentration for Maximum $k_{\text{eff}}$ of 0.95*

The calculations crediting soluble boron in the spent fuel pool to ensure that the reactivity does not exceed 0.95 are also performed. Calculations for a uniform loading of spent fuel are performed for enrichment and cooling time combinations of 2.0 wt%  $^{235}\text{U}$  at 0 years cooling,

4.95 wt%  $^{235}\text{U}$  at 0 years cooling and 4.95 wt%  $^{235}\text{U}$  at 20 years cooling at a soluble boron level of 400ppm. Calculations with peripheral storage cells are performed for various burnup and enrichment combinations in the central region and the peripheral locations. The minimum soluble boron requirement is determined by linear interpolation between soluble boron levels to achieve a target maximum  $k_{\text{eff}}$  of 0.9450. In all cases, the maximum  $k_{\text{eff}}$  including all applicable biases and uncertainties is below the regulatory limit of 0.95. The results for 4.95 wt% initial enrichment, including the required soluble boron, is also listed in Table 4.7.4 for uniform loading of spent fuel and Table 4.7.7 for low burnup assemblies in the peripheral cells.

#### 4.7.2.14 *Abnormal and Accident Conditions*

The effects on reactivity of credible abnormal and accident conditions are examined in this section. This section identifies which of the credible abnormal or accident conditions will result in exceeding the limiting reactivity ( $k_{\text{eff}} \leq 0.95$ ). For those accident or abnormal conditions that result in exceeding the limiting reactivity, a minimum soluble boron concentration is determined to ensure that  $k_{\text{eff}} \leq 0.95$ . The double contingency principle of ANS-8.1/N16.1-1975 [4.8] (and the USNRC letter of April 1978) specifies that it shall require at least two unlikely independent and concurrent events to produce a criticality accident. This principle precludes the necessity of considering the simultaneous occurrence of multiple accident conditions.

##### 4.7.2.14.1 Abnormal Temperature

All calculations for Region 2 are performed at the maximum temperature of 150°F. As shown in Section 4.7.2.9 above, the temperature coefficient of reactivity is positive, and temperatures above the maximum would cause an increase in the reactivity, and therefore are treated as accidents. Additional calculations at higher temperatures and with soluble boron concentrations of 400ppm were performed to determine the minimum soluble boron concentration necessary to ensure that the maximum  $k_{\text{eff}}$  is below 0.95. The calculations to determine the soluble boron content necessary to offset the reactivity effect of the increase in temperature are shown in Table 4.7.17.

#### 4.7.2.14.2 Dropped Assembly - Horizontal

For the case in which a fuel assembly is assumed to be dropped on top of a rack, the fuel assembly will come to rest horizontally on top of the rack with a minimum separation distance from the active fuel region of more than 12 inches, which is sufficient to preclude neutron coupling (i.e., an effectively infinite separation). Consequently, the horizontal fuel assembly drop accident will not result in a significant increase in reactivity. Furthermore, the soluble boron in the spent fuel pool water assures that the true reactivity is always less than the limiting value for this dropped fuel accident.

#### 4.7.2.14.3 Dropped Assembly - Vertical

It is also possible to vertically drop an assembly into a location that might be occupied by another assembly or that might be empty. Such a vertical impact would at most cause a small compression of the stored assembly, if present, or result in a small deformation of the baseplate for an empty cell. These deformations could potentially increase reactivity. Although these deformations would not have a significant reactivity effect, any reactivity increase would be small compared to the reactivity increase created by the misloading of a fresh assembly discussed in the following section. The vertical drop is therefore bounded by this misloading accident and no separate calculation is performed for the drop accident.

#### 4.7.2.14.4 Abnormal Location of a Fuel Assembly

##### 4.7.2.14.4.1 Misloaded Fresh Fuel Assembly

The misloading of a fresh unburned fuel assembly could, in the absence of soluble poison, result in exceeding the regulatory limit ( $k_{\text{eff}}$  of 0.95). This could possibly occur if a fresh fuel assembly of the highest permissible enrichment (4.95 wt%) were to be inadvertently misloaded into a storage cell intended to be empty in the checkerboard pattern or used for spent fuel in the uniform loading pattern. For the misloading accident in the Region 2 rack filled with spent fuel, enrichment and burnup combinations of 2.0 wt%  $^{235}\text{U}$  at 0 years cooling time, 4.95 wt%  $^{235}\text{U}$  at 0 years cooling time and 4.95 wt%  $^{235}\text{U}$  at 20 years cooling time were analyzed at the appropriate burnup. Additionally,

the reactivity consequence of this accident was determined for the Region 2 racks with lower burned fuel stored in the peripheral cells. Various combinations of burnup and enrichment requirements for both the central region and the peripheral cells were investigated.

The corresponding calculational model consists of a 7x7 array of Region 2 storage cells with a single, fresh unburned assembly in the center cell. The calculational model with low burned fuel stored in the peripheral cells consists of a 7x7 array of Region 2 storage cells with low burned assemblies on the rack periphery and a single, fresh unburned assembly in the corner cell of the central region, directly adjacent to three low burned assemblies. The model is surrounded by either periodic or reflective boundary conditions, as appropriate. Calculations are performed with 400ppm, 800ppm and 1200ppm (if necessary) soluble boron, and the final soluble boron concentration is determined by linear interpolation. The most limiting results are given in Table 4.7.11.

#### 4.7.2.14.4.2 Mislocated Fresh Fuel Assembly

The mislocation of a fresh unburned fuel assembly could, in the absence of soluble poison, result in exceeding the regulatory limit ( $k_{\text{eff}}$  of 0.95). This could possibly occur if a fresh fuel assembly of the highest permissible enrichment (4.95 wt%) were to be accidentally mislocated outside of a storage rack adjacent to other fuel assemblies. For the checkerboard pattern, it is assumed that the mislocated assembly is placed adjacent to a storage cell containing another fresh fuel assembly. For the mislocated assembly accident outside the Region 2 rack filled with spent fuel, enrichment and burnup combinations of 4.95 wt%  $^{235}\text{U}$  at 0 years cooling time and 4.95 wt%  $^{235}\text{U}$  at 20 years cooling time were analyzed at the appropriate burnup. Additionally, the reactivity consequence of this accident was determined for the Region 2 racks with lower burned fuel stored in the peripheral cells. Various combinations of burnup and enrichment requirements for both the central region and the peripheral cells were investigated.

The MCNP4a model consists of a 7x7 array of Region 2 fuel storage cells with a single fresh, unburned assembly placed adjacent to the rack and a 30 cm water reflector. The calculational model with low burned fuel assemblies stored in the peripheral cells consists of a 7x7 array of Region 2

storage cells with low burned assemblies on the rack periphery and a single, fresh unburned assembly placed adjacent to the rack and a 30 cm water reflector. The other 3 sides of the model consist of reflecting boundary conditions. The mislocated fuel assembly is placed as close to the rack face as possible to maximize the possible reactivity effect. Calculations are performed with 400 ppm and 800 ppm soluble boron, and the final soluble boron concentration is determined by linear interpolation. The most limiting results are given in Table 4.7.11.

### **4.7.3 Interfaces Within and Between Racks**

#### *4.7.3.1 Normal Conditions*

In addition to the calculations performed for each individual rack detailed in the preceding sections, the possibility of an increased reactivity effect due to the rack interfaces within and between the racks was determined. Figure 4.5.5 is a layout of the existing ANO Unit 2 spent fuel pool, with the gaps between Region 2 racks detailed for each interface. The gaps provided in Figure 4.5.5, denoted by a "B" or "T" at the rack corners, are measured from the outside surfaces of the adjacent storage cells. Table 4.5.7 summarizes the existing rack interfaces and the gaps between these racks. The values provided in Table 4.5.7 for the Region 1 to Region 1 rack interface and the Region 1 to Region 2 interface are based on the size and location of the new Region 1 racks to be placed in the ANO Unit 2 spent fuel pool.

Table 4.7.12 provides a summary of the various interface calculations performed for the ANO Unit 2 spent fuel pool. Interfaces within the rack include spent and fresh fuel loading patterns within the same rack to determine acceptability. Interface calculations between racks include Region 2-Region 2, Region 1-Region 2. Figures 4.7.1a through 4.7.5 are referenced in Table 4.7.12 and provide a visual representation of the interface calculation performed. The figures show the loading pattern assumed in each rack and the value for the water gap between the racks. The calculated reactivity from the interface calculation is then compared to the calculated reactivity from the reference infinite array calculations.

#### 4.7.3.2 Rack Lateral Motion – Seismic Event

A seismic event, could, in the absence of soluble boron, result in exceeding the regulatory limit (maximum  $k_{\text{eff}}$  of 0.95). This could possibly occur if the seismic event caused sufficient movement of the rack to a closer proximity. The seismic analysis identifies a maximum differential displacement between racks during a seismic event of almost 4 inches. Selected cases from the interface calculations described in the previous section were chosen to address this potential accident condition. The MCNP4a models described above were modified to reduce the gap between racks. In some cases the racks are modeled closer together than physically possible due to the baseplate extensions. Calculations were performed with 800ppm of soluble boron. The calculated reactivities from MCNP4a show that all calculated reactivities for this accident condition are below 0.90. Even with the addition of the applicable bias' and uncertainties, the maximum  $k_{\text{eff}}$  would be below 0.95.

#### 4.7.4 Boron Dilution Evaluation

The soluble boron in the spent fuel pool water is conservatively assumed to contain a minimum of 2000 ppm under operating conditions. Significant loss or dilution of the soluble boron concentration is extremely unlikely, if not incredible. Nonetheless, an evaluation was performed based on the ANO spent fuel pool data.

The required minimum soluble boron concentration is 452 ppm under normal conditions and 881 ppm for the most serious credible accident scenario. The volume of water in the pool is approximately 198,000 gallons. Large amounts of unborated water would be necessary to reduce the boron concentration from 2000 ppm to 881 ppm or to 452 ppm. Abnormal or accident conditions are discussed below for either low dilution rates (abnormal conditions) or high dilution rates (accident conditions). The general equation for boron dilution is,

$$C_t = C_o e^{-\left(\frac{F}{V}\right)t},$$

where

$C_t$  the boron concentration at time  $t$ ,  
 $C_o$  the initial boron concentration,

V is the volume of water in the pool, and

F is the flow rate of unborated water into the pool

This equation conservatively assumes the unborated water flowing into the pool mixes instantaneously with the water in the pool.

For convenience, the above equation may be re-arranged to permit calculating the time required to dilute the soluble boron from its initial concentration to a specified minimum concentration, which is given below.

$$t = \frac{V}{F} \ln(C_o / C_i)$$

If V is expressed in gallons and F in gallons per minute (gpm), the time, t, will be in minutes.

#### *4.7.4.1 Low Flow Rate Dilution.*

Small dilution flow around pump seals and valve stems or mis-aligned valves could possibly occur in the normal soluble boron control system or related systems. Such failures might not be immediately detected. These flow rates would be of the order of 2 gpm maximum and the increased frequency of makeup flow might not be observed. However, an assumed loss flow-rate of 2 gpm dilution flow rate would require approximately 100 days to reduce the boron concentration to the minimum required 452 ppm under normal conditions or 56 days to reach the 881 ppm required for the most severe fuel handling accident. Routine surveillance measurements of the soluble boron concentration would readily detect the reduction in soluble boron concentration with ample time for corrective action.

Administrative controls require a measurement of the soluble boron concentration in the pool water at least weekly. Thus, the longest time period that a potential boron dilution might exist without a direct measurement of the boron concentration is 7 days. In this time period, an undetected dilution flow rate of 29.2 gpm would be required to reduce the boron concentration to 452 ppm. No known dilution flow rate of this magnitude has been identified. Further, a total of about 300,000 gallons of unborated water would be associated with the dilution event and such a

large flow of unborated water would be readily evident by high-level alarms and by visual inspection on daily walk-downs of the storage pool area.

#### *4.7.4.2 High Flow Rate Dilution*

Under certain accident conditions, it is conceivable that a high flow rate of unborated water could flow onto the top of the pool. Such an accident scenario could result from rupture of a unborated water supply line or possibly the rupture of a fire protection system header, both events potentially allowing unborated water to spray onto the pool. A flow rate of up to 2500 gpm could possibly spray onto the spent fuel pool as a result of a rupture of the fire protection line. This would be the most serious condition and bounds all other accident scenarios. Conservatively assuming that all the unborated water from the break poured onto the top of the pool and further assuming instantaneous mixing of the unborated water with the pool water, it would take approximately 119 minutes to dilute the soluble boron concentration to 452 ppm, which is the minimum required concentration to maintain  $k_{eff}$  below 0.95 under normally operating conditions. In this dilution accident, some 300,000 gallons of water would spill on the auxiliary building floor and into the air-conditioning duct system. Well before the spilling of such a large volume of water, multiple alarms would have alerted the control room of the accident consequences (including the fuel pool high-level alarm, the fire protection system pump operation alarm, and the floor drain receiving tank high level alarm). For this high flow rate condition, 64 minutes would be required to reach the 881 ppm required for the most severe fuel handling accident.

Instantaneous mixing of pool water with the water from the rupture of the unborated water supply line is an extremely conservative assumption. Water falling on to the pool surface would mix with the top layer of pool water and the portions of the mixed volumes would continuously spill out of the pool. The density difference between water at 150 °F (maximum permissible pool bulk water temperature) and at the temperature of the unborated water supply is small. This density difference will not cause the water falling on to the pool surface to instantaneously sink down into the racks overcoming the principal driving force for the flow in the pool, which is the

buoyancy force generated in the spent fuel pool racks region due to the heat generation from the spent fuel in the racks. This would further enhance the mixing process between the pool water and spilled water above the racks.

For the fire protection system line break, upon the initial break, the fire protection system header pressure would drop to the auto start set point of the fire protection pumps. The start is accompanied with an alarm in the main control room. The annunciator response is to dispatch an operator to find the source of the pump start. Approximately 1 minute into the event, a Spent Fuel Pool high level alarm would be received in the main control room, assuming that the Spent Fuel Pool level started at the low alarm. The annunciator response for high Spent Fuel Pool level is to investigate the cause. The coincidence of the 2 alarms would quickly lead to the discovery of the failure of the fire protection system and sufficient time to isolate the failure.

The maximum flow rate from the demineralized water supply would provide approximately 200 gpm into the Spent Fuel Pool. Failure of the demineralized water header is not accompanied with an alarm; however, the time to dilute the Spent Fuel Pool from 2000 to 452 ppm is greater than the bounding case described above. An alarm on high Spent Fuel Pool level would be received in the main control room approximately 9 minutes into the event, assuming that the Spent Fuel Pool level started at the low alarm. In this scenario, there is sufficient time to isolate the failure and to prevent the spilling of some 300,000 gallons of water.

The analysis assumes that for a double-ended break in the fire protection system piping, the stream of water will arch through the air some 46 feet falling on top of the pool. This is virtually an incredible event. Should the stream of water fall upon the pool deck, a 3 inch high curb would channel some of the water to the pool drain and prevent all of the water from reaching the pool. Furthermore, the evaluation also assumes at least 3 independent and concurrent accidents occur simultaneously:

- ◆ Large amounts of water flowing from the double-ended pipe break would remain undetected and are ignored.
- ◆ Pool water high level alarms either fail or are ignored.

- ◆ Alarms indicating large amounts of water flowing into the floor drain have failed or are ignored.

Considering all related facts, a significant dilution of the pool soluble boron concentration in a short period of time without corrective action is not considered a credible event.

It is not considered credible that multiple alarms would fail or be ignored or that the spilling of large volumes of water would not be observed. Therefore, such a major failure would be detected in sufficient time for corrective action to avoid violation of an administrative guideline and to assure that the health and safety of the public is protected.

#### **4.8 New Fuel Storage Racks Criticality Analysis**

The New Fuel Storage Vault is intended for the receipt and storage of fresh fuel under normally dry conditions where the reactivity is very low. To assure the criticality safety under accident conditions and to conform to the requirements of General Design Criterion 62, "Prevention of Criticality in Fuel Storage and Handling," two separate criteria must be satisfied as defined in NUREG-0800, Standard Review Plan 9.1.1, "New Fuel Storage." These criteria are as follows:

- When fully loaded with fuel of the highest anticipated reactivity and flooded with clean, unborated water, the maximum reactivity, including uncertainties, shall not exceed a  $k_{\text{eff}}$  of 0.95.
- With fuel of the highest anticipated reactivity in place and assuming optimum hypothetical low density moderation (i.e., fog or foam), the maximum reactivity shall not exceed a  $k_{\text{eff}}$  of 0.98.

The New Fuel Storage Vault provides a 7 x 9 storage cell array arranged on a 26 inch lattice spacing as shown in Figure 4.8.1. The analytical model uses a conservatively small distance between the fuel assemblies and the surrounding walls on all four sides. Calculations were made with the MCNP4a [4.2] code package, a three-dimensional Monte Carlo analytical technique, with fresh fuel assemblies with 4.95 wt% nominal initial enrichment. These calculations were made for various moderator densities and the results are shown in Figure 4.8.2; the peak reactivity (optimum moderation) occurs at 6% moderator density. Results of the criticality safety analysis are summarized in Table 4.8.1 for the two accident conditions for fuel assemblies of  $4.95 \pm 0.05$  wt% initial enrichment. The maximum reactivity at 6% moderator density,

including uncertainties, is within the regulatory limit of 0.98, thus confirming the acceptability of the New Fuel Vault for  $4.95 \pm 0.05$  wt% fuel.

For the fully flooded accident condition, calculations are performed with the same calculational model as described above. Under these conditions and with fuel of 5.0 wt% enrichment, the maximum reactivity, including all uncertainties is less than the regulatory limit of 0.95 for  $k_{\text{eff}}$ , thus confirming the acceptability of the NFV for 5.0 wt% fuel in the fully flooded accident condition. Results of the criticality safety analysis for the fully flooded condition are summarized in Table 4.8.1.

## **4.9 Fuel Handling Equipment**

### *4.9.1 New Fuel Elevator and Fuel Carriage*

Criticality safety evaluations were also performed for handling of fresh fuel assemblies during transfer from the new fuel vault to the reactor core, including the new-fuel elevator and fuel carriage. The conservative calculational model for these configurations is a single assembly in a large water body. The maximum  $k_{\text{eff}}$  of this configuration is shown in Table 4.9.1. The maximum  $k_{\text{eff}}$  value is below the regulatory limit for this case.

An additional calculation is performed to evaluate the potential effect of an accidental dropped or misplaced fresh assembly next to an assembly in the fuel handling equipment. The two assemblies are assumed to be directly next to each other. This is very conservative, since the fuel handling equipment would prevent two assemblies to be in direct close contact. Since this is an accident condition, the presence of soluble boron in the water is credited. The maximum  $k_{\text{eff}}$  of this configuration is shown in Table 4.9.1, assuming 800 ppm soluble boron in the water. The maximum  $k_{\text{eff}}$  value is below the regulatory limit for this case.

### *4.9.2 Fuel Upender*

The fuel upender had the ability to handle two assemblies at a time with a minimum center-to-center assembly pitch of 12.04 inches. The fuel assemblies are surrounded by a large body of

water and the steel structure of the upender is neglected. The calculational model is shown in Figure 4.9.1, created with the 2-dimensional MCNP plotter. The maximum  $k_{\text{eff}}$  of this configuration is shown in Table 4.9.2. Without, soluble boron, the maximum  $k_{\text{eff}}$  is below 1.0. Credit is taken for soluble boron (400 ppm) to shown that the maximum  $k_{\text{eff}}$  is below 0.95.

As additional calculation is performed to evaluate the potential effect of an accidentally dropped or misplaced fresh assembly next to the fuel upender. The third assembly is assumed to be placed as close as possible to the two assemblies in the fuel upender, with the center of the third assembly placed at the midplane between the two assemblies in the fuel upender. This is very conservative, since the fuel upender would prevent the third assembly from being in direct close contact. Since this is an accident condition, the presence of soluble boron in the water is credited. The maximum  $k_{\text{eff}}$  of this configuration is shown in Table 4.9.2, assuming 1000ppm soluble boron in the water. The maximum  $k_{\text{eff}}$  value is below 0.95.

#### *4.9.3 Temporary Storage Rack in the Refuel Canal*

The refuel canal incorporates a 4-cell temporary storage rack on a linear array at a 17.8125 inch spacing. To bound the normal and any accident condition in the calculational model, a fifth assembly is modeled adjacent to the rack on the long side. It is assumed that this assembly is on the same pitch. This is conservative, since the structure that supports the rack would prevent an assembly to be that close to the rack. The calculational model is shown in Figure 4.9.2, created with the 2-dimensional MCNP plotter. The results for this condition are shown in Table 4.9.3. The maximum  $k_{\text{eff}}$  is below the regulatory limit.

## 4.10 References

- [4.1] M.G. Natrella, Experimental Statistics, National Bureau of Standards, Handbook 91, August 1963.
- [4.2] J.F. Briesmeister, Editor, "MCNP - A General Monte Carlo N-Particle Transport Code, Version 4A," LA-12625, Los Alamos National Laboratory (1993).
- [4.3] "Lumped Fission Product and Pm148m Cross Sections for MCNP," Holtec Report HI-2033031, Rev 0, September 2003.
- [4.4] M. Edenius, K. Ekberg, B.H. Forssén, and D. Knott, "CASMO-4 A Fuel Assembly Burnup Program User's Manual," Studsvik/SOA-95/1, Studsvik of America, Inc. and Studsvik Core Analysis AB (proprietary).
- [4.5] D. Knott, "CASMO-4 Benchmark Against Critical Experiments", SOA-94/13, Studsvik of America, Inc., (proprietary).
- [4.6] D. Knott, "CASMO-4 Benchmark Against MCNP," SOA-94/12, Studsvik of America, Inc., (proprietary).
- [4.7] L.I. Kopp, "Guidance on the Regulatory Requirements for Criticality Analysis of Fuel Storage at Light-Water Reactor Power Plants," NRC Memorandum from L. Kopp to T. Collins, August 19, 1998.
- [4.8] ANS-8.1/N16.1-1975, "American National Standard for Nuclear Criticality Safety in Operations with Fissionable Materials Outside Reactors," April 14, 1975
- [4.9] S.E. Turner, "Uncertainty Analysis - Burnup Distributions", presented at the DOE/SANDIA Technical Meeting on Fuel Burnup Credit, Special Session, ANS/ENS Conference, Washington, D.C., November 2, 1988.
- [4.10] "Study of the Effect of Integral Burnable Absorbers for PWR Burnup Credit," NUREG/CR-6760, ORNL/TM-2000-321, March 2002.

Table 4.5.1: PWR Fuel Assembly Specifications<sup>3</sup>

<b>Fuel Rod Data</b>		
<b>Assembly type</b>	<b>16x16 Standard</b>	<b>16x16 NGF</b>
[ ] <sup>4</sup> , <sup>a, c</sup>	[ ] <sup>a, c</sup>	[ ] <sup>a, c</sup>
Fuel pellet outside diameter, in.	0.3250 [ ] <sup>a, c</sup>	0.3225 [ ] <sup>a, c</sup>
Cladding inside diameter, in.	0.3320 [ ] <sup>a, c</sup>	0.329 [ ] <sup>a, c</sup>
Cladding outside diameter, in.	0.3820 [ ] <sup>a, c</sup>	0.374 [ ] <sup>a, c</sup>
Cladding material	Zircaloy-4	Optimized Zirlo
Stack density, g/cc	10.412 [ ] <sup>a, c</sup>	10.522 [ ] <sup>a, c</sup>
Maximum enrichment, wt% <sup>235</sup> U	4.95 [ ] <sup>a, c</sup>	4.95 [ ] <sup>a, c</sup>
<b>Fuel Assembly Data</b>		
Fuel rod array	16x16	16x16
Number of fuel rods	236	236
Fuel rod pitch <sup>5</sup> , in.	0.5060 [ ] <sup>a, c</sup>	0.5060 [ ] <sup>a, c</sup>
ZrB <sub>2</sub> Coating Loading (mg <sup>10</sup> B/inch)	3.14 (Cycle 18) 2.95 (Cycle 19)	3.14
[ ] <sup>a, c</sup>	[ ] <sup>a, c</sup> (Cycle 18) [ ] <sup>a, c</sup> (Cycle 19)	[ ] <sup>a, c</sup>
ZrB <sub>2</sub> Coating Length <sup>6</sup> , in.	134 (Cycle 18) 136 (Cycle 19)	138
Number of tubes (4 guide/ 1 instrument)	5	5
Guide Tube inside diameter, in.	0.900 [ ] <sup>a, c</sup>	0.900 [ ] <sup>a, c</sup>
Guide Tube outside diameter, in.	0.980 [ ] <sup>a, c</sup>	0.980 [ ] <sup>a, c</sup>
Nom. Active fuel Length <sup>7</sup> , in.	[ ] <sup>a, c</sup>	150.0

<sup>3</sup> [ ]<sup>a, c</sup>

<sup>4</sup> [ ]<sup>a, c</sup>

<sup>5</sup> [ ]<sup>a, c</sup>

<sup>6</sup> The ZrB<sub>2</sub> Coating Length is conservatively modeled to cover the entire active fuel length.

<sup>7</sup> The active fuel length is conservatively modeled as 150 inches.

Table 4.5.2: Core Operating Parameter for Depletion Analyses

Parameter	
Soluble Boron Concentration (cycle average), ppm	1000
Reactor Specific Power, MW/MTU	42.9
Core Average Fuel Temperature, °F	1073
Core Average Moderator Temperature at the Top of the Active Region, °F	620.4
In-Core Assembly Pitch, Inches	8.18

Table 4.5.3: Axial Burnup Profile; Burnup  $\leq 25.0$  GWD/MTU, All enrichments

Axial Segment (cm)	Relative Burnup
0 to 20.00	0.48
20.00 to 35.00	0.68
35.00 to 55.00	0.90
55.00 to 121.92	1.10
121.92 to 182.88	1.10
182.88 to 243.84	1.07
243.84 to 304.80	1.05
304.80 to 335.28	1.02
335.28 to 350.52	0.89
350.52 to 365.76	0.73
365.76 to 381.00	0.41

Table 4.5.4: Axial Burnup Profile; Burnup > 25.0 GWD/MTU, All enrichments

Axial Segment (cm)	Relative Burnup
0 to 12.7	0.553
12.7 to 25.4	0.775
25.4 to 38.1	0.923
38.1 to 50.8	0.998
50.8 to 63.5	1.031
63.5 to 76.2	1.043
76.2 to 88.9	1.047
88.9 to 101.6	1.047
101.6 to 114.3	1.047
114.3 to 127.0	1.047
127.0 to 139.7	1.047
139.7 to 152.4	1.047
152.4 to 165.1	1.047
165.1 to 177.8	1.047
177.8 to 190.5	1.048
190.5 to 203.2	1.048
203.2 to 215.9	1.049
215.9 to 228.6	1.049
228.6 to 241.3	1.049
241.3 to 254.0	1.050
254.0 to 266.7	1.051
266.7 to 279.4	1.050
279.4 to 292.1	1.042
292.1 to 304.8	1.030
304.8 to 317.5	1.011
317.5 to 330.2	0.979
330.2 to 342.9	0.927
342.9 to 355.6	0.844
355.6 to 368.3	0.707
368.3 to 381.0	0.489

Table 4.5.5: Fuel Rack Specifications – Region 1 Racks

Parameter	Value
Cell ID, Inches	8.58 [ ] <sup>a, b</sup>
Box Wall Thickness, Inches	0.075 [ ] <sup>a, b</sup>
Inner Sheathing Thickness <sup>8</sup> , Inches	0.035 [ ] <sup>a, b</sup>
Cell Pitch, Inches	9.8 [ ] <sup>a, b</sup>
Water Gap <sup>9</sup> , Inches	0.76 [ ] <sup>a, b</sup>
Metamic Pocket Thickness, Inches	0.118 (min)
Metamic Width <sup>10</sup> , Inches	7.2 [ ] <sup>a, b</sup>
Metamic Thickness, Inches	0.106 [ ] <sup>a, b</sup>
Metamic B <sub>4</sub> C Weight Percent	30.5 [ ] <sup>a, b</sup>

<sup>8</sup> The sheathing thickness on the outside surfaces of the rack is 0.075 [ ]<sup>a, b</sup> inches. The sheathing for the Region 1 racks are conservatively modeled as the thinner inner sheathing thickness of [ ]<sup>a, b</sup>.

<sup>9</sup> The Water gap tolerance is based on the tolerances of the cell pitch and cell ID.

<sup>10</sup> The Metamic width tolerance was conservatively modeled as [ ]<sup>a, b</sup> inches as shown in Section 4.7.1.3.

Table 4.5.6: Fuel Rack Specifications – Region 2 Racks

Parameter	Value
Cell ID, Inches	8.68 [ ] <sup>a, b</sup>
Box Wall Thickness, Inches	0.075 [ ] <sup>a, b</sup>
Cell Pitch, Inches	9.8
Water Gap, Inches	0.97 [ ] <sup>a, b</sup>

Table 4.5.7: Identification of Possible Rack Interaction and Minimum Distances Between Racks

Rack-to-Rack Interaction	Distance Between Racks
Region 1 to Region 1	1.75 in. (lower bound)
Region 2 to Region 2	1.25 in. (Figure 4.5.5)
Region 1 to Region 2	2 in. (lower bound)

Table 4.5.8: New Fuel Vault and Refuel Canal Rack Dimensions

Description	Value
New Fuel Vault	
Assembly Pitch	26 ± 0.25 Inches
Lateral Distance between assembly center and concrete wall	40 Inches (lower bound)
Axial distance between bottom of active length and concrete floor	11.8 Inches (lower bound)
Refuel Canal Racks	
Assembly Pitch	17.8125 ± 0.125 Inches
Lateral Distance between assembly center and concrete wall	8.75 Inches
Fuel Upender	
Assembly Pitch	12.04 Inches

Table 4.7.1: Summary of the Criticality Safety Analyses for Region 1 without Soluble Boron

Design Basis Burnup at 4.95 wt% <sup>235</sup> U	0.0 GWD/MTU
Soluble Boron	0 ppm
<b>Uncertainties</b>	
Bias Uncertainty (95%/95%)	± 0.0011
Calculational Statistics (95%/95%, 2.0×σ)	± 0.0012
Fuel Eccentricity	Negative
Rack Tolerances	± 0.0070
Fuel Tolerances	± 0.0050
Depletion Uncertainty	± 0.0000
Statistical Combination of Uncertainties	± 0.0087
Reference k <sub>eff</sub> (MCNP4a)	0.9859
Total Uncertainty (above)	0.0087
Temperature Bias	0.0023
Calculational Bias (see Appendix A)	0.0009
<b>Maximum k<sub>eff</sub></b>	<b>0.9978</b>
<b>Regulatory Limiting k<sub>eff</sub></b>	<b>1.0000</b>

Table 4.7.2: Summary of the Criticality Safety Analyses for Region 1 with Soluble Boron

Design Basis Burnup at 4.95 wt% <sup>235</sup> U	0.0 GWD/MTU
Soluble Boron	452 ppm
<b>Uncertainties</b>	
Bias Uncertainty (95%/95%)	± 0.0011
Calculational Statistics (95%/95%, 2.0×σ)	± 0.0012
Fuel Eccentricity	Negative
Rack Tolerances	± 0.0070
Fuel Tolerances	± 0.0050
Depletion Uncertainty	± 0.0000
Statistical Combination of Uncertainties	± 0.0087
Reference k <sub>eff</sub> (MCNP4a)	0.9331
Total Uncertainty (above)	0.0087
Temperature Bias	0.0023
Calculational Bias (see Appendix A)	0.0009
<b>Maximum k<sub>eff</sub></b>	<b>0.9450</b>
<b>Regulatory Limiting k<sub>eff</sub></b>	<b>0.9500</b>

Table 4.7.3: Summary of the Criticality Safety Analyses for a Uniform Loading of Spent Fuel in Region 2 without Soluble Boron at 0 Years Cooling Time

Design Basis Burnup at 4.95 wt% <sup>235</sup> U	46.8 GWD/MTU
Soluble Boron	0 ppm
<b>Uncertainties</b>	
Bias Uncertainty (95%/95%)	± 0.0011
Calculational Statistics (95%/95%, 2.0×σ)	± 0.0010
Fuel Eccentricity	+ 0.0049
Rack Tolerances	± 0.0038
Fuel Tolerances	± 0.0077
Depletion Uncertainty	± 0.0165
Statistical Combination of Uncertainties	± 0.0193
Reference k <sub>eff</sub> (MCNP4a)	0.9592
Total Uncertainty (above)	0.0193
Fuel Type Correction	0.0020
IFBA Bias	0.0056
Temperature Bias	0.0080
Calculational Bias (see Appendix A)	0.0009
<b>Maximum k<sub>eff</sub></b>	<b>0.9950</b>
<b>Regulatory Limiting k<sub>eff</sub></b>	<b>1.0000</b>

Table 4.7.4: Summary of the Criticality Safety Analyses for a Uniform Loading of Spent Fuel in Region 2 with Soluble Boron at 0 Years Cooling Time

Design Basis Burnup at 4.95 wt% <sup>235</sup> U	46.8 GWD/MTU
Soluble Boron	244 ppm <sup>11</sup>
<b>Uncertainties</b>	
Bias Uncertainty (95%/95%)	± 0.0011
Calculational Statistics (95%/95%, 2.0×σ)	± 0.0010
Fuel Eccentricity	+ 0.0049
Rack Tolerances	± 0.0038
Fuel Tolerances	± 0.0077
Depletion Uncertainty	± 0.0165
Statistical Combination of Uncertainties	± 0.0193
Reference k <sub>eff</sub> (MCNP4a)	0.9092
Total Uncertainty (above)	0.0193
Fuel Type Correction	0.0020
IFBA Bias	0.0056
Temperature Bias	0.0080
Calculational Bias (see Appendix A)	0.0009
<b>Maximum k<sub>eff</sub></b>	<b>0.9450</b>
<b>Regulatory Limiting k<sub>eff</sub></b>	<b>0.9500</b>

<sup>11</sup> Calculations performed for 4.95 wt% fuel with a burnup of 38.9 GWD/MTU at 20 years cooling time, resulted in a slightly higher soluble boron requirement of 245ppm.

Table 4.7.5: Summary of the Criticality Safety Analyses for Region 2 without Soluble Boron for a 2x2 Checkerboard of Fresh Fuel and Empty Cells

Design Basis Burnup at 4.95 wt% <sup>235</sup> U	0 GWD/MTU
Soluble Boron	0 ppm
<b>Uncertainties</b>	
Bias Uncertainty (95%/95%)	± 0.0011
Calculational Statistics (95%/95%, 2.0×σ)	± 0.0012
Fuel Eccentricity	+ 0.0024
Rack Tolerances	± 0.0050
Fuel Tolerances	± 0.0073
Depletion Uncertainty	N/A
Statistical Combination of Uncertainties	± 0.0093
Reference $k_{eff}$ (MCNP4a)	0.9274
Total Uncertainty (above)	0.0093
Temperature Bias	0.0090
Calculational Bias (see Appendix A)	0.0009
<b>Maximum <math>k_{eff}</math></b>	<b>0.9466</b>
<b>Regulatory Limiting <math>k_{eff}</math></b>	<b>1.0000</b>

Table 4.7.6: Summary of the Criticality Safety Analyses for Low Burnup Peripheral Cells in Region 2 without Soluble Boron at 0 Years Cooling Time

Design Basis Burnup in Central Storage Cells at 4.95 wt% <sup>235</sup> U	46.8 GWD/MTU
Design Basis Burnup in Peripheral Storage Cells at 4.95 wt% <sup>235</sup> U	33.3 GWD/MTU
Soluble Boron	0 ppm
<b>Uncertainties</b>	
Bias Uncertainty (95%/95%)	± 0.0011
Calculational Statistics (95%/95%, 2.0×σ)	± 0.0008
Fuel Eccentricity	+ 0.0049
Rack Tolerances	± 0.0038
Fuel Tolerances	± 0.0077
Depletion Uncertainty	± 0.0165
Statistical Combination of Uncertainties	± 0.0193
Reference $k_{eff}$ (MCNP4a)	0.9592
Total Uncertainty (above)	0.0193
Fuel Type Correction	0.0020
IFBA Bias	0.0056
Temperature Bias	0.0080
Calculational Bias (see Appendix A)	0.0009
<b>Maximum <math>k_{eff}</math></b>	<b>0.9950</b>
<b>Regulatory Limiting <math>k_{eff}</math></b>	<b>1.0000</b>

Table 4.7.7: Summary of the Criticality Safety Analyses for Low Burnup Peripheral Cells in Region 2 with Soluble Boron at 0 Years Cooling Time

Design Basis Burnup in Central Storage Cells at 4.95 wt% $^{235}\text{U}$	46.8 GWD/MTU
Design Basis Burnup in Peripheral Storage Cells at 4.95 wt% $^{235}\text{U}$	33.3 GWD/MTU
Soluble Boron	244 ppm
<b>Uncertainties</b>	
Bias Uncertainty (95%/95%)	$\pm 0.0011$
Calculational Statistics (95%/95%, $2.0 \times \sigma$ )	$\pm 0.0009$
Fuel Eccentricity	+ 0.0049
Rack Tolerances	$\pm 0.0038$
Fuel Tolerances	$\pm 0.0077$
Depletion Uncertainty	$\pm 0.0165$
Statistical Combination of Uncertainties	$\pm 0.0193$
Reference $k_{\text{eff}}$ (MCNP4a)	0.9092
Total Uncertainty (above)	0.0193
Fuel Type Correction	0.0020
IFBA Bias	0.0056
Temperature Bias	0.0080
Calculational Bias (see Appendix A)	0.0009
<b>Maximum <math>k_{\text{eff}}</math></b>	<b>0.9450</b>
<b>Regulatory Limiting <math>k_{\text{eff}}</math></b>	<b>0.9500</b>

**Table 4.7.8: Minimum Burnup versus Enrichment Values for Region 2 Racks with Spent Fuel<sup>12,13</sup>**

Enrichment	2.0	2.5	3.0	3.5	4.0	4.5	4.95
Cooling Time	Minimum Burnup (GWD/MTU)						
0	6.4	13.7	21.2	27.9	33.8	40.7	46.8
1	NC	NC	NC	27.1	33.0	39.5	45.8
2	NC	NC	NC	26.7	32.5	38.9	44.8
3	NC	NC	NC	26.5	32.1	38.4	44.3
4	NC	NC	NC	26.2	31.6	38.0	43.7
5	5.9	12.6	19.3	26.1	31.2	37.4	43.1
10	5.7	12.0	18.4	25.3	29.7	35.6	41.1
15	5.6	11.6	18.1	25.0	29.1	34.4	39.7
20	5.4	11.4	17.5	24.3	28.6	34.0	38.9

<sup>12</sup> Linear interpolation between burnups for a given cooling time is allowed. However, linear interpolation between cooling times is not allowed, therefore the cooling time of a given assembly must be rounded down to the nearest cooling time.

<sup>13</sup> NC = Not Calculated

**Table 4.7.9: Minimum Burnup versus Enrichment Values for Peripheral Cells in Region 2 Racks with Spent Fuel at 0 Years Cooling Time<sup>14</sup>**

Enrichment (wt% <sup>235</sup> U)	Minimum Burnup (GWD/MTU)
2.0	0
2.5	4.7
3.0	9.7
3.5	15.0
4.0	21.8
4.5	27.6
4.95	33.3

<sup>14</sup> Linear interpolation between burnups is allowed.

Table 4.7.10: Soluble Boron Requirements for Region 1 Accident Conditions

<b>Abnormal/Accident Condition</b>	<b>Soluble Boron Requirement</b>
Dropped Assembly – Horizontal	Negligible
Dropped Assembly – Vertical Into Storage Cell	Negligible
Dropped Assembly – Vertical Onto Rack Wall	See Section 4.7.1.7.4
Misloaded Assembly	Not Possible
Mislocated Assembly	Not Possible

Table 4.7.11: Soluble Boron Requirements for Region 2 Accident Conditions

<b>Abnormal/Accident Condition</b>	<b>Soluble Boron Requirement</b>
Abnormal Temperature – Spent Fuel – Uniform	324 ppm
Abnormal Temperature – Spent Fuel – Peripheral	324 ppm
Abnormal Temperature – Fresh Fuel	134 ppm
Dropped Assembly – Horizontal	Negligible
Dropped Assembly – Vertical	Negligible
Misloaded Assembly – Spent Fuel – Uniform	532 ppm
Misloaded Assembly – Spent Fuel – Peripheral	633 ppm
Misloaded Assembly – Fresh Fuel	881 ppm
Mislocated Assembly – Spent Fuel – Uniform	322 ppm
Mislocated Assembly – Spent Fuel – Peripheral	517 ppm
Mislocated Assembly – Fresh Fuel	667 ppm
<b>Maximum</b>	<b>881 ppm</b>

Table 4.7.12: Summary of Calculations for the Interfaces Between Racks and Loading Schemes

Interface Calculation	Figure #	Reactivity ( $k_{calc}$ )	Reference Reactivity ( $k_{calc}$ )	Delta k	Acceptable?
Region 2 – Checkerboard and Spent Fuel in same rack.	4.7.1a	0.9508	0.9592	-0.0084	Yes
Region 2 – Checkerboard and Spent Fuel in same rack.	4.7.1b	0.9712	0.9592	+0.0120	No
Region 2 – Checkerboard and Spent Fuel in same rack.	4.7.1c	0.9530	0.9592	-0.0062	Yes
Region 2 – Checkerboard and Spent Fuel in same rack.	4.7.1d	0.9786	0.9592	+0.0194	No
Region 2 – Checkerboard and Spent Fuel in same rack.	4.7.1e	0.9731	0.9592	+0.0139	No
Region 2 – Checkerboard and Spent Fuel in same rack.	4.7.1f	0.9500	0.9592	-0.0092	Yes
Region 2 – Checkerboard and Spent Fuel in same rack.	4.7.1g	0.9486	0.9592	-0.0106	Yes
Region 2 – Checkerboard and Spent Fuel in same rack.	4.7.1h	0.9519	0.9592	-0.0073	Yes
Region 2 – Checkerboard and Spent Fuel in same rack.	4.7.1i	0.9613	0.9592	+0.0021	No
Region 2 to Region 2 with fresh fuel checkerboard in each rack. Fresh fuel assemblies facing in adjacent racks.	4.7.2	0.9420	0.9274	+0.0146	No
Region 2 to Region 2 with a checkerboard of fresh fuel assemblies facing uniform loading of spent fuel in the adjacent rack.	4.7.3	0.9507	0.9592	-0.0085	Yes
Region 1 to Region 2, Fresh Fuel Checkerboard in Region 2	4.7.4	0.9782	0.9859	-0.0077	Yes
Region 1 to Region 2, Spent Fuel in Region 2 rack	4.7.5	0.9781	0.9859	-0.0078	Yes

Table 4.7.13: Reactivity Effect of IFBA Rods Enrichment 4.95 wt% <sup>235</sup>U

Burnup (GWD/MTU)	Calculated k <sub>eff</sub>		
	No IFBA	IFBA (Cycle 18)	IFBA (Cycle 19)
0.0	1.27644	1.00045	0.97409
1.0	1.25952	1.01228	0.98927
3.0	1.24337	1.04321	1.02546
5.0	1.22782	1.0676	1.05388
7.0	1.21231	1.08577	1.07518
9.0	1.19712	1.09852	1.09033
10.0	1.18967	1.10314	1.09593
12.5	1.17149	1.11006	1.1048
15.0	1.15388	1.11131	1.10748
17.5	1.13661	1.10804	1.10525
20.0	1.11966	1.10121	1.09918
22.5	1.10298	1.09183	1.09038
25.0	1.08649	1.0805	1.07946
27.5	1.07011	1.06769	1.06696
30.0	1.05382	1.05385	1.05337
32.5	1.03761	1.03931	1.03901
35.0	1.02146	1.02432	1.02415
37.5	1.00539	1.00903	1.00897
40.0	0.9894	0.99359	0.99361
42.5	0.97351	0.97808	0.97816
45.0	0.95775	0.96269	0.96271
47.5	0.94214	0.94722	0.94746
50.0	0.92674	0.93195	0.93217
52.5	0.91159	0.91687	0.91714
55.0	0.89673	0.90205	0.90234

Table 4.7.14: Reactivity Effect of Fuel and Rack Tolerances for Region 1 Racks

<b>Tolerance</b>	<b>4.95 wt%, 0 GWD/MTU</b>
<b>Fuel Tolerance</b>	<b><math>\Delta k</math></b>
Fuel Density	0.0018
Fuel Enrichment	0.0017
Fuel Rod Pitch	0.0039
Fuel Rod Clad OD	0.0018
Fuel Rod Clad ID	0.0000
Fuel Pellet OD	0.0003
Guide Tube OD	0.0002
Guide Tube ID	0.0001
<b>Statistical Combination</b>	<b>0.0050</b>
<b>Rack Tolerance</b>	<b><math>\Delta k</math></b>
Cell ID, Constant Water Gap	0.0004
Water Gap, Constant Cell Pitch	0.0059
Box Wall Thickness	0.0022
Sheathing Thickness	0.0006
Metamic Thickness	0.0015
Metamic Width	0.0021
Metamic B <sub>4</sub> C Weight %	0.0012
<b>Statistical Combination</b>	<b>0.0070</b>

Table 4.7.15: Reactivity Effect of Temperature Variation in Region 1 Racks

Temperature (°F)	4.95 wt%, 0 GWD/MTU
	$\Delta k$
39.2 (4 °C)	Reference
68 (20 °C)	-0.0015
80.33 (300K)	-0.0023
150 (max normal temp)	-0.0090
254 (123 °C)	-0.0233
254 + 10% Void	-0.0497

Table 4.7.16: Reactivity Effect of Fuel and Rack Tolerances for Region 2 Racks (0 Cooling Time)

<b>Tolerance</b>	<b>4.95 wt%, 55.0 GWD/MTU</b>	<b>4.95 wt%, 0 GWD/MTU</b>
<b>Fuel Tolerance</b>	<b><math>\Delta k</math></b>	<b><math>\Delta k</math></b>
Fuel Density	0.0035	0.0011
Fuel Enrichment	0.0033	0.0020
Fuel Rod Pitch	0.0062	0.0068
Fuel Rod Clad OD	0.0004	0.0008
Fuel Rod Clad ID	0.0002	0.0003
Fuel Pellet OD	0.0007	0.0002
Guide Tube OD	0.0000	0.0001
Guide Tube ID	0.0000	0.0001
<b>Statistical Combination</b>	<b>0.0079</b>	<b>0.0073</b>
<b>Rack Tolerance</b>	<b><math>\Delta k</math></b>	<b><math>\Delta k</math></b>
Cell ID, Constant Water Gap	0.0025	0.0037
Water Gap, Constant Cell Pitch	0.0003	0.0006
Box Wall Thickness	0.0026	0.0033
<b>Statistical Combination</b>	<b>0.0036</b>	<b>0.0050</b>

Table 4.7.17: Reactivity Effect of Temperature Variation in Region 2 Racks (0 Cooling Time)

Temperature (°F)	4.95 wt%, 55.0 GWD/MTU	4.95 wt%, 0 GWD/MTU
	$\Delta k$	$\Delta k$
32 (0 °C)	-0.0143	-0.0157
68 (20 °C)	-0.0098	-0.0107
80.33 (300K)	-0.0083	-0.0090
150 (max normal temp)	Reference	Reference
254 (123 °C)	0.0127	0.0129
254 + 10% Void	0.0168	0.0219

Table 4.8.1: Summary of New Fuel Vault Criticality Safety Analysis

	<b>OPTIMUM MODERATION</b>	<b>FULLY FLOODED</b>
Initial Enrichment, wt%	4.95± 0.05	5.00
Assembly	Standard	NGF
Calculated $k_{eff}$	0.9673	0.9185
Calculational bias, $\Delta k$	0.0009	0.0009
Uncertainties		
MCNP Bias	0.0011	0.0011
MCNP Statistics	0.0016	0.0018
Lattice Spacing	0.0059	included in calculated $k_{eff}$
Fuel Density	0.0035	included in calculated $k_{eff}$
Fuel Enrichment	0.0042	included in calculated $k_{eff}$
Statistical Combination	0.0083	0.0021
Total $k_{eff}$	0.9682 ± 0.0083	0.9194 ± 0.0021
Maximum k-eff	0.9765	0.9215
Regulatory Limit	0.98	0.95

Table 4.9.1: Summary of Criticality Safety Analysis for Fuel Handling Equipment

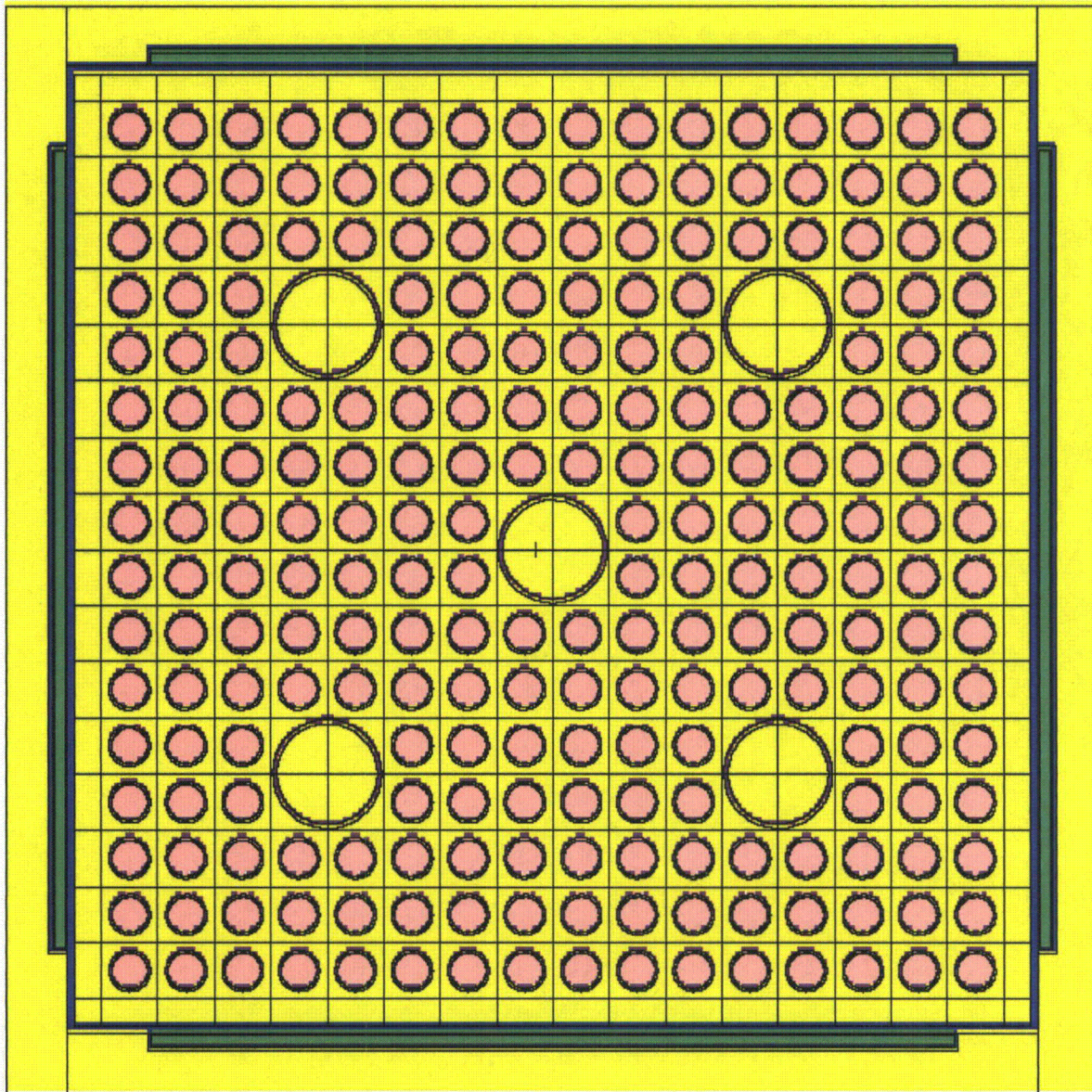
	NORMAL CONDITION	ACCIDENT CONDITION
Initial Enrichment, wt%	5.00	5.00
Soluble Boron	0 ppm	800 ppm
Assembly	NGF	NGF
Calculated $k_{eff}$	0.9188	0.9145
Calculational bias, $\Delta k$	0.0009	0.0009
Uncertainties		
MCNP Bias	0.0011	0.0011
MCNP Statistics	0.0014	0.0016
Fuel Density	included in calculated $k_{eff}$	included in calculated $k_{eff}$
Fuel Enrichment	included in calculated $k_{eff}$	included in calculated $k_{eff}$
Statistical Combination	0.0018	0.0019
Total $k_{eff}$	$0.9197 \pm 0.0018$	$0.9154 \pm 0.0019$
Maximum k-eff	0.9215	0.9173
Regulatory Limit	0.95	0.95

Table 4.9.2: Summary of Criticality Safety Analysis for the Fuel Upender

	NORMAL CONDITION		ACCIDENT CONDITION
Initial Enrichment, wt%	5.00	5.00	5.00
Soluble Boron	0 ppm	400ppm	1000 ppm
Assembly	NGF	NGF	NGF
Calculated $k_{eff}$	0.9532	0.8607	0.8677
Calculational bias, $\Delta k$	0.0009	0.0009	0.0009
Uncertainties			
MCNP Bias	0.0011	0.0011	0.0011
MCNP Statistics	0.0016	0.0016	0.0016
Fuel Density	included in calculated $k_{eff}$	included in calculated $k_{eff}$	included in calculated $k_{eff}$
Fuel Enrichment	included in calculated $k_{eff}$	included in calculated $k_{eff}$	included in calculated $k_{eff}$
Statistical Combination	0.0019	0.0019	0.0019
Total $k_{eff}$	$0.9541 \pm 0.0019$	$0.8616 \pm 0.0019$	$0.8686 \pm 0.0019$
Maximum k-eff	0.9560	0.8635	0.8705
Regulatory Limit	1.0	0.95	0.95

Table 4.9.3: Summary of Criticality Safety Analysis for Refuel Canal Rack

Initial Enrichment, wt%	5.00
Assembly	NGF
Calculated $k_{eff}$	0.9188
Calculational bias, $\Delta k$	0.0009
Uncertainties	
MCNP Bias	0.0011
MCNP Statistics	0.0018
Lattice Spacing	included in calculated $k_{eff}$
Fuel Density	included in calculated $k_{eff}$
Fuel Enrichment	included in calculated $k_{eff}$
Statistical Combination	0.0021
Total $k_{eff}$	$0.9197 \pm 0.0021$
Maximum k-eff	0.9218
Regulatory Limit	0.95



**FIGURE 4.5.1: A TWO-DIMENSIONAL REPRESENTATION OF THE ACTUAL CALCULATIONAL MODEL USED FOR THE REGION 1 RACK ANALYSIS FOR UNIFORM LOADING OF SPENT FUEL.**

This Figure was Drawn (To Scale) with the Two-Dimensional Plotter in MCNP4a.

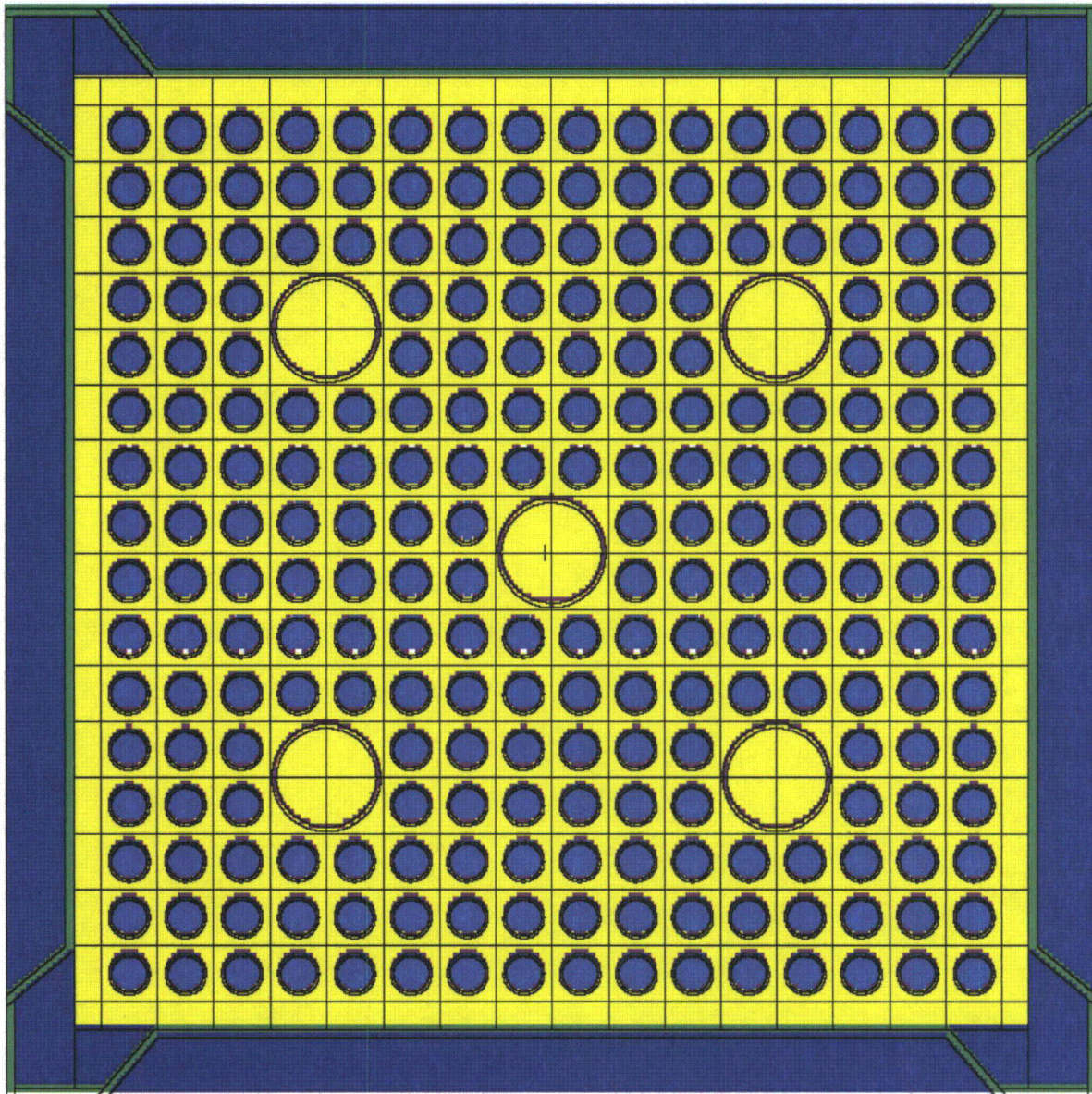


**FIGURE 4.5.2: A TWO-DIMENSIONAL REPRESENTATION OF THE ACTUAL CALCULATIONAL MODEL USED FOR THE REGION 2 RACK ANALYSIS FOR UNIFORM LOADING OF SPENT FUEL.**

This Figure was drawn (To Scale) with the Two-Dimensional Plotter in MCNP4a.

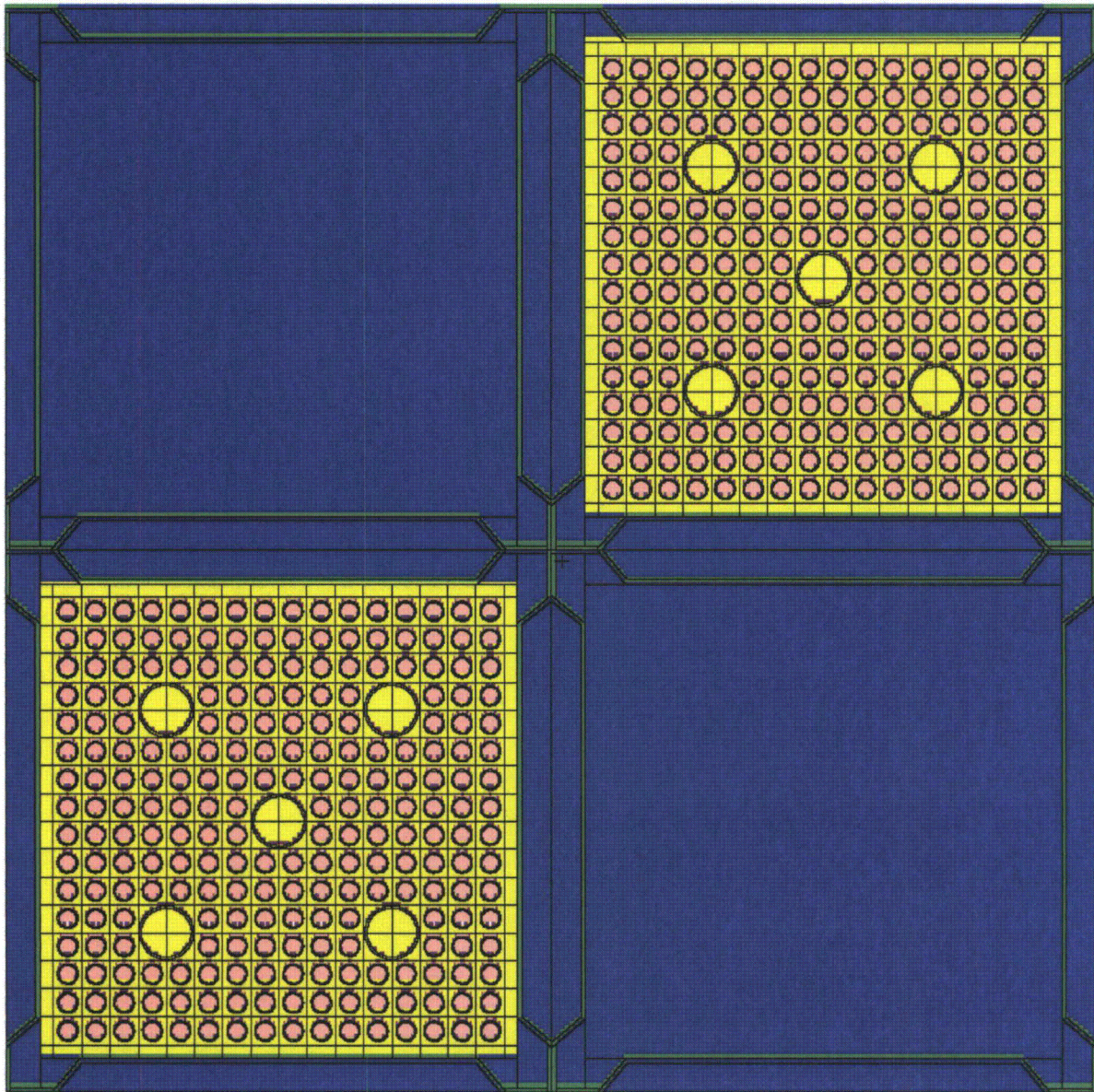


**FIGURE 4.5.3: A TWO-DIMENSIONAL REPRESENTATION OF THE ACTUAL CALCULATIONAL MODEL USED FOR THE REGION 2 RACK ANALYSIS FOR CHECKERBOARD LOADING OF FRESH FUEL.**

This Figure was Drawn (To Scale) with the Two-Dimensional Plotter in MCNP4a.

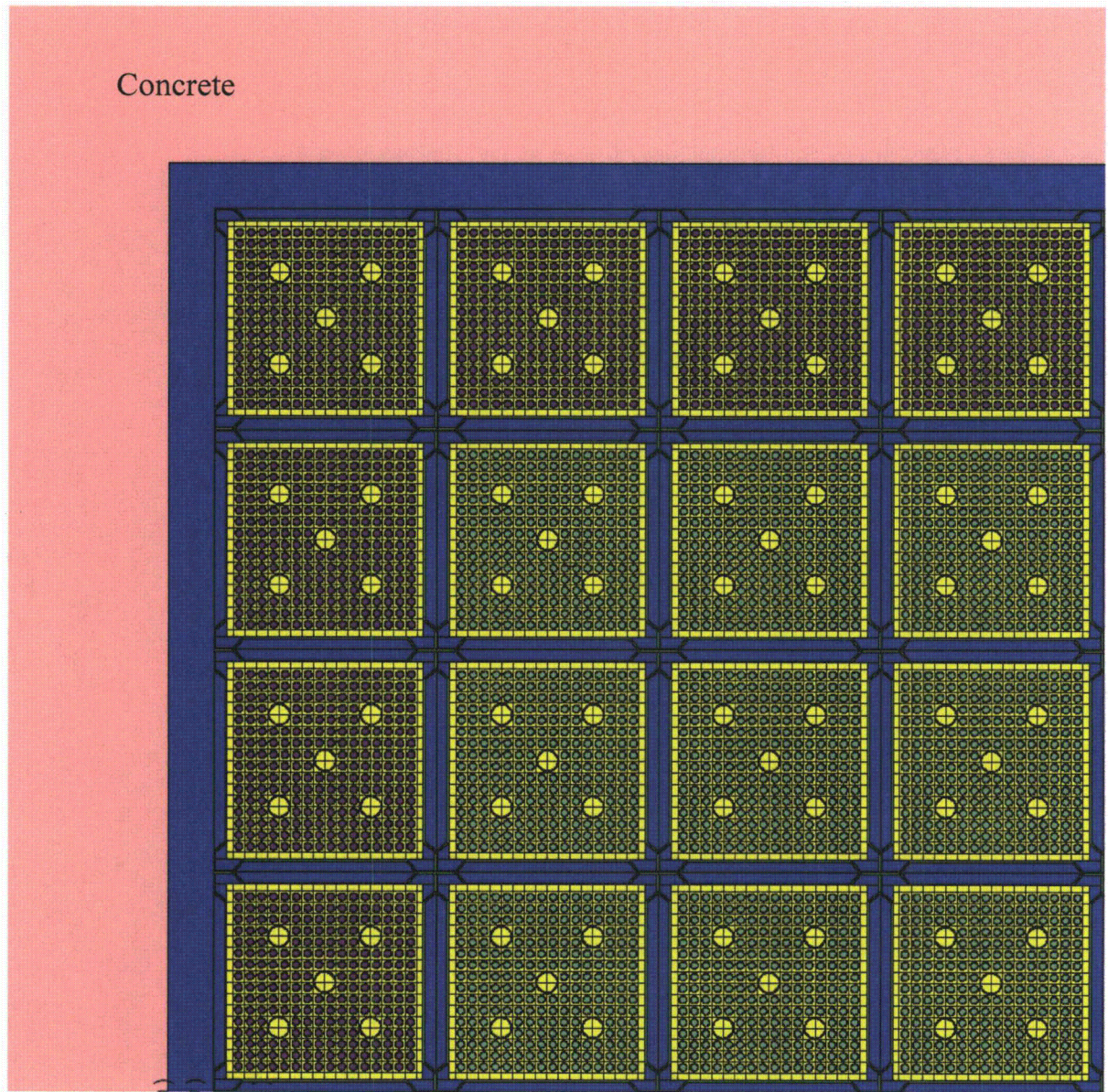


**FIGURE 4.5.4: A TWO-DIMENSIONAL REPRESENTATION OF THE ACTUAL CALCULATIONAL MODEL USED FOR THE REGION 2 RACK ANALYSIS FOR PERIPHERAL CELLS.**

This Figure was Drawn (To Scale) with the Two-Dimensional Plotter in MCNP4a.

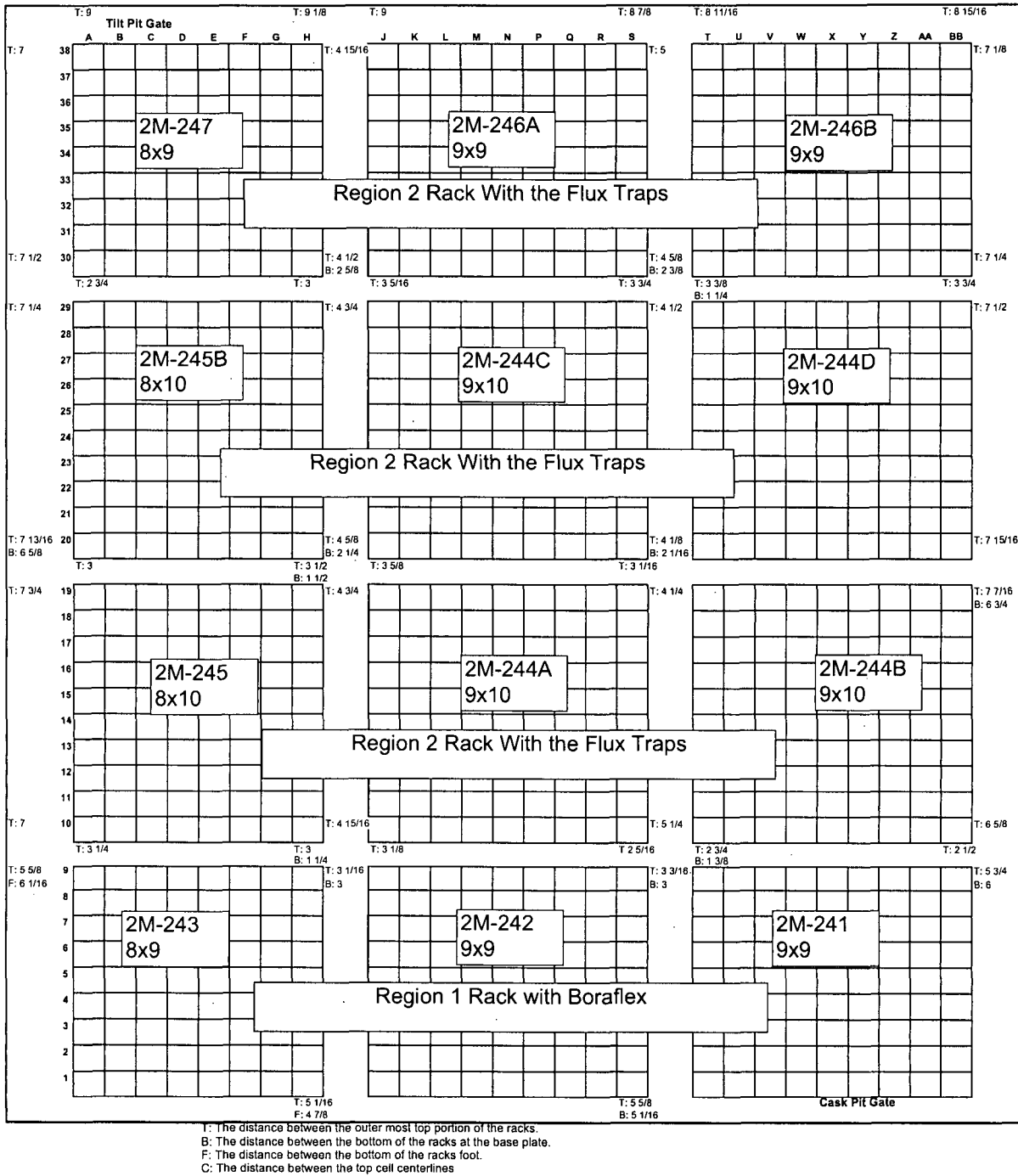


**FIGURE 4.5.5: A TWO-DIMENSIONAL REPRESENTATION OF THE EXISTING ANO UNIT 2 SPENT FUEL POOL LAYOUT WITH RACK REGION LAYOUT AND GAPS BETWEEN ADJACENT RACKS**

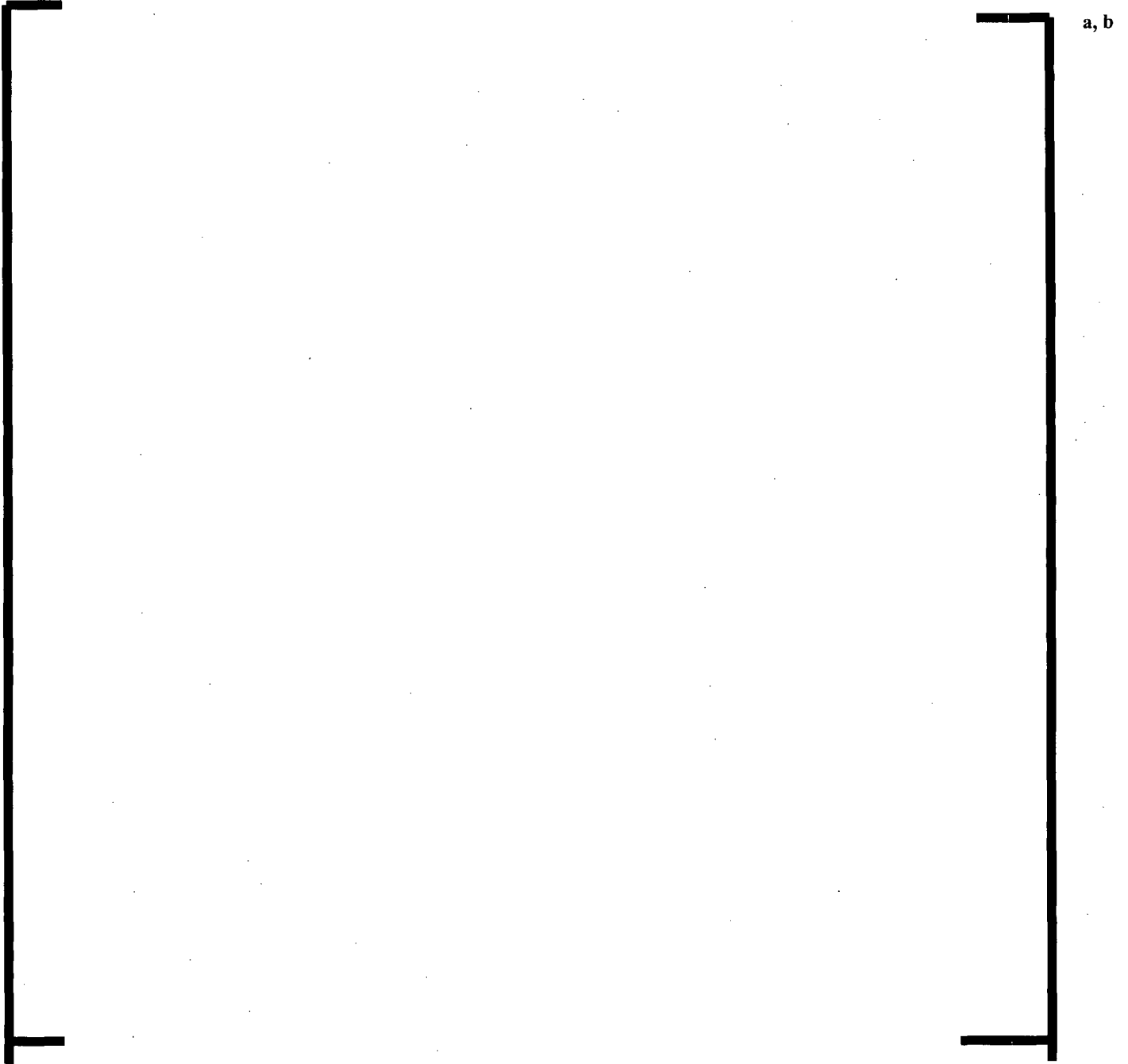


**FIGURE 4.5.6: SKETCH OF REGION 1 RACKS, DETAILING IMPORTANT DIMENSIONS AND TOLERANCES**

(NOT TO SCALE, all dimensions in inches)

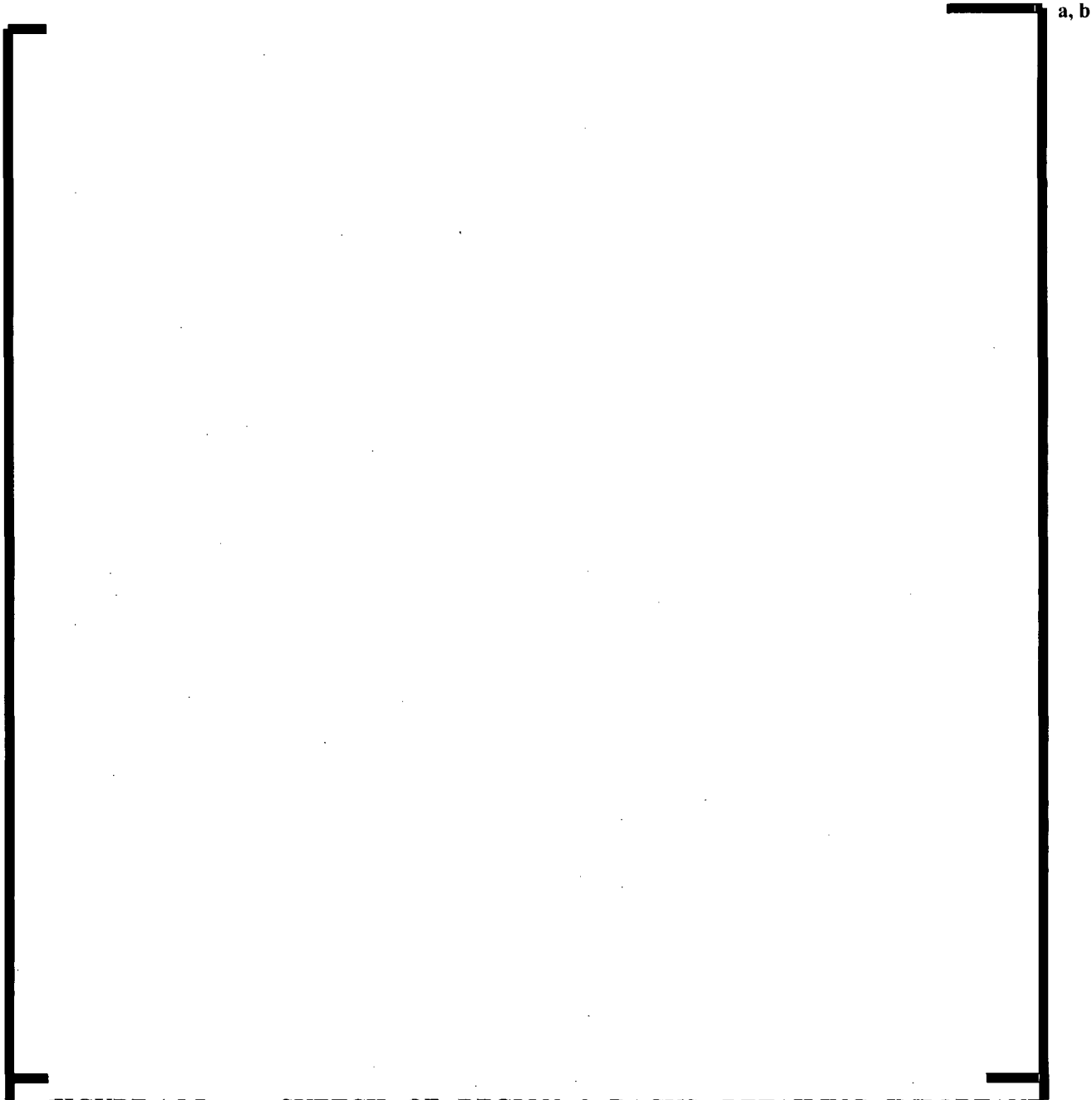


**FIGURE 4.5.7: SKETCH OF REGION 2 RACKS, DETAILING IMPORTANT DIMENSIONS AND TOLERANCES. (NOT TO SCALE, all dimensions in inches)<sup>15</sup>**

<sup>15</sup> In order to preserve the pitch due to a conservative reduction of the flux trap gap width from a design reference value of 1.07 inches to 0.97 inches (based on measurements), the nominal cell ID was modeled as 8.68 [ ]<sup>a,b</sup>.

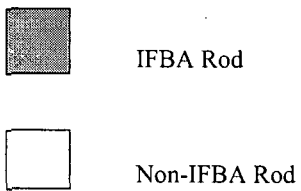
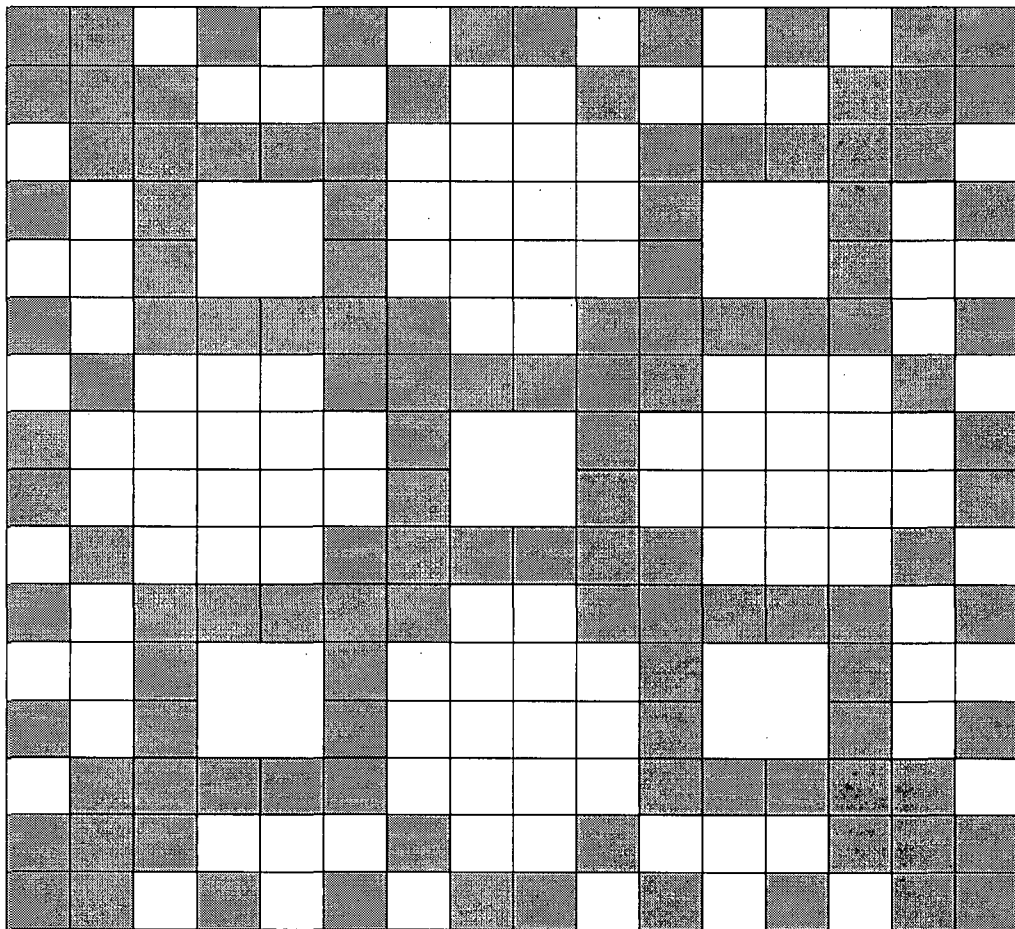


**FIGURE 4.5.8: IFBA FUEL ROD CONFIGURATION, CYCLE 18 (124 ZRB<sub>2</sub> RODS)**

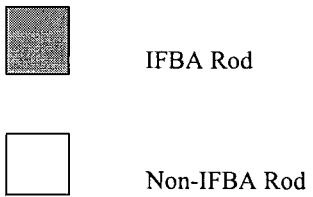
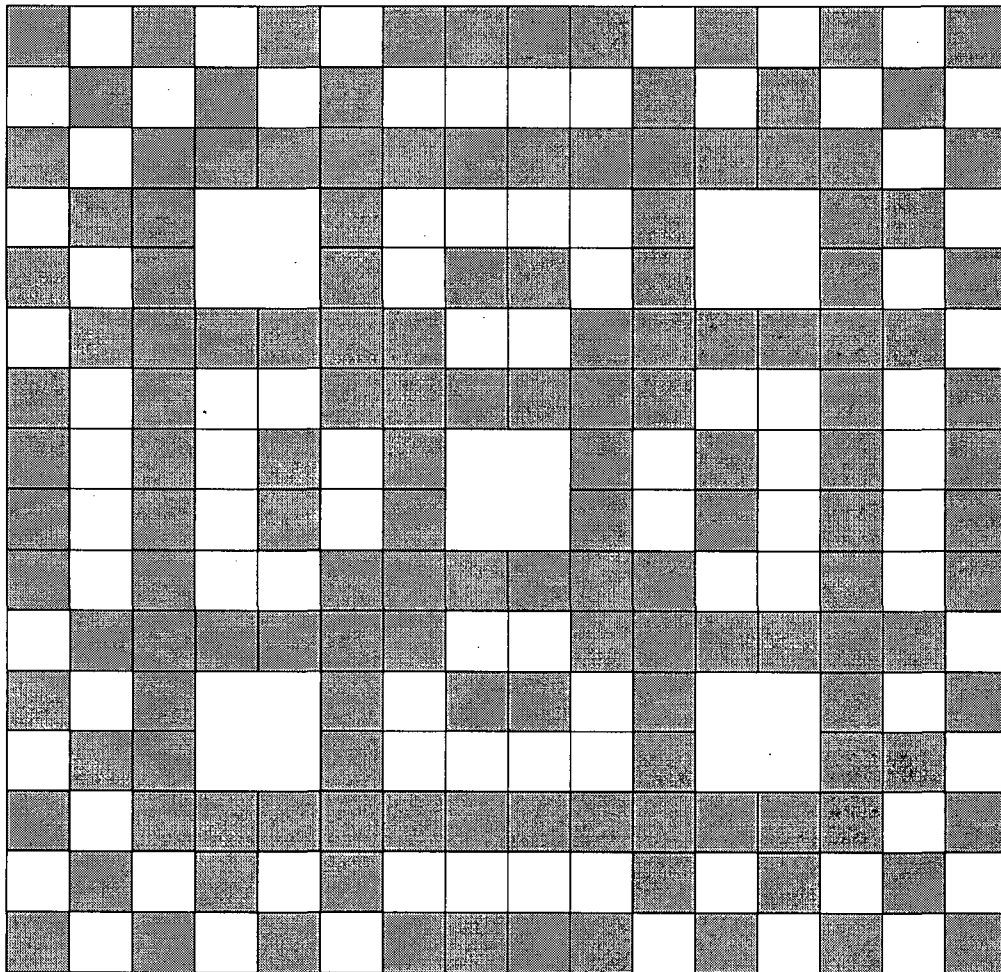


**FIGURE 4.5.9: IFBA FUEL ROD CONFIGURATION, CYCLE 19 AND BEYOND (148 ZRB<sub>2</sub> RODS)**

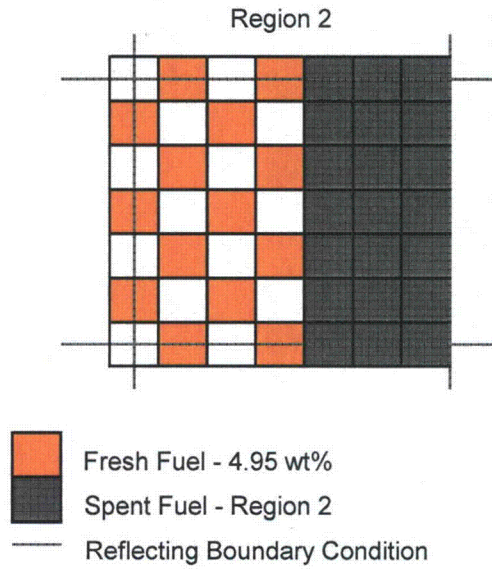


**FIGURE 4.7.1a: FRESH FUEL CHECKERBOARD AND SPENT FUEL IN SAME REGION 2 RACK – ACCEPTABLE.**

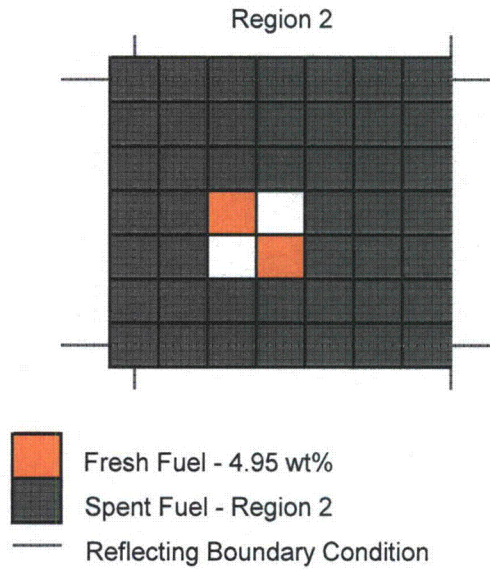


**FIGURE 4.7.1b: FRESH FUEL CHECKERBOARD AND SPENT FUEL IN SAME REGION 2 RACK – NOT ACCEPTABLE**

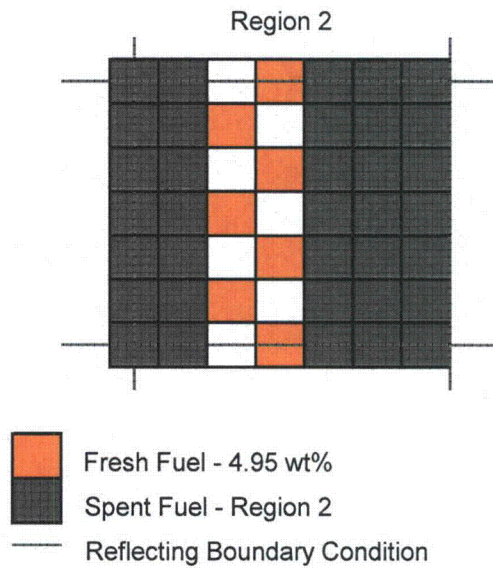


**FIGURE 4.7.1c: FRESH FUEL CHECKERBOARD AND SPENT FUEL IN SAME REGION 2 RACK – ACCEPTABLE**

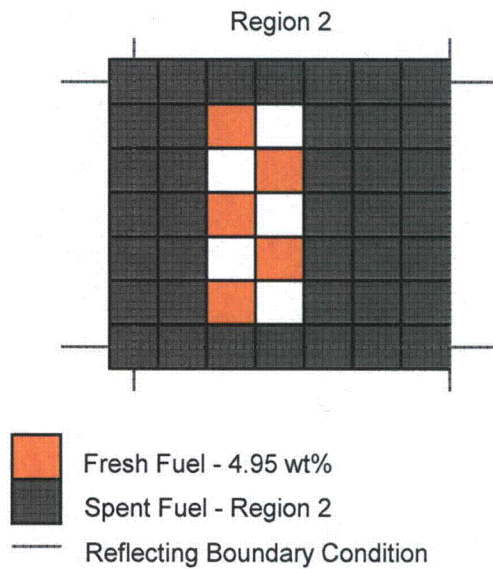


**FIGURE 4.7.1d: FRESH FUEL CHECKERBOARD AND SPENT FUEL IN SAME REGION 2 RACK – NOT ACCEPTABLE**

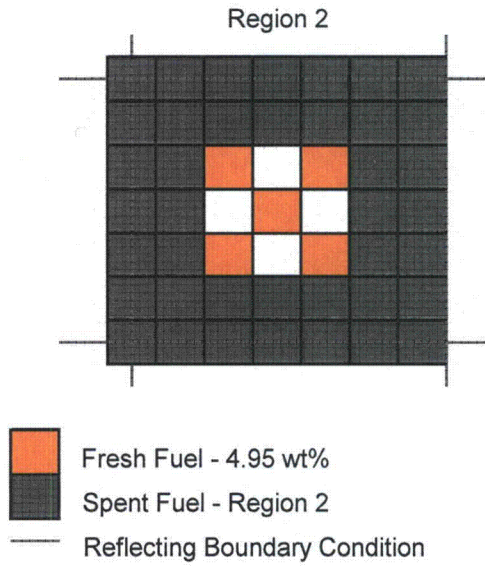


**FIGURE 4.7.1e: FRESH FUEL CHECKERBOARD AND SPENT FUEL IN SAME REGION 2 RACK – NOT ACCEPTABLE**

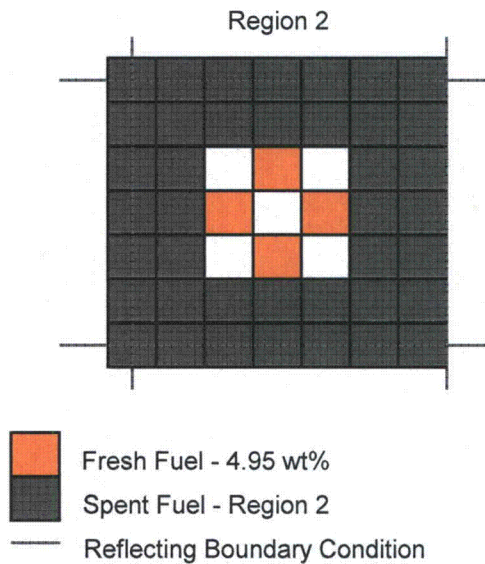


**FIGURE 4.7.1f: FRESH FUEL CHECKERBOARD AND SPENT FUEL IN SAME REGION 2 RACK – ACCEPTABLE**

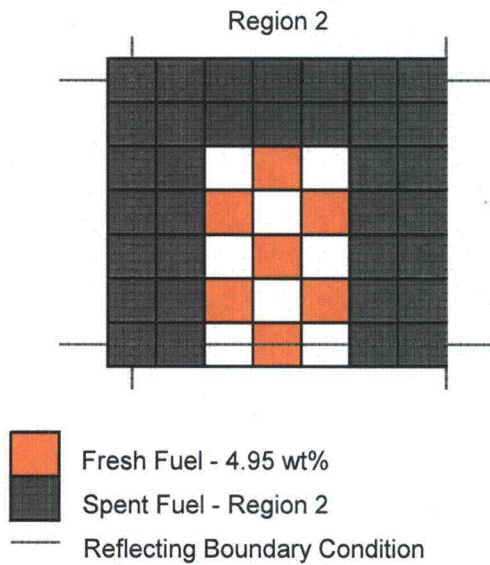


**FIGURE 4.7.1g: FRESH FUEL CHECKERBOARD AND SPENT FUEL IN SAME REGION 2 RACK – ACCEPTABLE**

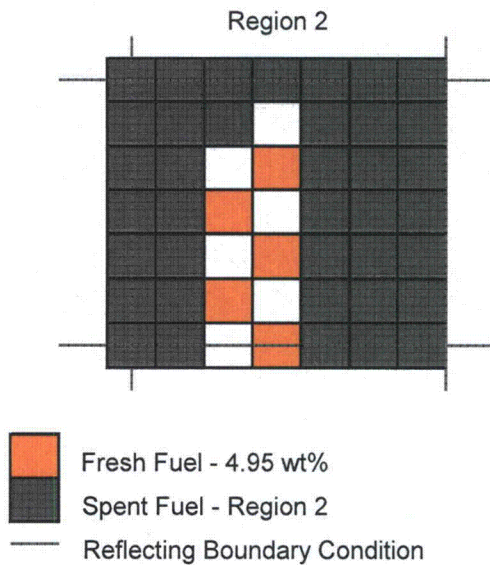


**FIGURE 4.7.1h: FRESH FUEL CHECKERBOARD AND SPENT FUEL IN SAME REGION 2 RACK – ACCEPTABLE**

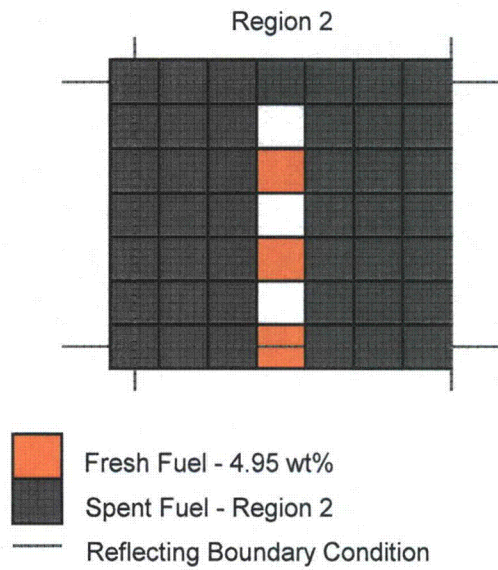


**FIGURE 4.7.1i: FRESH FUEL CHECKERBOARD AND SPENT FUEL IN SAME REGION 2 RACK – NOT ACCEPTABLE**

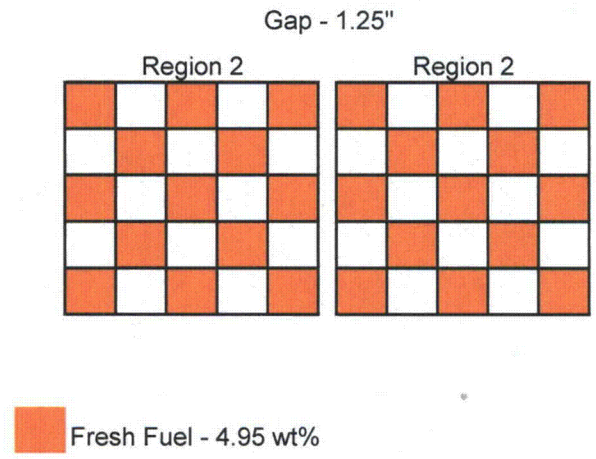


**FIGURE 4.7.2: INTERFACE CALCULATION FOR ADJACENT REGION 2 RACKS CONTAINING FRESH FUEL CHECKERBOARDS WITH FRESH FUEL ASSEMBLIES FACING ACROSS THE GAP – NOT ACCEPTABLE.**

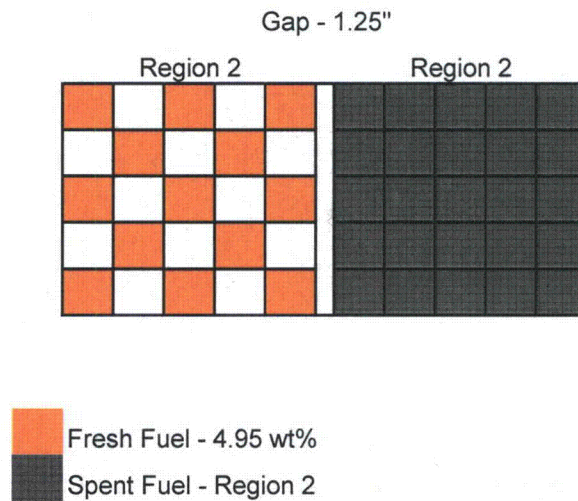


**FIGURE 4.7.3: INTERFACE CALCULATION FOR ADJACENT REGION 2 RACKS CONTAINING FRESH FUEL CHECKERBOARD AND UNIFORM LOADING OF SPENT FUEL - ACCEPTABLE.**

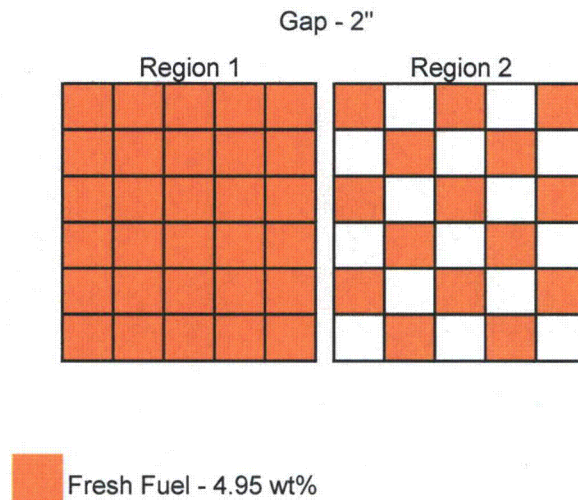


**FIGURE 4.7.4: INTERFACE CALCULATION FOR REGION 1 AND REGION 2 RACKS; FRESH FUEL CHECKERBOARD IN REGION 2 RACK - ACCEPTABLE.**

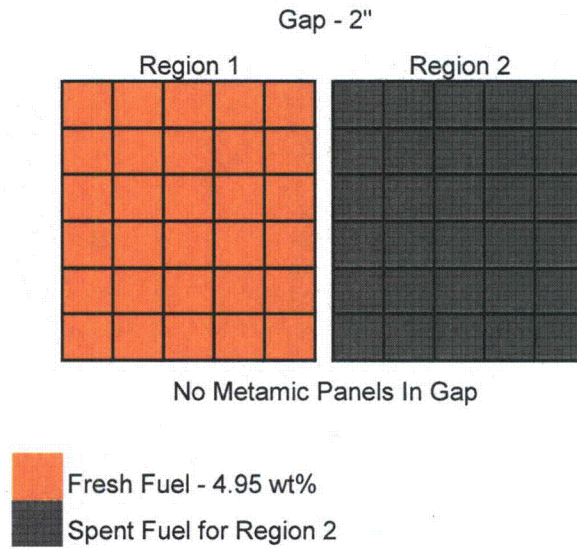


**FIGURE 4.7.5: INTERFACE CALCULATION FOR REGION 1 AND REGION 2 RACKS. UNIFORM LOADING OF SPENT FUEL IN REGION 2 RACK – ACCEPTABLE.**

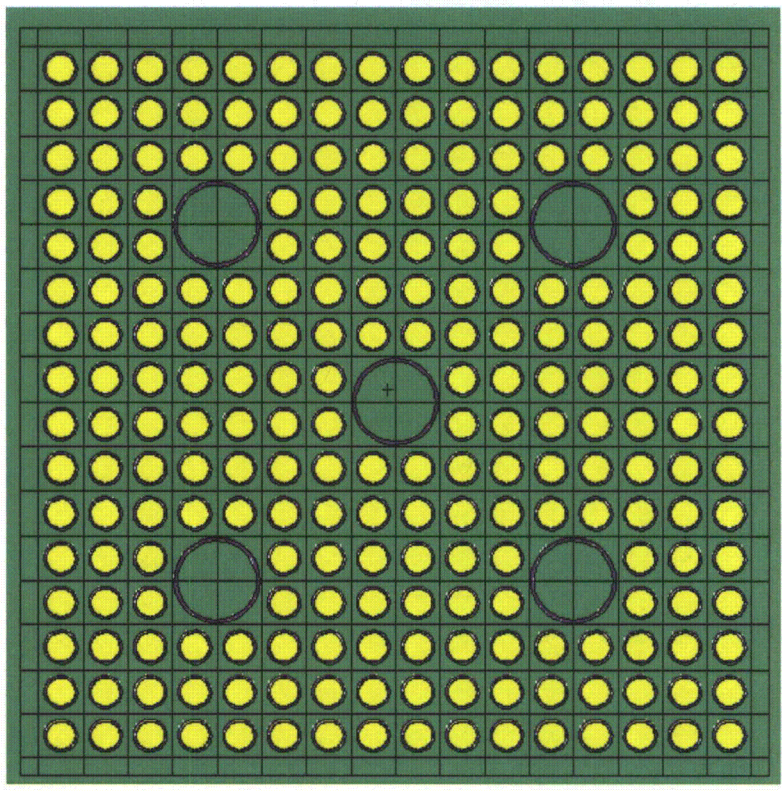
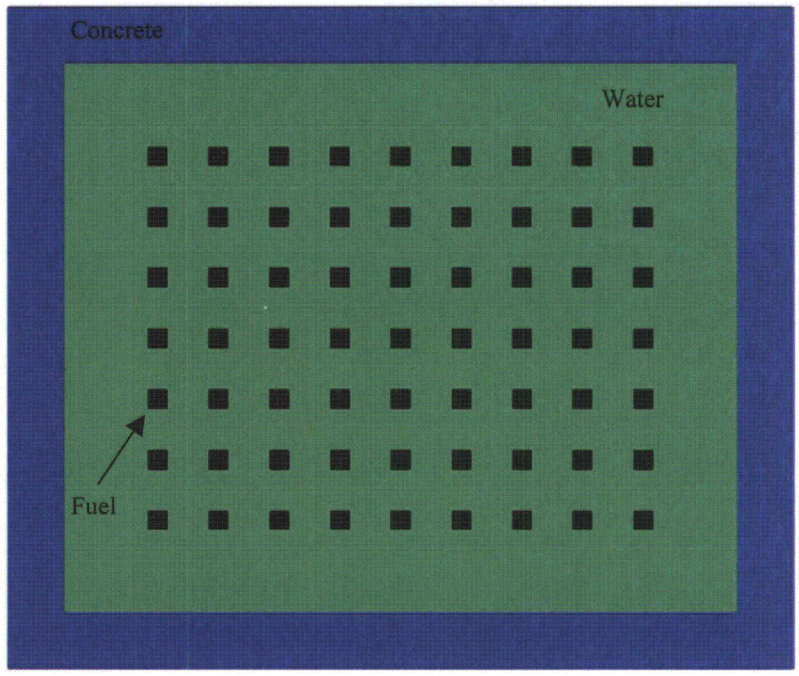


**FIGURE 4.8.1: TWO-DIMENSIONAL REPRESENTATIONS (CROSS SECTIONS) OF THE ACTUAL CALCULATIONAL MODEL USED FOR THE NEW FUEL VAULT ANALYSIS: ENTIRE VAULT (TOP) AND INDIVIDUAL ASSEMBLY (BOTTOM)**

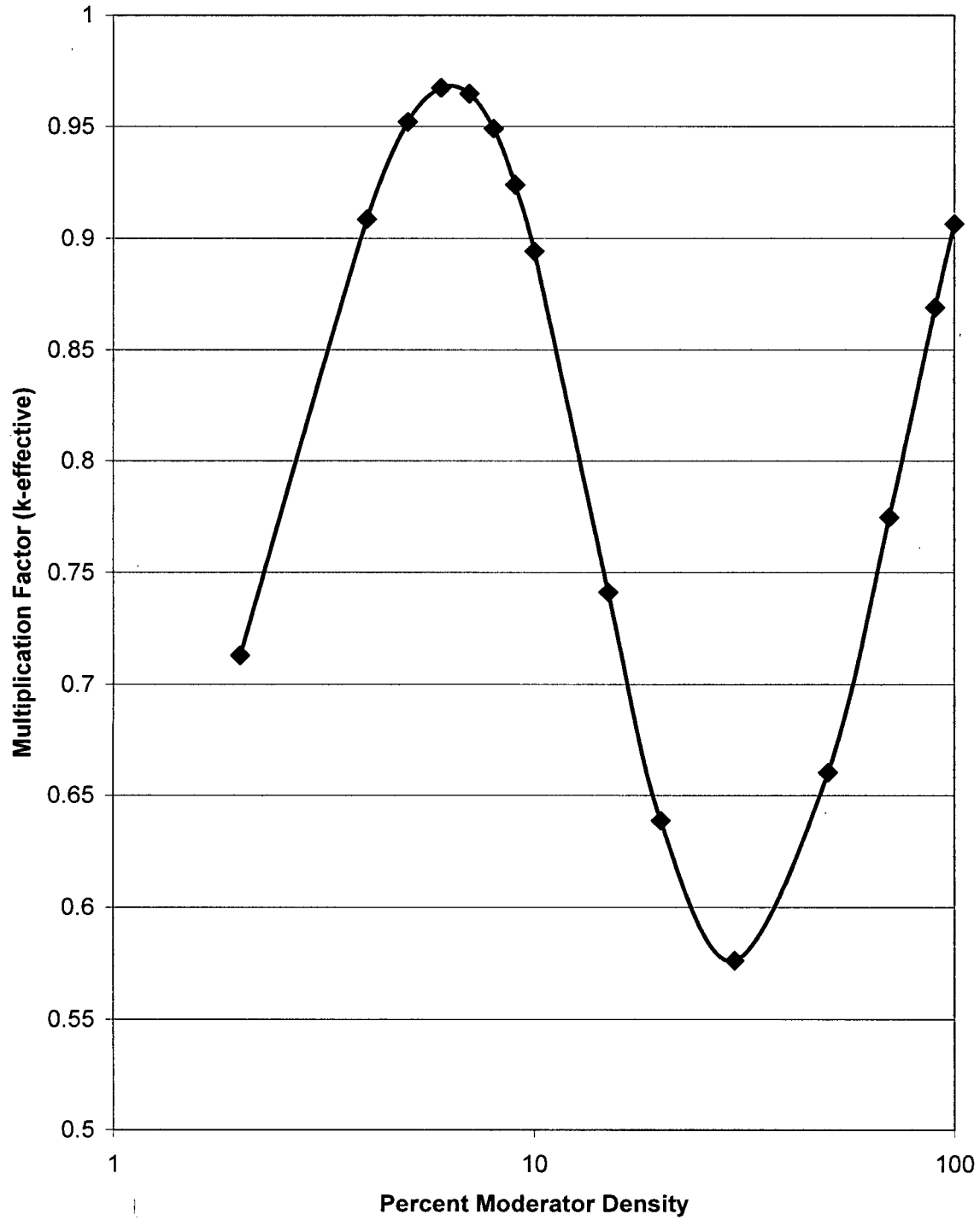


**FIGURE 4.8.2: CALCULATED  $K_{EFF}$  AS A FUNCTION OF WATER DENSITY IN THE NEW FUEL VAULT.**

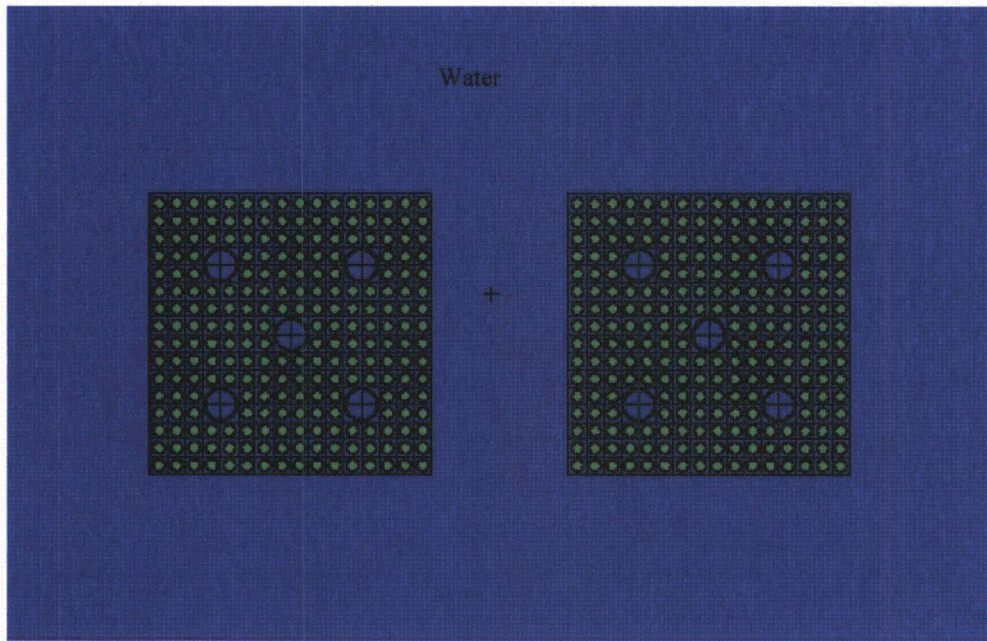


**FIGURE 4.9.1**      **TWO-DIMENSIONAL REPRESENTATION (CROSS SECTION) OF THE ACTUAL CALCULATIONAL MODEL USED FOR THE FUEL UPENDER ANALYSIS**

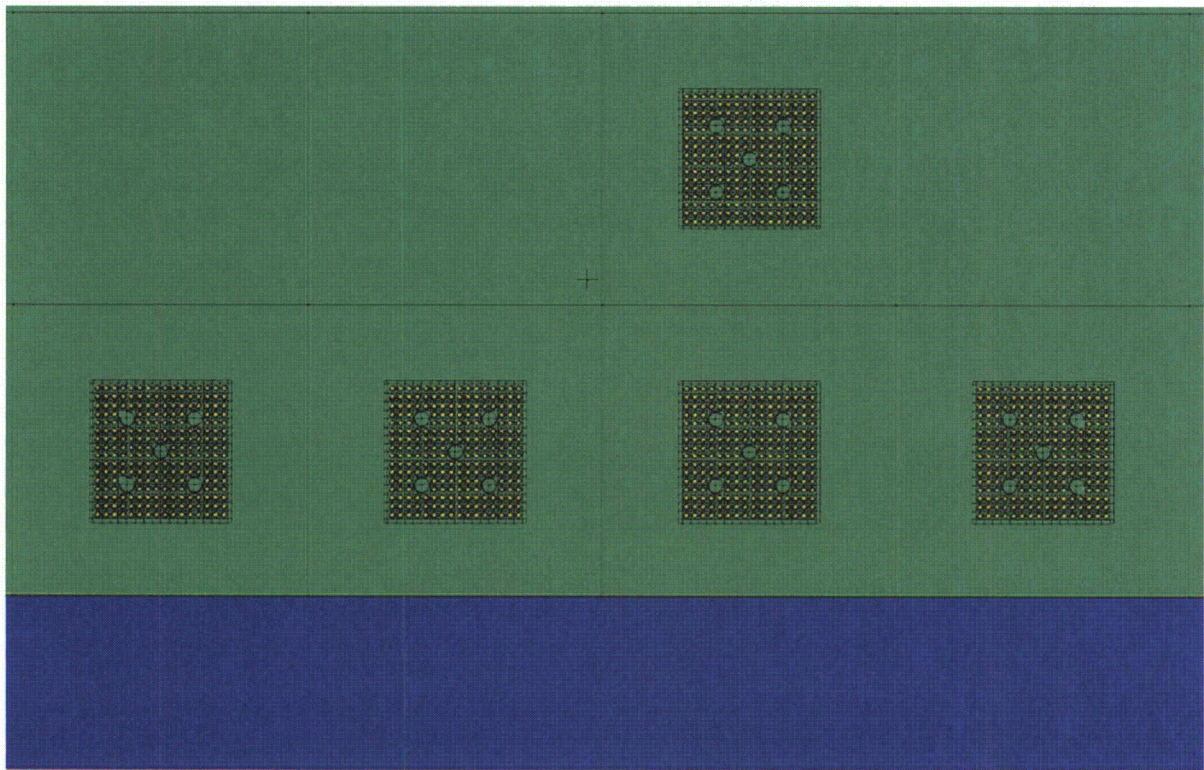


**FIGURE 4.9.2** TWO-DIMENSIONAL REPRESENTATION (CROSS SECTION) OF THE ACTUAL CALCULATIONAL MODEL USED FOR THE REFUEL CANAL ANALYSIS.

## **Appendix 4A: Benchmark Calculations**

(total number of pages: 26 including this page)

Note: because this appendix was taken from a different report, the next page is labeled "Appendix 4A, Page 1"

## APPENDIX 4A: BENCHMARK CALCULATIONS

### 4A.1 INTRODUCTION AND SUMMARY

Benchmark calculations have been made on selected critical experiments, chosen, in so far as possible, to bound the range of variables in the rack designs. Two independent methods of analysis were used, differing in cross section libraries and in the treatment of the cross sections. MCNP4a [4A.1] is a continuous energy Monte Carlo code and KENO5a [4A.2] uses group-dependent cross sections. For the KENO5a analyses reported here, the 238-group library was chosen, processed through the NITAWL-II [4A.2] program to create a working library and to account for resonance self-shielding in uranium-238 (Nordheim integral treatment). The 238 group library was chosen to avoid or minimize the errors<sup>†</sup> (trends) that have been reported (e.g., [4A.3 through 4A.5]) for calculations with collapsed cross section sets.

In rack designs, the three most significant parameters affecting criticality are (1) the fuel enrichment, (2) the <sup>10</sup>B loading in the neutron absorber, and (3) the lattice spacing (or water-gap thickness if a flux-trap design is used). Other parameters, within the normal range of rack and fuel designs, have a smaller effect, but are also included in the analyses.

Table 4A.1 summarizes results of the benchmark calculations for all cases selected and analyzed, as referenced in the table. The effect of the major variables are discussed in subsequent sections below. It is important to note that there is obviously considerable overlap in parameters since it is not possible to vary a single parameter and maintain criticality; some other parameter or parameters must be concurrently varied to maintain criticality.

One possible way of representing the data is through a spectrum index that incorporates all of the variations in parameters. KENO5a computes and prints the "energy of the average lethargy causing fission" (EALF). In MCNP4a, by utilizing the tally option with the identical 238-group energy structure as in KENO5a, the number of fissions in each group may be collected and the EALF determined (post-processing).

---

<sup>†</sup> Small but observable trends (errors) have been reported for calculations with the 27-group and 44-group collapsed libraries. These errors are probably due to the use of a single collapsing spectrum when the spectrum should be different for the various cases analyzed, as evidenced by the spectrum indices.

Figures 4A.1 and 4A.2 show the calculated  $k_{\text{eff}}$  for the benchmark critical experiments as a function of the EALF for MCNP4a and KENO5a, respectively ( $\text{UO}_2$  fuel only). The scatter in the data (even for comparatively minor variation in critical parameters) represents experimental error<sup>†</sup> in performing the critical experiments within each laboratory, as well as between the various testing laboratories. The B&W critical experiments show a larger experimental error than the PNL criticals. This would be expected since the B&W criticals encompass a greater range of critical parameters than the PNL criticals.

Linear regression analysis of the data in Figures 4A.1 and 4A.2 show that there are no trends, as evidenced by very low values of the correlation coefficient (0.13 for MCNP4a and 0.21 for KENO5a). The total bias (systematic error, or mean of the deviation from a  $k_{\text{eff}}$  of exactly 1.000) for the two methods of analysis are shown in the table below.

Calculational Bias of MCNP4a and KENO5a	
MCNP4a	0.0009 ± 0.0011
KENO5a	0.0030 ± 0.0012

The bias and standard error of the bias were derived directly from the calculated  $k_{\text{eff}}$  values in Table 4A.1 using the following equations<sup>††</sup>, with the standard error multiplied by the one-sided K-factor for 95% probability at the 95% confidence level from NBS Handbook 91 [4A.18] (for the number of cases analyzed, the K-factor is ~2.05 or slightly more than 2).

$$\bar{k} = \frac{1}{n} \sum_i^n k_i \quad (4A.1)$$

---

† A classical example of experimental error is the corrected enrichment in the PNL experiments, first as an addendum to the initial report and, secondly, by revised values in subsequent reports for the same fuel rods.

†† These equations may be found in any standard text on statistics, for example, reference [4A.6] (or the MCNP4a manual) and is the same methodology used in MCNP4a and in KENO5a.

$$\sigma_k^2 = \frac{\sum_{i=1}^n k_i^2 - (\sum_{i=1}^n k_i)^2 / n}{n(n-1)} \quad (4A.2)$$

$$Bias = (1 - \bar{k}) \pm K \sigma_{\bar{k}} \quad (4A.3)$$

where  $k_i$  are the calculated reactivities of  $n$  critical experiments;  $\sigma_k$  is the unbiased estimator of the standard deviation of the mean (also called the standard error of the bias (mean));  $K$  is the one-sided multiplier for 95% probability at the 95% confidence level (NBS Handbook 91 [4A.18]).

Formula 4.A.3 is based on the methodology of the National Bureau of Standards (now NIST) and is used to calculate the values presented on page 4.A-2. The first portion of the equation,  $(1 - \bar{k})$ , is the actual bias which is added to the MCNP4a and KENO5a results. The second term,  $K \sigma_{\bar{k}}$ , is the uncertainty or standard error associated with the bias. The  $K$  values used were obtained from the National Bureau of Standards Handbook 91 and are for one-sided statistical tolerance limits for 95% probability at the 95% confidence level. The actual  $K$  values for the 56 critical experiments evaluated with MCNP4a and the 53 critical experiments evaluated with KENO5a are 2.04 and 2.05, respectively.

The bias values are used to evaluate the maximum  $k_{eff}$  values for the rack designs. KENO5a has a slightly larger systematic error than MCNP4a, but both result in greater precision than published data [4A.3 through 4A.5] would indicate for collapsed cross section sets in KENO5a (SCALE) calculations.

#### 4A.2 Effect of Enrichment

The benchmark critical experiments include those with enrichments ranging from 2.46 w/o to 5.74 w/o and therefore span the enrichment range for rack designs. Figures 4A.3 and 4A.4 show the calculated  $k_{eff}$  values (Table 4A.1) as a function of the fuel enrichment reported for the critical experiments. Linear regression analyses for these data confirms that there are no trends, as indicated by low values of the correlation coefficients (0.03 for MCNP4a and 0.38 for KENO5a). Thus, there are no corrections to the bias for the various enrichments.

As further confirmation of the absence of any trends with enrichment, a typical configuration was calculated with both MCNP4a and KENO5a for various enrichments. The cross-comparison of calculations with codes of comparable sophistication is suggested in Reg. Guide 3.41. Results of this comparison, shown in Table 4A.2 and Figure 4A.5, confirm no significant difference in the calculated values of  $k_{\text{eff}}$  for the two independent codes as evidenced by the 45° slope of the curve. Since it is very unlikely that two independent methods of analysis would be subject to the same error, this comparison is considered confirmation of the absence of an enrichment effect (trend) in the bias.

#### 4A.3 Effect of $^{10}\text{B}$ Loading

Several laboratories have performed critical experiments with a variety of thin absorber panels similar to the Boral panels in the rack designs. Of these critical experiments, those performed by B&W are the most representative of the rack designs. PNL has also made some measurements with absorber plates, but, with one exception (a flux-trap experiment), the reactivity worth of the absorbers in the PNL tests is very low and any significant errors that might exist in the treatment of strong thin absorbers could not be revealed.

Table 4A.3 lists the subset of experiments using thin neutron absorbers (from Table 4A.1) and shows the reactivity worth ( $\Delta k$ ) of the absorber.<sup>†</sup>

No trends with reactivity worth of the absorber are evident, although based on the calculations shown in Table 4A.3, some of the B&W critical experiments seem to have unusually large experimental errors. B&W made an effort to report some of their experimental errors. Other laboratories did not evaluate their experimental errors.

To further confirm the absence of a significant trend with  $^{10}\text{B}$  concentration in the absorber, a cross-comparison was made with MCNP4a and KENO5a (as suggested in Reg. Guide 3.41). Results are shown in Figure 4A.6 and Table 4A.4 for a typical geometry. These data substantiate the absence of any error (trend) in either of the two codes for the conditions analyzed (data points fall on a 45° line, within an expected 95% probability limit).

---

<sup>†</sup> The reactivity worth of the absorber panels was determined by repeating the calculation with the absorber analytically removed and calculating the incremental ( $\Delta k$ ) change in reactivity due to the absorber.

#### 4A.4 Miscellaneous and Minor Parameters

##### 4A.4.1 Reflector Material and Spacings

PNL has performed a number of critical experiments with thick steel and lead reflectors.<sup>†</sup> Analysis of these critical experiments are listed in Table 4A.5 (subset of data in Table 4A.1). There appears to be a small tendency toward overprediction of  $k_{eff}$  at the lower spacing, although there are an insufficient number of data points in each series to allow a quantitative determination of any trends. The tendency toward overprediction at close spacing means that the rack calculations may be slightly more conservative than otherwise.

##### 4A.4.2 Fuel Pellet Diameter and Lattice Pitch

The critical experiments selected for analysis cover a range of fuel pellet diameters from 0.311 to 0.444 inches, and lattice spacings from 0.476 to 1.00 inches. In the rack designs, the fuel pellet diameters range from 0.303 to 0.3805 inches O.D. (0.496 to 0.580 inch lattice spacing) for PWR fuel and from 0.3224 to 0.494 inches O.D. (0.488 to 0.740 inch lattice spacing) for BWR fuel. Thus, the critical experiments analyzed provide a reasonable representation of power reactor fuel. Based on the data in Table 4A.1, there does not appear to be any observable trend with either fuel pellet diameter or lattice pitch, at least over the range of the critical experiments applicable to rack designs.

##### 4A.4.3 Soluble Boron Concentration Effects

Various soluble boron concentrations were used in the B&W series of critical experiments and in one PNL experiment, with boron concentrations ranging up to 2550 ppm. Results of MCNP4a (and one KENO5a) calculations are shown in Table 4A.6. Analyses of the very high boron concentration experiments (> 1300 ppm) show a tendency to slightly overpredict reactivity for the three experiments exceeding 1300 ppm. In turn, this would suggest that the evaluation of the racks with higher soluble boron concentrations could be slightly conservative.

---

<sup>†</sup> Parallel experiments with a depleted uranium reflector were also performed but not included in the present analysis since they are not pertinent to the Holtec rack design.

#### 4A.5 MOX Fuel

The number of critical experiments with  $\text{PuO}_2$  bearing fuel (MOX) is more limited than for  $\text{UO}_2$  fuel. However, a number of MOX critical experiments have been analyzed and the results are shown in Table 4A.7. Results of these analyses are generally above a  $k_{\text{eff}}$  of 1.00, indicating that when Pu is present, both MCNP4a and KENO5a overpredict the reactivity. This may indicate that calculation for MOX fuel will be expected to be conservative, especially with MCNP4a. It may be noted that for the larger lattice spacings, the KENO5a calculated reactivities are below 1.00, suggesting that a small trend may exist with KENO5a. It is also possible that the overprediction in  $k_{\text{eff}}$  for both codes may be due to a small inadequacy in the determination of the Pu-241 decay and Am-241 growth. This possibility is supported by the consistency in calculated  $k_{\text{eff}}$  over a wide range of the spectral index (energy of the average lethargy causing fission).

References

- [4A.1] J.F. Briesmeister, Ed., "MCNP4a - A General Monte Carlo N-Particle Transport Code, Version 4A; Los Alamos National Laboratory, LA-12625-M (1993).
- [4A.2] SCALE 4.3, "A Modular Code System for Performing Standardized Computer Analyses for Licensing Evaluation", NUREG-0200 (ORNL-NUREG-CSD-2/U2/R5, Revision 5, Oak Ridge National Laboratory, September 1995.
- [4A.3] M.D. DeHart and S.M. Bowman, "Validation of the SCALE Broad Structure 44-G Group ENDF/B-Y Cross-Section Library for Use in Criticality Safety Analyses", NUREG/CR-6102 (ORNL/TM-12460) Oak Ridge National Laboratory, September 1994.
- [4A.4] W.C. Jordan et al., "Validation of KENO.V.a", CSD/TM-238, Martin Marietta Energy Systems, Inc., Oak Ridge National Laboratory, December 1986.
- [4A.5] O.W. Hermann et al., "Validation of the Scale System for PWR Spent Fuel Isotopic Composition Analysis", ORNL-TM-12667, Oak Ridge National Laboratory, undated.
- [4A.6] R.J. Larsen and M.L. Marx, An Introduction to Mathematical Statistics and its Applications, Prentice-Hall, 1986.
- [4A.7] M.N. Baldwin et al., Critical Experiments Supporting Close Proximity Water Storage of Power Reactor Fuel, BAW-1484-7, Babcock and Wilcox Company, July 1979.
- [4A.8] G.S. Hoovier et al., Critical Experiments Supporting Underwater Storage of Tightly Packed Configurations of Spent Fuel Pins, BAW-1645-4, Babcock & Wilcox Company, November 1991.
- [4A.9] L.W. Newman et al., Urania Gadolinia: Nuclear Model Development and Critical Experiment Benchmark, BAW-1810, Babcock and Wilcox Company, April 1984.

- [4A.10] J.C. Manaranche et al., "Dissolution and Storage Experimental Program with 4.75 w/o Enriched Uranium-Oxide Rods," Trans. Am. Nucl. Soc. 33: 362-364 (1979).
- [4A.11] S.R. Bierman and E.D. Clayton, Criticality Experiments with Subcritical Clusters of 2.35 w/o and 4.31 w/o  $^{235}\text{U}$  Enriched  $\text{UO}_2$  Rods in Water with Steel Reflecting Walls, PNL-3602, Battelle Pacific Northwest Laboratory, April 1981.
- [4A.12] S.R. Bierman et al., Criticality Experiments with Subcritical Clusters of 2.35 w/o and 4.31 w/o  $^{235}\text{U}$  Enriched  $\text{UO}_2$  Rods in Water with Uranium or Lead Reflecting Walls, PNL-3926, Battelle Pacific Northwest Laboratory, December, 1981.
- [4A.13] S.R. Bierman et al., Critical Separation Between Subcritical Clusters of 4.31 w/o  $^{235}\text{U}$  Enriched  $\text{UO}_2$  Rods in Water with Fixed Neutron Poisons, PNL-2615, Battelle Pacific Northwest Laboratory, October 1977.
- [4A.14] S.R. Bierman, Criticality Experiments with Neutron Flux Traps Containing Voids, PNL-7167, Battelle Pacific Northwest Laboratory, April 1990.
- [4A.15] B.M. Durst et al., Critical Experiments with 4.31 wt %  $^{235}\text{U}$  Enriched  $\text{UO}_2$  Rods in Highly Borated Water Lattices, PNL-4267, Battelle Pacific Northwest Laboratory, August 1982.
- [4A.16] S.R. Bierman, Criticality Experiments with Fast Test Reactor Fuel Pins in Organic Moderator, PNL-5803, Battelle Pacific Northwest Laboratory, December 1981.
- [4A.17] E.G. Taylor et al., Saxton Plutonium Program Critical Experiments for the Saxton Partial Plutonium Core, WCAP-3385-54, Westinghouse Electric Corp., Atomic Power Division, December 1965.
- [4A.18] M.G. Natrella, Experimental Statistics, National Bureau of Standards, Handbook 91, August 1963.

Table 4A.1

Summary of Criticality Benchmark Calculations

Reference	Identification	Enrich.	Calculated $k_{eff}$		EALF <sup>†</sup> (eV)		
			MCNP4a	KENO5a	MCNP4a	KENO5a	
1	B&W-1484 (4A.7)	Core I	2.46	0.9964 ± 0.0010	0.9898 ± 0.0006	0.1759	0.1753
2	B&W-1484 (4A.7)	Core II	2.46	1.0008 ± 0.0011	1.0015 ± 0.0005	0.2553	0.2446
3	B&W-1484 (4A.7)	Core III	2.46	1.0010 ± 0.0012	1.0005 ± 0.0005	0.1999	0.1939
4	B&W-1484 (4A.7)	Core IX	2.46	0.9956 ± 0.0012	0.9901 ± 0.0006	0.1422	0.1426
5	B&W-1484 (4A.7)	Core X	2.46	0.9980 ± 0.0014	0.9922 ± 0.0006	0.1513	0.1499
6	B&W-1484 (4A.7)	Core XI	2.46	0.9978 ± 0.0012	1.0005 ± 0.0005	0.2031	0.1947
7	B&W-1484 (4A.7)	Core XII	2.46	0.9988 ± 0.0011	0.9978 ± 0.0006	0.1718	0.1662
8	B&W-1484 (4A.7)	Core XIII	2.46	1.0020 ± 0.0010	0.9952 ± 0.0006	0.1988	0.1965
9	B&W-1484 (4A.7)	Core XIV	2.46	0.9953 ± 0.0011	0.9928 ± 0.0006	0.2022	0.1986
10	B&W-1484 (4A.7)	Core XV <sup>††</sup>	2.46	0.9910 ± 0.0011	0.9909 ± 0.0006	0.2092	0.2014
11	B&W-1484 (4A.7)	Core XVI <sup>††</sup>	2.46	0.9935 ± 0.0010	0.9889 ± 0.0006	0.1757	0.1713
12	B&W-1484 (4A.7)	Core XVII	2.46	0.9962 ± 0.0012	0.9942 ± 0.0005	0.2083	0.2021
13	B&W-1484 (4A.7)	Core XVIII	2.46	1.0036 ± 0.0012	0.9931 ± 0.0006	0.1705	0.1708

**Table 4A.1**  
**Summary of Criticality Benchmark Calculations**

	Reference	Identification	Eurich.	Calculated $k_{eff}$		EALF <sup>†</sup> (eV)	
				MCNP4a	KENO5a	MCNP4a	KENO5a
14	B&W-1484 (4A.7)	Core XIX	2.46	0.9961 ± 0.0012	0.9971 ± 0.0005	0.2103	0.2011
15	B&W-1484 (4A.7)	Core XX	2.46	1.0008 ± 0.0011	0.9932 ± 0.0006	0.1724	0.1701
16	B&W-1484 (4A.7)	Core XXI	2.46	0.9994 ± 0.0010	0.9918 ± 0.0006	0.1544	0.1536
17	B&W-1645 (4A.8)	S-type Fuel, w/886 ppm B	2.46	0.9970 ± 0.0010	0.9924 ± 0.0006	1.4475	1.4680
18	B&W-1645 (4A.8)	S-type Fuel, w/746 ppm B	2.46	0.9990 ± 0.0010	0.9913 ± 0.0006	1.5463	1.5660
19	B&W-1645 (4A.8)	SO-type Fuel, w/1156 ppm B	2.46	0.9972 ± 0.0009	0.9949 ± 0.0005	0.4241	0.4331
20	B&W-1810 (4A.9)	Case 1 1337 ppm B	2.46	1.0023 ± 0.0010	NC	0.1531	NC
21	B&W-1810 (4A.9)	Case 12 1899 ppm B	2.46/4.02	1.0060 ± 0.0009	NC	0.4493	NC
22	French (4A.10)	Water Moderator 0 gap	4.75	0.9966 ± 0.0013	NC	0.2172	NC
23	French (4A.10)	Water Moderator 2.5 cm gap	4.75	0.9952 ± 0.0012	NC	0.1778	NC
24	French (4A.10)	Water Moderator 5 cm gap	4.75	0.9943 ± 0.0010	NC	0.1677	NC
25	French (4A.10)	Water Moderator 10 cm gap	4.75	0.9979 ± 0.0010	NC	0.1736	NC
26	PNL-3602 (4A.11)	Steel Reflector, 0 separation	2.35	NC	1.0004 ± 0.0006	NC	0.1018

**Table 4A.1**  
**Summary of Criticality Benchmark Calculations**

Reference	Identification	Enrich.	Calculated $k_{eff}$		EALF <sup>†</sup> (eV)		
			MCNP4a	KENO5a	MCNP4a	KENO5a	
27	PNL-3602 (4A.11)	Steel Reflector, 1.321 cm sepn.	2.35	0.9980 ± 0.0009	0.9992 ± 0.0006	0.1000	0.0909
28	PNL-3602 (4A.11)	Steel Reflector, 2.616 cm sepn	2.35	0.9968 ± 0.0009	0.9964 ± 0.0006	0.0981	0.0975
29	PNL-3602 (4A.11)	Steel Reflector, 3.912 cm sepn.	2.35	0.9974 ± 0.0010	0.9980 ± 0.0006	0.0976	0.0970
30	PNL-3602 (4A.11)	Steel Reflector, infinite sepn.	2.35	0.9962 ± 0.0008	0.9939 ± 0.0006	0.0973	0.0968
31	PNL-3602 (4A.11)	Steel Reflector, 0 cm sepn.	4.306	NC	1.0003 ± 0.0007	NC	0.3282
32	PNL-3602 (4A.11)	Steel Reflector, 1.321 cm sepn.	4.306	0.9997 ± 0.0010	1.0012 ± 0.0007	0.3016	0.3039
33	PNL-3602 (4A.11)	Steel Reflector, 2.616 cm sepn.	4.306	0.9994 ± 0.0012	0.9974 ± 0.0007	0.2911	0.2927
34	PNL-3602 (4A.11)	Steel Reflector, 5.405 cm sepn.	4.306	0.9969 ± 0.0011	0.9951 ± 0.0007	0.2828	0.2860
35	PNL-3602 (4A.11)	Steel Reflector, Infinite sepn. <sup>††</sup>	4.306	0.9910 ± 0.0020	0.9947 ± 0.0007	0.2851	0.2864
36	PNL-3602 (4A.11)	Steel Reflector, with Boral Sheets	4.306	0.9941 ± 0.0011	0.9970 ± 0.0007	0.3135	0.3150
37	PNL-3926 (4A.12)	Lead Reflector, 0 cm sepn.	4.306	NC	1.0003 ± 0.0007	NC	0.3159
38	PNL-3926 (4A.12)	Lead Reflector, 0.55 cm sepn.	4.306	1.0025 ± 0.0011	0.9997 ± 0.0007	0.3030	0.3044
39	PNL-3926 (4A.12)	Lead Reflector, 1.956 cm sepn.	4.306	1.0000 ± 0.0012	0.9985 ± 0.0007	0.2883	0.2930

**Table 4A.1**  
**Summary of Criticality Benchmark Calculations**

Reference	Identification	Enrich.	Calculated $k_{eff}$		EALF <sup>†</sup> (eV)		
			MCNP4a	KENO5a	MCNP4a	KENO5a	
40	PNL-3926 (4A.12)	Lead Reflector, 5.405 cm sepn.	4.306	0.9971 ± 0.0012	0.9946 ± 0.0007	0.2831	0.2854
41	PNL-2615 (4A.13)	Experiment 004/032 - no absorber	4.306	0.9925 ± 0.0012	0.9950 ± 0.0007	0.1155	0.1159
42	PNL-2615 (4A.13)	Experiment 030 - Zr plates	4.306	NC	0.9971 ± 0.0007	NC	0.1154
43	PNL-2615 (4A.13)	Experiment 013 - Steel plates	4.306	NC	0.9965 ± 0.0007	NC	0.1164
44	PNL-2615 (4A.13)	Experiment 014 - Steel plates	4.306	NC	0.9972 ± 0.0007	NC	0.1164
45	PNL-2615 (4A.13)	Exp. 009 1.05% Boron-Steel plates	4.306	0.9982 ± 0.0010	0.9981 ± 0.0007	0.1172	0.1162
46	PNL-2615 (4A.13)	Exp. 012 1.62% Boron-Steel plates	4.306	0.9996 ± 0.0012	0.9982 ± 0.0007	0.1161	0.1173
47	PNL-2615 (4A.13)	Exp. 031 - Boral plates	4.306	0.9994 ± 0.0012	0.9969 ± 0.0007	0.1165	0.1171
48	PNL-7167 (4A.14)	Experiment 214R - with flux trap	4.306	0.9991 ± 0.0011	0.9956 ± 0.0007	0.3722	0.3812
49	PNL-7167 (4A.14)	Experiment 214V3 - with flux trap	4.306	0.9969 ± 0.0011	0.9963 ± 0.0007	0.3742	0.3826
50	PNL-4267 (4A.15)	Case 173 - 0 ppm B	4.306	0.9974 ± 0.0012	NC	0.2893	NC
51	PNL-4267 (4A.15)	Case 177 - 2550 ppm B	4.306	1.0057 ± 0.0010	NC	0.5509	NC
52	PNL-5803 (4A.16)	MOX Fuel - Type 3.2 Exp. 21	20% Pu	1.0041 ± 0.0011	1.0046 ± 0.0006	0.9171	0.8868

Table 4A.1

Summary of Criticality Benchmark Calculations

Reference	Identification	Enrich.	Calculated $k_{eff}$		EALF <sup>†</sup> (eV)		
			MCNP4a	KENO5a	MCNP4a	KENO5a	
53	PNL-5803 (4A.16)	MOX Fuel - Type 3.2 Exp. 43	20% Pu	1.0058 ± 0.0012	1.0036 ± 0.0006	0.2968	0.2944
54	PNL-5803 (4A.16)	MOX Fuel - Type 3.2 Exp. 13	20% Pu	1.0083 ± 0.0011	0.9989 ± 0.0006	0.1665	0.1706
55	PNL-5803 (4A.16)	MOX Fuel - Type 3.2 Exp. 32	20% Pu	1.0079 ± 0.0011	0.9966 ± 0.0006	0.1139	0.1165
56	WCAP-3385 (4A.17)	Saxton Case 52 PuO <sub>2</sub> 0.52" pitch	6.6% Pu	0.9996 ± 0.0011	1.0005 ± 0.0006	0.8665	0.8417
57	WCAP-3385 (4A.17)	Saxton Case 52 U 0.52" pitch	5.74	1.0000 ± 0.0010	0.9956 ± 0.0007	0.4476	0.4580
58	WCAP-3385 (4A.17)	Saxton Case 56 PuO <sub>2</sub> 0.56" pitch	6.6% Pu	1.0036 ± 0.0011	1.0047 ± 0.0006	0.5289	0.5197
59	WCAP-3385 (4A.17)	Saxton Case 56 borated PuO <sub>2</sub>	6.6% Pu	1.0008 ± 0.0010	NC	0.6389	NC
60	WCAP-3385 (4A.17)	Saxton Case 56 U 0.56" pitch	5.74	0.9994 ± 0.0011	0.9967 ± 0.0007	0.2923	0.2954
61	WCAP-3385 (4A.17)	Saxton Case 79 PuO <sub>2</sub> 0.79" pitch	6.6% Pu	1.0063 ± 0.0011	1.0133 ± 0.0006	0.1520	0.1555
62	WCAP-3385 (4A.17)	Saxton Case 79 U 0.79" pitch	5.74	1.0039 ± 0.0011	1.0008 ± 0.0006	0.1036	0.1047

Notes: NC stands for not calculated.

<sup>†</sup> EALF is the energy of the average lethargy causing fission.

<sup>††</sup> These experimental results appear to be statistical outliers (> 3σ) suggesting the possibility of unusually large experimental error. Although they could justifiably be excluded, for conservatism, they were retained in determining the calculational basis.

Table 4A.2

COMPARISON OF MCNP4a AND KENO5a CALCULATED REACTIVITIES<sup>†</sup>  
FOR VARIOUS ENRICHMENTS

Enrichment	Calculated $k_{eff} \pm 1\sigma$	
	MCNP4a	KENO5a
3.0	0.8465 $\pm$ 0.0011	0.8478 $\pm$ 0.0004
3.5	0.8820 $\pm$ 0.0011	0.8841 $\pm$ 0.0004
3.75	0.9019 $\pm$ 0.0011	0.8987 $\pm$ 0.0004
4.0	0.9132 $\pm$ 0.0010	0.9140 $\pm$ 0.0004
4.2	0.9276 $\pm$ 0.0011	0.9237 $\pm$ 0.0004
4.5	0.9400 $\pm$ 0.0011	0.9388 $\pm$ 0.0004

---

<sup>†</sup> Based on the GE 8x8R fuel assembly.

Table 4A.3

MCNP4a CALCULATED REACTIVITIES FOR  
CRITICAL EXPERIMENTS WITH NEUTRON ABSORBERS

Ref.	Experiment		$\Delta k$ Worth of Absorber	MCNP4a Calculated $k_{eff}$	EALF <sup>†</sup> (eV)
4A.13	PNL-2615	Boral Sheet	0.0139	0.9994 ± 0.0012	0.1165
4A.7	B&W-1484	Core XX	0.0165	1.0008 ± 0.0011	0.1724
4A.13	PNL-2615	1.62% Boron-steel	0.0165	0.9996 ± 0.0012	0.1161
4A.7	B&W-1484	Core XIX	0.0202	0.9961 ± 0.0012	0.2103
4A.7	B&W-1484	Core XXI	0.0243	0.9994 ± 0.0010	0.1544
4A.7	B&W-1484	Core XVII	0.0519	0.9962 ± 0.0012	0.2083
4A.11	PNL-3602	Boral Sheet	0.0708	0.9941 ± 0.0011	0.3135
4A.7	B&W-1484	Core XV	0.0786	0.9910 ± 0.0011	0.2092
4A.7	B&W-1484	Core XVI	0.0845	0.9935 ± 0.0010	0.1757
4A.7	B&W-1484	Core XIV	0.1575	0.9953 ± 0.0011	0.2022
4A.7	B&W-1484	Core XIII	0.1738	1.0020 ± 0.0011	0.1988
4A.14	PNL-7167	Expt 214R flux trap	0.1931	0.9991 ± 0.0011	0.3722

<sup>†</sup>EALF is the energy of the average lethargy causing fission.

Table 4A.4

COMPARISON OF MCNP4a AND KENO5a  
CALCULATED REACTIVITIES<sup>†</sup> FOR VARIOUS <sup>10</sup>B LOADINGS

<sup>10</sup> B, g/cm <sup>2</sup>	Calculated $k_{\text{eff}} \pm 1\sigma$	
	MCNP4a	KENO5a
0.005	1.0381 $\pm$ 0.0012	1.0340 $\pm$ 0.0004
0.010	0.9960 $\pm$ 0.0010	0.9941 $\pm$ 0.0004
0.015	0.9727 $\pm$ 0.0009	0.9713 $\pm$ 0.0004
0.020	0.9541 $\pm$ 0.0012	0.9560 $\pm$ 0.0004
0.025	0.9433 $\pm$ 0.0011	0.9428 $\pm$ 0.0004
0.03	0.9325 $\pm$ 0.0011	0.9338 $\pm$ 0.0004
0.035	0.9234 $\pm$ 0.0011	0.9251 $\pm$ 0.0004
0.04	0.9173 $\pm$ 0.0011	0.9179 $\pm$ 0.0004

---

<sup>†</sup> Based on a 4.5% enriched GE 8x8R fuel assembly.

Table 4A.5

**CALCULATIONS FOR CRITICAL EXPERIMENTS WITH  
THICK LEAD AND STEEL REFLECTORS<sup>†</sup>**

Ref.	Case	E, wt%	Separation, cm	MCNP4a $k_{eff}$	KENO5a $k_{eff}$
4A.11	Steel Reflector	2.35	1.321	$0.9980 \pm 0.0009$	$0.9992 \pm 0.0006$
		2.35	2.616	$0.9968 \pm 0.0009$	$0.9964 \pm 0.0006$
		2.35	3.912	$0.9974 \pm 0.0010$	$0.9980 \pm 0.0006$
		2.35	$\infty$	$0.9962 \pm 0.0008$	$0.9939 \pm 0.0006$
4A.11	Steel Reflector	4.306	1.321	$0.9997 \pm 0.0010$	$1.0012 \pm 0.0007$
		4.306	2.616	$0.9994 \pm 0.0012$	$0.9974 \pm 0.0007$
		4.306	3.405	$0.9969 \pm 0.0011$	$0.9951 \pm 0.0007$
		4.306	$\infty$	$0.9910 \pm 0.0020$	$0.9947 \pm 0.0007$
4A.12	Lead Reflector	4.306	0.55	$1.0025 \pm 0.0011$	$0.9997 \pm 0.0007$
		4.306	1.956	$1.0000 \pm 0.0012$	$0.9985 \pm 0.0007$
		4.306	5.405	$0.9971 \pm 0.0012$	$0.9946 \pm 0.0007$

<sup>†</sup> Arranged in order of increasing reflector-fuel spacing.

Table 4A.6

CALCULATIONS FOR CRITICAL EXPERIMENTS WITH VARIOUS SOLUBLE BORON CONCENTRATIONS

Reference	Experiment	Boron Concentration, ppm	Calculated $k_{eff}$	
			MCNP4a	KENO5a
4A.15	PNL-4267	0	$0.9974 \pm 0.0012$	-
4A.8	B&W-1645	886	$0.9970 \pm 0.0010$	$0.9924 \pm 0.0006$
4A.9	B&W-1810	1337	$1.0023 \pm 0.0010$	-
4A.9	B&W-1810	1899	$1.0060 \pm 0.0009$	-
4A.15	PNL-4267	2550	$1.0057 \pm 0.0010$	-

Table 4A.7

## CALCULATIONS FOR CRITICAL EXPERIMENTS WITH MOX FUEL

Reference	Case <sup>†</sup>	MCNP4a		KENO5a	
		$k_{eff}$	EALF <sup>††</sup>	$k_{eff}$	EALF <sup>††</sup>
PNL-5803 [4A.16]	MOX Fuel - Exp. No. 21	1.0041 ± 0.0011	0.9171	1.0046 ± 0.0006	0.8868
	MOX Fuel - Exp. No. 43	1.0058 ± 0.0012	0.2968	1.0036 ± 0.0006	0.2944
	MOX Fuel - Exp. No. 13	1.0083 ± 0.0011	0.1665	0.9989 ± 0.0006	0.1706
	MOX Fuel - Exp. No. 32	1.0079 ± 0.0011	0.1139	0.9966 ± 0.0006	0.1165
WCAP-3385-54 [4A.17]	Saxton @ 0.52" pitch	0.9996 ± 0.0011	0.8665	1.0005 ± 0.0006	0.8417
	Saxton @ 0.56" pitch	1.0036 ± 0.0011	0.5289	1.0047 ± 0.0006	0.5197
	Saxton @ 0.56" pitch borated	1.0008 ± 0.0010	0.6389	NC	NC
	Saxton @ 0.79" pitch	1.0063 ± 0.0011	0.1520	1.0133 ± 0.0006	0.1555

Note: NC stands for not calculated

† Arranged in order of increasing lattice spacing.

†† EALF is the energy of the average lethargy causing fission.

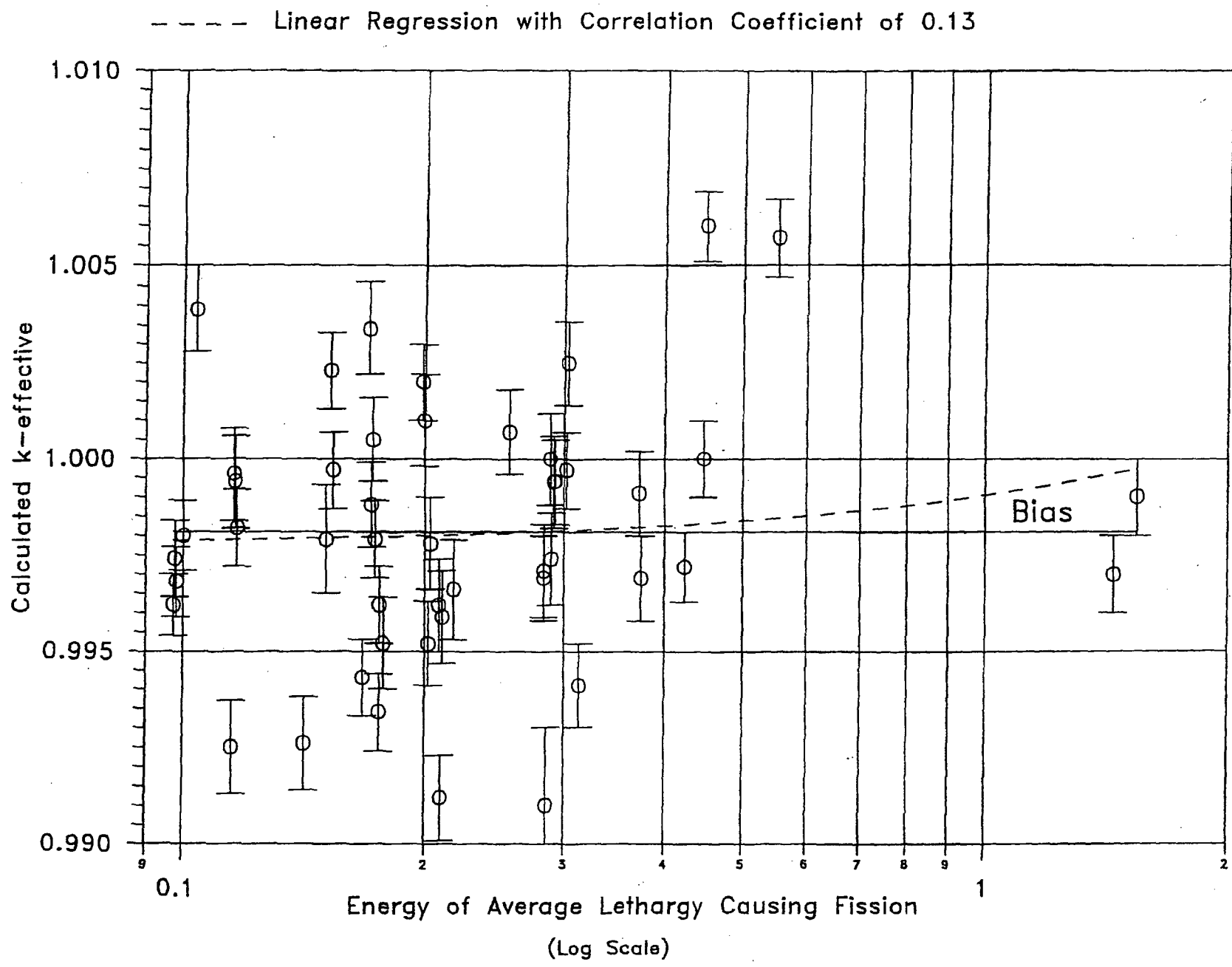


FIGURE 4A.1 MCNP CALCULATED k-eff VALUES for VARIOUS VALUES OF THE SPECTRAL INDEX

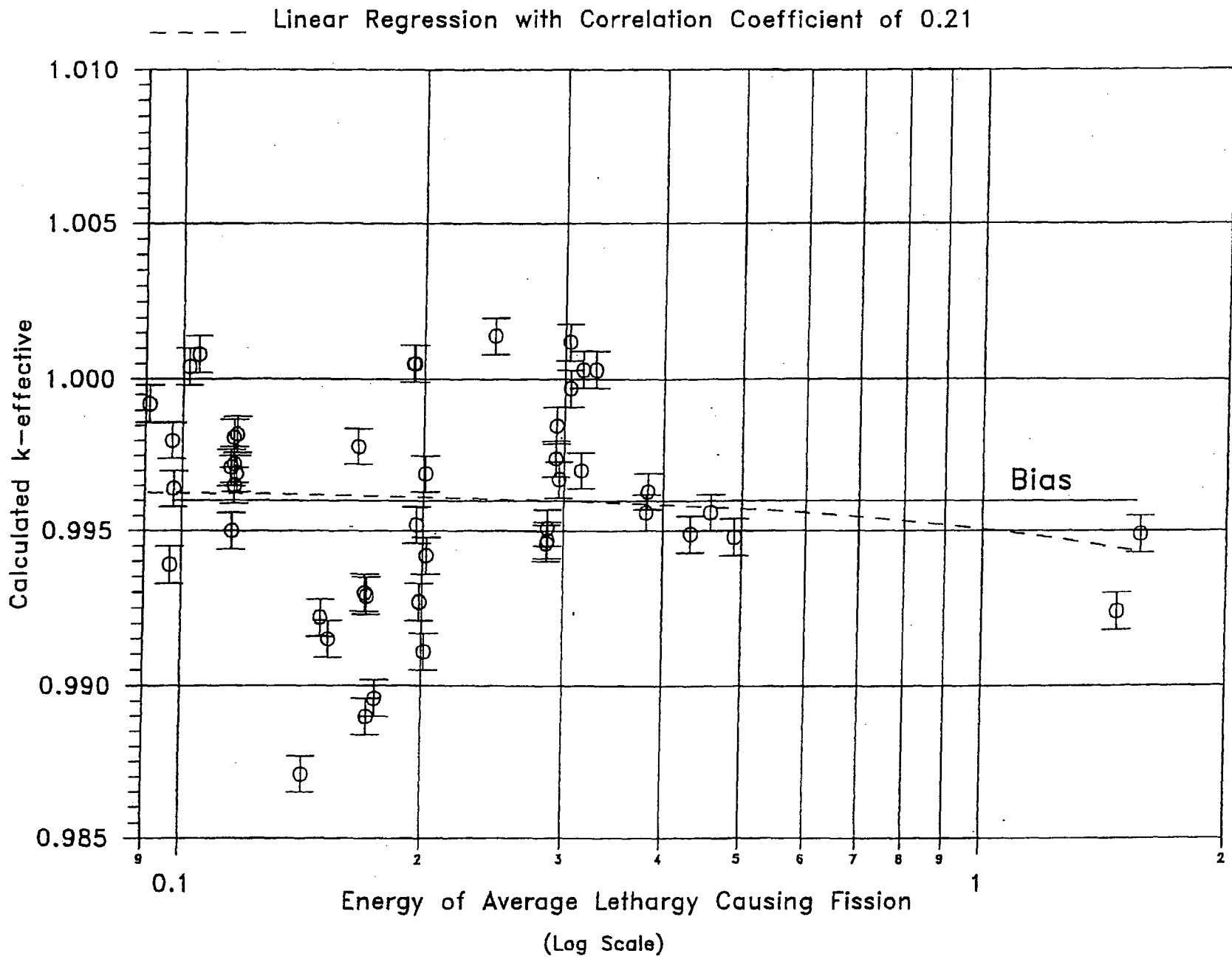


FIGURE 4A.2 KEN05a CALCULATED k-eff VALUES FOR VARIOUS VALUES OF THE SPECTRAL INDEX

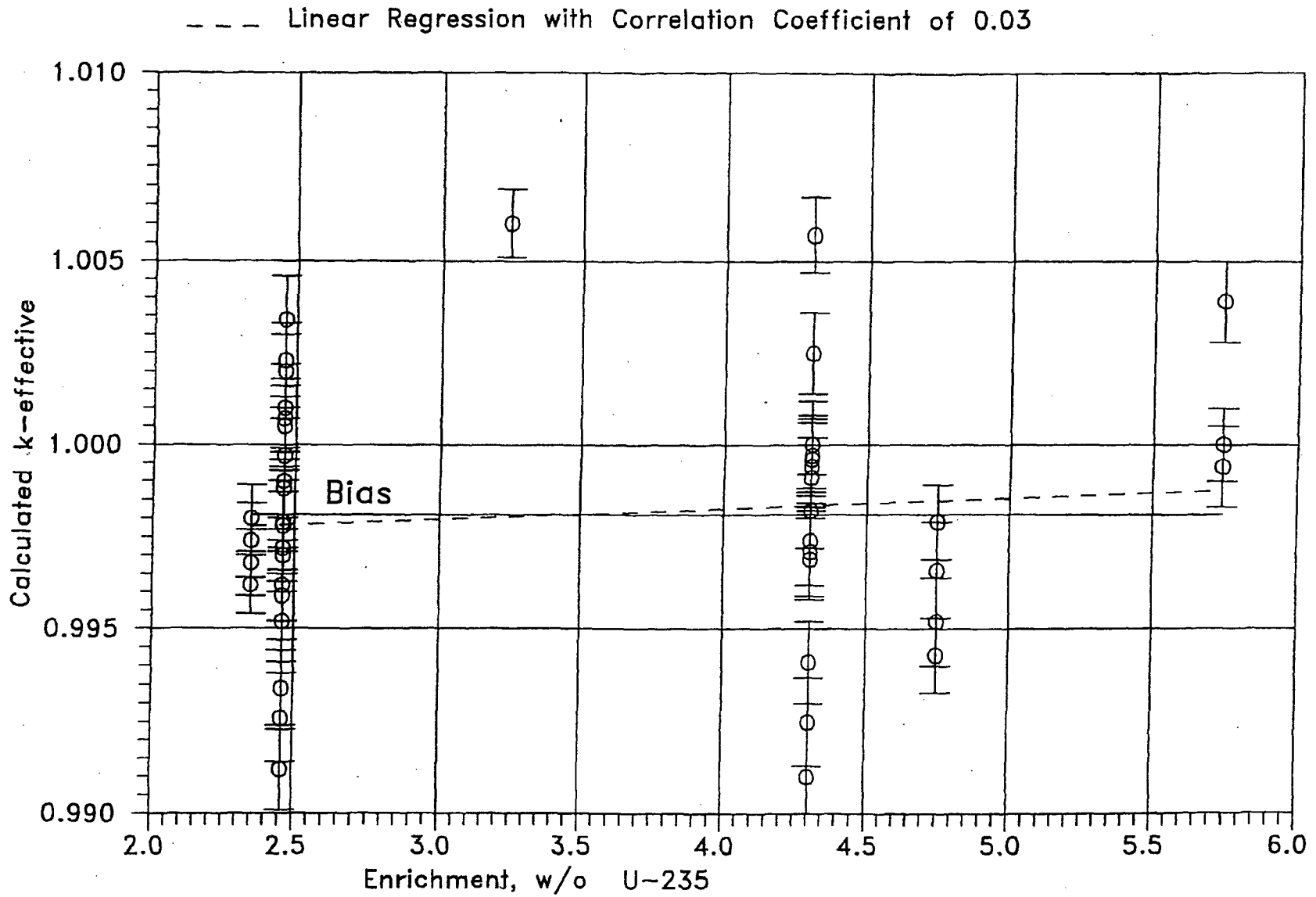


FIGURE 4A.3 MCNP CALCULATED k-eff VALUES AT VARIOUS U-235 ENRICHMENTS

--- Linear Regression with Correlation Coefficient of 0.38

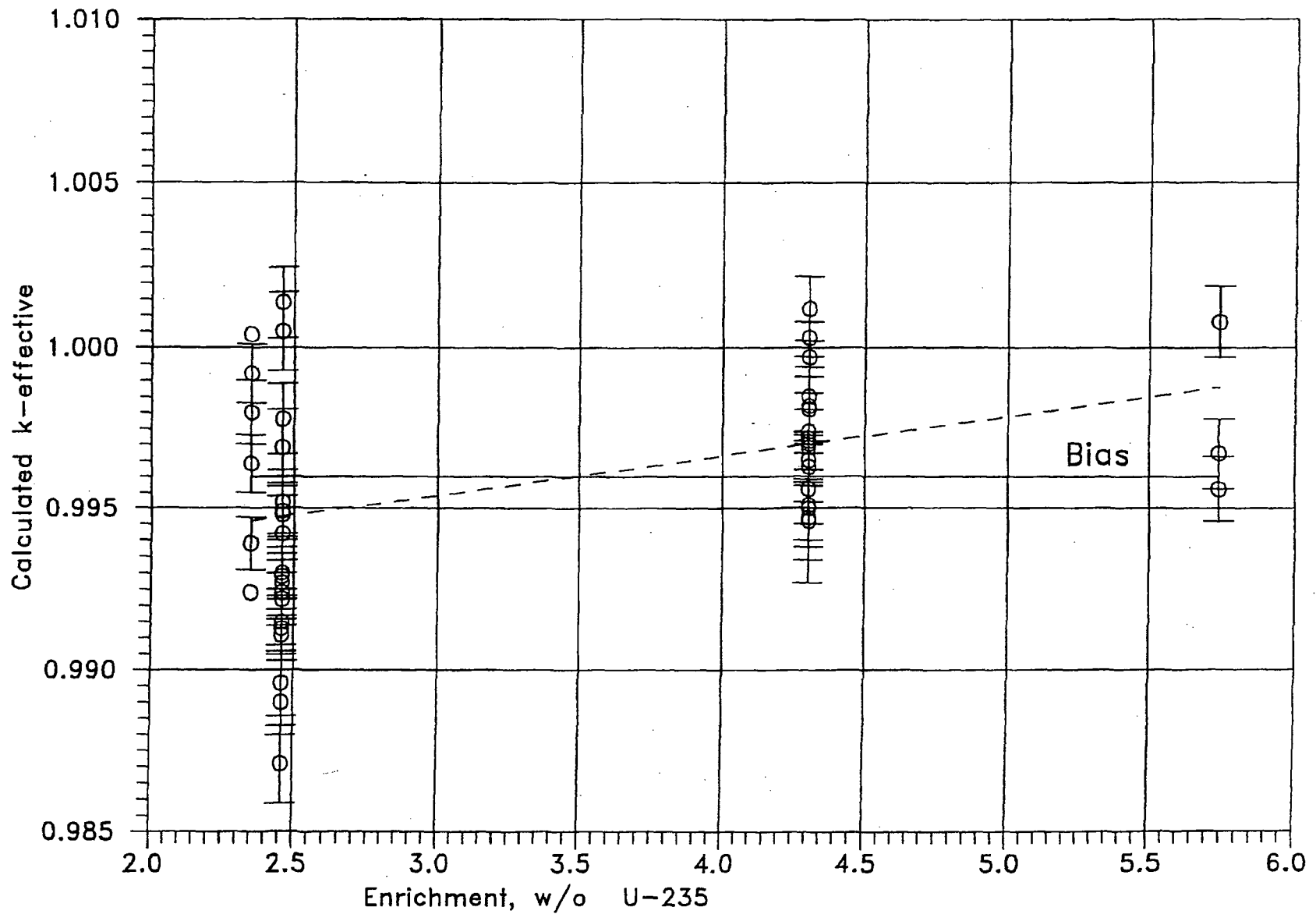


FIGURE 4A.4 KENO CALCULATED k-eff VALUES AT VARIOUS U-235 ENRICHMENTS

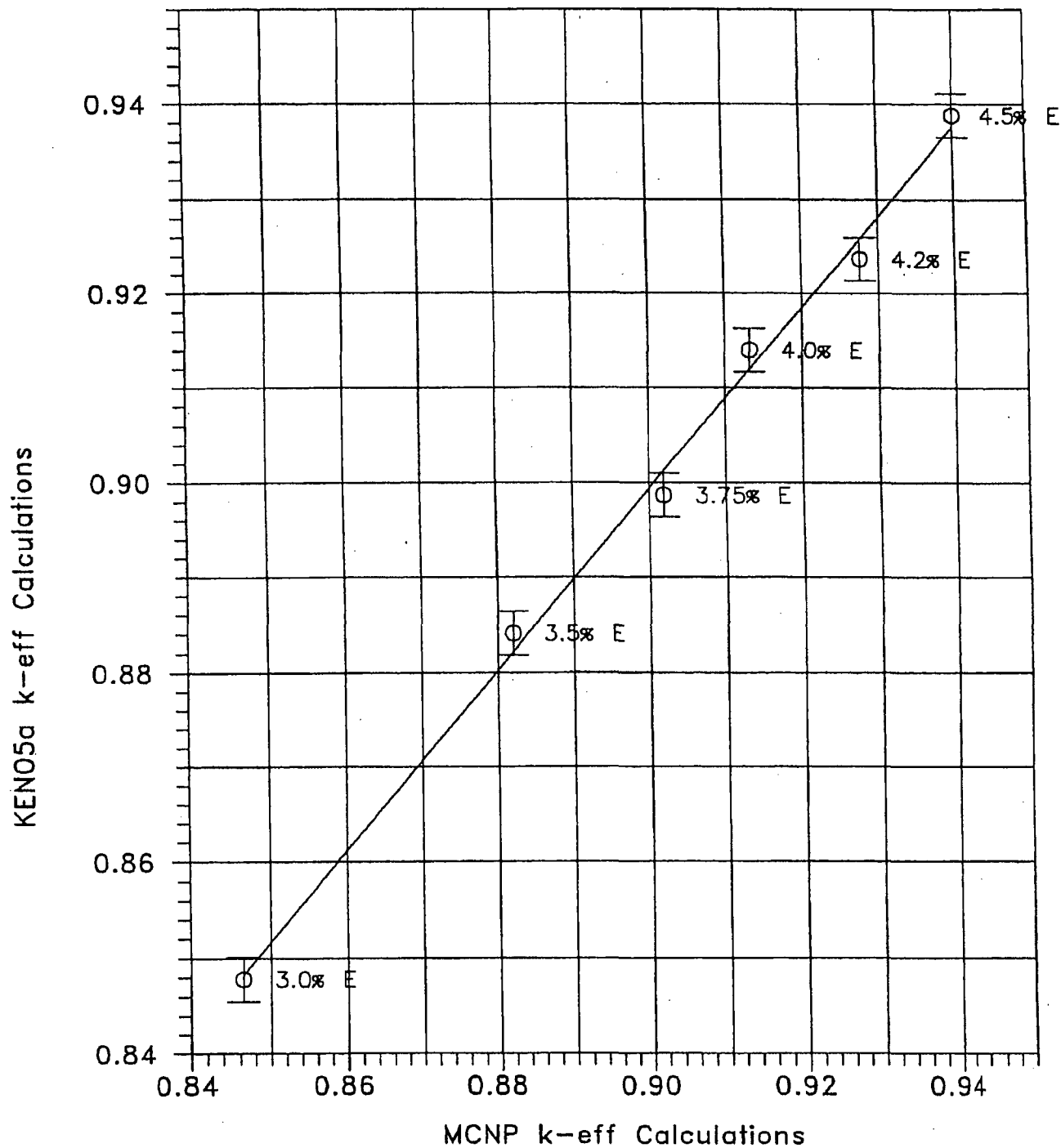


FIGURE 4A.5 COMPARISON OF MCNP AND KENO5A CALCULATIONS FOR VARIOUS FUEL ENRICHMENTS

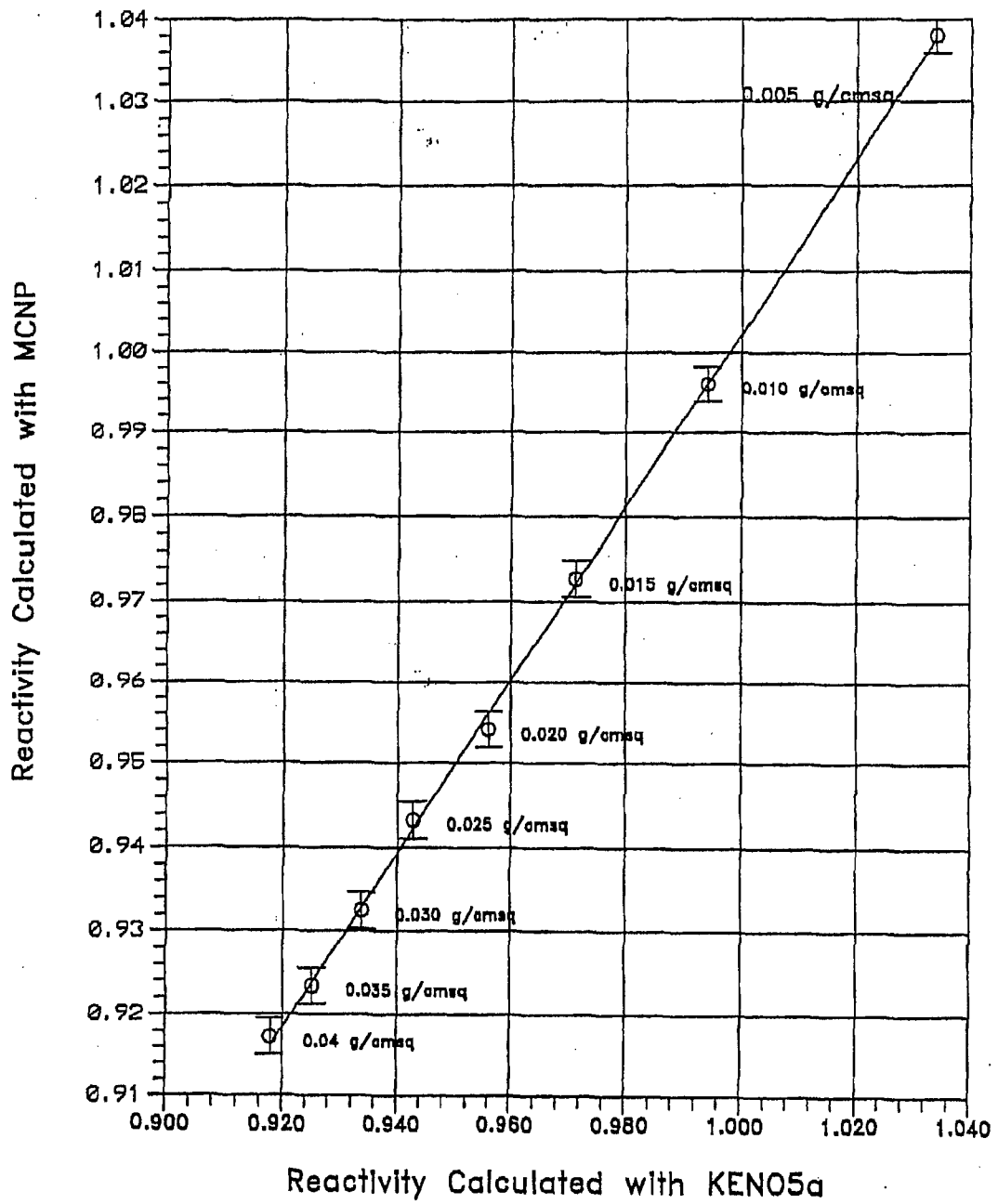


FIGURE 4A.6 COMPARISON OF MCNP AND KENO5a CALCULATIONS FOR VARIOUS BORON-10 AREAL DENSITIES

# Chapter 5: Thermal-Hydraulic Considerations

## 5.1 Introduction

This section provides a summary of the thermal-hydraulic analyses performed to demonstrate compliance of the ANO Unit 2 Spent Fuel Pool (SFP) and its attendant cooling system with the relevant provisions of USNRC Standard Review Plan (SRP) 9.1.3 (Spent Fuel Pool Cooling and Cleanup System, Rev. 1, July 1981) and Section III of the USNRC "OT Position Paper for Review and Acceptance of Spent Fuel Storage and Handling Applications," (April 14, 1978). Similar methods of thermal-hydraulic analysis have been used in the licensing evaluations for other SFP wet storage projects (e.g. USNRC Docket 50-313 (ANO-1), Dockets 50-275 and 50-323 (Diablo-Canyon 1 and 2), and 50-461 (Clinton)).

The thermal-hydraulic qualification analyses for the modified rack array may be broken down into the following categories:

- i. Evaluation of bounding maximum decay heat versus time profiles, used as input to subsequent analyses.
- ii. Evaluation of loss-of-forced cooling scenarios, to establish minimum times to perform corrective actions and the associated makeup water requirements.
- iii. Determination of the maximum local water temperature, at the instant when the pool decay heat reaches its maximum value, to establish that localized boiling in the Spent Fuel Storage Racks (SFSRs) is not possible while forced cooling is operating. The bulk pool temperature is postulated to be at the maximum limit.
- iv. Evaluation of the maximum fuel rod cladding temperature, at the instant when the pool decay heat reaches its maximum value, to establish that nucleate and film boiling are not possible while forced cooling is operating. The bulk pool temperature is postulated to be at the maximum limit.

The following sections present plant system descriptions, analysis methodologies and assumptions, a synopsis of the input data employed, and summaries of the calculated results.

## 5.2 Cooling System Description

The Spent Fuel Cooling (SFC) System is designed to maintain the water quality and clarity and to remove the decay heat from the stored fuel in the spent fuel pool. It is designed to maintain the spent fuel pool water less than or equal to 120°F under normal conditions. Refueling operations are administratively controlled in order to minimize the potential of exceeding a pool temperature of 150 °F during a full core discharge. The decay heat removal process is accomplished by recirculating spent fuel coolant water from the spent fuel pool through SFC system and back to the pool. The SFC system is a closed loop system consisting of two pumps and one full capacity shell and tube heat exchanger. The fuel pool water is drawn from the fuel pool near the surface and is circulated by the operating fuel pool pump through the tube side of the fuel pool heat exchanger, where heat is rejected to the service water flowing on the shell side. From the outlet of the fuel pool heat exchanger, the cooled fuel pool water is returned to the top of the fuel pool via a distribution header at the opposite end of the pool from the intake.

The clarity and purity of the water in the fuel pool, refueling cavity, and refueling water tank are maintained by the purification loop of the SFC System. The purification loop consists of the fuel pool purification pump, ion exchanger, filters, strainers, and an installed connection for a floating skimmer. The purification flow is drawn from the bottom of the fuel pool. A basket strainer is provided in the purification line to the pump suction to remove any relatively large particulate matter. The pump circulates the fuel pool water through a filter, which removes particulates larger than 5 microns in size, and through an ion exchanger to remove ionic material. Connections to the refueling water tank and refueling water cavity are provided for purification and makeup.

Makeup to the fuel pool is provided from the CVCS (Chemical and Volume Control System) via the blending tee, the refueling water tank via the purification pumps, or the BMS (Borated Makeup System) holdup tanks if chemistry specifications are met. In an emergency, Seismic Category I makeup is available from either service water system loop. The boric acid makeup tanks are also available for boration of the spent fuel pool. Overflow protection is provided by

transferring the fuel pool water on high level alarm to the refueling water tank or one of the BMS holdup tanks via the purification pump.

### 5.3 Spent Fuel Pool Decay Heat Loads

The decay heat in the SFP is generated in the spent fuel assemblies stored therein. In order to conservatively simplify the decay heat calculations, the total decay heat is considered as coming from two different groups of assemblies:

- i. Fuel assemblies from previous offloads already stored in the SFP
- ii. Fuel assemblies that are being offloaded from the reactor to the SFP

The fuel assemblies in the first group are referred to as previously offloaded fuel. Over the relatively short transient evaluation periods of this report the heat generation rate of these assemblies reduces very slowly with time, due to the exponential nature of radioactive decay and their relatively long decay periods. The decay heat contribution of these assemblies can therefore be conservatively treated as constant, neglecting any reduction in their decay heat contribution during the evaluation period. The fuel assemblies in the second group are referred to as recently offloaded fuel. The heat generation rate of these assemblies reduces rapidly with time, so the decay heat contribution of these assemblies is treated as time varying. The following equation defines the total decay heat generation in the SFP.

$$Q_{GEN}(\tau) = Q_P + F(\tau) \times Q_R(\tau) \quad (5-1)$$

where:

$Q_{GEN}(\tau)$  is the total time-varying decay heat generation rate in SFP, Btu/hr

$Q_P$  is the decay heat contribution of the previously offloaded fuel, Btu/hr

$F(\tau)$  is the fraction of the recently offloaded fuel transferred to the SFP

$Q_R(\tau)$  is the decay heat contribution of the recently offloaded fuel, Btu/hr

$\tau$  is the fuel decay time after reactor shutdown, hrs

Prior to the start of fuel transfer from the reactor to the SFP,  $F(\tau)$  is equal to zero and the total decay heat in the SFP will be equal to the invariant portion  $Q_P$ . During the fuel transfer,  $F(\tau)$  will increase linearly from zero to one, and the total decay heat in the SFP will increase to  $Q_P + Q_R(\tau)$ .

Following the completion of fuel transfer, the total decay heat in the SFP will decrease as  $Q_R(\tau)$  decreases.

The decay heat contributions of both the previously and recently offloaded fuel are determined using the Holtec QA validated computer program DECOR [5.3.1]. This computer program incorporates the Oak Ridge National Laboratory (ORNL) ORIGEN2 computer code [5.3.2] for performing decay heat calculations. The use of ORIGEN2 code has previously been accepted by the NRC for SFP decay heat calculations on multiple docket [e.g. USNRC Dockets 50-461 and 50-395].

Based on the input data provided in Tables 5.3.1 and 5.3.2, the fuel decay heat is determined for the following two offload scenarios:

1. Partial Core Offload - A refueling batch of 92 assemblies is offloaded from the plant's reactor into the SFP, completely filling all available storage locations. The total SFP inventory prior to the offload is 920 fuel assemblies, for a final post-offload inventory of 1012 fuel assemblies. This conservatively exceeds the storage capacity of the ANO-2 SFP (and the ANO-2 TS 4.3.3 limit of 988 assemblies) and is used for calculation of decay heat loads, which is conservative.
2. Full Core Offload - The full core of 177 assemblies is offloaded from the plant's reactor into the SFP, completely filling all available storage locations. The total SFP inventory prior to the offload is 920 fuel assemblies, for a final post-offload inventory of 1097 fuel assemblies. This conservatively exceeds the storage capacity of the ANO-2 SFP (and the ANO-2 TS limit of 988 assemblies) and is used for calculation of decay heat loads, which is conservative.

There are two types of fuel assemblies to be stored in the SFP: standard and NGF assemblies. While most of the differences between these two assembly types are minor from a heat-generation standpoint, the standard fuel contains approximately 2 kg more uranium per assembly that will result in higher decay heat loads. As such, all fuel assemblies discharged from the core are assumed to be the higher heat generating standard fuel assembly type.

## 5.4 Minimum Time-To-Boil And Maximum Boiloff Rate

The following conservatisms and assumptions are applied in the time-to-boil and boiloff rate calculations:

- The initial SFP bulk temperature is assumed to be equal to the bulk temperature limit of 150°F for the full core offload and 120°F for the partial core offload.
- The thermal inertia (thermal capacity) of the SFP is based on the net water volume only. This conservatively neglects the considerable thermal inertia of the fuel assemblies, stainless steel racks and stainless steel SFP liners.
- During the loss of forced cooling evaluations, it is assumed that makeup water is not available. This minimizes the thermal capacity of the SFP as water is boiled off, thus increasing the water level drop rate.
- The loss of forced cooling is assumed to occur coincident with the peak SFP bulk temperature and the maximum pool decay heat. Maximizing the initial temperature and the pool decay heat conservatively minimizes the calculated time-to-boil.

The governing enthalpy balance equation for this condition, subject to these conservative assumptions, can be written as:

$$C(\tau) \frac{dT}{d\tau} = Q_{gen} (\tau + \tau_0) \quad (5-2)$$

where:

$C(\tau)$  = Time-varying SFP thermal capacity (BTU/°F)

$\tau$  = Time after cooling is lost (hr)

$\tau_0$  = Loss of cooling time after shutdown (hr)

$T$  = Pool water temperature, (°F)

Equation 5-2 is solved to obtain the bulk pool temperature as a function of time, the time-to-boil, boil-off rate and water depth versus time. Once boiling begins, the ongoing evaporation of water will cause the water level of the SFP to decrease. The maximum water boil-off rate is determined by dividing the heat load by the latent heat of water at 212°F. The time required to drain the SFP

to the top of the fuel racks is determined by computing the amount of water above the racks and dividing by the boil-off rate. The major input values for these analyses are summarized in Table 5.4.1.

## 5.5 Maximum SFP Local Water Temperature

In order to determine an upper bound on the maximum SFP local water temperature, a series of conservative assumptions are made. The most important of these assumptions are:

- The walls and floor of the SFP are all modeled as adiabatic surfaces, thereby neglecting conduction heat loss through these items. This conservatively maximizes the net heat load, thereby maximizing both global and local temperatures.
- Heat losses by thermal radiation and natural convection from the hot SFP surface to the environment are neglected.
- No downcomer flow is assumed to exist between the rack modules.
- The hydraulic resistance parameters for the rack cells, permeability and inertial resistance, are conservatively adjusted by 10%. The conservatism bounds any small deviations in fuel assembly and rack geometry.
- The bottom plenum heights used in the model are less than the actual heights. This ensures that the effects of additional flow restrictions around rack pedestals and bearing pads are bounded in the model.
- The hydraulic resistance of every Spent Fuel Storage Rack (SFSR) cell includes the effects of blockage due to an assumed dropped fuel assembly lying horizontally on top of the SFSRs. This conservatively increases the total rack cell hydraulic resistance and bounds the thermal-hydraulic effects of a fuel assembly dropped anywhere in the spent fuel storage area.

The objective of this study is to demonstrate that the thermal-hydraulic criterion of ensuring local subcooled conditions in the SFP is met for all postulated fuel offload scenarios. The local

thermal-hydraulic analysis is performed such that slight fuel assembly variations are bounded. An outline of the Computational Fluid Dynamics (CFD) approach is described in the following. There are several significant geometric and thermal-hydraulic features of the ANO-2 SFP that need to be considered for a rigorous CFD analysis. From a fluid flow modeling standpoint, there are two regions to be considered. One region is the SFP bulk region where the classical Navier-Stokes equations [5.5.1] are solved, with turbulence effects included. The other region is the SFSRs containing heat generating fuel assemblies, located near the bottom of the SFP. In this region, water flow is directed vertically upwards due to buoyancy forces through relatively small flow channels formed by the fuel assemblies in each SFSR cell. This situation is modeled as a porous region with pressure drop in the flowing fluid governed by Darcy's Law as:

$$\frac{\partial P}{\partial X_i} = -\frac{\mu}{K(i)} V_i - C \rho |V| \frac{V_i}{2} \quad (5-3)$$

where  $\partial P/\partial X_i$  is the pressure gradient,  $K(i)$ ,  $V_i$  and  $C$  are the corresponding permeability, velocity and inertial resistance parameters,  $\rho$  is the fluid density, and  $\mu$  is the fluid viscosity. These terms are added as sink terms to the classic Navier-Stokes equations. The permeability and inertial resistance parameters for the rack cells loaded with fuel assemblies are determined based on friction factor correlations for the laminar flow conditions that would exist due to the low buoyancy induced velocities and the small size of the flow channels.

The ANO-2 SFP geometry requires an adequate portrayal of both large scale and small scale features, spatially distributed heat sources in the SFSRs and water inlet/outlet piping. Relatively cooler bulk water normally flows down between the perimeter of the fuel rack array and wall liner, a clearance known as the downcomer. Near the bottom of the racks the flow turns from a vertical to horizontal direction into the bottom plenum, supplying cooling water to the rack cells. Heated water flowing out of the top of the racks mixes with the bulk water. An adequate modeling of these features in the CFD program involves meshing the large scale bulk SFP region and small scale downcomer and bottom plenum regions with sufficient numbers of computational cells to capture both the global and local features of the flow field.

The distributed heat sources in the SFP racks are modeled by identifying distinct heat generation zones considering recently offloaded fuel, bounding peaking effects, and the presence of background decay heat from previous offloads. Two heat generating zones are modeled. The first consists of background fuel from previous offloads. The second zone consists of fuel from recently offloaded fuel assemblies. This is a conservative model, since all of the hot fuel assemblies from the recent offload are placed in a contiguous area. A uniformly distributed heat generation rate was applied throughout each distinct zone (i.e., there were no variations in heat generation rate within a single zone).

The CFD analysis was performed on the commercially available FLUENT [5.5.2] Computational Fluid Dynamics program, which has been benchmarked under Holtec's QA program. The FLUENT code enables buoyancy flow and turbulence effects to be included in the CFD analysis. Buoyancy forces are included by specifying a temperature-dependent density for water and applying an appropriate gravity vector. Turbulence effects are modeled by relating time-varying Reynolds' Stresses to the mean bulk flow quantities with the standard k- $\epsilon$  turbulence model.

Some of the major input values for this analysis are summarized in Table 5.5.1. An isometric view of the assembled CFD model is presented in Figure 5.5.1.

## **5.6 Fuel Rod Cladding Temperature**

The maximum fuel rod cladding temperature is determined to establish that nucleate and film boiling are not possible while forced cooling is operating. This requires demonstrating that the highest fuel rod cladding temperatures are less than the local saturation temperature of the adjacent SFP water. The maximum fuel cladding superheat above the local water temperature is calculated for the peak fuel rod heat emission rate.

A fuel rod can produce  $F_z$  times the average heat emission rate over a small length, where  $F_z$  is the axial peaking factor. The axial heat distribution in a rod is generally a maximum in the

central region, and tapers off at its two extremities. Thus, peak cladding heat flux over an infinitesimal rod section is given by the equation:

$$q_c = \frac{Q \times F_z}{A_c} \quad (5-4)$$

where  $Q$  is the rod average heat emission and  $A_c$  is the total cladding external heat transfer area in the active fuel length region. The axial peaking factor is given in Table 5.5.1.

As described previously, the maximum local water temperature was computed. Within each fuel assembly sub-channel, water is continuously heated by the cladding as it moves axially upwards under laminar flow conditions. Rohsenow and Hartnett [5.6.1] report a Nusselt-number for laminar flow heat transfer in a heated channel. The film temperature driving force ( $\Delta T_f$ ) at the peak cladding flux location is calculated as follows:

$$\begin{aligned} \Delta T_f &= \frac{q_c}{h_f} \\ h_f &= Nu \frac{K_w}{D_h} \end{aligned} \quad (5-5)$$

where  $h_f$  is the waterside film heat transfer coefficient,  $D_h$  is sub-channel hydraulic diameter,  $K_w$  is water thermal conductivity and  $Nu$  is the Nusselt number for laminar flow heat transfer.

In order to introduce some additional conservatism in the analysis, we assume that the fuel cladding has a crud deposit resistance  $R_c$  (equal to 0.0005 ft<sup>2</sup>-hr-°R/Btu) that covers the entire surface. Thus, including the temperature drop across the crud resistance, the cladding to water local temperature difference ( $\Delta T_c$ ) is given by the equation  $\Delta T_c = \Delta T_f + R_c \times q_c$ .

## 5.7 Results

This section contains results from the analyses performed for the postulated offload scenarios.

### **5.7.1 Decay Heat**

For the offload scenarios described in Section 5.3, the calculated SFP decay heat loads are summarized in Table 5.7.1. Given the conservatisms incorporated into the calculations, actual decay heat loads will be lower than these calculated values. Figures 5.7.1 and 5.7.2 each present profiles of net decay heat load versus time for the evaluated transient scenarios.

### **5.7.2 Minimum Time-To-Boil And Maximum Boiloff Rate**

For the offload scenarios and conditions described in Sections 5.3 and 5.4, the calculated times-to-boil and maximum boil-off rates are summarized in Table 5.7.2. These results show that, in the extremely unlikely event of a failure of forced cooling to the SFP, there would be at least 1.56 hours available for corrective actions prior to SFP boiling. Given the conservatisms incorporated into the calculations, actual times-to-boil will be higher than these calculated values. It is noted that a complete failure of forced cooling is extremely unlikely. The maximum water boiloff rate is less than or equal to 88 gpm.

### **5.7.3 Local Water and Fuel Cladding Temperatures**

Consistent with our approach to make conservative assessments of temperature, the local water temperature calculations described in Section 5.5 are performed for a SFP with a total decay heat generation equal to the calculated decay heat load coincident with the maximum SFP bulk temperature. Thus, the local water temperature evaluation is a calculation of the temperature increment over the theoretical spatially uniform value due to local hot spots (due to the presence of highly heat emissive fuel assemblies). As described in Section 5.6, the peak fuel clad superheat (i.e., the maximum clad-to-local water temperature difference) is determined. The resultant bounding superheat value was used to calculate a bounding maximum fuel clad temperature.

The numeric results of the maximum local water temperature and the bounding fuel cladding temperature evaluations are presented in Table 5.7.3. Figure 5.7.3 presents converged temperature contours in a vertical slice through the hot fuel region. Figure 5.7.4 presents converged velocity vectors in a vertical slice through the hot fuel region.

Both the maximum local water temperatures and the bounding fuel cladding temperatures are substantially lower than the 241°F, which is the boiling temperature at the depth of water corresponding to the top of the SFSRs. These results demonstrate that boiling cannot occur anywhere within the ANO-2 SFP.

Under a postulated accident scenario of the loss of all cooling, the water temperature will rise. Assuming a temperature of 212 °F at the inlet to the rack cells, and conservatively using the bounding bulk-to-local and local-to-clad temperature differences from Table 5.7.3, the maximum possible cladding temperature will be 280.3 °F, which is greater than the saturation temperature at the top of the active fuel length. Due to the low maximum assembly heat flux (approximately 2200 W/m<sup>2</sup>) and the critical heat flux required for departure from nucleate boiling (on the order of 10<sup>6</sup> W/m<sup>2</sup>), it can be concluded that the fuel cladding will not be subjected to departure from nucleate boiling, even under the postulated accident scenario of the loss of all SFP cooling, and the cladding integrity would be maintained.

## 5.8 References

- [5.3.1] "QA Documentation for DECOR," Holtec Report HI-971734, Revision 0.
- [5.3.2] A.G. Croff, "ORIGEN2 - A Revised and Updated Version of the Oak Ridge Isotope Generation and Depletion Code," ORNL-5621, Oak Ridge National Laboratory, 1980.
- [5.5.1] Batchelor, G.K., "An Introduction to Fluid Dynamics," Cambridge University Press, 1967.
- [5.5.2] FLUENT Version 5.5, Fluent Inc., 2001.
- [5.6.1] Rohsenow, N.M., and Hartnett, J.P., "Handbook of Heat Transfer," McGraw Hill Book Company, New York, 1973.

Table 5.3.1: Key Input Data for Decay Heat Computations

<b>Input Data Parameter</b>	<b>Value</b>
Reactor Thermal Power (MWt)	3100
Number of Assemblies in Reactor Core	177
Maximum Number of Storage Cells in SFP	988
Bounding Discharge Schedule	Table 5.3.2
Minimum In-Core Hold Time (hr)	100
Fuel Discharge Rate	5 per hour

Table 5.3.2: Offload Schedule

CYCLE NUMBER	CYCLE LENGTH (Months)	NUMBER OF DISCHARGED ASSEMBLIES
Cycle 1	18	92
Cycle 2	18	92
Cycle 3	18	92
Cycle 4	18	92
Cycle 5	18	92
Cycle 6	18	92
Cycle 7	18	92
Cycle 8	18	92
Cycle 9	18	92
Cycle 10	18	92

Table Notes:

1. To conservatively overestimate background decay heat, the refuel batch size and fuel burnup are maximized. Because a great bulk of the pool decay heat is contributed by the freshly discharged fuel, the overall impact of this overestimation on pool temperatures is quite modest.

**Table 5.4.1: Key Input Data for Time-To-Boil Evaluation**

SFP Surface Area	753.25 ft <sup>2</sup>
Pool Water Depth	39 feet 2 inches
Height of Racks	16.2 feet
SFP Net Water Volume	17299 ft <sup>3</sup>

**Note:**

The net water volume, used in these analyses, is the gross water volume (i.e., area times depth) above the fuel racks and stored fuel assemblies. This conservatively under-estimates the total thermal inertia of the pool.

**Table 5.5.1: Key Input Data for Local Temperature Evaluation**

Axial Peaking Factor	1.70
Number of Fuel Assemblies	988
Cooled SFP Water Flow Rate through SFC Heat Exchanger	3200 gpm*
Fuel Assembly Type	CE Standard/NGF 16x16
Fuel Rod Outer Diameter	0.382 inches
Active Fuel Length**	149.61 inches
Number of Rods per Assembly	236 rods
Rack Cell Inner Dimension	8.58 inches
Rack Cell Length	188.9 inches
Modeled Bottom Plenum Height	3 inches

\* Conservatively, a 20% lower flow rate than the two pumps capacity (each with a capacity of 2000 gpm) is used in the analysis.

\*\* Conservatively, the lowerbound value for the active fuel length for ANO-2 fuel assemblies is used in the analysis.

**Table 5.7.1: Result of SFP Decay Heat Calculations**

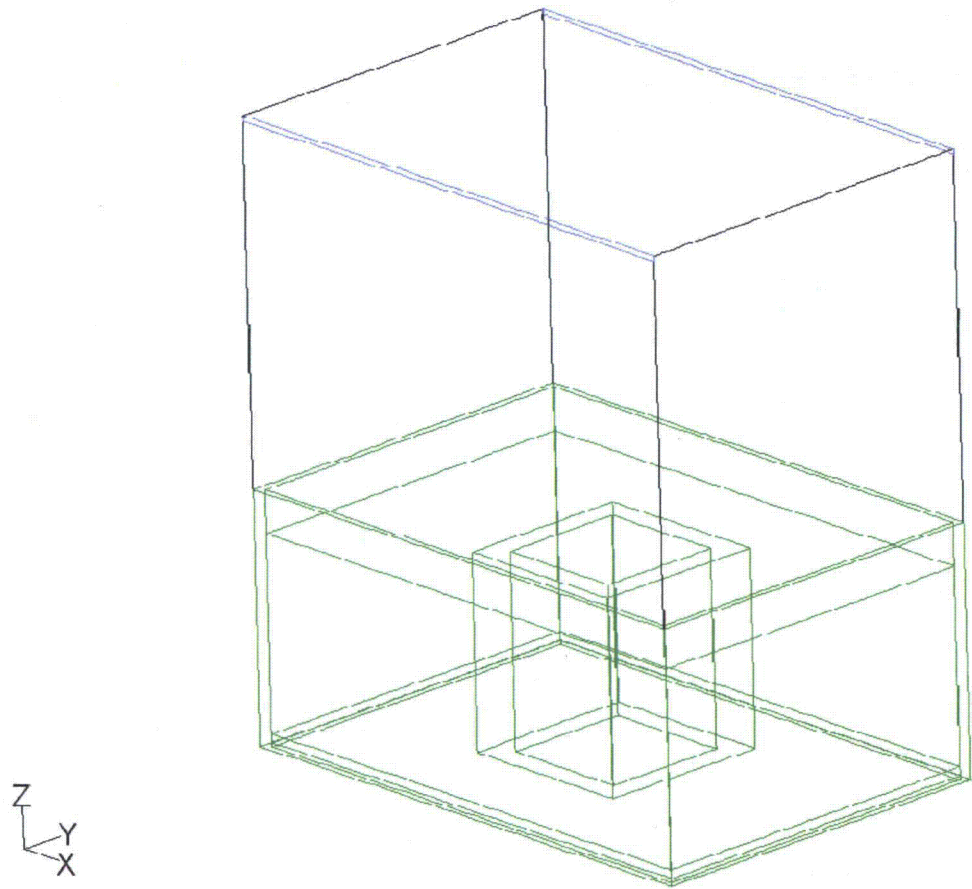
<b>Heat Load Component</b>	<b>Partial Core Offload Value (Btu/hr)</b>	<b>Full Core Offload Value (Btu/hr)</b>
Previously Discharged Fuel	$6.913 \times 10^6$	$6.913 \times 10^6$
Recently Discharged Fuel at End of Transfer	$19.737 \times 10^6$	$35.928 \times 10^6$
Total Bounding SFP Decay Heat	$26.65 \times 10^6$	$42.841 \times 10^6$

**Table 5.7.2: Results of Loss-of-Forced Cooling Evaluations**

<b>Calculate Result Parameter</b>	<b>Partial Core Offload Value</b>	<b>Full Core Offload Value</b>
Minimum Time-to-Boil	3.72 hours	1.56 hours
Maximum Boiloff Rate	55 gallons per minute	88 gallons per minute
Minimum Time for Water to Drop to Top of Racks	41.38 hours	24.98 hours

Table 5.7.3: Results of Maximum Local Water and Fuel Cladding Temperature Evaluations

<b>Parameter</b>	<b>Value</b>
Peak Local Water Temperature	188 °F
Peak Cladding Superheat	30.3 °F
Peak Local Fuel Cladding Temperature	218.3 °F



Grid

Oct 18, 2006  
FLUENT 5.5 (3d, segregated, ke)

**FIGURE 5.5.1: SCHEMATIC OF THE CFD MODEL OF THE ANO-2 SFP**

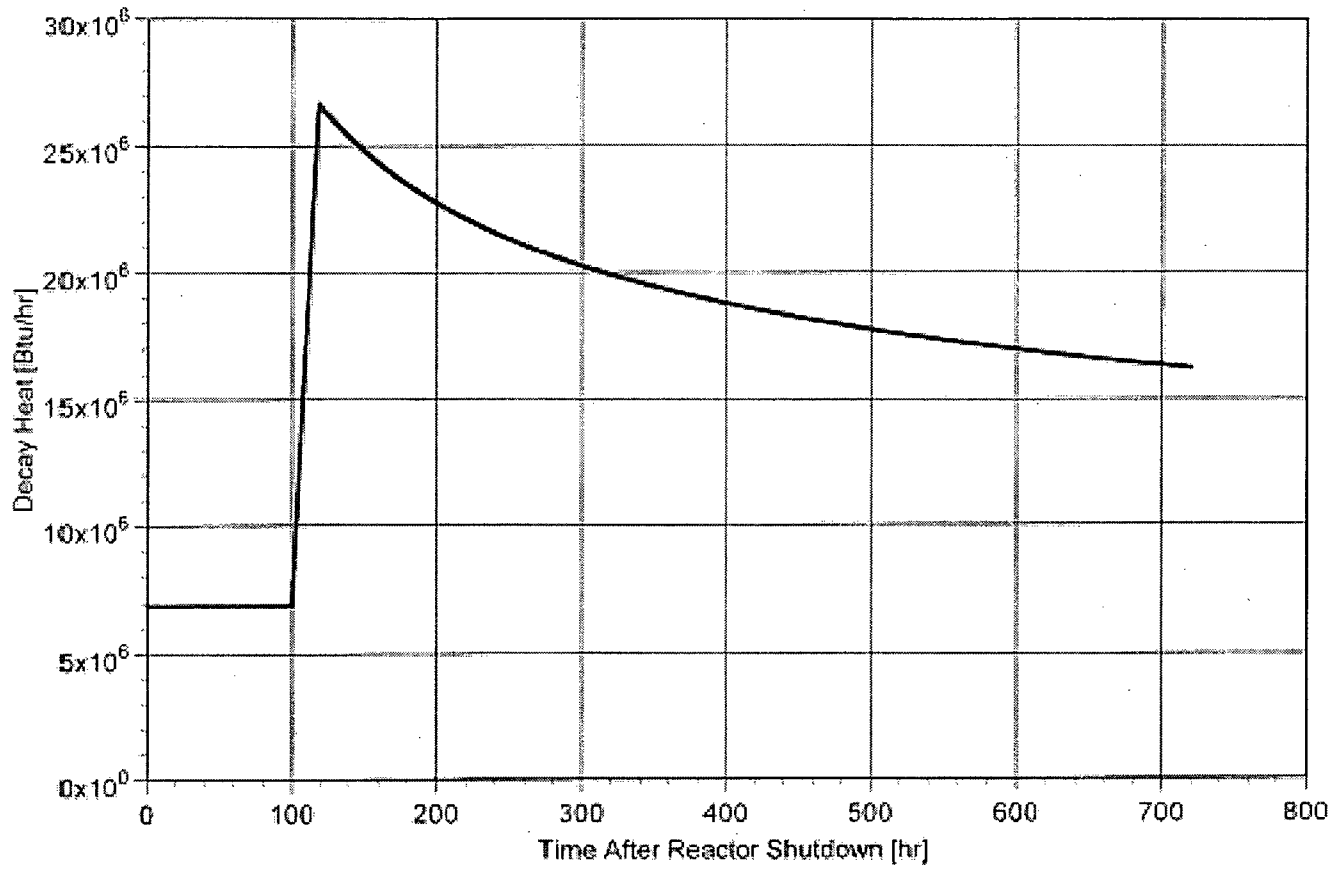


**FIGURE 5.7.1: NORMAL OFFLOAD BOUNDING SPENT FUEL HEAT LOAD**

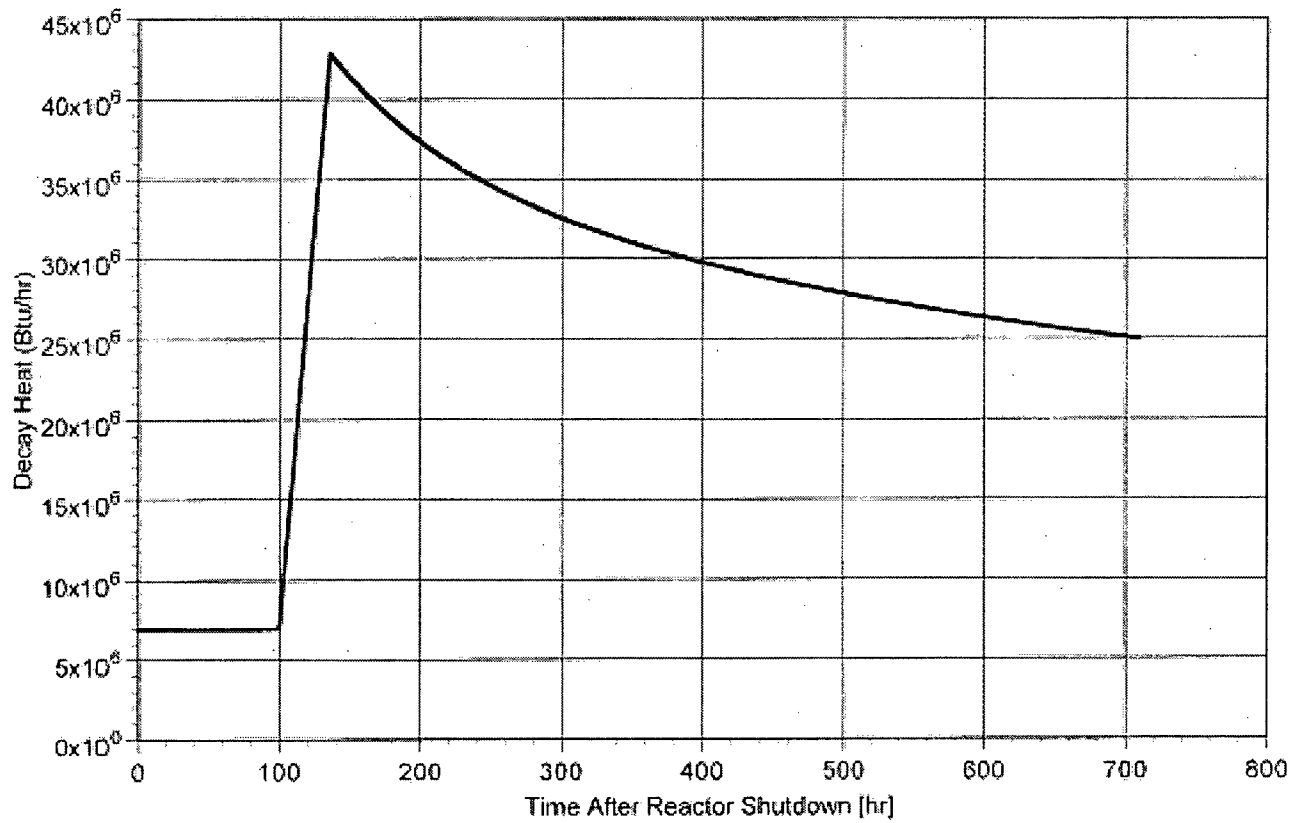
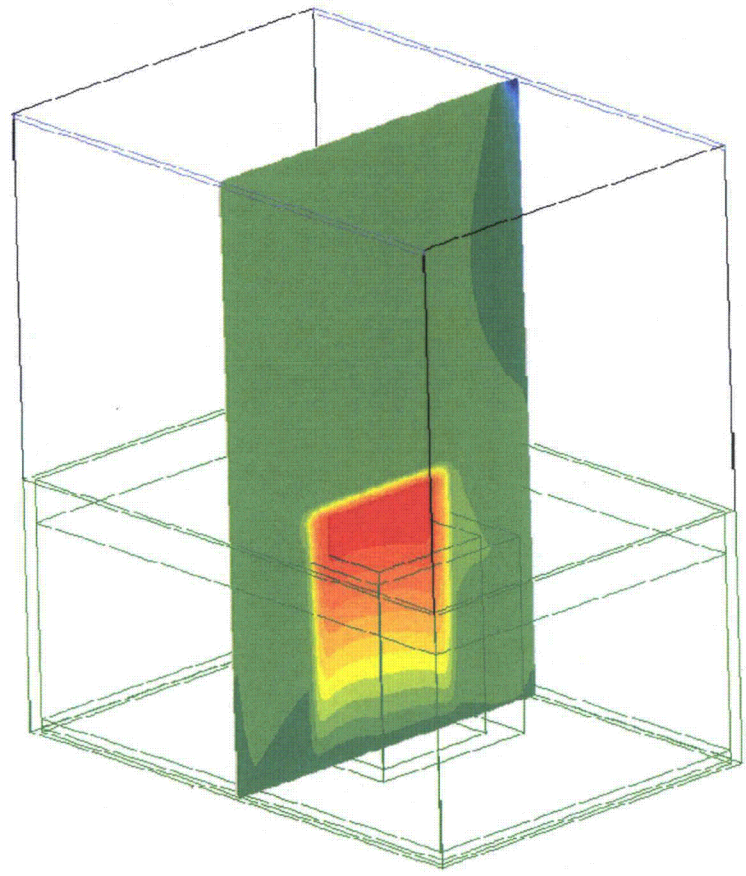
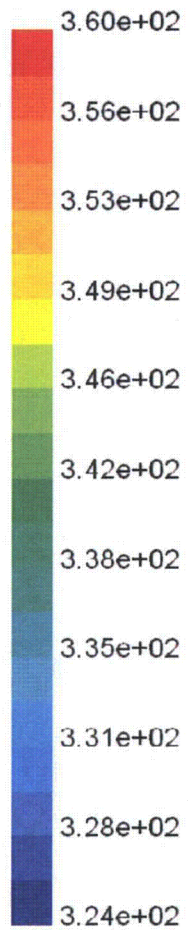


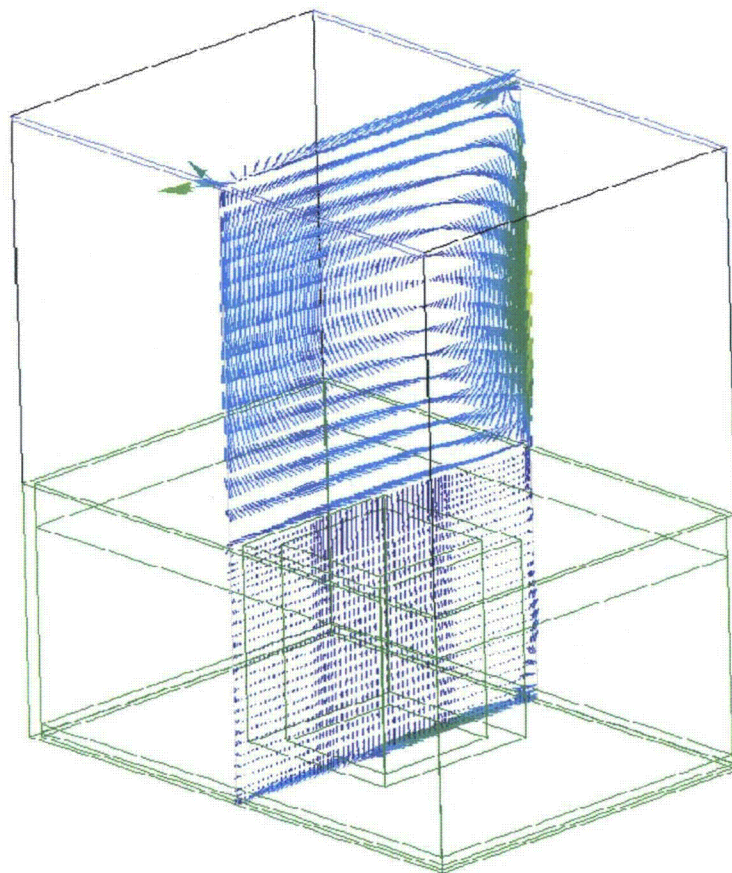
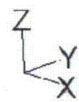
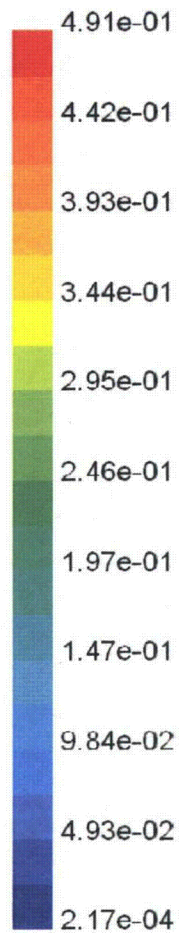
**FIGURE 5.7.2: FULL-CORE DISCHARGE OFFLOAD BOUNDING SPENT FUEL HEAT LOAD**



Contours of Static Temperature (k)

Oct 18, 2006  
 FLUENT 5.5 (3d, segregated, ke)

**FIGURE 5.7.3: CONTOURS OF STATIC TEMPERATURE IN A VERTICAL PLANE THROUGH THE CENTER OF THE SFP**



Velocity Vectors Colored By Velocity Magnitude (m/s)

Oct 18, 2006  
 FLUENT 5.5 (3d, segregated, ke)

**FIGURE 5.7.4: VELOCITY VECTOR PLOT IN A VERTICAL PLANE THROUGH THE CENTER OF THE SFP**

# Chapter 6: Installation

## 6.1 Introduction

The installation phase of the fuel storage rack project will be executed by Holtec International's Field Services Division. Holtec, serving as the installer, is responsible for performance of specialized services, such as welding operations, as necessary. All installation work will be performed in compliance with NUREG-0612 (invoked in Chapter 2), Holtec Quality Assurance Procedures, Holtec project specific rack installation procedures, and applicable site programs and procedures.

Crane and fuel bridge operators are trained in the operation of overhead cranes per the requirements of ANSI/ASME B30.2, and the plant's specific training program. Consistent with the installer's past practices, a videotape aided or equivalent training session is presented to the installation team, all of whom are required to successfully complete a written examination prior to the commencement of work. Fuel handling bridge operations are performed by site personnel, who are trained in accordance with site procedures.

Rack lifting devices are required for the handling of new racks and existing racks. The lifting devices are designed to engage and disengage on lift points at the bottom of the racks. The lifting devices comply with the provisions of ANSI N14.6-1978 and NUREG-0612, including compliance with the design stress criteria, load testing at a multiplier of maximum working load, and nondestructive examination of critical welds.

A surveillance and inspection program shall be maintained as part of the installation of the racks. A set of inspection points, which have been proven to eliminate any incidence of rework or erroneous installation in previous rack projects, is implemented by the installer.

Holtec International developed procedures will be used in conjunction with the site procedures to cover the scope of activities for the rack removal and installation effort. Similar procedures have been utilized and successfully implemented by Holtec on previous rereack projects. These

procedures are written to include ALARA (As Low As Reasonably Achievable) practices and provide requirements to assure equipment, personnel, and plant safety. These procedures are reviewed and approved in accordance with site administrative procedures prior to use. The following is a list of the Holtec procedures, used in addition to the site procedures to implement the installation phase of the project.

A. Installation/Removal and Handling Procedure:

This procedure provides direction for the installation, removal, and handling of the new and existing storage rack modules in the spent fuel pool. This procedure delineates the steps necessary to receive the new racks on site, the proper method for unloading and uprighting the racks, staging the racks prior to installation, removal and packaging of existing racks, and installation of the new racks. The procedure provides for the installation of the new racks, their height and level adjustments of the rack pedestals and verification of the as-built field configuration to ensure compliance with design documents.

B. Receipt Inspection Procedure:

This procedure delineates the steps necessary to perform a thorough receipt inspection of a new rack module after its arrival on site. The receipt inspection includes dimensional measurements, cleanliness inspection, visual weld examination, and verticality measurements.

C. Cleaning Procedure:

This procedure provides for the cleaning of a new rack module, if required. The modules are to meet the requirements of ANSI N45.2.1, Level B, prior to placement in the spent fuel pool. Methods and limitations on cleaning materials to be utilized are provided.

#### D. Pre- and Post-Installation Drag Test Procedure:

These two procedures stipulate the requirements for performing a functional test on a new rack module prior to and following installation. The procedures provide direction for inserting and withdrawing an insertion gage into designated cell locations, and establish an acceptance criterion in terms of maximum drag force. Pre-installation drag testing may be performed either at the fabrication facility or at the site.

#### E. ALARA Procedure:

Consistent with Holtec International's ALARA Program, this procedure provides guidance to minimize the total man-rem received during the rack installation project, by accounting for time, distance, and shielding. This procedure will be used in conjunction with the site ALARA program.

#### F. Underwater Welding Procedure:

Underwater welding procedures are utilized for welding back previously cut and removed spent fuel pool obstructions or as identified during installation of the new storage racks. The procedures contain appropriate qualification records documenting relevant variables, parameters, and limiting conditions. The weld procedure is qualified in accordance with ASME Section XI, or may be qualified to an alternate code accepted by both the owner and Holtec International.

## **6.2 Rack Arrangement**

The fuel storage rack project will not change the rack arrangement in the spent fuel pool. Three existing Region 1 racks will be replaced by three new Region 1 racks that have the same array sizes, storage capacities, cell pitch and approximate dimensions (length, width and height).

## **6.3 Rack Interferences**

The new Region 1 racks will have the same approximate dimensions (length, width and height) as the existing Region 1 racks. While several structures that interfere with rack removal and installation will be temporarily removed, there should be no new interferences following rack installation and restoration of these structures.

#### **6.4 SFP Cooling**

The pool cooling system shall be operated in order to maintain the pool water temperature at an acceptable level. It is anticipated that none of the installation activities will require the temporary shutdown of the spent fuel pool cooling system.

If a temporary shutdown of the spent fuel pool cooling system were required, the estimated time after shutdown to increase the pool bulk coolant temperature to a selected value of  $\leq 120^{\circ}\text{F}$  will be determined. A temperature of  $\leq 120^{\circ}\text{F}$  is chosen with enough margin such that cooling may be restored to ensure the pool bulk temperature will not exceed  $150^{\circ}\text{F}$ .

#### **6.5 Removal of Existing Racks and Installation of New Racks**

For existing rack removal from the spent fuel pool, the racks will be cleaned via pressure washing and surveyed by Health Physics prior to removal from the spent fuel pool. All existing rack handling shall be completed by the Fuel Building Crane. The removed racks shall be moved to a designated area for packaging and preparation for shipment to an approved disposal facility.

Installation of the new racks, supplied by Holtec International, involves the following activities. The racks are delivered in the horizontal position. A new rack module is removed from the shipping trailer using a suitably rated crane, while maintaining the horizontal configuration. The rack is placed on the up-ender and secured. Using two independent overhead hooks, or a single overhead hook and a spreader beam, the module is up-righted into a vertical position.

The new rack lifting device is engaged in the lift points at the bottom of the rack. The rack is then transported to a pre-leveled surface where, after leveling the rack, the appropriate quality control receipt inspection is performed (see Section 6.1, Items B and D).

The spent fuel pool floor is inspected and any debris that may inhibit the installation of the racks is removed. The new rack module is lifted with the Fuel Building Crane and transported along the pre-established safe load path. The rack module is carefully lowered into the spent fuel pool.

Elevation readings are taken to confirm that the module is level and the pedestal heights are adjusted as necessary to achieve level. In addition, rack-to-wall and rack-to-rack off-set distances (gaps) are also measured. Adjustments are made as necessary to ensure compliance with design documents. The lifting device is then disengaged and removed from the spent fuel pool under Health Physics direction. As directed by procedure, post-installation free path verification of individual cells is performed using an inspection gage (see Section 6.1, Item D).

All of the rack removal and installation activities in the SFP floor area will take place within a defined foreign material exclusion zone. At the completion of all activities, the SFP floor area shall be confirmed to be at the same level of cleanliness and condition that existed prior the start of installing the new racks.

## **6.6 Safety, Health Physics, and ALARA Methods**

### **6.6.1 Safety**

During the installation phase of the fuel storage rack project, personnel safety is of paramount importance. All work shall be carried out in compliance with applicable approved procedures.

### **6.6.2 Health Physics**

Health Physics is carried out per the requirements of the site radiation protection program.

### 6.6.3 ALARA

The key factors in maintaining project dose As Low As Reasonably Achievable (ALARA) are time, distance, and shielding. These factors are addressed by utilizing many mechanisms with respect to project planning and execution.

#### Time

Each member of the project team is trained and provided appropriate education and understanding of critical evolutions. Additionally, daily pre-job briefings are employed to acquaint each team member with the scope of work to be performed and the proper means of executing such tasks. Such pre-planning devices reduce worker time within the radiological controlled area and, therefore, project dose.

#### Distance

Remote tooling such as lift fixtures, pneumatic grippers, a support leveling device and a lift rod disengagement device have been developed to execute numerous activities from the SFP surface, where dose rates are relatively low.

#### Shielding

During the course of the fuel storage rack project, primary shielding is provided by the water in the spent fuel pool. The amount of water between an individual at the surface and an irradiated fuel assembly is an essential shield that reduces dose. Additionally, other shielding may be employed to mitigate dose when work is performed around high dose rate sources. If necessary, additional shielding may be utilized to meet ALARA principles.

## **6.7 Radwaste Material Control**

Radioactive waste generated from the rack installation will be controlled in accordance with established site procedures.

**Attachment 6**

**2CAN030706**

**Structural / Seismic Considerations  
for Replacement of Three Spent Fuel Racks at ANO-2**

**STRUCTURAL/SEISMIC CONSIDERATIONS FOR REPLACEMENT OF THREE  
SPENT FUEL RACKS AT ANO-2**

## 1.0 Introduction

The overall design objectives of the spent fuel storage pool at Arkansas Nuclear One (ANO) Unit 2 are governed by various Regulatory Guides, the Standard Review Plan, and industry standards. The replacement of the existing three boraflex poison rack modules, with new rack modules by Holtec, International, which use Metamic poison panels, increases the deadweight load from these racks, changes the load distribution from the racks to the pool, and additionally changes the seismic load effects from the affected racks on the pool structure. The structural adequacy of the new Spent Fuel Pool (SFP) rack modules at ANO Unit 2, and the effects of replacing the existing poison rack modules with the new rack modules on the SFP structure were evaluated using the appropriate regulatory and design standards. Postulated loadings for normal, seismic, and accident conditions at the ANO Unit 2 site are considered in this analysis and evaluation.

The design adequacy of the new racks is confirmed with analyses that are performed in compliance with the USNRC Standard Review Plan [1], the USNRC Office of Technology Position Paper [2], Lawrence Livermore Report UCRL52342 [3] and ANO Specification APL-C-2502 [4].

This report is a summary of the Ref. [5] detailed calculation performed to assess the design adequacy of the new Holtec racks, the Reference [6] calculation performed to assess the effect of the change in loads to the spent fuel pool structure, and the Reference [20] calculation performed to address a fuel assembly drop accident, and a SFP gate drop accident.

## 2.0 Rack Layout and Description

### 2.1 Rack Layout Description

The ANO Unit 2 Spent Fuel Pool contains twelve independent rack modules designed to hold the spent fuel assemblies and control element assemblies in storage for long term decay. There are two regions of racks. The current Region 1 racks use Boroflex as the poison material. Region 2 racks do not have any poison material. The Region 1 racks are being replaced by racks from Holtec, which use Metamic panels as the poison material. The pool layout is illustrated in Figure 2.1. Figure 2.2 shows the plan dimensions including the clearances between rack modules and between the rack modules and pool walls. The X and Y coordinate axes and rack identification used in the analytical model development are also indicated.

The existing racks are free standing on fourteen feet (or pedestals) that rest on the bottom of the pool. The twelve racks, originally designed by Westinghouse, are self-supporting and are not connected to each other or to the SFP walls. There are three basic configurations for the rack modules. Region 1 consists of one 8 cell x 9 cell rack module and two 9 cell x 9 cell rack modules. Region 2 consists of two 8 cell x 10 cell rack modules, four 9 cell x 10 cell rack modules, one 8 cell x 9 cell rack module, and two 9 cell x 9 cell rack modules. Aside from the cell configuration, the Westinghouse racks are structurally the same. The three Region 1 replacement rack modules by Holtec are also free standing, but have only four feet (pedestals) per rack module. The new Holtec racks consist of one 8 cell x 9 cell rack module, and two 9 cell x 9 cell rack modules, to match the existing configuration for the racks being replaced.

## Stevenson & Associates Report 06Q3571.07-01

In addition to the cell arrangements, the new Holtec racks with Metamic panels are dimensionally similar to the existing Westinghouse Boraflex racks. Cell ID is maintained at 8.58 inches and cell pitch is maintained at 9.8 inches. Overall height of 195.125 inches is slightly greater for the new racks, compared to 192.37 inches for the existing racks. The Metamic panels are contained in sheathing plates on the outside of the rack cells. The Metamic panels are considered non-structural, and are therefore included in the rack models as added mass. Due to Metamic being considerably "softer" than the stainless steel cell walls and sheathing, demonstration of structural adequacy for the cell walls and sheathing assures the Metamic panels are adequate for seismic load effects, without further review.

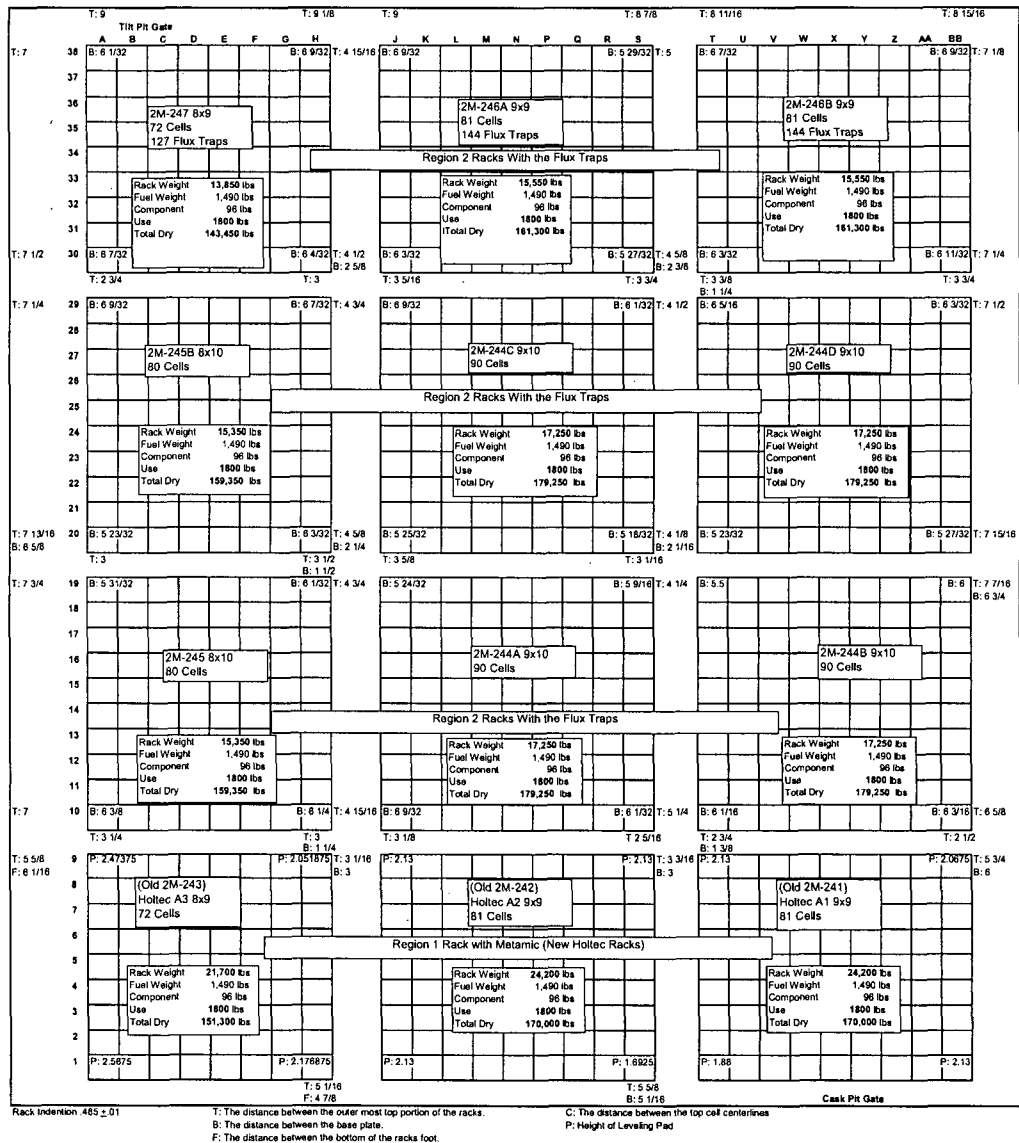


**Figure 2.1 - ANO Unit 2 Spent Fuel Pool Layout**

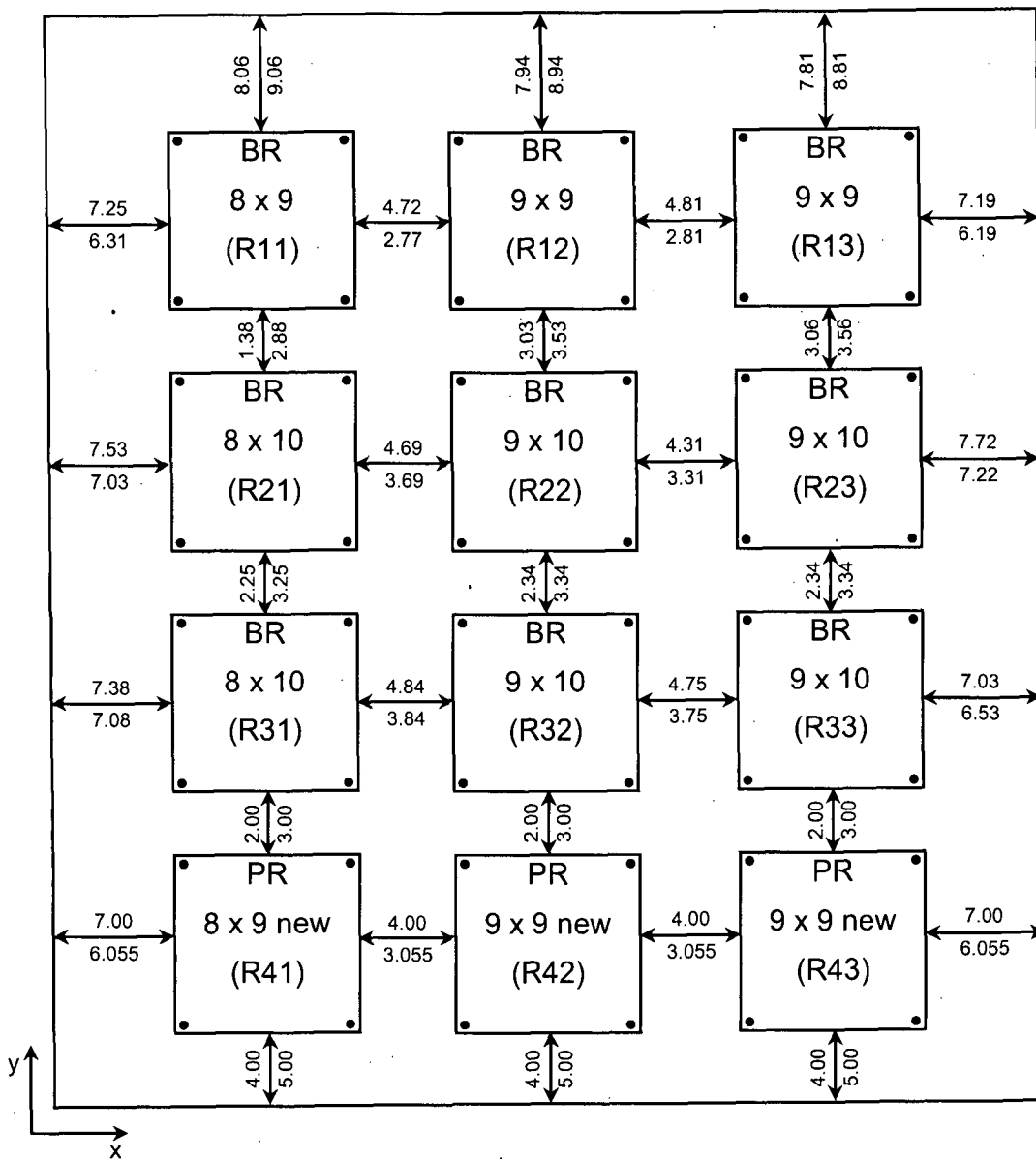


Figure 2.2 - ANO Unit 2 Spent Fuel Pool Layout Plan Dimensions  
 (All Dimensions in inches; BR=Burn-up Rack; PR=Poison Rack)

**2.2 Material Properties of Rack, Fuel and Poison Inserts (Design Inputs)**

The high density storage rack weights from References [8] and [9] are listed in Table 2.1 below.

<b>Table 2.1 -- RACK WEIGHT DATA</b>				
Rack #		Cells/Module	Array Size	Empty Rack Dry Weight (lbs)
Per Figure 2.1 and 2.2	Per Ref. 8			
2M-247—Region 2	07	72	8x9	13,850
2M-246A—Region 2	06	81	9x9	15,550
2M-246B—Region 2	06	81	9x9	15,550
2M-245B—Region 2	05	80	8x10	15,350
2M-244C—Region 2	04	90	9x10	17,250
2M-244D—Region 2	04	90	9x10	17,250
2M-245—Region 2	05	80	8x10	15,350
2M-244A—Region 2	04	90	9x10	17,250
2M-244B—Region 2	04	90	9x10	17,250
Poison Racks--Existing Designation	New Per Ref. 9			
2M-243—Region 1	A3	72	8x9	21,700
2M-242—Region 1	A2	81	9x9	24,200
2M-241—Region 1	A1	81	9x9	24,200

The Cartesian coordinate system used within the rack dynamic model has the following nomenclature:

- X = Horizontal axis along plant East
- Y = Horizontal axis along plant North
- Z = Vertical axis upward from the rack base

The material properties for the rack and support material are summarized in Table 2.2 below.

Table 2.2 -- RACK MATERIAL DATA (ASME – Appendices Ref. [12])			
MATERIAL DATA (T <sub>0</sub> = 150°F)			
Stainless Steel Material	Young's Modulus E (psi)	Yield Strength S <sub>y</sub> (psi)	Tensile Strength S <sub>u</sub> (psi)
SA240, Type 304	27.7 x 10 <sup>6</sup>	27,500	73,000
SA479, Type 304	27.7 x 10 <sup>6</sup>	27,500	73,000
SA564, Type 630 A.H. 1100 °F	28.9 x 10 <sup>6</sup>	110,650	140,000
MATERIAL DATA (T <sub>a</sub> = 254°F)			
SA240, Type 304	27.3 x 10 <sup>6</sup>	23,650	68,300
SA479, Type 304	27.3 x 10 <sup>6</sup>	23,650	68,300
SA564, Type 630 A.H. 1100 °F	28.5 x 10 <sup>6</sup>	104,100	140,000

### 3.0 Overview of Rack Structural Analysis Methodology

The response of a free-standing rack module to seismic loadings is nonlinear and involves a complex combination of motions (rocking, twisting, turning, and sliding). This could potentially cause impacts within the structure (fuel assemblies to the cell walls) and between modules, or between modules and the pool walls. Rack dynamic behavior includes a large portion of the total structural mass in a confined rattling motion. The rack pedestals are restricted from lateral motion only by friction at the base. In addition, there are large fluid coupling effects due to water around the assemblies and the independent adjacent structures.

Linear dynamic analysis methods cannot reasonably simulate the structural response of these highly nonlinear structures when subjected to earthquake loadings. An appropriate simulation can only be obtained by direct integration of the nonlinear equations of motion with three directional pool slab time-histories applied as forcing functions acting on the structures simultaneously.

Whole Pool Multi-Rack (WPMR) analysis is used to obtain final analysis results in order to simulate the dynamic behavior of the storage rack structures. This section describes the methodology used in the analysis.

### 3.1 Analysis Methodology Background

Reliable assessment of stresses within the rack components and stored fuel behavior within the rack modules requires a dynamic model that incorporates the appropriate attributes of the actual structure. The model must feature the ability to simultaneously simulate concurrent motions compatible with the rack and fuel storage installation.

The model has the capability to affect interactions, which occur due to rattling of fuel assemblies inside storage cells, and lift-off of the support pedestals on the pool floor. The contribution of the water mass in the spaces around the rack modules and within the storage cells is modeled in an accurate manner as described below.

The friction coefficient at the pedestal-to-pool liner (or bearing pad) interface may lie in a rather wide range and a conservative value of friction cannot be prescribed without performing bounding simulations. Different friction coefficients provide the governing results for different analysis parameters. For example, the lower bound friction results in the largest overall rack displacement, which may seem obvious, however other parameters such as the impact force between the rack and fuel assembly being largest with the upper bound friction is a result not immediately predictable.

The approach used in this evaluation was to develop single rack models for the new Region 1 type rack structures, since these are the racks being replaced relative to the current seismic qualification analysis (Reference 10). The three-dimensional single rack dynamic model addresses the parameters discussed above. Single rack simulations may not by themselves be sufficient in determining the maximum dynamic response. This is due to the participation of water around the racks, with hydraulic interaction that may either increase or decrease rack motion. The results of this evaluation confirm that the dynamics of one rack affect the motion of the others in the pool. Therefore, the dynamic simulation of one rack, while providing a great deal of insight into this behavior, may not adequately predict the motion or structural response (applied forces and internal stresses) of rack modules.

For this reason, the hydraulic and dynamic interaction of closely spaced racks is simulated by including all modules in one comprehensive simulation using a WPMR model. All rack modules are modeled simultaneously and the coupling effect due to multi-body motion is included in the analysis. Region 2 rack models for the whole pool model were developed in a similar manner as the new Region 1 rack models with appropriate modifications to the cell geometry and configurations. The Region 2 racks are all identical in construction except for the number of rows of cells.

The models developed as described below, consist of beam elements to model the rack and fuel elements. Spring/gap elements and contact surfaces were used to account for the racks being unanchored, and for possible impacts between the racks and pool walls, rack to rack, and fuel element to rack cell wall. Mass elements were used to include the added mass to account for hydrodynamic effects.

### 3.2 Equation of Motion

The SOLVIA general finite element program (Reference [7]) was used for the dynamic non-linear time history analysis of the single rack and WPMR model of the structures. Using the direct time integration method, the equations of motion are solved at each time step for acceleration time histories in each of the three degrees of freedom. The basic equations that SOLVIA is operating on are:

$$M\ddot{u}(t) + C\dot{u}(t) = R(t) - F(t)$$

where:

- $M$  = constant mass matrix,
- $C$  = constant damping matrix,
- $R(t)$  = external load vector applied at time  $t$ ,
- $F(t)$  = nodal point force vector equivalent to the element stresses at time  $t$ ,
- A superimposed dot denotes time derivative, e.g.,
- $\dot{u}(t)$  = nodal point velocity vector at time  $t$ .
- $\ddot{u}(t)$  = nodal point acceleration vector at time  $t$ .

An implicit time integration method (Nemark Method) is employed for this structural vibration problem.

There are several non-linear attributes and unique hydrodynamic properties of this structure that are modeled. Non-linear attributes in the WPMR include gaps or clearances between the racks and between the racks and the pool, the free-sliding and lift-off potential for the racks relative to their support on the pool floor, and the accounting for potential impact effects. Experimental verification was not implemented. Methodology used is consistent with industry practice (Reference [11]) for analysis of spent fuel racks, shielding blocks, and dry fuel casks. Use of the non-linear gapped-truss elements in SOLVIA provides a means to account for the gaps between the model components and impact forces if those gaps closed during the analysis. The "gapped truss" element is an axial force member, and hence is effectively a spring. The non-linear gap option allows it to be a compression-only element when the gap is closed, and to carry or transmit zero load when the gap is open.

The models were built by modeling each attribute and checking their effects one at a time. Each single rack model is developed by appropriately combining these attributes. The WPMR is modeled by combining the twelve modules and including the appropriate off diagonal stiffness matrix and mass matrix terms that include the interactions between the modules.

### 3.3 Friction Coefficient Between Rack Supports and Pool Floor

It is not possible to determine an accurate coefficient of friction ( $\mu$ ) between the pedestal supports and the pool floor. Data on austenitic stainless steel plates submerged in water show a mean value of  $\mu$  to be 0.503 [Ref. 11] with a standard deviation of 0.125. Upper and lower bounds (based on twice the standard deviation) are 0.753 and 0.253, respectively. Therefore, coefficient of friction values of 0.2 (lower limit) and 0.8 (upper limit) as well as a best estimate

value of 0.5 provide reasonable limits and provide a reasonable envelope for calculating the upper bound module response for each design parameter.

The friction interface between rack support pedestal and liner in the fuel rack simulations is simulated by linear contact (friction) elements. These elements function only when the pedestal is physically in contact with the pool floor. Friction elements are also included at the base of the fuel rod to rack base interface to reasonably model the behavior of the rod at this juncture. The coefficient of friction modeled at this interface was consistent with that used for the pedestal/pool bottom interface for a given analysis.

### 3.4 Rack Beam Behavior

The structural model using an equivalent beam stiffness developed for the full cell structure, was modeled using linear beam members to represent the elastic bending and twisting action.

The equivalent moment of inertia for the beam was estimated using a shell element model of a row of cells with the appropriate number of cells included for each horizontal direction. The axial area was estimated using a single cell model. The overall combined section properties for each type of rack module were then estimated from results of analysis of these models for applied unit displacements.

### 3.5 Impact Behavior

To include the impact behavior, compression-only gap elements are used to provide for opening and closing of interfaces such as the pedestal-to-pool floor interface and the fuel assembly-to-cell wall interface. These interface gaps are modeled using nonlinear spring elements (Gapped Truss elements in SOLVIA). The nonlinear spring is the mathematical representation of the condition where a restoring force is zero until the gap is closed and then is linearly proportional to displacement.

### 3.6 Fuel Loading to Cell Wall Behavior

The fuel assemblies are conservatively assumed to rattle in unison, which provides an upper bound for the contribution of impact against the cell wall. This is modeled with a single spent fuel assembly, which is a combination of all the assemblies contained in the rack. This single assembly is allowed to rattle against the cell walls of the rack modeled as an equivalent beam element. This results in the impact load being a combination of all 72 to 90 fuel assemblies hitting the wall at the same time.

From Reference 3, it is noted that impact damping is a significant source of damping for multiple impacting members. The same effective damping due to fuel to cell impact as a function of mass and stiffness presented in Reference [10] was used. From Reference [10], the damping coefficient was calculated as:

$$C = 2 \times \text{damping} \times \sqrt{Km}$$

where C = effective damping coefficient

K = impact stiffness

m = mass

damping = 2%

### 3.7 Fluid – Rack Coupling

The WPMR model used for this analysis handles simultaneous simulation of all racks in the pool as a WPMR three dimensional analysis. The WPMR analysis is appropriate for predicting maximum structural stresses with reasonable predictions of rack dynamic response.

During an earthquake, all racks in the pool are subject to the input excitation simultaneously. While the possibility of inter-rack impact is not a common occurrence and depends on rack spacing, the effect of water (the fluid coupling effect) is a factor. It is, therefore, essential that the contribution of the fluid forces be included in a comprehensive manner. This is possible when all racks in the pool are included in a three dimensional simulation using a mathematical model that includes all modules moving simultaneously. The fluid coupling effect encompasses interaction between every set of racks in the pool. The motion of one rack effects the fluid forces on all other racks and on the pool walls. Therefore, both near-field and far-field fluid coupling effects are included in the analysis.

### 3.8 Whole Pool Multi-Rack (WPMR) Methodology

The WPMR analysis must deal with both stress/displacement and impact criteria. The model development and analysis steps that are undertaken are summarized in the following steps.

- a. The section and mass properties of single cells are developed.
- b. Using the single cell section and mass properties, equivalent properties for each rack module are developed.
- c. Similarly, single element properties are calculated for the fuel assembly and the base pedestals. These are also used to develop equivalent properties for the rack module.
- d. Individual stiffness used in the gap elements are calculated for each of the interfaces included in the model. These include the pedestal base to pool floor, rack to rack, and rack to wall stiffness, and fuel assembly to rack wall interface. These are also appropriately combined to get equivalent module properties.
- e. Calculate the appropriate hydrodynamic properties for the spent fuel assemblies and rack. This includes the hydrodynamic mass and the off-diagonal hydrodynamic mass matrix terms.
- f. Develop the individual or single rack models in the pool.
- g. Combine the single rack models into one three-dimensional dynamic model suitable for a time-history analysis of the racks. These models include the assemblage of all rack modules in the pool. Include all fluid coupling interactions and mechanical coupling appropriate to performing an accurate non-linear simulation.
- h. Perform the three-dimensional dynamic analyses on various physical conditions (such as coefficient of friction and extent of cells containing fuel assemblies).

## Stevenson & Associates Report 06Q3571.07-01

Archive the appropriate displacement and load outputs from the dynamic model for post-processing.

- i. Using the force and moment outputs from the dynamic analyses, perform stress analysis of high stress areas for the limiting cases. Use simple modeling techniques to evaluate the local regions of the structure that need to be evaluated. Demonstrate compliance with ASME Code Section III, Subsection NF limits on stress and displacement.

### 4.0 Rack Model Development

#### 4.1 Single Rack Module Development

The new Region 1 racks include 72 (8 by 9) cells and 81 (9 by 9) cells. The weight of each component from Reference 9 and Figure 2-1 is as follows:

Fuel weight to use for analysis is conservatively specified in Reference [14].

8x9 Cell	Rack weight = 21,700 lb
	Fuel weight = 1,800 lb* 72 Assemblies = 129,600 lb
	Total weight (dry) = 151,300 lb
9x9 Cell	Rack weight = 24,200 lb
	Fuel weight = 1,800 lb* 81 Assemblies = 145,800 lb
	Total weight (dry) = 170,000 lb

The material properties for the stainless steel racks used in the analysis are as follows:

Type 304, SA240 18CR-8N (Ref. 12):

Modulus of Elasticity:  $E_s = 27.7 \times 10^6$  psi

Poisson's Ratio:  $\mu_s = 0.3$  (Steel)

Density (Stainless Steel--weight units):  $\delta_{(w)} = 0.29$  lb/in<sup>3</sup>

The calculated material properties used for the pool concrete, for model development, from Ref. 13:

Compressive Strength,  $f'_c = 4000$  psi (assumed for stiffness calculation)

Modulus of Elasticity,  $E_c = 57000\sqrt{f'_c} = 57000\sqrt{4000}$  psi = 3.60E6 psi

Poisson's Ratio  $\mu_c = 0.16$  (Concrete)

Density (Concrete--weight units)  $\delta_{(w)} = 0.0868$  lb/in<sup>3</sup>

**Stevenson & Associates Report 06Q3571.07-01**

Fuel weight  $W_f = 1800$  lb (assume the weight is uniformly distributed)

The Single Rack combined structural section properties [Moment of Inertias ( $I_x$ ,  $I_y$ , and  $I_t$ ), Area (A), and Weight] for the Rack modules are shown in Table 4.1. Combined structural section properties [Moment of Inertias ( $I_x$ ,  $I_y$ , and  $I_t$ ), Area (A), and Weight] for the fuel assemblies are shown in Table 4.2.

<b>Table 4.1 -- Stick models properties</b>					
Rack (region)	Area [in <sup>2</sup> ]	$I_x$ [in <sup>4</sup> ]	$I_y$ [in <sup>4</sup> ]	$I_t$ [in <sup>4</sup> ]	Weight [lbs]
Poison Rack 8x9 (Region 1)	244.80	98,280	85,354	183,634	21,700
Poison Rack 9x9 (Region 1)	275.40	110,563	110,563	221,126	24,200
Burnup Rack 8x9 (Region 2)	216.58	101,917	85,358	187,275	13,850
Burnup Rack 9x9 (Region 2)	243.65	114,657	114,657	229,314	15,550
Burnup Rack 8x10 (Region 2)	240.64	131,626	94,843	226,469	15,350
Burnup Rack 9x10 (Region 2)	270.72	148,080	127,397	275,477	17,250

<b>Table 4.2 -- Beam equivalent properties for fuel assemblies</b>				
Rack (region)	Area [in <sup>2</sup> ]	$I_x = I_y$ [in <sup>4</sup> ]	$I_t$ [in <sup>4</sup> ]	Weight [lbs]
Poison Rack 8x9 (Region 1)	460.1	14.688	29.376	129,600
Poison Rack 9x9 (Region 1)	517.6	16.524	33.048	145,800
Burnup Rack 8x9 (Region 2)	460.1	14.688	29.376	129,600
Burnup Rack 9x9 (Region 2)	517.6	16.524	33.048	145,800
Burnup Rack 8x10 (Region 2)	511.2	16.320	32.640	144,000
Burnup Rack 9x10 (Region 2)	575.1	18.360	36.720	162,000

The stiffness for the gap compression-only elements at the base for the new poison racks is as follows:  $K_{ped} = 4.031 \times 10^7$  lb/in.

The stiffness for the gap compression-only elements at the base for the existing burn-up racks is as follows:  $K_{ped} = 1.166 \times 10^7$  lb/in. for single pedestals, and  $K_{ped} = 2.332 \times 10^7$  lb/in. for double pedestals.

#### 4.2 Single Rack to Multi-Rack Model Development

The single rack models are combined into the WPMR model and the inter-rack gap stiffness springs are attached. When the gaps are closed during the analysis, the stiffnesses shown in Table 4.3 were in effect between these interfaces.

Impact Spring Type	Spring Constant [lb/in]
Poison Rack to Poison Rack (top)	341,250
Burn-up Rack to Burn-up Rack (top)	341,185
Burn-up Rack to Poison Rack (top)	339,675
Poison Rack to Poison Rack (bottom)	1,591,000
Burn-up Rack to Burn-up Rack (bottom)	1,062,000
Burn-up Rack to Poison Rack (bottom)	1,062,000
Poison Rack to Pool Wall (top)	642,000
Burn-up Rack to Pool Wall (top)	642,000
Poison Rack to Pool Wall (bottom)	2,125,000
Burn-up Rack to Pool Wall (bottom)	1,511,000

Similarly, fuel-rack gap stiffness springs are attached between the rack cells and fuel assemblies. When the gaps are closed during the analysis, the stiffnesses shown in Table 4.4 were in effect between these interfaces. Additionally, the damping associated with the fuel-rack impact is shown in Table 4.4. Note, for the single rack models, the appropriate fuel-rack gap stiffnesses and damping values from Table 4.4 were also included.

Rack (region)	Fuel-cell impact stiffness [lb/in]	Total damping [lb-sec/in]	Damping top [lb-sec/in]	Damping middle [lb-sec/in]	Damping bottom [lb-sec/in]
Poison Rack 8x9 (Region 1)	$0.54 \cdot 10^6$	708.4	177.1	354.2	177.1
Poison Rack 9x9 (Region 1)	$0.61 \cdot 10^6$	752.8	188.2	376.4	188.2
Burnup Rack 8x9 (Region 2)	$1.12 \cdot 10^6$	1020.1	255.0	510.1	255.0
Burnup Rack 9x9 (Region 2)	$1.35 \cdot 10^6$	1120.0	280.0	560.0	280.0
Burnup Rack 8x10 (Region 2)	$1.33 \cdot 10^6$	1111.6	277.9	555.8	277.9
Burnup Rack 9x10 (Region 2)	$1.5 \cdot 10^6$	1180.6	295.1	590.4	295.1

### 4.3 Model Details and Description

The rack structure dynamic model was prepared by considering nonlinearities and parametric variations. Particulars of modeling details and assumptions for the WPMR analysis of racks are given in the following subsections.

#### 4.3.1 Modeling Details and Assumptions

- a. The model for the rack is supported at the base level, on four (corner) pedestals, modeled using non-linear compression-only gap spring elements and eight linear friction spring elements. These elements are located with respect to the centerline of the rack beam to allow for arbitrary rocking and sliding motions.
- b. The fuel rack structure motion is simulated by modeling the rack using 6 degrees-of-freedom at each mass point of the model. This includes the displacements and rotations at each of these points. The response of the module relative to the base is simulated in the dynamic analyses using suitable springs to couple the rack degrees-of-freedom and simulate rack stiffness.
- c. Fluid coupling between the rack and fuel assemblies and between the rack and wall is simulated by appropriately modeling the off diagonal mass matrix terms. Inclusion of these effects uses rack/assembly coupling and rack-to-rack coupling as described in subsection 4.3.3.
- d. Fluid damping and velocity drag due to water particle velocity are not modeled. These effects are considered implicitly in the fluid coupling and fluid assumption mass modeling described in c. and i.
- e. Rattling fuel assemblies within the rack are modeled by five lumped masses located at  $H$ ,  $0.75H$ ,  $0.5H$ ,  $0.25H$ , and at the rack base ( $H$  is the rack height measured above the base-plate). Each lumped fuel mass has two horizontal displacement degrees-of-freedom. Vertical motion of the fuel assembly mass is assumed equal to rack vertical motion at the base-plate level.
- f. Seismic motion of a fuel rack is characterized assuming that fuel assemblies in their individual storage location move together in phase. This is the worst case computed dynamic loading on the rack structure for this phenomenon.
- g. Potential impacts between the cell walls of the racks and the contained fuel assemblies are accounted for by appropriate compression-only gap elements between the masses involved. The possible incidence of rack-to-wall or rack-to-rack impact is simulated by gap elements at the top and bottom of the rack in two horizontal directions. Bottom gap elements are located at the base-plate elevation. The initial gaps reflect the presence of base-plate extensions, and the rack stiffnesses are chosen to simulate the local structural detail.

- h. Pedestals are modeled using gap elements in the vertical direction and as “rigid links” for transferring horizontal forces. Each pedestal support is linked to the pool liner (or bearing pad) by two friction springs. The spring rate for the friction springs includes any lateral elasticity of the stub pedestals. Local pedestal vertical spring stiffness accounts for floor elasticity and for local rack elasticity just above the pedestal.
- i. Rattling of fuel assemblies inside the storage locations causes the gap between fuel assemblies and cell wall to change from a maximum of twice the nominal gap to a theoretical zero gap. Fluid coupling coefficients are based on the nominal gap in order to provide a measure of fluid resistance to gap closure.

**4.3.2 Element Details**

The dynamic model of a single rack is shown in Figures 4.1 and 4.2. Figure 4.1 shows many of the characteristics of the model including the fuel to rack gap springs, the rack and fuel bundle elements and the gapped and friction springs at the base that are linked with rigid members.

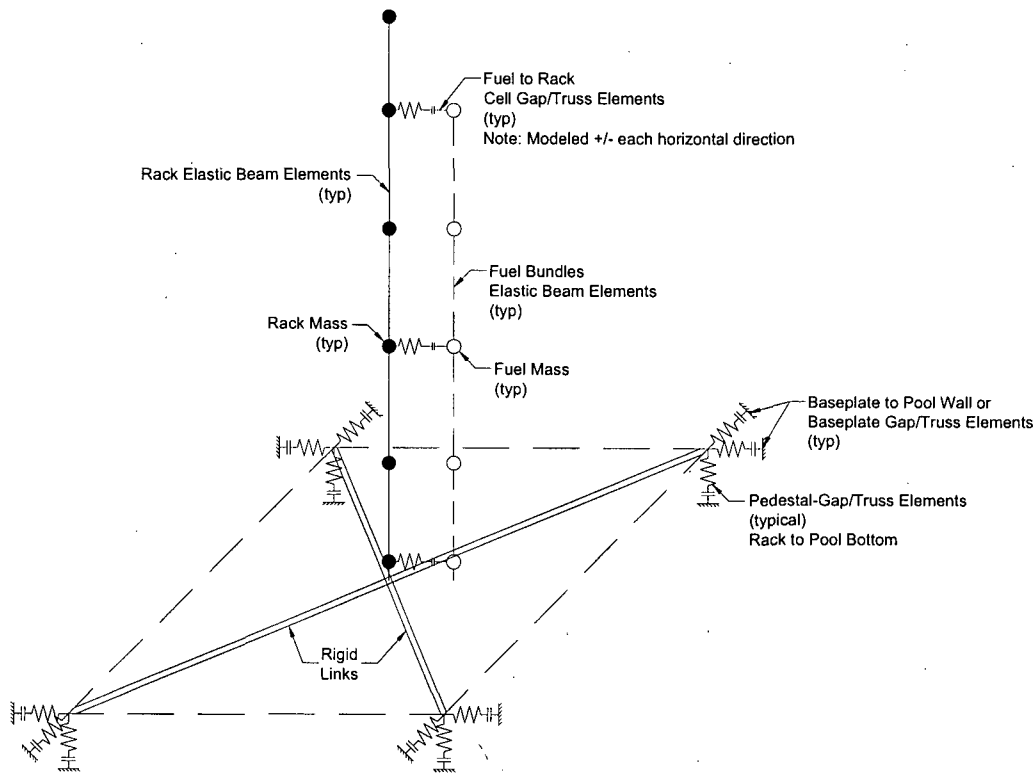


**Figure 4.1 – Schematic of the Single Rack Dynamic Model**

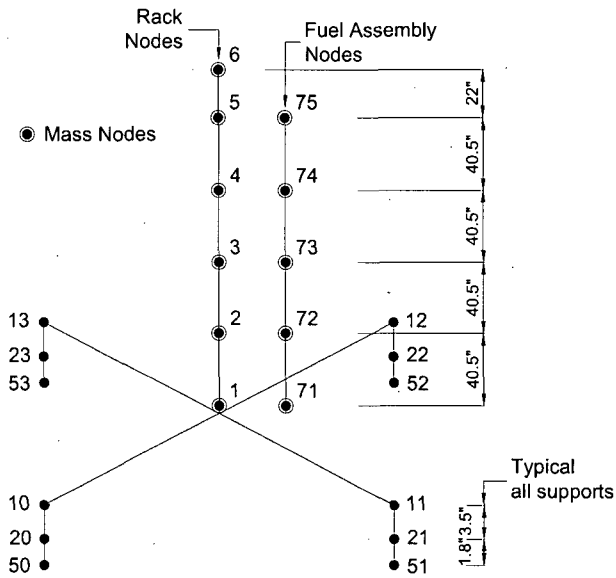


Figure 4.2 – Sketch of the Single Rack Dynamic Model

#### 4.3.3 Hydrodynamic Coupling Modeling (Single and Multi-Body Coupling)

The hydrodynamic coupling between any two masses is described as “adding” force due to relative motion of the two masses in the X direction. The formulation for this added force is given in Ref. [3] and is summarized using the following mass matrix formulation:

$$\begin{Bmatrix} F_{x1} \\ F_{x2} \end{Bmatrix} = \begin{bmatrix} M_H & -(M_1 + M_H) \\ -(M_1 + M_H) & M_1 + M_2 + M_H \end{bmatrix} \begin{Bmatrix} \ddot{X}_1 \\ \ddot{X}_2 \end{Bmatrix}$$

where,

- $F_{x1}$  - adding force acted on Mass 1
- $F_{x2}$  - adding force acted on Mass 2 (Mass 2 is assumed contained inside Mass 1)
- $M_1$  - water mass enclosed by Mass 1
- $M_2$  - displaced water mass by Mass 2
- $M_H$  - hydrodynamic mass
- $\ddot{X}_1$  - absolute acceleration of Mass 1
- $\ddot{X}_2$  - absolute acceleration of Mass 2

The diagonal terms ( $M_1 = M_2 + M_H$ ) and  $M_H$  are added mass terms for the two bodies (for example, the pool wall as one body and the rack as the other body), and the off-diagonal terms – ( $M_1 + M_H$ ) are the inertial coupling terms.

Therefore, the mass matrix for adding the hydrodynamic coupling force between any two masses is included in the solution process by adding the water masses  $M_1$ ,  $M_2$ , and the hydrodynamic mass  $M_H$  in each direction to the SOLVIA structural model.

Using the above formulation, the motion of one body affects the force field on another. This force field is a function of inter-body gap and can be large when the gaps are small. The lateral motion of a fuel assembly inside a storage location encounters this effect. The rack analysis contains inertial fluid coupling terms, which model the effect of fluid in the gaps between adjacent racks.

Rack-to-rack gap elements have initial gaps set to the entire physical gap between the racks or between outermost racks and the adjacent pool walls. Masses including the hydrodynamic mass were calculated by setting the kinetic energy of hydrodynamic mass to be equal to kinetic energy of the fluid flow, maintaining continuity between the body and fluid flow area, and combining the mass for all of the cells.

#### 4.3.4 Stiffness Element

There are three element types used in the SOLVIA rack module models. The first element type is a linear elastic beam element used to represent the beam-like behavior of the integrated rack cell matrix. The second element type is the linear friction springs used to develop the forces between the rack pedestals and the supporting floor. The third element type is a non-linear gap element, which models gap closures and impact loadings between fuel assemblies and the storage cell inner walls and racks.

The gap elements modeling impact between fuel assemblies and racks have local stiffness  $K_i$ . Support pedestal spring rates,  $K_s$ , are modeled by gap elements. Local behavior of the pedestal on the concrete floor is included in  $K_s$ . The friction elements are included as  $K_f$ . The beam elements for the rack and fuel model the combined stiffness of these components for the racks.

Friction at the support to pool floor interface is modeled by the linear friction springs with stiffness  $K_f$  up to the limiting lateral load  $\mu N$ , where  $N$  is the current compression load at the interface between support and liner. At every time-step during time history analysis, the current value of  $N$  (either zero, if the pedestal has lifted off the floor, or a restraining force) is computed.

The modeling of the effective compression stiffness with the gap element of stiffness  $K_i$  includes the pedestal stiffness and local stiffness of the underlying pool slab.

#### 4.3.5 Friction Modeling Between Rack Supports and Pool Floor

As discussed in Section 3.3, simulations are performed with friction coefficients of 0.2, 0.5, and 0.8 in order to bound the range of realistic results for the earthquake event.

**5.0 Load Combinations and Load Development**

**5.1 Loads and Load Combinations**

The applicable loads and load combinations to be considered in the seismic analysis of rack modules are taken from the OT Position [2] and are included in Table 5.1 below: The acceptance criteria is defined in Subsection NF of the ASME Code [15].

<b>Table 5.1 -- Load Combinations for the SFP Rack Analysis</b>	
<b>Loading Combination</b>	<b>Acceptance Limit</b>
<i>D + L</i> <i>D + L + E</i>	Normal Limits of NF3231.1a <sup>(1)</sup> , Ref. [15]
<i>D + L + T<sub>o</sub></i> <i>D + L + T<sub>o</sub> + E</i> <i>D + L + T<sub>a</sub> + E</i>	Lesser of 2 S <sub>y</sub> or S <sub>u</sub> – Stress Range
<i>D + L + T<sub>a</sub> + E'</i>	Faulted Condition Limits of NF 3231.1c <sup>(2)</sup> , Ref. [15]

Notes:

- 1) The design basis for the existing racks is Reference 2 and ASME Subsection NF, 1980 through the Winter 1981 Addendum. The new racks are evaluated to these requirements.
- 2) Faulted conditions in the ASME code are defined as Service Level D condition [15]. NF3231.1c ultimately references Appendix F for this evaluation.

Where:

- D* = Dead weight-induced loads (including fuel assembly and poison insert weights)
- L* = Live Load (not applicable for the fuel rack, since there are no moving objects in the rack load path)
- E* = Operating Basis Earthquake (OBE), including the effects of impacts occurring during the earthquake event.
- E'* = Safe Shutdown Earthquake (DBE), including the effects of impacts occurring during the earthquake event.
- T<sub>o</sub>* = Differential temperature induced loads (normal operating or shutdown condition based on the most critical transient or steady state condition)
- T<sub>a</sub>* = Differential temperature induced loads (the highest temperature associated with the postulated abnormal design conditions).

## Stevenson & Associates Report 06Q3571.07-01

The basic generally governing load combinations evaluated are as follows:

$D + L + E$  (Acceptance Limit Normal Limits of NF3231.1a, Ref. [15])

$D + L + T_a + E'$  Faulted Condition Limits of NF3231.1c and Appendix F, Ref. [15]

For ease of analysis, the elastic modulus at 150° F was used for both the OBE and DBE dynamic analyses, which results in the best estimate global forces and displacements. The allowable stresses calculated in Sections 7.2 and 7.3 use the yield and ultimate strength properties at 150° F and 254° F respectively for the OBE and DBE.

For impact of the fuel assemblies with the cell walls, as discussed in the OT Position [2], "for impact loading the ductility ratios utilized to absorb kinetic energy in the tensile, flexural, compressive, and shearing modes should be quantified." Maximum impact loads and therefore maximum ductility ratios were derived from the DBE event. Also ductility ratios are applicable only for faulted condition limits. Therefore, impact loading was only evaluated in detail locally for the cell walls for the DBE load case. In addition the impact acceptance criteria includes a provision that insures that the consequent impact loads on the fuel assembly does not lead to damage of the fuel in accordance with the OT Position [2]. Impact load effects were included for both OBE and DBE for all other acceptance considerations for the racks.

### 5.2 Synthetic Earthquake Time Histories OBE and DBE

The synthetic time-histories in three orthogonal directions (N-S, E-W, and vertical) are generated in accordance with the provisions of SRP [1], Section 3.7.1. In order to prepare an acceptable set of acceleration time-histories, Stevenson and Associates' commercial code THSPEC [16] is used. It is noted that program THSPEC is a derivative of Program SIMQKE, developed at MIT.

The response spectrum and the power spectral density (PSD) corresponding to the generated acceleration time-history is to envelope their target (design basis) spectrum and PSD with only finite enveloping infractions. The target floor response spectra were developed by interpolating the 2% damped horizontal OBE and DBE spectra between Elevations 354' and 372' to obtain spectra at 362'. It is noted that time history acceleration is independent of damping level. However, due to smoothing and enveloping when developing design spectra, the time history may not envelop all response spectra at a given location developed with different damping coefficients. It is reasonable to use a 2% damped target since this is the damping used in the analysis of welded steel structures. The time-histories used for the rack analyses were generated to satisfy the enveloping criterion for synthetic time-histories in Section 3.7.1 of the SRP [1]. The seismic files also satisfy the requirements of statistical independence required by SRP 3.7.1 [1]. The absolute value of correlation function of the three OBE time-histories and three DBE time-histories relative to one another are shown in Tables 5.2 and 5.3. As can be seen all are less than 0.30 (the statistical independence criterion) indicating that the three data sets are statistically independent.

**Stevenson & Associates Report 06Q3571.07-01**

Table 5.2 -- Correlation Coefficients Between Time History Components (DBE)			
Component Pair	Maximum Accelerations (g)	Mean Accelerations (g)	Correlation
Horz X	0.25	-2.3E-5	0.193
Horz Y	0.25	6.19E-5	
Horz. X	0.25	-2.3E-5	0.018
Vertical	0.139	4.89E-5	
Horz Y	0.25	6.19E-5	0.036
Vertical	0.139	4.89E-5	

Table 5.3 -- Correlation Coefficients Between Time History Components (OBE)			
Component Pair	Maximum Accelerations (g)	Mean Accelerations (g)	Correlation
Horz X	0.1988	3.88E-5	0.057
Horz Y	0.194	-1.24E-5	
Horz X	0.1988	3.88E-5	0.020
Vertical	0.069	5.70E-6	
Horz Y	0.194	-1.24E-5	0.043
Vertical	0.069	5.70E-6	

Plots showing the comparison of the Response Spectra generated by each of the artificial time histories to the target floor response spectra are provided as follows:

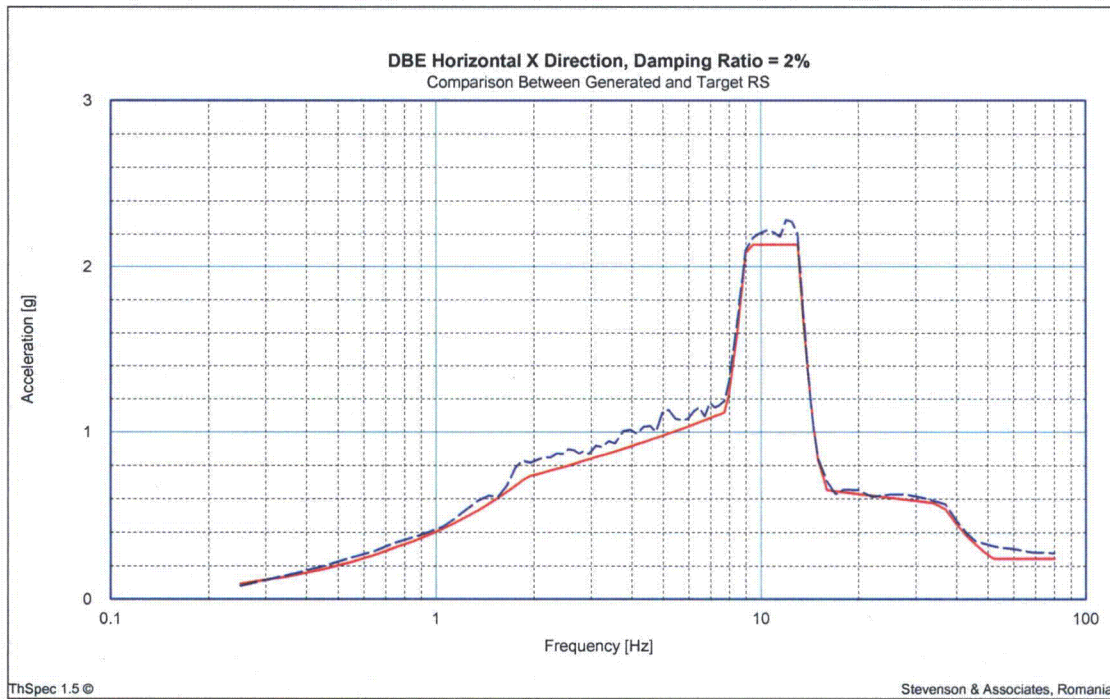


Figure 5.1 – Comparison of Generated Response Spectrum (Dashed Line) to Target Floor Response Spectrum (Solid Line), Horizontal, DBE X-Direction

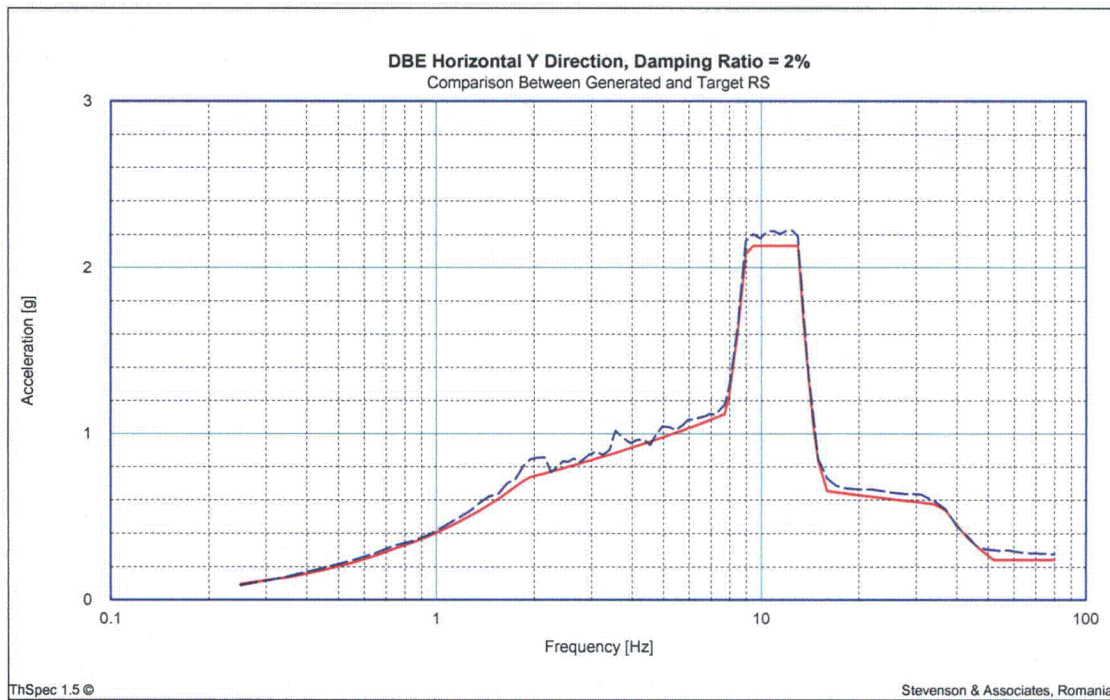


Figure 5.2 – Comparison of Generated Response Spectrum (Dashed Line) to Target Floor Response Spectrum (Solid Line), Horizontal, DBE Y-Direction

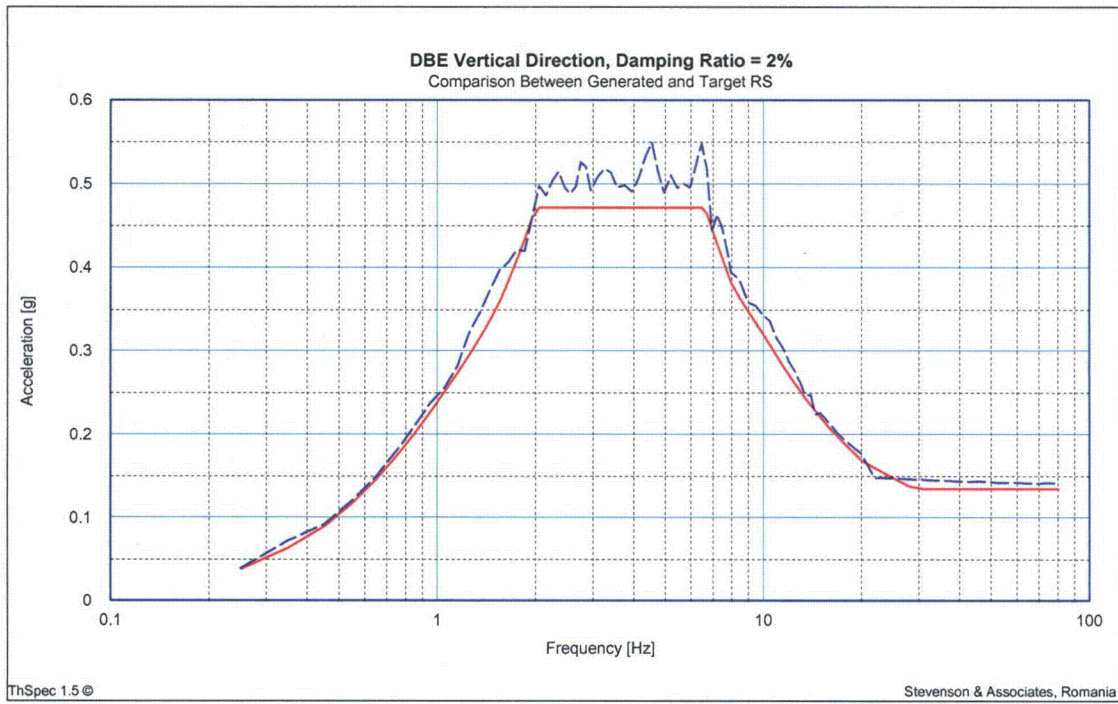


Figure 5.3 – Comparison of Generated Response Spectrum (Dashed Line) to Target Floor Response Spectrum (Solid Line), DBE Vertical Direction

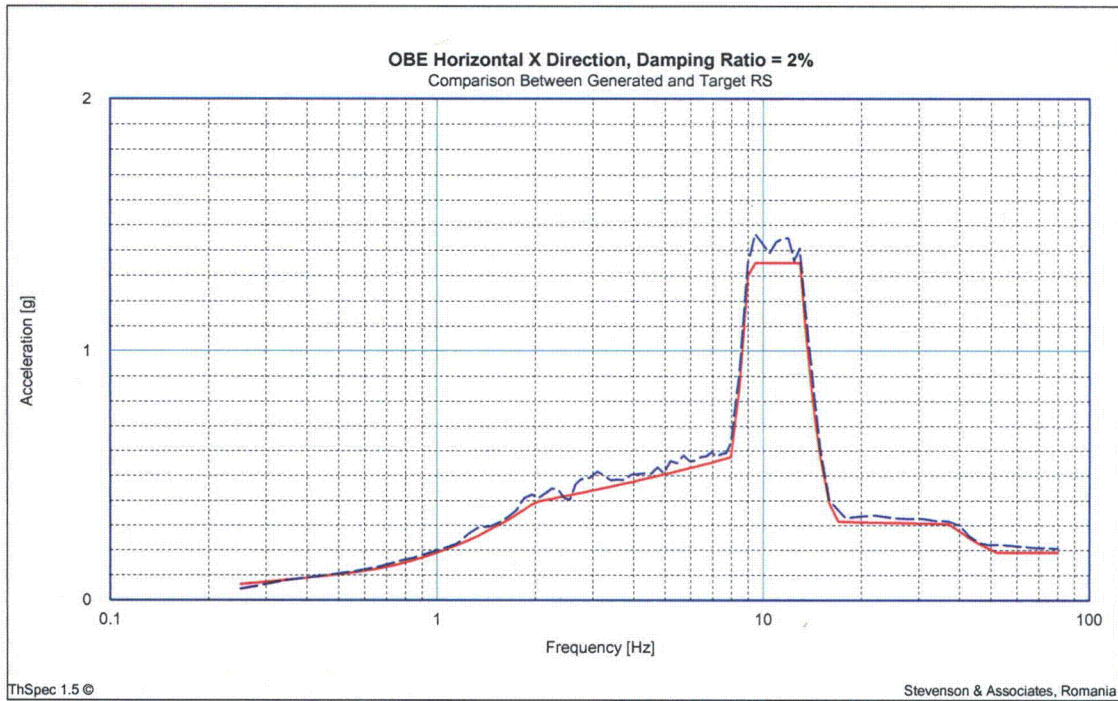


Figure 5.4 – Comparison of Generated Response Spectrum (Dashed Line) to Target Floor Response Spectrum (Solid Line), Horizontal, OBE X-Direction

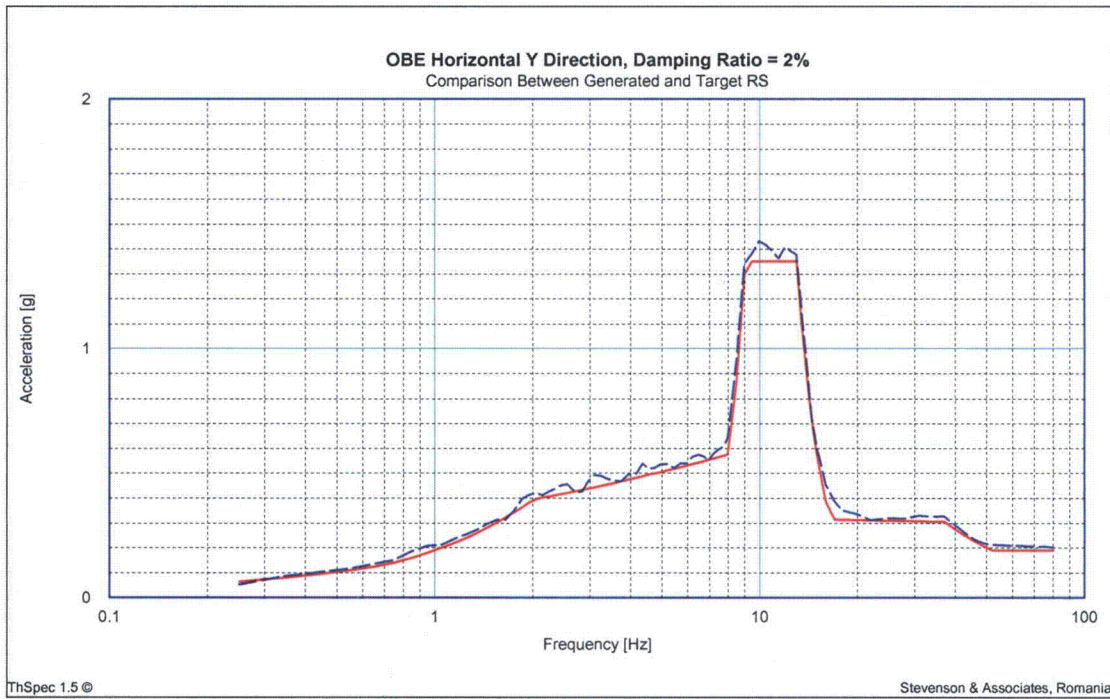


Figure 5.5 – Comparison of Generated Response Spectrum (Dashed Line) to Target Floor Response Spectrum (Solid Line), Horizontal, OBE Y-Direction

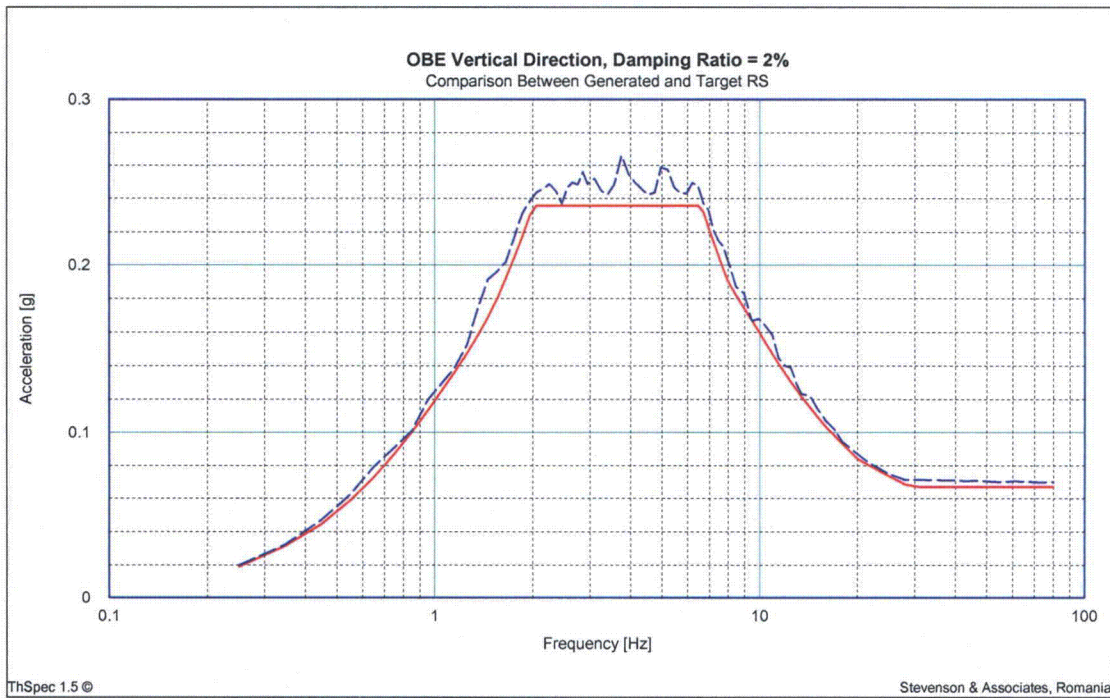


Figure 5.6 – Comparison of Generated Response Spectrum (Dashed Line) to Target Floor Response Spectrum (Solid Line), Horizontal, OBE Vertical Direction

### **5.3 Impact Load Consideration and Combination with other Loads**

The impact loading effect on the global rack assemblies is implicitly included by the modeling and dynamic simulations. As described in the modeling, impacts are considered as the gap elements open and close during the analysis.

## **6.0 Summary of Analyses Performed**

### **6.1 Single Rack Analysis**

As previously discussed in Section 4.1, single rack models were developed for each module type in order to use them as building blocks for the WPMR analysis. In addition the single rack models are employed to study the effect of top loading the rack with miscellaneous equipment. The top loaded rack simulation is performed using the 0.8 coefficient of friction, DBE load case to produce the maximum overturning moment. A bounding 2,000 lbf mass, with three translational degrees-of-freedom, is rigidly attached to the rack 24" above the top of the cell structure. The analysis results, with and without the weight, are studied. It is noted that the results indicate that the additional mass has an insignificant effect on the rack module analysis results.

### **6.2 Whole Pool Multi-Rack (WPMR) Analysis**

The multiple rack models use the fluid coupling effects for all racks in the pool. The twelve racks are modeled with proper interface fluid gaps and a coefficient of friction at the support interface locations as described in Section 4.3. The response to both DBE and OBE seismic excitation is determined.

### **6.3 Parametric Simulations**

#### **6.3.1 Friction Coefficient Variation**

The WPMR simulations listed in Table 6.1 have been performed to investigate the structural integrity of the new Holtec racks.

<b>Table 6.1 -- LIST OF WPMR AND SINGLE RACK SIMULATIONS</b>				
<b>Case</b>	<b>Model</b>	<b>Load Case</b>	<b>COF</b>	<b>Event</b>
1	WPMR & Single	All racks fully loaded	0.5	OBE
2	WPMR & Single	All racks fully loaded	0.2	OBE
3	WPMR & Single	All racks fully loaded	0.8	OBE
4	WPMR & Single	All racks fully loaded	0.5	DBE
5	WPMR & Single	All racks fully loaded	0.2	DBE
6	WPMR & Single	All racks fully loaded	0.8	DBE

COF = Coefficient of Friction

Note 1: A 50% full simulation was performed in Reference [17] to determine whether there was a possibility that the racks could exhibit greater displacement when all the cells within the rack are not in use (empty). It was shown that the fully loaded racks were the governing case.

Note 2: No numerical convergence or instability problems were encountered in any of the analyses.

## 7.0 Acceptance Criteria Development

### 7.1 Displacement and Rocking Acceptance Criteria

According to Section 3.8.5 of Ref. [1], the minimum required safety margins against overturning under the OBE and DBE events are 1.5 and 1.1 respectively. The maximum rotations of the rack (about the two principal axes) are obtained from a post processing of the rack time-history response output. The margin of safety against overturning is given by the ratio of the rotation required to produce incipient tipping in either principal plane to the actual maximum rotation in that plane predicted by the time-history solution.

All ratios for the OBE and DBE events are greater than 1.5 and 1.1 respectively, and satisfy the regulatory acceptance criteria.

### 7.2 Stress Evaluations – OBE Load Case

The stress limits presented apply to the rack structure and are derived from the ASME Code, Section III, Subsection NF [15]. Parameters and terminology are in accordance with the ASME Code. Material properties are obtained from the ASME Code Appendices and are listed in Table 2.2. Enumerated allowable stress values below are relative to the SA240, Type 304 material.

### 7.2.1 Tension Allowable Stress - OBE

Allowable stress in tension on a net section is:

$$F_t = 0.6 S_y$$

$$F_t = 0.6 * 27,500 \text{ psi} = 16,500 \text{ psi}$$

Where  $S_y$  = yield stress at temperature, and  $F_t$  is equivalent to primary membrane stress.

### 7.2.2 Compression Allowable Stress - OBE

Allowable stress for compression members on a net section is (ASME XVII-2213.1):

$$F_a = \frac{\left[ 1 - \frac{(Kl/r)^2}{2C_c^2} \right] S_y}{\frac{5}{3} + \left[ \frac{3(Kl/r)}{8C_c} \right] - \left[ \frac{(Kl/r)^3}{8C_c^3} \right]}$$

where:

$$C_c = \sqrt{\frac{2\pi^2 E}{S_y}}$$

$l$  = unsupported length of component

$K$  = length coefficient which gives influence of boundary conditions.

$r$  = radius of gyration of component

For local buckling considerations of the cell walls, from Reference 26, the critical buckling stress is given by:

$$F_{cr} = \frac{k\pi^2 E}{12(1-\mu^2)} \left( \frac{t}{b} \right)^2$$

Where:  $F_{cr}$  = critical buckling stress

$k$  = buckling stress coefficient (= 4.0 for simply supported unloaded edges)

$E$  = initial modulus of elasticity

$\mu$  = Poisson's ratio

$t$  = plate thickness

$b$  = effective width

From ASME XVII-2210(b), the allowable stress for buckling of the cell walls shall be limited to:

$$2/3(F_{cr})$$

### 7.2.3 Shear Allowable Stress - OBE

Allowable stress in shear on a net section is (ASME XVII-2212.1):

$$F_v = 0.4 S_y$$

$$F_v = .4 * 27,500 \text{ psi} = 11,000 \text{ psi}$$

### 7.2.4 Bending Allowable Stress - OBE

Maximum allowable bending stress at the outermost fiber of a net section, due to flexure about one plane of symmetry is:

$$F_b = 0.60 S_y \quad (\text{equivalent to primary bending})$$

$$F_b = 0.6 * (27,500 \text{ psi}) = 16,500 \text{ psi}$$

### 7.2.5 Combined Bending and Tension or Compression Allowable Stress - OBE

Combined bending and compression on a net section satisfies (ASME XVII-2215.1):

$$\frac{f_a}{F_a} + \frac{C_{mx} f_{bx}}{D_x F_{bx}} + \frac{C_{my} f_{by}}{D_y F_{by}} < 1$$

where:

$f_a$  = Direct compressive stress in the section

$f_{bx}$  = Maximum bending stress along x-axis

$f_{by}$  = Maximum bending stress along y-axis

$C_{mx}$  = 0.85

$C_{my}$  = 0.85

$D_x$  =  $1 - (f_a/F'_{ex})$

$D_y$  =  $1 - (f_a/F'_{ey})$

$F'_{ex,ey}$  =  $(\pi^2 E)/(2.15 (kl/r)^2_{x,y})$

$E$  = Young's Modulus

and subscripts x,y reflect the particular bending plane.

Combined flexure and compression (or tension) on a net section:

## Stevenson & Associates Report 06Q3571.07-01

$$\frac{f_a}{0.6S_y} + \frac{f_{bx}}{F_{bx}} + \frac{f_{by}}{F_{by}} < 1.0$$

The above requirements are to be met for direct tension or compression.

### 7.2.6 Weld Allowable Stress or Force – OBE

Allowable maximum tension, compression, or shear stress on the effective throat of full penetration (all directions) and partial penetration (all directions except tension normal to the axis) groove welds is given by (NF-3292.1):

Same as for Base Metal

Allowable maximum shear stress on the effective throat of fillet welds and tension normal to the axis of partial penetration groove welds is given by (NF-3292.1):

$$F_w = 21 \text{ ksi for base metal with } S_u \text{ in range of 61-70 ksi}$$

$$F_w = 24 \text{ ksi for base metal with } S_u \text{ in range of 71-80 ksi}$$

where:  $S_u$  = base material ultimate strength at temperature

### 7.3 Stress Evaluations - DBE Load Case

Section F-1370 (ASME Section III, Appendix F, Reference 12), states that for the Level D (faulted) condition allowable stresses from ASME Appendix XVII-2000 may be increased by a factor of  $1.2(S_y/F_t)$  but not to exceed  $0.7(S_u/F_t)$ , where  $S_y$  is the material yield stress at temperature,  $F_t$  is the allowable tensile stress, and  $S_u$  is the material tensile stress at temperature. Additionally, axial loads should not exceed 0.67 times the critical buckling strength at temperature.

For the Type 304 stainless steel:

$$1.2(S_y/F_t) = 1.2(23,650 \text{ psi} / (0.6(23,650) \text{ psi})) = 2.0 \leftarrow \text{Governs}$$

$$0.7(S_u/F_t) = 0.7(68,300 \text{ psi} / 16,500 \text{ psi}) = 2.9$$

#### 7.3.1 Tension Allowable Stress - DBE

Allowable stress in tension on a net section is:

$$F_t = 2.0 * 0.6 * 23,650 \text{ psi} = 28,380 \text{ psi}$$

#### 7.3.2 Compression Allowable Stress - DBE

Axial Compression Loads applicable to the overall rack structure are limited to 2/3 of the calculated buckling load.

$$F_a = .667 * F_e \leq 28,380 \text{ psi}$$

## Stevenson & Associates Report 06Q3571.07-01

where:  $F_e$  is the Euler Buckling Load (stress units)

For local buckling considerations of the cell walls, the acceptance criterion is taken the same for OBE above.

### 7.3.3 Shear Allowable Stress - DBE

Stresses in shear are limited to the lesser of  $0.72S_y$  or  $0.42S_u$ . In the case of the Austenitic Stainless material used here,  $0.72S_y$  governs.

Allowable stress in shear on a net section is:  $F_v = 0.72 * 23,650 \text{ psi} = 17,028 \text{ psi}$

### 7.3.4 Bending Allowable Stress - DBE

Maximum allowable bending stress at the outermost fiber of a net section, due to flexure about one plane of symmetry is:

$$F_b = 2.0 * 0.6 * (23,650 \text{ psi}) = 28,380 \text{ psi}$$

### 7.3.5 Combined Bending and Tension or Compression Allowable Stress - DBE

Combined bending and compression on a net section satisfies:

$$\frac{f_a}{0.667 * F_e} + \frac{C_{mx} f_{bx}}{D_x F_{bx}} + \frac{C_{my} f_{by}}{D_y F_{by}} < 1$$

Where all of the terms have been defined above for OBE stress evaluation.

### 7.3.6 Weld Allowable Stress - DBE

Allowable maximum tension, compression, or shear stress on the effective throat of full penetration (all directions) and partial penetration (all directions except tension normal to the axis) groove welds is given by (NF-3292.1):

Same as for Base Metal

Allowable maximum shear stress on the effective throat of fillet welds and tension normal to the axis of partial penetration groove welds is given by (NF-3292.1) factored for DBE:

$$F_w = 2.0 \times 21 \text{ ksi} = 42 \text{ ksi for base metal with } S_u \text{ in range of 61-70 ksi}$$

$$F_w = 2.0 \times 24 \text{ ksi} = 48 \text{ ksi for base metal with } S_u \text{ in range of 71-80 ksi}$$

where:  $S_u$  = base material ultimate strength at temperature

### 7.3.7 Impact Acceptance Criteria - DBE

Impact allowable stress will be calculated as follows:

For general Primary Membrane Stress;

$$P_m < 0.7S_u = .7 * 68,300 \text{ psi} = 47,810 \text{ psi}$$

## Stevenson & Associates Report 06Q3571.07-01

And for the maximum Primary Stress (including bending from the impact);

$$P_m < 0.9S_u = .9 * 68,300 \text{ psi} = 61,470 \text{ psi}$$

### 7.4 OBE with Thermal Stresses:

Lessor of  $2S_y$  or  $S_u$  stress range

For SA240, Type 304,

$$S_y = 27,500 \text{ psi at } 150^\circ\text{F}$$

$$S_u = 73,000 \text{ psi at } 150^\circ\text{F}$$

$$2 S_y = 2(27,500 \text{ psi}) = 55,000 \text{ psi} < 73,000 \text{ psi}$$

Therefore OBE combinations with thermal stresses are limited to an allowable stress range of 55,000 psi.

### 7.5 DBE with Thermal Stresses:

NF-3231.1c does not require inclusion of thermal stresses and hence specific limits are not provided. Therefore, the same limits as for OBE are used:

Lessor of  $2S_y$  or  $S_u$  stress range

For SA240, Type 304,

$$S_y = 23,650 \text{ psi at } 254^\circ\text{F}$$

$$S_u = 68,300 \text{ psi at } 254^\circ\text{F}$$

$$2 S_y = 2(23,650 \text{ psi}) = 47,300 \text{ psi} < 68,300 \text{ psi}$$

Therefore the DBE combination with thermal stresses are limited to an allowable stress range of 47,300 psi.

### 7.6 Fuel Assembly Lateral Impact Load

The permissible lateral load on an irradiated spent fuel assembly has been studied by the Lawrence Livermore National Laboratory (LLNL). The LLNL report (Ref. 18) states that "...for the most vulnerable fuel assembly, axial buckling varies from 82g's at initial storage to 95g's after 20 years' storage. In a side drop, no yielding is expected below 63g's at initial storage to 74g's after 20 years' [dry] storage."

### 7.7 Fatigue Analysis

SPEC-06-0002-A [14] requires that it be verified that multiple seismic events will not cause the Cumulative Damage factor to exceed 1.

Cyclic loads that the racks are generally subjected to are primarily limited to thermal fluctuations of the pool water. Seismic loadings have relatively low number of cycles. ASME Section III, Subsection NF [15] (with reference to ASME III, Appendix XVII [12]) considers fatigue primarily for Class 1 (ASME III classification) equipment and pipe supports. As considered in Appendix XVII a single loading with a unique stress range and known cycles is assumed, and fatigue is addressed by reducing the allowable stresses based on the number of cycles. For the racks, multiple stress ranges with differing numbers of cycles exist. Therefore, the linear damage rule will be used, where the cumulative damage factor is determined as:

$$\sum \frac{n_i}{N_i} \leq 1.0$$

Where:  $n_i$  = number of applied cycles for the  $i_{th}$  stress range  
 $N_i$  = allowable number of cycles for the  $i_{th}$  stress range

ASME III, Appendix I [12], Table I-9.1 and Figure I-9.2 for austenitic steels will be used to determine allowable number of cycles.

## 7.8 Fuel Assembly and Gate Drop Analysis

For the fuel assembly and gate drop analysis, the acceptance criteria are different depending on the scenario analyzed, but all criteria are imposed by maintaining the storage elements affected subcritical.

For all shallow drop scenarios the acceptance criteria is that the impact resulting from the drop of the fuel assembly will either not cause permanent damage into the active fuel region, or that the consequences of damage into the active fuel region are shown by a criticality analysis to maintain a neutron multiplication factor less than 0.95. The Metamic poison panels are contained on the sides of the cells from 3.2" to 157.2" above the rack baseplate. This means that the allowable depth of cell that could be crushed during impacts without affecting the criticality of the structure is  $189" - 157.2" = 31.8"$ . This allowable depth was considered as acceptance criteria for the structure, where if the depth of excessive plastic deformations is less than this value, acceptance is demonstrated, and if exceeded, a criticality analysis is required to demonstrate acceptance.

For the deep drop through the central cell (that affects the baseplate), the acceptance criteria will be that the impact will not lead to a gross failure or excessive deflection of the baseplate, which could result in unacceptable criticality consequences.

For the deep drop through the cell located above the pedestal, the most affected structural elements (the elements of the supporting structure from the SFP floor and the supporting concrete) must not lead to uncontrollable water leakage. This means that the liner must remain intact or exhibit only small plastic deformations on a restraint area, and that the concrete structural integrity will not be affected.

## **8.0 Analysis Results and Comparison to Acceptance Criteria**

### **8.1 Time-History Simulation Results**

The results from the seismic analyses are provided in the form of maximum values of the parameters of interest; namely overall forces and moments, displacements, support pedestal forces, and impact loads. Tables 8.1 through 8.4 summarize the overall global response of the various Single Rack and WPMR OBE and DBE Analyses.

The new racks in the pool are at the south end of the pool. Maintaining the same system of identification as previously identified in Figure 2.2 (with the R11 rack in the northern left corner of the pool and the rack R43 on the southern right corner of the pool), the new racks are identified as R41 (8x9 rack) and R42, R43 (9x9 racks).

Table 8.1 -- Result Summary – Load Case = D+L+OBE						
Rack Global Forces	Single Rack Analysis (SRA) (R41)			Full Pool Analysis (FPA) (R41)		
	F.Coeff=0.2	F.Coeff=0.5	F.Coeff=0.8	F.Coeff=0.2	F.Coeff=0.5	F.Coeff=0.8
Base S <sub>hx</sub>	6.042x10 <sup>4</sup>	1.144x10 <sup>5</sup>	1.561x10 <sup>5</sup>	4.838x10 <sup>4</sup>	1.094x10 <sup>5</sup>	1.429x10 <sup>5</sup>
Base S <sub>hy</sub>	5.406x10 <sup>4</sup>	1.060x10 <sup>5</sup>	1.292x10 <sup>5</sup>	4.788x10 <sup>4</sup>	1.087x10 <sup>5</sup>	1.235x10 <sup>5</sup>
Axial F	-1.898x10 <sup>4</sup>	-1.898x10 <sup>4</sup>	-1.898x10 <sup>4</sup>	-1.898x10 <sup>4</sup>	-1.898x10 <sup>5</sup>	-1.898x10 <sup>4</sup>
Base M <sub>xx</sub>	7.561x10 <sup>6</sup>	1.413x10 <sup>7</sup>	1.896x10 <sup>7</sup>	6.667x10 <sup>6</sup>	1.435x10 <sup>7</sup>	1.716x10 <sup>7</sup>
Base M <sub>yy</sub>	8.193x10 <sup>6</sup>	1.606x10 <sup>7</sup>	2.186x10 <sup>6</sup>	6.864x10 <sup>6</sup>	1.579x10 <sup>7</sup>	2.054x10 <sup>6</sup>
Base D <sub>x</sub>	1.116	0.387	0.231	0.761	0.214	0.096
Base D <sub>y</sub>	1.795	0.534	0.377	1.189	0.124	0.072
Top D <sub>x</sub>	1.133	0.446	0.269	0.769	0.259	0.174
Top D <sub>y</sub>	1.810	0.577	0.459	1.197	0.160	0.140
Base Acc <sub>x</sub>	77.63	113.70	148.21	82.95	165.11	169.91
Base Acc <sub>y</sub>	102.01	105.71	148.87	94.57	120.36	132.69
Top Acc <sub>x</sub>	160.35	225.57	235.81	155.11	261.08	331.69
Top Acc <sub>y</sub>	160.30	237.70	283.06	166.20	304.11	325.89
Max. Fuel Impact	2.249x10 <sup>4</sup>	4.069x10 <sup>4</sup>	4.564x10 <sup>4</sup>	2.396x10 <sup>4</sup>	4.100x10 <sup>4</sup>	4.839x10 <sup>4</sup>
Foot-1	-9.188x10 <sup>4</sup>	-1.615x10 <sup>5</sup>	-2.332x10 <sup>5</sup>	-9.483x10 <sup>4</sup>	-1.595x10 <sup>5</sup>	-2.211x10 <sup>5</sup>
Foot-2	-1.040x10 <sup>5</sup>	-1.841x10 <sup>5</sup>	-2.319x10 <sup>5</sup>	-1.009x10 <sup>5</sup>	-1.738x10 <sup>5</sup>	-2.292x10 <sup>5</sup>
Foot-3	-1.032x10 <sup>5</sup>	-1.692x10 <sup>5</sup>	-2.175x10 <sup>5</sup>	-9.064x10 <sup>4</sup>	-1.663x10 <sup>5</sup>	-2.276x10 <sup>5</sup>
Foot-4	-1.032x10 <sup>5</sup>	-1.690x10 <sup>5</sup>	-2.423x10 <sup>5</sup>	-9.680x10 <sup>4</sup>	-1.784x10 <sup>5</sup>	-2.479x10 <sup>5</sup>

Note: Results are for the 8x9 rack (region 1), Units: Displacement [in]; Forces [lb]; Moments [lb-in], Accelerations [in/sec<sup>2</sup>]; Foot-1 – SW corner of the rack, Foot-2 – SE corner of the rack, Foot-3 – NE corner of the rack, Foot-4 – NW corner of the rack. S<sub>hx</sub> and S<sub>hy</sub> are horizontal shear forces with units of (lb).

Table 8.2 -- Result Summary – Load Case = D+L+OBE						
Rack Global Forces	Full Pool Analysis (FPA) (R42)			Full Pool Analysis (FPA) (R43)		
	F.Coeff=0.2	F.Coeff=0.5	F.Coeff=0.8	F.Coeff=0.2	F.Coeff=0.5	F.Coeff=0.8
Base S <sub>hx</sub>	6.374x10 <sup>4</sup>	1.460x10 <sup>5</sup>	1.883x10 <sup>4</sup>	5.793x10 <sup>4</sup>	1.271x10 <sup>5</sup>	1.811x10 <sup>5</sup>
Base S <sub>hy</sub>	6.270x10 <sup>4</sup>	1.182x10 <sup>5</sup>	1.721x10 <sup>5</sup>	6.043x10 <sup>4</sup>	1.292x10 <sup>5</sup>	1.520x10 <sup>5</sup>
Axial F	-2.123x10 <sup>4</sup>	-2.123x10 <sup>4</sup>	-2.123x10 <sup>4</sup>	-2.123x10 <sup>4</sup>	-2.123x10 <sup>4</sup>	-2.123x10 <sup>4</sup>
Base M <sub>xx</sub>	8.801x10 <sup>6</sup>	1.671x10 <sup>7</sup>	2.230x10 <sup>7</sup>	8.578x10 <sup>6</sup>	1.815x10 <sup>7</sup>	2.133x10 <sup>7</sup>
Base M <sub>yy</sub>	9.256x10 <sup>6</sup>	1.965x10 <sup>7</sup>	2.694x10 <sup>7</sup>	8.068x10 <sup>6</sup>	1.763x10 <sup>7</sup>	2.614x10 <sup>7</sup>
Base D <sub>x</sub>	0.821	0.260	0.157	0.750	0.292	0.087
Base D <sub>y</sub>	1.391	0.295	0.167	1.335	0.165	0.124
Top D <sub>x</sub>	0.830	0.308	0.202	0.759	0.329	0.153
Top D <sub>y</sub>	1.397	0.326	0.232	1.340	0.209	0.212
Base Acc <sub>x</sub>	120.35	151.38	151.98	92.86	131.95	173.87
Base Acc <sub>y</sub>	90.03	115.64	147.43	82.51	123.48	140.10
Top Acc <sub>x</sub>	166.71	261.31	331.08	162.15	226.56	320.84
Top Acc <sub>y</sub>	169.20	279.18	333.53	176.44	303.33	373.05
Max. Fuel Impact	2.398x10 <sup>4</sup>	4.581x10 <sup>4</sup>	5.506x10 <sup>4</sup>	2.672x10 <sup>4</sup>	4.682x10 <sup>4</sup>	5.506x10 <sup>4</sup>
Foot -1	-1.204x10 <sup>5</sup>	-1.932x10 <sup>5</sup>	-2.703x10 <sup>5</sup>	-1.137x10 <sup>5</sup>	-1.945x10 <sup>5</sup>	-2.583x10 <sup>5</sup>
Foot-2	-1.100x10 <sup>5</sup>	-1.993x10 <sup>5</sup>	-2.684x10 <sup>5</sup>	-1.129x10 <sup>5</sup>	-1.996x10 <sup>5</sup>	-2.637x10 <sup>5</sup>
Foot-3	-1.041x10 <sup>5</sup>	-1.909x10 <sup>5</sup>	-2.619x10 <sup>5</sup>	-1.002x10 <sup>5</sup>	-1.709x10 <sup>5</sup>	-2.468x10 <sup>5</sup>
Foot-4	-1.028x10 <sup>5</sup>	-1.906x10 <sup>5</sup>	-2.350x10 <sup>5</sup>	-1.079x10 <sup>5</sup>	-2.066x10 <sup>5</sup>	-2.418x10 <sup>5</sup>

Note: Results are for the 9x9 racks (Region 1), Units: Displacement [in]; Forces [lb]; Moments [lb-in], Accelerations [in/sec<sup>2</sup>]; Foot-1 – SW corner of the rack, Foot-2 – SE corner of the rack, Foot-3 – NE corner of the rack, Foot-4 – NW corner of the rack. S<sub>hx</sub> and S<sub>hy</sub> are horizontal shear forces with units of (lb).

Table 8.3 -- Result Summary – Load Case = D+L+DBE						
Rack Global Forces	Single Rack Analysis (SRA) (R41)			Full Pool Analysis (FPA) (R41)		
	F.Coeff=0.2*	F.Coeff=0.5	F.Coeff=0.8	F.Coeff=0.2	F.Coeff=0.5	F.Coeff=0.8
Base S <sub>hx</sub>	2.315x10 <sup>5</sup>	1.298x10 <sup>5</sup>	1.768x10 <sup>5</sup>	5.151x10 <sup>4</sup>	9.948x10 <sup>4</sup>	1.545x10 <sup>5</sup>
Base S <sub>hy</sub>	1.896x10 <sup>5</sup>	1.167x10 <sup>5</sup>	1.482x10 <sup>5</sup>	5.346x10 <sup>4</sup>	1.142x10 <sup>5</sup>	1.530x10 <sup>5</sup>
Axial F	-1.994x10 <sup>4</sup>	-1.994x10 <sup>4</sup>	-1.994x10 <sup>4</sup>	-1.994x10 <sup>4</sup>	-1.994x10 <sup>4</sup>	-1.994x10 <sup>4</sup>
Base M <sub>xx</sub>	2.706x10 <sup>7</sup>	1.576x10 <sup>7</sup>	2.140x10 <sup>7</sup>	7.449x10 <sup>6</sup>	1.539x10 <sup>7</sup>	2.118x10 <sup>7</sup>
Base M <sub>yy</sub>	3.302x10 <sup>7</sup>	1.869x10 <sup>7</sup>	2.432x10 <sup>7</sup>	7.131x10 <sup>6</sup>	1.418x10 <sup>7</sup>	2.093x10 <sup>7</sup>
Base D <sub>x</sub>	3.472	2.887	0.972	4.686	1.462	0.515
Base D <sub>y</sub>	4.162	2.117	1.227	4.557	1.055	0.722
Top D <sub>x</sub>	3.471	2.927	0.994	4.691	1.479	0.565
Top D <sub>y</sub>	4.313	2.167	1.268	4.559	1.072	0.777
Base Acc <sub>x</sub>	120.74	150.56	187.41	135.04	164.60	193.07
Base Acc <sub>y</sub>	220.68	159.48	169.15	136.46	183.50	213.78
Top Acc <sub>x</sub>	335.63	284.04	318.85	222.50	326.80	383.63
Top Acc <sub>y</sub>	371.87	270.17	311.04	191.91	316.02	421.29
Max. Fuel Impact	5.100x10 <sup>4</sup>	5.652x10 <sup>4</sup>	7.166x10 <sup>4</sup>	2.289x10 <sup>4</sup>	5.446x10 <sup>4</sup>	6.403x10 <sup>4</sup>
Foot -1	-2.670x10 <sup>5</sup>	-1.834x10 <sup>5</sup>	-2.821x10 <sup>5</sup>	-1.216x10 <sup>5</sup>	-2.161x10 <sup>5</sup>	-2.864x10 <sup>5</sup>
Foot-2	-2.304x10 <sup>5</sup>	-1.904x10 <sup>5</sup>	-2.805x10 <sup>5</sup>	-1.053x10 <sup>5</sup>	-1.787x10 <sup>5</sup>	-2.247x10 <sup>5</sup>
Foot-3	-2.330x10 <sup>5</sup>	-2.000x10 <sup>5</sup>	-2.809x10 <sup>5</sup>	-1.040x10 <sup>5</sup>	-1.965x10 <sup>5</sup>	-2.783x10 <sup>5</sup>
Foot-4	-1.427x10 <sup>5</sup>	-1.864x10 <sup>5</sup>	-2.843x10 <sup>5</sup>	-9.574x10 <sup>4</sup>	-1.964x10 <sup>5</sup>	-2.253x10 <sup>5</sup>

Note: Results are for the 8x9 rack (Region 1), Units: Displacement [in]; Forces [lb]; Moments [lb-in], Accelerations [in/sec<sup>2</sup>]; Foot-1 – SW corner of the rack, Foot-2 – SE corner of the rack, Foot-3 – NE corner of the rack, Foot-4 – NW corner of the rack. S<sub>hx</sub> and S<sub>hy</sub> are horizontal shear forces with units of (lb).

\* The results for this case are unrealistic. During the analysis some impacts (with the fixed boundaries simulating the presence of other racks or pool walls) took place, which do not occur in the full pool analysis (see Figure 8-1), due to the fact that during this analysis the neighboring racks were moving. Analyses have been carried out for the single rack and full pool analysis that capture the so called "group effect". The "group effect" is also documented in Ref. [3]. The difference is due to the fact that the neighboring racks are moving and transfer interaction forces to each other, and all racks have a tendency to have a degree of synchronization. Note however, that the values used to check the racks envelop all the single and full pool analysis results, hence these results were still considered.

Analyzing Figure 8-1 it can be seen that for the single rack analysis (using rack R41) there are three impacts. The first impact for the R41 single rack model (upper right) is with the rack R31 (modeled as a fixed point), which took place at 5.725 sec. This impact added 1.874·10<sup>5</sup> lbs to the dynamics of the rack, perturbing its kinematics. The subsequent impacts (located closer – at 6.765 and 6.995 seconds) with the R42 rack (also modeled as a fixed point) and the southern

pool wall could be considered consequences of this perturbation in kinematics (as they are not evident in the full pool analysis results).

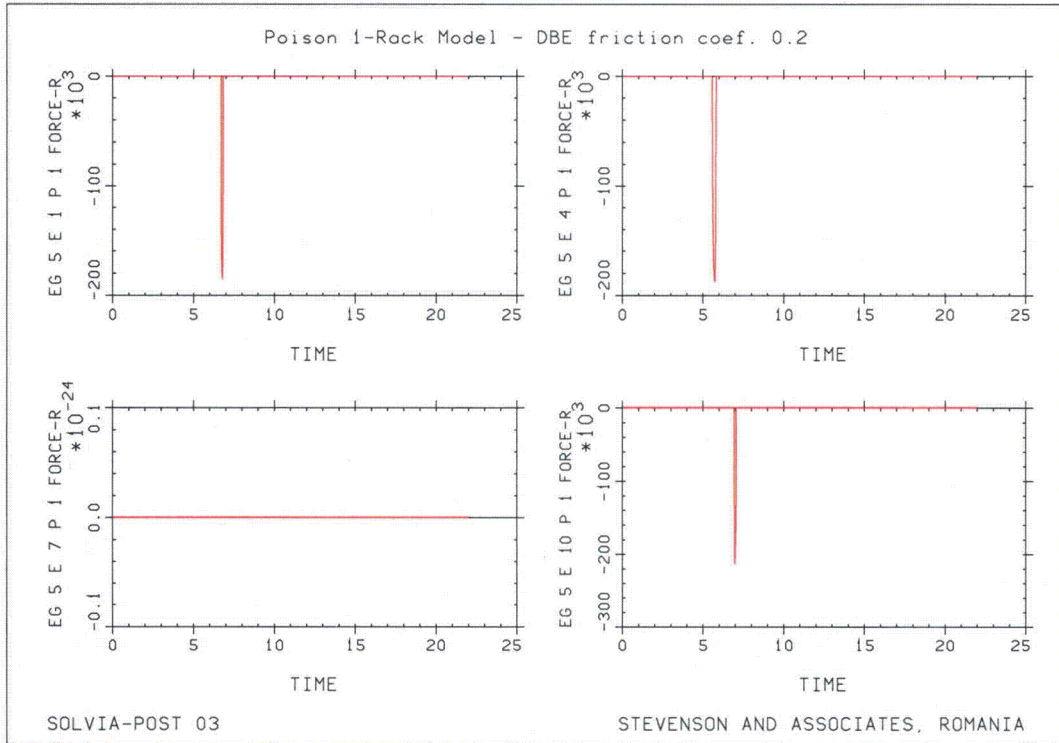


Figure 8-1 -- Single rack analysis – impacts at base of the R41 rack with other racks and pool wall  
(Note, other racks and pool walls were modeled as fixed points for the single rack model)

Stevenson & Associates Report 06Q3571.07-01

Table 8.4 -- Result Summary – Load Case = D+L+DBE						
Rack Global Forces	Full Pool Analysis (FPA) (R42)			Full Pool Analysis (FPA) (R43)		
	F.Coeff=0.2	F.Coeff=0.5	F.Coeff=0.8	F.Coeff=0.2	F.Coeff=0.5	F.Coeff=0.8
Base S <sub>hx</sub>	5.784x10 <sup>4</sup>	1.285x10 <sup>5</sup>	2.142x10 <sup>5</sup>	5.405x10 <sup>4</sup>	1.357x10 <sup>5</sup>	1.912x10 <sup>5</sup>
Base S <sub>hy</sub>	7.026x10 <sup>4</sup>	1.290x10 <sup>5</sup>	2.017x10 <sup>5</sup>	6.571x10 <sup>4</sup>	1.373x10 <sup>5</sup>	1.845x10 <sup>5</sup>
Axial F	-2.230x10 <sup>4</sup>	-2.230x10 <sup>4</sup>	-2.230x10 <sup>4</sup>	-2.230x10 <sup>4</sup>	-2.230x10 <sup>4</sup>	-2.230x10 <sup>4</sup>
Base M <sub>xx</sub>	9.426x10 <sup>6</sup>	1.854x10 <sup>7</sup>	2.639x10 <sup>7</sup>	9.107x10 <sup>6</sup>	1.910x10 <sup>7</sup>	2.479x10 <sup>7</sup>
Base M <sub>yy</sub>	7.311x10 <sup>6</sup>	1.833x10 <sup>7</sup>	2.736x10 <sup>7</sup>	7.662x10 <sup>6</sup>	1.801x10 <sup>7</sup>	2.509x10 <sup>7</sup>
Base D <sub>x</sub>	4.832	1.634	0.683	4.777	1.514	0.604
Base D <sub>y</sub>	5.354	1.672	0.694	4.858	1.328	0.720
Top D <sub>x</sub>	4.835	1.636	0.731	4.775	1.528	0.608
Top D <sub>y</sub>	5.352	1.712	0.741	4.859	1.351	0.772
Base Acc <sub>x</sub>	142.95	191.27	207.34	142.10	172.38	188.67
Base Acc <sub>y</sub>	129.36	156.04	186.77	144.57	172.14	214.66
Top Acc <sub>x</sub>	240.48	350.16	391.05	217.64	330.66	363.22
Top Acc <sub>y</sub>	175.17	235.43	342.51	185.98	308.96	381.83
Max. Fuel Impact	2.596x10 <sup>4</sup>	6.091x10 <sup>4</sup>	6.662x10 <sup>4</sup>	2.497x10 <sup>4</sup>	5.821x10 <sup>4</sup>	6.758x10 <sup>4</sup>
Foot -1	-1.455x10 <sup>5</sup>	-2.181x10 <sup>5</sup>	-3.038x10 <sup>5</sup>	-1.398x10 <sup>5</sup>	-2.354x10 <sup>5</sup>	-2.825x10 <sup>5</sup>
Foot-2	-1.128x10 <sup>5</sup>	-2.141x10 <sup>5</sup>	-2.749x10 <sup>5</sup>	-1.124x10 <sup>5</sup>	-1.920x10 <sup>5</sup>	-2.518x10 <sup>5</sup>
Foot-3	-1.350x10 <sup>5</sup>	-2.228x10 <sup>5</sup>	-3.007x10 <sup>5</sup>	-1.236x10 <sup>4</sup>	-2.070x10 <sup>5</sup>	-2.978x10 <sup>5</sup>
Foot-4	-1.118x10 <sup>5</sup>	-2.131x10 <sup>5</sup>	-2.653x10 <sup>5</sup>	-1.019x10 <sup>5</sup>	-2.059x10 <sup>5</sup>	-2.583x10 <sup>5</sup>

Note: Results are for the 9x9 racks (Region 1), Units: Displacement [in]; Forces [lb]; Moments [lb-in], Accelerations [in/sec<sup>2</sup>]; Foot-1 – SW corner of the rack, Foot-2 – SE corner of the rack, Foot-3 – NE corner of the rack, Foot-4 – NW corner of the rack. S<sub>hx</sub> and S<sub>hy</sub> are horizontal shear forces with units of (lb).

## 8.2 Consideration of Dummy Fuel Assembly and Miscellaneous Equipment

From Reference [14], ANO will use the racks to store fuel assemblies and other miscellaneous items such as damaged fuel assemblies, control element assemblies, debris canisters, or consolidated fuel canisters in the storage cells. Reference [14] hence specifies, that 1 dummy fuel assembly in inventory in the spent fuel pool that weighs 2400 lb, be considered. This dummy fuel assembly is assumed to be placed anywhere (in a fuel cell) in any rack in the pool. In addition, Reference [14] indicates that miscellaneous equipment weighing as much as 2000 lb may be temporarily mounted on a fuel rack. Reference [14] specifies that for structural qualification, the equipment shall be simulated as a rigid body with its center of gravity no more than 24" above the top of the racks. Qualification for applicable seismic excitations is necessary. Also, a single load rigid body of 200 lb with a center of gravity no more than 12" above the top of the racks is to be considered.

In order to evaluate the impact of the presence of a dummy fuel assembly (weighing 2,400 lb) inside of the 8x9 new rack, a single rack analysis was performed and the results are compared with those obtained in the regular single rack analysis. The additional mass was considered when the fuel mass was computed.

The same model was also used for considering some miscellaneous equipment laying on top of the rack (2000 lb at 2 ft above). The entire mass was considered concentrated at a point located 24 inches above the top of the rack. The point was rigidly connected with the top of the rack. This 2000 lb load is considered to bound the effects of the 200 lb load.

Table 8.5 presents the comparison of the two situations described to the regular case for the 8x9 new poison rack. The analysis assumed DBE seismic load and a friction coefficient of 0.8.

<b>Table 8.5 – Analysis of Dummy Fuel and Miscellaneous Equipment</b>			
Rack Global Forces	Single Rack Analysis (SRA) (R41)		
	Normal	dummy fuel	miscellaneous equipment
Base S <sub>hx</sub>	1.768x10 <sup>5</sup>	1.772x10 <sup>5</sup>	1.780x10 <sup>5</sup>
Base S <sub>hy</sub>	1.482x10 <sup>5</sup>	1.558x10 <sup>5</sup>	1.585x10 <sup>5</sup>
Axial F	-1.994x10 <sup>4</sup>	-1.994x10 <sup>4</sup>	-2.219x10 <sup>4</sup>
Base M <sub>xx</sub>	2.140x10 <sup>7</sup>	2.217x10 <sup>7</sup>	2.242x10 <sup>7</sup>
Base M <sub>yy</sub>	2.432x10 <sup>7</sup>	2.451x10 <sup>7</sup>	2.425x10 <sup>7</sup>
Base D <sub>x</sub>	0.972	1.037	0.924
Base D <sub>y</sub>	1.227	1.086	1.170
Top D <sub>x</sub>	0.994	1.054	0.971
Top D <sub>y</sub>	1.268	1.134	1.210
Base Acc <sub>x</sub>	187.41	171.48	191.59
Base Acc <sub>y</sub>	169.15	200.50	192.66
Top Acc <sub>x</sub>	318.85	300.02	325.26
Top Acc <sub>y</sub>	311.04	329.43	341.21
Max. Fuel Impact	7.166x10 <sup>4</sup>	8.262x10 <sup>4</sup>	7.273x10 <sup>4</sup>
Foot -1	-2.821x10 <sup>5</sup>	-2.838x10 <sup>5</sup>	-2.855x10 <sup>5</sup>
Foot-2	-2.805x10 <sup>5</sup>	-2.827x10 <sup>5</sup>	-2.946x10 <sup>5</sup>
Foot-3	-2.809x10 <sup>5</sup>	-3.014x10 <sup>5</sup>	-2.968x10 <sup>5</sup>
Foot-4	-2.843x10 <sup>5</sup>	-2.880x10 <sup>5</sup>	-2.949x10 <sup>5</sup>

Note: Results are for the 8x9 new rack (Region 1), Units: Displacement [in]; Forces [lb]; Moments [lb-in], Accelerations [in/sec<sup>2</sup>]; Foot-1 – SW corner of the rack, Foot-2 – SE corner of the rack, Foot-3 – NE corner of the rack, Foot-4 – NW corner of the rack. S<sub>hx</sub> and S<sub>hy</sub> are horizontal shear forces with units of (lb).

From the comparisons between the normal situation to the rack with the dummy fuel loaded, and to the rack with miscellaneous equipment laying on top, it can be seen that the changes are not significant, except for the fuel-rack impact for the dummy fuel case. Hence, from this result, the analysis of the fuel-rack impact load considered an increase of 15.3% in load magnitude.

### 8.3 Maximum Rack Displacements and Rocking

#### 8.3.1 Lateral Seismic Displacements

Except for the single rack analysis case discussed above, no impacts were recorded between the racks, or between the racks and the pool walls for all analysis cases.

The kinematics of the new racks nodes (extreme values of displacements on both lateral axes) are listed in Table 8.6.

Rack	Node	dxmax (in)	dxmin (in)	dymax (in)	dymin (in)
R41 (8x9)	9001	4.686	-1.061	4.556	-1.052
	9002	4.686	-1.062	4.557	-1.053
	9003	4.686	-1.064	4.557	-1.055
	9004	4.687	-1.067	4.557	-1.058
	9005	4.689	-1.071	4.558	-1.061
	9006	4.691	-1.073	4.559	-1.063
R42 (9x9)	10,001	4.832	-1.085	5.354	-1.100
	10,002	4.832	-1.085	5.354	-1.101
	10,003	4.832	-1.086	5.354	-1.102
	10,004	4.832	-1.087	5.353	-1.103
	10,005	4.834	-1.088	5.353	-1.105
	10,006	4.835	-1.088	5.352	-1.105
R43 (9x9)	11,001	4.777	-1.116	4.858	-1.109
	11,002	4.776	-1.117	4.858	-1.109
	11,003	4.775	-1.119	4.858	-1.110
	11,004	4.774	-1.121	4.859	-1.111
	11,005	4.774	-1.124	4.859	-1.112
	11,006	4.775	-1.126	4.859	-1.113

Note: All displacements are in inches. Nodes progress from base (e.g. 9001) to top (e.g. 9006) for each rack.

#### 8.3.2 Rack Lift-off Stability

The energy which produced rack lift-off is calculated for various loading scenarios. The allowable lift-off energy corresponds to the zero stability moment.

The following parameters are used for calculation of the lift off energy and allowable lift off:

For Rack with 8x9 cells:

Maximum horizontal displacement (relative to base):	0.193 in
Rigid body rotation angle:	0.001 rad
Maximum uplift of the center of the weight :	0.035 in
Fuel center of the weight: $167/2+0.5+3+1.88 =$	88.88 in
Minimum distance between pedestals:	68.3 in
Distance to the empty rack CG $L_{RS} =$	34.3 in

## Stevenson & Associates Report 06Q3571.07-01

Rack empty weight	21700 lb
Fuel design weight	1800 lb
Rack full weight	151,300 lb
Rack per cell	2101.389 lb
Lift-off Energy /cell	73.458 lb-in/cell

The calculation of the lift off CG, allowable lift off, and safety factors was conducted for various loading conditions. From these calculations the minimum safety factor is 59 corresponding to the case with three rows loaded with spent fuel. This satisfies OBE and DBE criteria of 1.5 and 1.1.

### 8.4 Pedestal Evaluation

#### 8.4.1 Maximum Pedestal Vertical Forces

The maximum loads on any pedestal for the new racks are  $2.703 \times 10^5$  lb for the OBE load combination, and  $3.038 \times 10^5$  lb for DBE load combination. Both correspond to the analysis cases with a friction coefficient of 0.8.

#### 8.4.2 Maximum Pedestal Horizontal Forces (From Friction)

The maximum interface shear force values for the new racks were not explicitly extracted from the analyses. Limiting values are obtained by considering the maximum vertical forces (normal load) times the coefficient of friction. From this, the maximum limiting shear forces from the new racks at the base of the pedestals is 216,240 lb for the OBE load combination, and 243,040 lb for the DBE load combination.

#### 8.4.3 Pedestal and Pedestal Connection Structural Evaluation

Pedestals consist of the female part (3" thick x 18" square plates at each corner using SA-240-304 material) and the male part (4½" diameter round bar using SA-564-630 material). Stress on the pedestal components is controlled by the shear on the female threads due to the effective engagement lengths less than the thread diameter, and the relatively high material strength of the male part ( $F_{y\text{-male}} = 104100$  psi versus  $F_{y\text{-female}} = 23650$  psi).

For the OBE condition the maximum shear stress in the pedestal support threads was:

$$9859.6 \text{ psi} < 11,000 \text{ psi allowable (Ref. [5])}$$

For the DBE condition the maximum shear stress in the pedestal support threads was:

$$11081.5 \text{ psi} < 17,028 \text{ psi allowable (Ref. [5])}$$

## 8.5 Rack Structural Evaluation

### 8.5.1 Rack Member Evaluations

To analyze the new rack modules for stresses, full 3-D models were developed for both new rack configurations using shell elements. These models were analyzed using ANSYS to determine stresses in the racks from deadweight plus seismic loading by applying maximum differential displacements from the results of the time-history beam model analyses.

Separately, these models were used to analyze the new racks for thermal expansion loading.

The limiting maximum combined rack stress interaction coefficient for axial and bending stresses for the OBE load combination =  $0.878 < 1.0$  allowable, and for the DBE load combination =  $0.638 < 1.0$  allowable. These evaluations are for the worst case point for the rack cell plates.

Stresses at the welds were also analyzed with a 3-D model. The limiting maximum combined stress interaction coefficient for any of the welds for the OBE load combination =  $0.75 < 1.0$  allowable, and for any of the welds for the DBE load combination =  $0.455 < 1.0$  allowable. These evaluations are for the worst case point for the rack cell plates.

## 8.6 Impact Evaluation

### 8.6.1 Local Stress Evaluations Due to Impact Between the Fuel Assembly and Cell Wall

Local cell wall integrity is conservatively estimated from peak impact loads.

From Table 8.1 to 8.4 the maximum impact forces are:

- for OBE:  $5.506 \times 10^4$  lbs (FPA, OBE,  $\mu = 0.8 - R42, R43$ )  
 $4.564 \times 10^4$  lbs (SRA, OBE,  $\mu = 0.8 - R41$ )
- for DBE:  $7.166 \times 10^4$  lbs (SRA, DBE,  $\mu = 0.8 - R41$ )  
 $6.758 \times 10^4$  lbs (FPA, DBE,  $\mu = 0.8 - R43$ )

Effective impact forces for one fuel assembly impacting on one cell wall:

- for OBE:  $5.506 \times 10^4$  lbs / 81 = 679.75 lbs (FPA, OBE,  $\mu = 0.8 - R42, R43$ )  
 $4.564 \times 10^4$  lbs / 72 = 633.88 lbs (SRA, OBE,  $\mu = 0.8 - R41$ )
- for DBE:  $7.166 \times 10^4$  lbs / 72 = 995.28 lbs (SRA, DBE,  $\mu = 0.8 - R41$ )  
 $6.758 \times 10^4$  lbs / 81 = 834.32 lbs (FPA, DBE,  $\mu = 0.8 - R43$ )

The analyses are done using the two-cell assembly model (which is the same for the 8x9 and 9x9 racks – see Figure 8-2) using these maximum impact loads from seismic loading plus an additional 15.3% to account for the possible presence of a dummy fuel assembly. It means:

Stevenson & Associates Report 06Q3571.07-01

- for OBE: 784 lbs
- for DBE: 1148 lbs

The results are listed in Table 8.7.

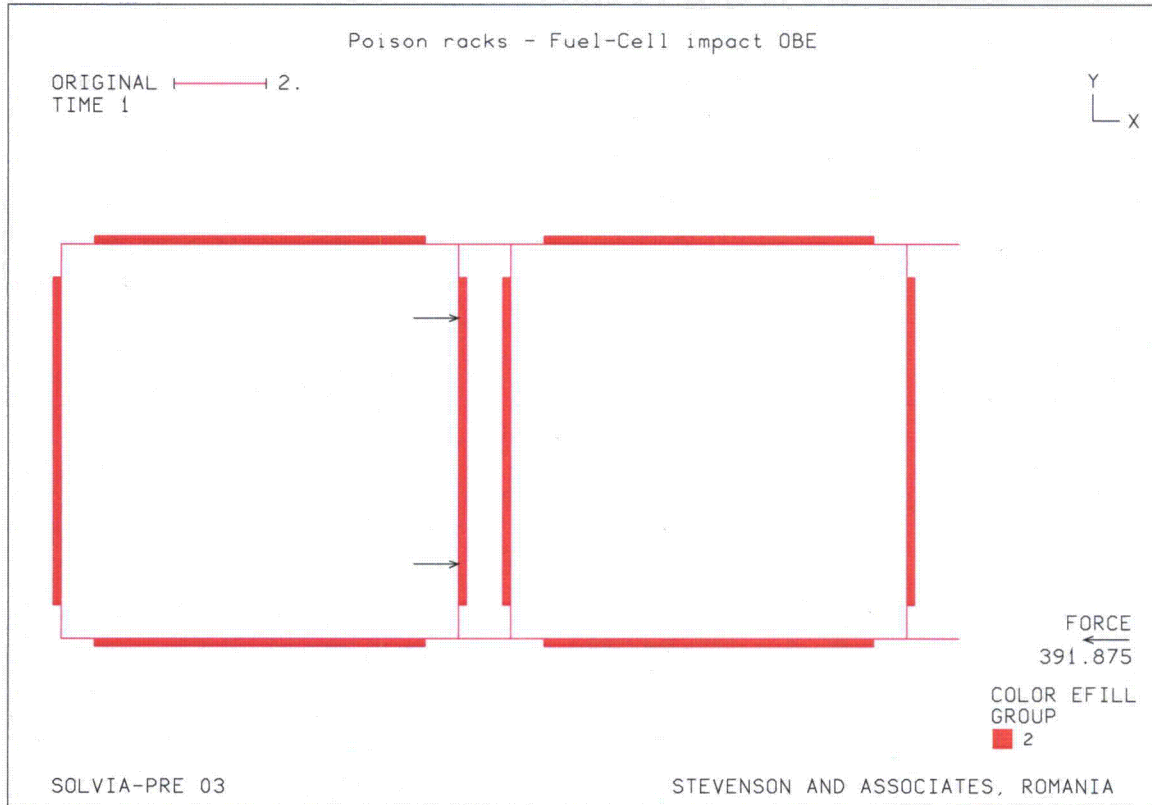


Figure 8-2 -- Two-cell model for local fuel-rack impact

Seismic Load	Von Mises Stress [psi]	Stress Limit [psi]
OBE	1,785	$0.6 \cdot S_y = 16,500$
DBE	2,613	$2 \cdot (0.6 \cdot S_y) = 28,380$

It can be seen that the OBE and DBE computed Von Mises stresses are much lower than the stress limits of  $0.6S_y$  for OBE and  $2(0.6 S_y)$  for DBE.

### 8.6.2 Evaluation of the Fuel Assembly

The permissible lateral load on an irradiated spent fuel assembly has been studied by the Lawrence Livermore National Laboratory (LLNL). The LLNL report [18] states that "...for the most vulnerable fuel assembly, axial buckling varies from 82g's at initial storage to 95g's after

20 years' storage. In a side drop, no yielding is expected below 63g's at initial storage to 74g's after 20 years' [dry] storage."

The maximum fuel-to-storage cell rattling force from the WPMR runs is 1,148 lb calculated above. The weight of a fuel assembly is conservatively defined as 1800 lb. By inspection, the impact force from a side drop at 63 g's of the 1800 lb assembly is much greater than the 1148 lb impact load from the analysis and therefore, the fuel assembly is acceptable.

### 8.6.3 Rack to Wall or Rack to Rack Impact Loads

The storage racks do not impact the pool walls or adjacent racks under any simulation. The rack to rack or rack to wall gap elements did not close during the analytical simulations.

## 8.7 Fuel Assembly and Gate Drop Analysis Results

The 3-D models as used for thermal expansion analysis and stress analysis were modified and used to perform the accident drop analyses (Reference [20]). LS-DYNA (Reference [21]) was used to perform these analyses.

Due to the refueling operations of new and existing fuel, the new racks have the following limiting Kinetic Energy for all possible potentially new events. For these drop analyses, kinetic energy is determined using actual mass (weight) of the fuel assemblies and attached lifting devices.

Deep Drop: 1747 lb drop weight, 4.5212 lb-s<sup>2</sup>/in mass, Impact Velocity with Rack = 514.74 in/s

$$KE = \frac{1}{2}mv^2 = 0.5 * 4.5212 \text{ lb-s}^2/\text{in} * (514.74 \text{ in/s})^2 = 598,962 \text{ in-lb (Controls for Rack)}$$

Deep Drop: 1747 lb drop weight, 4.5212 lb-s<sup>2</sup>/in mass, Impact Velocity with Rack Base Plate = 477.92 in/s

$$KE = \frac{1}{2}mv^2 = 0.5 * 4.5212 \text{ lb-s}^2/\text{in} * (477.92 \text{ in/s})^2 = 516,338 \text{ in-lb (Controls for Rack Base)}$$

Shallow Drop: 2000 lb drop weight, 5.176 lb-s<sup>2</sup>/in mass, Impact Velocity with Rack Base at the Pedestal = 108.3 in/s

$$KE = \frac{1}{2}mv^2 = 0.5 * 5.176 \text{ lb-s}^2/\text{in} * (108.3 \text{ in/s})^2 = 30,354 \text{ in-lb (Controls at Pedestal)}$$

The postulated drop for the spent fuel gate is enveloped by the fuel assembly drops indicated, and will not control the impact on the top of the racks.

**Stevenson & Associates Report 06Q3571.07-01**

Notation for drop cases is as follows:

Load Case ID	Load Case description	Type of fuel assembly	Height of drop	Velocity [in/sec]
SDCSF	Drop on the corner of the corner cell of the rack from Spent Fuel Machine (SFM)	Spent fuel	14.9 in	100.40
SDESF	Drop on the edge of the corner cell of the rack from SFM	Spent Fuel	14.9 in	100.40
SDCFF	Drop on the corner of the corner cell of the rack from crane	Fresh Fuel	37.5 ft	514.74
SDEFF	Drop on the edge of the corner cell of the rack from crane	Fresh Fuel	37.5 ft	514.74
DDCFF	Drop through a central cell from crane	Fresh Fuel	37.5 ft	477.92
DDPSF	Drop through a cell located on the pedestal	Spent Fuel	14.9 in	108.3

Acceptance criteria	Load case covered	Computed quantity	Criteria check
The depth of excessive deformed area of cell wall must not exceed 31.8 inches, or a criticality analysis must be performed.	SDCSF SDESF SDCFF SDEFF	Maximum depth of excessively deformed area is 34.78 in.	Criticality Analysis Performed (Ref. 19) and all criteria satisfied.
No gross failure or excessive deflection of the baseplate	DDCFF	Maximum vertical deflection of baseplate is 1.518. Maximum total strain is 0.21 in/in	√
No failure of steel liner or area of crushed concrete	DDPSF	Maximum strain in the liner is 0.0004. Maximum stress in the bearing structure is elastic. The concrete exhibits plastic deformation of 0.00342 level on a very small area under the embedded plate	√

From the results presented the following conclusions are obtained:

1. The maximum depth of excessively deformed area of the cell wall as a result of an impact at the top of the rack (from the SFM at a height of 14.9 inches for a spent fuel assembly or from the crane at a height of 37.5 feet for a fresh fuel assembly) is 34.78 inches which is greater than the cell depth of 31.8 inches from the top of the rack to the top of the metamic poison panels.
2. The baseplate and the neighboring cells have no gross failure (maximum total strain 0.21 in/in) due to a drop of a fresh fuel assembly from 37.5 feet above the top of the rack through

## Stevenson & Associates Report 06Q3571.07-01

a central cell. Also, the maximum deflection is 1.518 inches which maintains the rack structure subcritical.

3. The steel liner that covers the SFP floor experiences stresses within the elastic range and has no damage subsequent to the impact by the accidental drop of a spent fuel assembly through the pedestal cell. The maximum strain is 0.0004 (under the yield limit of 0.002). The maximum Von Mises stress in the bearing steel elements is 12,480 psi (lower than the yield stress – 26,700 psi). The stresses in the concrete do not exceed the concrete strength.

Except as noted in 1. above, the new Region 1 racks as well as additional structures (as bearing structure) will resist the impacts resulting from postulated accidental drops of spent or fresh fuel assemblies maintaining their structural integrity. Stress and strain state is within design limits. Since the maximum depth of deformed area extends into the active fuel region, a criticality check was performed in Calculation CALC-06-E-0014-03 [19], and summarized in Chapter 4 of this submittal.

**8.8 Summary of Stress Results**

The stresses for the new Holtec rack components are summarized in Tables 8.8 and 8.9.

<b>Table 8.8 – Summary of Stress Results for OBE Load Case</b>				
Component	Stress Type	D + L + E		
		Calculated Stress (psi)	Allowable Stress (psi)	Stress Interaction
Cell Plates	Axial+Bending	14,487	16,500	0.878
Base Plates	Axial+Bending	11,013	16,500	0.667
Welds—Cells to Baseplate	Shear	844	21,000	0.040
Welds—Cell plates	Shear	15,749	21,000	0.750
Impact Loads on Cells	Membrane Tension	1,785	16,500	0.108
Pedestals – Threads	Shear	9,859.6	11,000	0.896
Bearing Plate	Bending	17,000	24,750	0.687
	Bearing (plate)	2,155	16,500	0.131
	Bearing (pool)	3,566	4,570	0.78 <sup>(2)</sup>
D + L + E + T <sub>a</sub> <sup>(1)</sup>				
Component	Stress Type	Calculated Stress (psi)	Allowable Stress (psi)	Stress Interaction
Cell Plates	Axial+Bending	17,566	55,000	0.319
Base Plates	Axial+Bending	16,628	55,000	0.302

Notes: (1) Load case uses T<sub>a</sub>. This load case envelopes other thermal cases except for DBE case reported below.  
 (2) Also indicates increased local loading on pool floor due to reduction from fourteen pedestals to four pedestals is acceptable.

**Stevenson & Associates Report 06Q3571.07-01**

<b>Table 8.9 -- Summary of Stress Results for DBE Load Case</b>				
Component	Stress Type	D + L + E <sup>(1)</sup>		
		Calculated Stress (psi)	Allowable Stress (psi)	Stress Interaction
Cell Plates	Axial+Bending	18,108	28,380	0.638
Base Plate	Axial+Bending	13,766	28,380	0.485
Welds—Cells to Baseplate	Shear	1,056	42,000	0.025
Welds—Cell plates	Shear	19,089	42,000	0.455
Impact Loads on Cells	Membrane Tension	2,613	28,380	0.092
Pedestals -- Threads	Shear	11,082	17,028	0.651
Bearing Plate	Bending	20,805	42,570	0.489
	Bearing (plate)	2,637	28,380	0.093
	Bearing (pool)	2,871	4,570	0.628 <sup>(2)</sup>
D + L + T <sub>a</sub> + E'				
Component	Stress Type	Applied Stress (psi)	Allowable Stress (psi)	Stress Interaction
Cell Plates	Axial+Bending	21,187	47,300	0.448
Base Plates	Axial+Bending	19,381	47,300	0.410

Notes: (1) Results presented without T<sub>a</sub> included.

(2) Also indicates increased local loading on pool floor due to reduction from fourteen pedestals to four pedestals is acceptable.

SPEC-06-0002-A requires that it be verified that multiple seismic events will not cause the Cumulative Damage Factor (CUF) to exceed 1. A fatigue analysis was conducted considering cyclic thermal and seismic loads. A CUF of 0.0061 < 1.0 was obtained.

## 9.0 Evaluation of Spent Fuel Pool Structural Integrity for Increased Loads from Spent Fuel Racks

The ANO-2 spent fuel pool consists of 4'-0" thick reinforced concrete walls and a 5'-9" thick floor slab. The pool is supported below by thick foundation walls. Concrete compressive strength for structural analysis for the ANO-2 spent fuel pool is 3000 psi minimum and reinforcement used was Grade 40.

The spent fuel pool was originally designed by Bechtel Corp. (Reference [22]) in accordance with the ACI 318-63 reinforced concrete building code, for loadings including deadweight of the structure, water, and spent fuel racks, hydrodynamic pressure from the water, operating thermal, accident thermal, seismic, tornado and flood loads. Rack loads were treated as a uniform load spread across the pool floor slab.

In 1981-1982, a reanalysis of the spent fuel pool structure including the foundation walls, refueling canal, and cask storage area was performed by Structural Dynamics Inc. (References [23] and [24]) in support of the re-rack project for ANO-2. Finite element methodology was used for this analysis. The same loads as described above in the Bechtel design were included in the analysis. The loads from the spent fuel racks included their deadweight (treated as live load on the pool floor slab) and vertical and horizontal seismic load effects. Rack loads were provided by Westinghouse Corp. This analysis, again used the acceptance criteria in the ACI 318-63 code, but supplemented the strength design methodology using provisions from the ACI 349-80 Nuclear Structure Reinforced Concrete Code [28]. The load combinations used were in accordance with Standard Review Plan, Section 3.8.

The dominant load effects were due to thermal expansion from the accident thermal loading for both analyses of the ANO-2 Spent Fuel Pool.

The analysis of the new spent fuel racks by Holtec International as described in Sections 3 through 8, resulted in revised loads imparted from the racks to the pool floor slab.

A review of the pool structure was performed using the 1981-1982 analysis by Structural Dynamics with the applied loads including the rack load effects. These effects were amplified using conservatively determined factors to account for the increased loads from the racks. Specifically, the deadweight loading of the racks was factored up by the ratio of the maximum deadweight increase for any of the racks. Similarly, the seismic load contributions were recalculated by factoring the seismic rack loads by the maximum ratio calculated for the worst case rack in either the horizontal or vertical directions. Combined forces and moments were then recalculated and compared to the 1981-1982 results.

For the 1981-1982 analysis, section moments were reported at 21 points in 7 locations. Review of the contributing load effects to the various fuel pool structure locations indicates the load effects from the racks have the highest contribution to the locations of the Pool Floor Slab, and the Pool Foundation Walls. This is due to the load path being primarily from the racks to the floor slab, and then to the foundation walls, with little loading from the racks being transferred to the structural elements above the fuel pool floor level. Five points were selected and checked

**Stevenson & Associates Report 06Q3571.07-01**

for the Pool Floor Slab and Pool Foundation Wall locations. For the other locations, by comparison to the conservative changes for these five points and the significant margin still obtained, the selected locations are bounding.

The section strengths for the five locations for the ANO-2 spent fuel pool were reviewed in detail relative to the increased loads from the new Holtec spent fuel racks. The assumptions as to the effective increase in loads are conservative. The results are summarized in Table 9.1, with comparison to the previous (Reference [21] and [22]) analysis results.

<b>Table 9.1 -- Summary of Section Strength Review of Selected Locations</b>			
Location	Section Strength Parameter	Previous Analysis Ratio to Code Allowable	Conservative Estimate of Ratio to Code Allowable for Increased Rack Loads
Pool Floor Slab East-West Section	Moment	0.54	0.570
	Transverse Shear	0.27	0.411
	In-Plane Shear	0.15	0.218
Pool Floor Slab North-South Section	Moment	0.49	0.531
	Transverse Shear	0.37	0.840
	In-Plane Shear	0.21	0.278
Pool Foundation North Wall	Moment	0.18	0.161
	Transverse Shear	0.29	0.321
	In-Plane Shear	0.40	0.600
Pool Foundation East Wall	Moment	0.30	0.270
	Transverse Shear	0.26	0.229
	In-Plane Shear	0.76	0.848
Pool Foundation West Wall	Moment	0.36	0.349
	Transverse Shear	0.29	0.332
	In-Plane Shear	0.64	0.777

From Table 9.1 it can be seen that for the increased loads from the Reference 5 rack analysis, the pool structure section moments and shears remain within allowable limits.

## 10.0 Conclusions

The overall design objectives of the spent fuel storage pool at ANO Unit 2 have been shown to meet the various Regulatory Guides, the Standard Review Plan, and industry standards.

The structural adequacy of the new Holtec poison spent fuel racks at ANO Unit 2 with the Metamic poison panels have been evaluated using the appropriate regulatory and design standards. Postulated loadings for normal, seismic, and accident conditions at the ANO Unit 2 site were considered in this analysis and evaluation.

The design adequacy of the racks and the poison panels has been confirmed with analyses that were performed in compliance with the USNRC Standard Review Plan [1], the USNRC Office of Technology Position Paper [2], Lawrence Livermore Report UCRL52342 [3], and ANO Specification APL-C-2502 [4]. All applicable displacement and stress acceptance criteria have been met for the racks and the new poison inserts, as summarized for the OBE and DBE in Tables 8.1 through 8.4 and Tables 8.6 through 8.9. Results for the Pool Structure Analysis are summarized in Table 9.1.

For the fuel drop accident, for one case, the damage area was determined to extend into the region of the metamic poison panels. This situation was analyzed relative to criticality concerns, and is addressed and discussed in Chapter 4 of this submittal.

## 11.0 References

- [1] USNRC NUREG-0800, Standard Review Plan, June 1987.
- [2] (USNRC Office of Technology) "OT Position for Review and Acceptance of Spent Fuel Storage and Handling Applications," dated April 14, 1978, and January 18, 1979 amendment thereto.
- [3] R.G. Dong, "Effective Mass and Damping of Submerged Structures," Lawrence Livermore National Laboratory, UCRL52342, April 1, 1978.
- [4] ANO Technical Specification APL-C-2502, "Technical Specifications for Earthquake Resistance Design of Structures and/or Components Located in the Auxiliary Building for the Arkansas Nuclear One Unit 2 Power Plant," Rev. 2, 4-22-87.
- [5] Calculation CALC-06-E-0014-01, "ANO-2 Holtec Rack Seismic Analysis," Rev. 0, March 16, 2007.
- [6] Calculation ANO-ER-02-011, "Review of Structural Analysis of the Arkansas Nuclear One Unit 2 Spent Fuel Pool For Revised Fuel Rack Loads," Rev. 0, March, 16, 2007.
- [7] SOLVIA, Finite Element System, Version 03, Solvia Engineering, AB, Sweden, 1987-2006.
- [8] Westinghouse Drawing 6130E47, "AP&L Unit 2 Spent Fuel Storage Rack Installation," Sheet 1 or 4, (2-W62A-016(1)-0).
- [9] Holtec International Drawing 4906, Revision 5, "Spent Fuel Pool Racks," 2-22-2007.
- [10] Calculation 91E-0079-02, Revision 3, "Design Report of Spent Fuel Storage Racks for Arkansas Power and Light Company, Plant Applicability, Arkansas Nuclear One, Unit 2" 1-08-2002 (analysis performed in 1983).
- [11] NUREG/CR-5912, BNL-NUREG-52335, "Review of the Technical Basis and Verification of Current Analysis Methods Used to Predict Seismic Response of Spent Fuel Storage Racks," Brookhaven National Laboratory, October 1992.
- [12] ASME Boiler & Pressure Vessel Code, Section III, Appendices, 1980, through Winter 1981 Addendum.
- [13] ACI 318-71, Building Code Requirements for Structural Concrete, American Concrete Institute, Detroit, Michigan, 1971.
- [14] SPEC-06-0002-A, "ANO-2 Spent Fuel Pool Partial Re-Rack," Revision 1.
- [15] ASME Boiler & Pressure Vessel Code, Section III, Subsection NF, 1980, through Winter 1981 Addendum.
- [16] S&A-RO Computer code TH-Spec, Version 1.5/2005.

**Stevenson & Associates Report 06Q3571.07-01**

- [17] Calculation ANO-ER-02-051, "Seismic Requalification of the Arkansas Nuclear One Unit 1 Spent Fuel Racks," Rev. 0, July 17, 2006.
- [18] Chun, R., Witte, M. and Schwartz, M., "Dynamic Impact Effects on Spent Fuel Assemblies," UCID-21246, Lawrence Livermore National Laboratory, October 1987. (fuel impact)
- [19] Calculation CALC-06-E-0014-03, "Criticality Safety Evaluation of the ANO Unit 2 Spent Fuel Racks," Rev. 0.
- [20] Calculation CALC-06-E-0014-02, "ANO-2 Holtec Rack Structural Drop Analysis," Rev. 0, March 16, 2007.
- [21] "ANSYS LS-DYNA User Manual", Version 10.0, 2005.
- [22] Bechtel Job No. 6600-2, Calculation No. 2.4.6.2, "Spent Fuel Pool -- Concrete Design and Seismic Analysis," Rev. 5, December 19, 1996.
- [23] Calculation No. 88-E-0035-08, "Structural Evaluation of the Arkansas Nuclear One--Unit 2 Spent Fuel Storage Facility, for Consolidated Fuel Storage," by Structural Dynamics Technology, Inc. APL-02-013, November 24, 1982. (Calculation: Revision 0, date, August 22, 1988).
- [24] Calculation No. 83-D-2021-02, Rev. 1, "Analysis of SF Pool Structure For High Density Storage Racks," by Structural Dynamics Technology, Inc. APL-0200-3000, April 15, 1983.
- [25] ASCE Standard 4-98, "Seismic Analysis of Safety Related Nuclear Structures and Commentary," American Society of Civil Engineers, Copyright 2000.
- [26] Chajes, A., "Principles of Structural Stability Theory," Prentice-Hall, New Jersey, 1974.
- [27] ACI 349-80, "Code Requirements for Nuclear Safety Related Concrete Structures," American Concrete Institute, Detroit, October 1980.

**Attachment 7**

**2CAN030706**

**List of Regulatory Commitments**

### List of Regulatory Commitments

The following table identifies those actions committed to by Entergy in this document. Any other statements in this submittal are provided for information purposes and are not considered to be regulatory commitments.

COMMITMENT	TYPE (Check one)		SCHEDULED COMPLETION DATE (If Required)
	ONE- TIME ACTION	CONTINUING COMPLIANCE	
The surveillance coupons will be approximately 4" x 8" and 0.106" thick, identical in composition and manufacturing process as the Metamic™ in the inserts (i.e., created from the same manufacturing lot used to manufacture the Metamic™ PIAs).		x	
The coupons will be mounted in stainless steel jackets simulating the actual insert design.		x	
The coupon tree will have ten coupons.		x	
The coupon tree will be installed within a cell in Region 2.		x	
The coupons will be staggered and placed adjacent to the active fuel region where, based on the burnup profile, the localized burnup is greater than the assembly average burnup.		x	
No welding will be used on the Metamic™ as per the PIA design.		x	
Scratches will be simulated by the mechanical etching or scribing the surface of the coupons. The scratches will be formed using hardened materials made out of carbon steel, stainless steel, and Metamic™. The scratches will not be cleaned after being applied to ensure an evaluation will be performed of the corrosion affects of leaving the trace material in a scratch.		x	
Coupons will be examined on a two year basis for the first three intervals and thereafter on a 4 to 5 year interval over the service life of the inserts.		x	
During the first six years, freshly discharged fuel assemblies will be placed on two sides of the coupon tree to ensure that the dose to the coupons is maximized.		x	

COMMITMENT	TYPE (Check one)		SCHEDULED COMPLETION DATE (If Required)
	ONE- TIME ACTION	CONTINUING COMPLIANCE	
Upon receipt of a coupon for testing, the exposed coupon should be carefully examined and photographed to document the appearance of the coupon, noting any sign of degradation that may be observed. Special attention will be paid to any edge or corner defects and to any discoloration, swelling, or surface pitting that might exist.		x	
<p>Measurements to be performed at each inspection will be as follows:</p> <ul style="list-style-type: none"> <li>• Physical observations of the surface appearance to detect pitting, swelling or other degradation,</li> <li>• Length, width, and thickness measurements to monitor for bulging and swelling (Measurements will be taken in five procedurally defined locations prior to placing the coupons in the ANO-2 SFP. When the coupon is removed, measurements will be taken in the same locations as the original measurements.) Length and width dimensions shall not exceed <math>\pm 0.125</math> inches when compared to the initial width or length. Thickness is used to monitor swelling and an increase in thickness at any point shall not exceed <math>\pm 0.01</math> inches of the initial thickness at that point</li> <li>• Weight and density to monitor for material loss (The weight of each coupon should be obtained within <math>\pm 5\%</math> of the initial coupon weight.), and</li> <li>• Neutron attenuation to confirm the <math>B_{10}</math> concentration or destructive chemical testing to determine the boron content.</li> </ul>		x	

**Attachment 9**

**2CAN030706**

**Affidavits for Withholding Information**

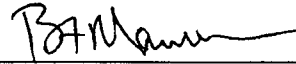
AFFIDAVIT

COMMONWEALTH OF PENNSYLVANIA:

ss

COUNTY OF ALLEGHENY:

Before me, the undersigned authority, personally appeared B. F. Maurer, who, being by me duly sworn according to law, deposes and says that he is authorized to execute this Affidavit on behalf of Westinghouse Electric Company LLC (Westinghouse), and that the averments of fact set forth in this Affidavit are true and correct to the best of his knowledge, information, and belief:

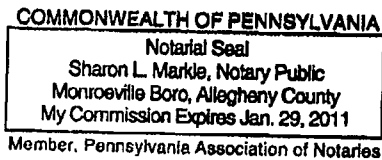


B. F. Maurer, Acting Manager  
Regulatory Compliance and Plant Licensing

Sworn to and subscribed before me  
this 23<sup>rd</sup> day of March, 2007



Notary Public



- (1) I am Acting Manager, Regulatory Compliance and Plant Licensing, in Nuclear Services, Westinghouse Electric Company LLC (Westinghouse), and as such, I have been specifically delegated the function of reviewing the proprietary information sought to be withheld from public disclosure in connection with nuclear power plant licensing and rule making proceedings, and am authorized to apply for its withholding on behalf of Westinghouse.
- (2) I am making this Affidavit in conformance with the provisions of 10 CFR Section 2.390 of the Commission's regulations and in conjunction with the Westinghouse application for withholding accompanying this Affidavit.
- (3) I have personal knowledge of the criteria and procedures utilized by Westinghouse in designating information as a trade secret, privileged or as confidential commercial or financial information.
- (4) Pursuant to the provisions of paragraph (b)(4) of Section 2.390 of the Commission's regulations, the following is furnished for consideration by the Commission in determining whether the information sought to be withheld from public disclosure should be withheld.
  - (i) The information sought to be withheld from public disclosure is owned and has been held in confidence by Westinghouse.
  - (ii) The information is of a type customarily held in confidence by Westinghouse and not customarily disclosed to the public. Westinghouse has a rational basis for determining the types of information customarily held in confidence by it and, in that connection, utilizes a system to determine when and whether to hold certain types of information in confidence. The application of that system and the substance of that system constitutes Westinghouse policy and provides the rational basis required.

Under that system, information is held in confidence if it falls in one or more of several types, the release of which might result in the loss of an existing or potential competitive advantage, as follows:

- (a) The information reveals the distinguishing aspects of a process (or component, structure, tool, method, etc.) where prevention of its use by any of Westinghouse's competitors without license from Westinghouse constitutes a competitive economic advantage over other companies.
- (b) It consists of supporting data, including test data, relative to a process (or component, structure, tool, method, etc.), the application of which data secures a competitive economic advantage, e.g., by optimization or improved marketability.
- (c) Its use by a competitor would reduce his expenditure of resources or improve his competitive position in the design, manufacture, shipment, installation, assurance of quality, or licensing a similar product.

- (d) It reveals cost or price information, production capacities, budget levels, or commercial strategies of Westinghouse, its customers or suppliers.
- (e) It reveals aspects of past, present, or future Westinghouse or customer funded development plans and programs of potential commercial value to Westinghouse.
- (f) It contains patentable ideas, for which patent protection may be desirable.

There are sound policy reasons behind the Westinghouse system which include the following:

- (a) The use of such information by Westinghouse gives Westinghouse a competitive advantage over its competitors. It is, therefore, withheld from disclosure to protect the Westinghouse competitive position.
  - (b) It is information that is marketable in many ways. The extent to which such information is available to competitors diminishes the Westinghouse ability to sell products and services involving the use of the information.
  - (c) Use by our competitor would put Westinghouse at a competitive disadvantage by reducing his expenditure of resources at our expense.
  - (d) Each component of proprietary information pertinent to a particular competitive advantage is potentially as valuable as the total competitive advantage. If competitors acquire components of proprietary information, any one component may be the key to the entire puzzle, thereby depriving Westinghouse of a competitive advantage.
  - (e) Unrestricted disclosure would jeopardize the position of prominence of Westinghouse in the world market, and thereby give a market advantage to the competition of those countries.
  - (f) The Westinghouse capacity to invest corporate assets in research and development depends upon the success in obtaining and maintaining a competitive advantage.
- (iii) The information is being transmitted to the Commission in confidence and, under the provisions of 10 CFR Section 2.390, it is to be received in confidence by the Commission.
  - (iv) The information sought to be protected is not available in public sources or available information has not been previously employed in the same original manner or method to the best of our knowledge and belief.

- (v) The proprietary information sought to be withheld in this submittal is that which is appropriately marked in Table 4.5.1 PWR Fuel Assembly Specifications contained in "Licensing Report for ANO Unit 2 Partial Rerack" Holtec Report No. HI-2063601 (Proprietary) being transmitted by Entergy Operations, Inc. letter and Application for Withholding Proprietary Information from Public Disclosure, to the Document Control Desk. The proprietary information as submitted by Westinghouse for ANO Unit 2 is for review and approval.

This information is part of that which will enable Westinghouse to:

- (a) Provide technical information in support of spent fuel pool rack criticality analysis licensing.

Further this information has substantial commercial value as follows:

- (a) Westinghouse can use this information to further enhance their licensing position with their competitors.
- (b) Assist customers to obtain license changes.

Public disclosure of this proprietary information is likely to cause substantial harm to the competitive position of Westinghouse because it would enhance the ability of competitors to provide similar analyses and licensing defense services for commercial power reactors without commensurate expenses. Also, public disclosure of the information would enable others to use the information to meet NRC requirements for licensing documentation without purchasing the right to use the information.

The development of the technology described in part by the information is the result of applying the results of many years of experience in an intensive Westinghouse effort and the expenditure of a considerable sum of money.

In order for competitors of Westinghouse to duplicate this information, similar technical programs would have to be performed and a significant manpower effort, having the requisite talent and experience, would have to be expended.

Further the deponent sayeth not.



**H O L T E C**  
I N T E R N A T I O N A L

Holtec Center, 555 Lincoln Drive West, Marlton, NJ 08053

Telephone (856) 797-0900

Fax (856) 797-0909

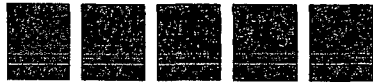
U.S. Nuclear Regulatory Commission  
ATTN: Document Control Desk

**AFFIDAVIT PURSUANT TO 10 CFR 2.390**

---

I, Debabrata Mitra-Majumdar, being duly sworn, depose and state as follows:

- (1) I am the Holtec International Project Manager for the Arkansas Nuclear One Unit 2 Partial Re-Rack Project (Holtec Project 1572) and have reviewed the information described in paragraph (2) which is sought to be withheld, and am authorized to apply for its withholding.
- (2) The information sought to be withheld is contained in Revision 0 of Holtec Report HI-2063601. Rack tolerances and poison material dimension tolerances are considered Holtec proprietary information.
- (3) In making this application for withholding of proprietary information of which it is the owner, Holtec International relies upon the exemption from disclosure set forth in the Freedom of Information Act ("FOIA"), 5 USC Sec. 552(b)(4) and the Trade Secrets Act, 18 USC Sec. 1905, and NRC regulations 10CFR Part 9.17(a)(4), 2.390(a)(4), and 2.390(b)(1) for "trade secrets and commercial or financial information obtained from a person and privileged or confidential" (Exemption 4). The material for which exemption from disclosure is here sought is all "confidential commercial information", and some portions also qualify under the narrower definition of "trade secret", within the meanings assigned to those terms for purposes of FOIA Exemption 4 in, respectively, Critical Mass Energy Project v. Nuclear Regulatory Commission, 975F2d871 (DC Cir. 1992), and Public Citizen Health Research Group v. FDA, 704F2d1280 (DC Cir. 1983).



**H O L T E C**  
I N T E R N A T I O N A L

Holtec Center, 555 Lincoln Drive West, Marlton, NJ 08053

Telephone (856) 797-0900

Fax (856) 797-0909

U.S. Nuclear Regulatory Commission  
ATTN: Document Control Desk

**AFFIDAVIT PURSUANT TO 10 CFR 2.390**

---

- (4) Some examples of categories of information which fit into the definition of proprietary information are:
- a. Information that discloses a process, method, or apparatus, including supporting data and analyses, where prevention of its use by Holtec's competitors without license from Holtec International constitutes a competitive economic advantage over other companies;
  - b. Information which, if used by a competitor, would reduce his expenditure of resources or improve his competitive position in the design, manufacture, shipment, installation, assurance of quality, or licensing of a similar product.
  - c. Information which reveals cost or price information, production, capacities, budget levels, or commercial strategies of Holtec International, its customers, or its suppliers;
  - d. Information which reveals aspects of past, present, or future Holtec International customer-funded development plans and programs of potential commercial value to Holtec International;
  - e. Information which discloses patentable subject matter for which it may be desirable to obtain patent protection.

The information sought to be withheld is considered to be proprietary for the reasons set forth in paragraphs 4.a and 4.b, above.

- (5) The information sought to be withheld is being submitted to the NRC in confidence. The information (including that compiled from many sources) is of a sort customarily held in confidence by Holtec International, and is in fact so



Holtec Center, 555 Lincoln Drive West, Marlton, NJ 08053

Telephone (856) 797-0900

Fax (856) 797-0909

U.S. Nuclear Regulatory Commission  
ATTN: Document Control Desk

**AFFIDAVIT PURSUANT TO 10 CFR 2.390**

---

held. The information sought to be withheld has, to the best of my knowledge and belief, consistently been held in confidence by Holtec International. No public disclosure has been made, and it is not available in public sources. All disclosures to third parties, including any required transmittals to the NRC, have been made, or must be made, pursuant to regulatory provisions or proprietary agreements which provide for maintenance of the information in confidence. Its initial designation as proprietary information, and the subsequent steps taken to prevent its unauthorized disclosure, are as set forth in paragraphs (6) and (7) following.

- (6) Initial approval of proprietary treatment of a document is made by the manager of the originating component, the person most likely to be acquainted with the value and sensitivity of the information in relation to industry knowledge. Access to such documents within Holtec International is limited on a "need to know" basis.
- (7) The procedure for approval of external release of such a document typically requires review by the staff manager, project manager, principal scientist or other equivalent authority, by the manager of the cognizant marketing function (or his designee), and by the Legal Operation, for technical content, competitive effect, and determination of the accuracy of the proprietary designation. Disclosures outside Holtec International are limited to regulatory bodies, customers, and potential customers, and their agents, suppliers, and licensees, and others with a legitimate need for the information, and then only in accordance with appropriate regulatory provisions or proprietary agreements.
- (8) The information classified as proprietary was developed and compiled by Holtec International at a significant cost to Holtec International. This information is classified as proprietary because it contains detailed descriptions of analytical approaches and methodologies not available elsewhere. This information would provide other parties, including competitors, with information from Holtec



**H O L T E C**  
I N T E R N A T I O N A L

Holtec Center, 555 Lincoln Drive West, Marlton, NJ 08053

Telephone (856) 797-0900

Fax (856) 797-0909

U.S. Nuclear Regulatory Commission  
ATTN: Document Control Desk

**AFFIDAVIT PURSUANT TO 10 CFR 2.390**

---

International's technical database and the results of evaluations performed by Holtec International. A substantial effort has been expended by Holtec International to develop this information. Release of this information would improve a competitor's position because it would enable Holtec's competitor to copy our technology and offer it for sale in competition with our company, causing us financial injury.

- (9) Public disclosure of the information sought to be withheld is likely to cause substantial harm to Holtec International's competitive position and foreclose or reduce the availability of profit-making opportunities. The information is part of Holtec International's comprehensive spent fuel storage technology base, and its commercial value extends beyond the original development cost. The value of the technology base goes beyond the extensive physical database and analytical methodology, and includes development of the expertise to determine and apply the appropriate evaluation process.

The research, development, engineering, and analytical costs comprise a substantial investment of time and money by Holtec International.

The precise value of the expertise to devise an evaluation process and apply the correct analytical methodology is difficult to quantify, but it clearly is substantial.

Holtec International's competitive advantage will be lost if its competitors are able to use the results of the Holtec International experience to normalize or verify their own process or if they are able to claim an equivalent understanding by demonstrating that they can arrive at the same or similar conclusions.

The value of this information to Holtec International would be lost if the information were disclosed to the public. Making such information available to competitors without their having been required to undertake a similar

